Charles University in Prague
Faculty of Science

Ph.D. Program: Immunology

Jana Balounová

Toll like receptors and myeloid cells in development and disease
Toll like receptory a myeloidní buňky ve vývoji a nemoci

Ph.D. Thesis

Supervisor: Dominik Filipp
Consultant: Jan Černý

Immunobiology group

Institute of Molecular Genetics of the ASCR, v. v. i.

Prague, 2014

Declaration

I hereby declare that thesis is a presentation of my original research work. Wherever contribution of others is involved, every effort is made to indicate this clearly, with reference the literature and acknowledgement of collaborative research and discussions. This thesis contains no material that has been submitted previously, in whole or in part, for the award of any other academic degree or diploma.
Prague, 1st of April, 2014

Signature:

Acknowledgements

Abbreviations

AGM	aorta gonad mesonephros
APC	antigen presenting cell
BAC	bacterial artificial chromosome
BaP	basophil progenitor
BM	bone marrow
BMCP	basophil/mast-cell progenitor
CFU	colony forming unit
CHORI	Children's Hospital Oakland Research Institute
CLP	common lymphoid progenitor
CMEP	common myeloid-erythroid progenitor
CMP	common myeloid progenitor
CMLP	common myelo-lymphoid progenitor
Cre	Cyclic recombinase
DC	dendritic cell
DHD	defensin high diabetic
DND	defensin normal diabetic
DRM	detergent resistant microdomain
EoP	eosinophil progenitor
EP	embryo proper
EPO	erythropoietin
ER	estrogen receptor
EryP	primitive erythrocytes
EYFP	enhanced yellow fluorescent protein
FACS	fluorescence actiated cell sorting
FDR	false discovery rate
FL	fetal liver
FT	fetal thymus
GMP	granulocyte-monocyte progenitor
HPC	hematopoietic progenitor cell
HSC	hematopoietic stem cell
HSPC	hematopoietic stem and progenitor cell
IFN	interferon
Lin	lineage
LPS	lipopolysaccharide
LSK	Lin$^-$ Sca$^+$c-kit$^+$ cells
LTML	long term multi lineage
LVS	live vaccine strain

MCP	mast-cell progenitor
MDP	macrophage-dendritic cell progenitor
MEP	megakaryocyte and erythroid progenitor
MPP	multipotent progenitor
Neo	neomycin
NET	neutrophil extracellular trap
NMP	neutrophil-monocyte progenitor
ON	overnight
PAMP	pathogen associated molecular pattern
PNI	pronuclear injection
PCR	polymerase chain reaction
PRR	pattern-recognition receptor
PSp	para-aortic splanchnopleura
ROS	reactive oxygen species
TIR	Toll-IL-1 receptor
TLR	Toll like receptor
TPO	thrombopoietin
T1D	Type 1 diabetes mellitus
wt	wild type
YFP	yellow fluorescent protein
YS	yolk sac
4-OHT	4-hydroxytamoxifen

Contents

Preface

Toll like receptors (TLRs) are critically important in the pathogen recognition and regulation of the innate and adaptive immune response (Akira et al. 2001; Medzhitov 2007). In addition, it has been recently shown that direct pathogen sensing of bone marrow hematopoietic stem cells (HSCs) and hematopoietic progenitors via TLRs seems to play a crucial role in directing the hematopoietic cell fates under inflammatory conditions (Nagai et al. 2006; Sioud et al. 2006; Boiko and Borghesi 2011).

In the past decades the role of TLRs in adult hematopoiesis and immune responses has been studied intensively. However, their expression pattern and role in early stages of embryonic development are so far largely overlooked.

The presented thesis is based on three manuscripts and an overview of my current work focused on the role of TLRs in early embryonic hematopoietic events including generation of two transgenic mice strains.

The first chapter is based on a manuscript (submitted to Genes and Development, in revision) that describes the existence of TLR2+ erythro-myeloid progenitors in very early stages of embryonic development.

The following chapter describes the generation of two transgenic TLR2-reporter mouse strains suitable for lineage tracing of cells with activated *Tlr2* regulatory elements (unpublished data).

The third chapter is represented by a published article that characterizes the role of embryonic, yolk sac derived phagocytes expressing TLRs in developmental homeostasis and iron metabolism.

Finally, the last two chapters include two papers dedicated to the role of myeloid cells in disease. One paper describes the induction of autophagy pathway in macrophages at the early time of *Francisella tularensis* LVS infection. The other paper reveals the role of myeloid α-defensins produced by eosinophils in peripheral blood of type 1 diabetes patients.

The manuscripts and published papers directly related to this thesis:

Balounová J, Vavrochová T, Benešová M, Alberich-Jordà M, Jurisicova A, Sung H, Filipp D. **Toll-like receptor 2 tracks the emergence of earliest erythro-myeloid progenitors in precirculation embryo**. *Submitted in 2013, currently in revision in Genes & Development.*

Balounová J, Vavrochová T, Benešová M, Ballek O, Kolář M, Filipp D. **Toll-like receptors expressed on embryonic macrophages couple inflammatory signals to iron metabolism during early ontogenesis.** *Eur J Immunol. Accepted manuscript, 2014 Jan 27. doi: 10.1002/eji.201344040. [Epub ahead of print]*

Härtlova A, Link M, **Balounova J**, Benesova M, Resch U, Straskova A, Sobol M, Philimonenko A, Hozak P, Krocova Z, Gekara N, Filipp D, Stulik J. **Quantitative Proteomics Analysis of Macrophage-Derived Lipid Rafts Reveals Induction of Autophagy Pathway at the Early Time of *Francisella tularensis* LVS Infection**. *Journal of Proteome Research. 2014, 13(2):796-804.*

Neuwirth A, Dobes J, **Oujezdska J**, Ballek O, Benesova M, Sumnik Z, Vcelakova J, Kolouskova S, Obermannova B, Kolar M, Stechova K, Filipp D. **Eosinophils from patients with type 1 diabetes mellitus express high level of myeloid α-defensins and myeloperoxidase**. *Cell Immunol. 2012, 273(2):158-63.*

In addition, during her Ph.D. studies, the defendant published several scientific papers related to the above listed articles by their methodological approaches.

Specifically, defendant's expertise in immunodetection including western-blotting, multicolor FACS analysis and fluorescence microscopy granted the co-authorship in following studies:

Dobes J, Neuwirth A, Benesova M, Voboril M, **Balounova J**, Ballek O, Lebl J, Meloni A, Krohn K, Kluger N, Ranki A, Filipp D. **Enteric α−defensins as novel and clinically relevant intestinal autoantigens in APECED patients**. *Submitted in 2013, currently in revision in the Journal of Experimental Medicine.*

Faldyna M, Samankova P, Leva L, Cerny J, **Oujezdska J**, Rehakova Z, Sinkora J. **Cross-reactive anti-human monoclonal antibodies as a tool for B-cell identification in dogs and pigs.** *Vet Immunol Immunopathol. 2007, 119(1-2):56-62*

Abstract

Toll like receptors (TLRs) are germline-encoded pattern recognition receptors (PRRs) that play a central role in host cell recognition and responses to pathogens. Primarily they are responsible for induction and regulation of the innate and adaptive immune responses whereby the effector function is executed chiefly by differentiated myeloid cells. Somewhat unexpectedly, TLRs have been also shown to be involved in direct pathogen sensing by bone marrow-derived hematopoietic stem cells (HSCs) and hematopoietic progenitors when, under inflammatory conditions, the rapid generation of innate immune effector cells that effectively combat the infection is of utmost priority. While it has been recognized that the release of inflammatory cytokines from inflamed tissues along with the changes in proportions of differentiating cells in the bone marrow (BM) as well as the BM niche can nudge the differentiation of adult BM-derived cells towards myeloid cells and granulocytes, a direct role of TLRs expressed by HSCs in this process has been demonstrated only recently. However, whether a similar mechanism operates also during embryonic hematopoiesis is unknown. Here we show that TLRs and their adaptor proteins are functionally expressed during early stages of embryogenesis by short-lived maternally-transferred myeloid cells, which are then replaced by differentiated embryonic myeloid cells. Unexpectedly, the earliest hematopoietic multipotent progenitors, which appear at day 6.5 of mouse embryogenesis (E6.5), also express TLRs and similar to differentiated embryonic myeloid cells, respond to TLR2 triggering by enhanced proliferation and myeloid differentiation rates in a MyD88-adaptor protein-dependent manner. In order to trace the relationship of established hematopoietic lineages to these TLR2+ early hematopoietic progenitors, we describe here the generation of two transgenic *Tlr2*-reporter mouse strains that enable a direct lineage tracing of embryonic cells with an active *Tlr2* locus. In addition to providing gene expression profiling and multiple lines of evidence for the functionality of embryonically expressed TLRs, we demonstrate the involvement of TLR2 signaling in the regulation of iron metabolism pathway in E10.5 TLR2+ yolk sac-derived macrophages. In respect to the role of myeloid cells in health and disease, particularly focusing on pathogen-host interactions, we describe the early activation of *Francisella tularensis*-triggered autophagy pathway in macrophages which is controlled by the adaptor protein p62, a process that is likely initiated by TLR triggering. Lastly, we also show that myeloid α-defensins and myeloperoxidase are highly expressed in eosinophils that are isolated from peripheral capillary blood of patients with the type 1 diabetes, where they could serve as molecular markers of transcriptionally active eosinophils. Collectively, our work demonstrates so far unrecognized functions of TLRs in myeloid cells in development and disease.

Abstrakt

Receptory odvozené od receptoru Toll (TLR) rozeznávají specifické evolučně konzervované struktury společné mnohým patogenům a hrají klíčovou roli v jejich rozpoznání a eliminaci hostitelem. V první řadě jsou zodpovědné za iniciaci a regulaci vrozené i specifické imunitní odpovědi, která je zprostředkována zejména diferenciovanými myeloidními buňkami. Poněkud překvapivé je nedávné zjištění, že v průběhu zánětlivé odpovědi, kdy je prioritou organismu produkovat dostatečné množství buněk imunitního systému pro boj s infekcí, hematopoetické kmenové buňky (HKB) a jejich progenitory mohou prostřednictvím TLR přímo rozpoznávat mikrobiální struktury. Tento nedávno popsaný mechanismus můžeme zahrnout mezi další již dříve popsané způsoby indukce diferenciace HKB v myeloidní buňky a granulocyty. Jmenovitě vliv zánětlivých cytokinů produkovaných infikovanou tkání a reakci na pokles počtu diferencovaných buněk, či jejich prekurzorů, v důsledku mobilizace těchto buněk z kostní dřeni. Není nicméně známo, zda se tento mechanismus uplatňuje také v embryonální krvetvorbě. Naše výsledky ukazují, že receptory TLR a jejich adaptorové proteiny jsou v časných stádiích embryogeneze funkčně exprimovány nejprve maternálními myeloidními buňkami, které jsou postupně nahrazeny diferenciovanými embryonálními fagocyty. Za povšimnutí stojí fakt, že stejně jako diferencované embryonální myeloidní buňky, i nejčasnější hematopoetické multipotentní progenitory, které se objevující ve dni 6.5 embryonálního (E6.5) vývoje myši exprimují receptory TLR, a po stimulaci agonistou receptoru TLR2 odpovídají zvýšením úrovně proliferace a myeloidní diferenciace v závislosti na přítomnosti adaptorového proteinu MyD88. Abychom porozuměli vztahům vznikajících hematopoetických linií a TLR2+ časných embryonálních hematopoetických progenitorů, vytvořili jsme dva transgenní *Tlr2*-reportérové myší modely umožňující neinvazivní genetické sledování embryonálních buněk s aktivním lokusem genu *Tlr2*. Vedle zmapování expresního profilu E10.5 embryonálních fagocytů pocházejících vývojově ze žloutkového váčku, a prověření funkčnosti jejich receptorů TLR, naše data ukazují i na účast signalizace TLR2 v regulaci metabolismu železa v těchto embryonálních makrofázích. S ohledem na roli myeloidních buněk v rozvoji onemocnění, a to zejména při interakci patogen-hostitel, popisujeme časnou aktivaci autofagie indukované v makrofázích po infekci bakterií *Francisella tularensis* prostřednictvím adaptorového proteinu p62. Tento proces může být spuštěn aktivací receptorů TLR. Následně demonstrujeme, že myeloidní α-defensiny a myeloperoxidáza jsou produkovány eosinofily izolovanými z kapilární krve pacientů s diabetem 1. typu a mohly by tak představovat molekulární markery transkripčně aktivních eosinofilů. Naše práce poukazuje na doposud nepopsané funkce receptorů TLR v myeloidních buňkách v průběhu vývoje i patologických stavů.

1. Literature review

1.1. Toll like receptors

Toll like receptors are critically important in triggering immune responses to infections. The interaction of TLRs with their ligands initiates several distinct signaling pathways resulting in global and robust changes in the gene expression leading to effective innate immune responses and regulated development of antigen-specific immunity (reviewed in (Akira et al. 2001; Medzhitov 2007).

1.1.1. TLR discovery

Originally, the *Toll* gene was described to be responsible for the dorso-ventral patterning in developing *Drosophila* embryo (Anderson et al. 1985). Later, the striking structural and functional similarities in Toll/dorsal signaling cascade and cytokine induced activation of NF-kB pathway in mammals led the team of Jules Hoffman to the discovery of new function for Toll receptor in *Drosophila* immune responses to fungal infections (Lemaitre et al. 1996). One year later, a mammalian homolog of the Toll receptor, currently known as TLR4, was shown to induce the expression of genes involved in inflammatory responses (Medzhitov et al. 1997). This seminal observation was quickly complemented by an excellent study by Beutler and colleagues who identified murine TLR4 as a key signal-transducing receptor for LPS (Poltorak et al. 1998). Subsequent intense database search identified 10 human and 12 murine TLRs that recognize other immunologically-relevant microbial structures such as proteins, lipoproteins, carbohydrates and nucleic acids, as depicted in Figure 1 (Kumar et al. 2011). TLR1-TLR9 are conserved between the human and mouse, whereas functional TLR10 is expressed only in humans. In contrast, mice express also TLR11, TLR12 and TLR13 which lack functional homologs in humans (Akira and Takeda 2004). TLRs were the first identified pattern-recognition receptors (PRRs) that recognize molecular structures broadly shared by pathogens, known as pathogen-associated molecular patterns (PAMPs). It is of historical interest that while the existence of PRRs was predicted by Charlie Janeway several years before their discovery (Janeway 1989), Bruce Beutler and Jules Hoffman received the Nobel prize in 2011 for the experimental demonstration of their importance for the regulation of immune responses.

1.1.2. TLR structure, specificity and localization

The TLRs are the type I integral membrane glycoproteins consisting of an extracellular domain with 19-25 tandem copies of leucine-rich repeats, a single transmembrane segment and an intracellular domain, highly similar to the IL-1 receptor domain (TIR; Toll-IL-1 receptor) (Akira et al. 2006). Despite this similarity, the extracellular portions of both types of receptors are structurally unrelated allowing recognition of a wide spectrum of non-self ligands (Akira and Takeda 2004). These include lipoproteins (recognized by TLR1, TLR2, and TLR6), double-stranded RNA (TLR3), lipopolysaccharide (TLR4), flagellin (TLR5), single-stranded RNA (TLR7 and TLR8), and DNA (TLR9) (Figure 1) (Akira et al. 2006).

Based on cellular localization, two groups of TLRs can be distinguished: TLR1, TLR2, TLR4, TLR5, and TLR6 are localized on the cell surface and largely recognize microbial membrane components whereas TLR3, TLR7, TLR8, TLR9, TLR11 and TLR13 are expressed within intracellular vesicles and recognize mainly nucleic acids (Blasius and Beutler 2010). The intracellular localization within innate immune cells enables TLRs to recognize nucleic acids delivered to the intracellular compartments after the uptake of viruses and other pathogens or infected cells and prevents their activation by harmless nucleic acids present in the cytosol. However, there are some exemptions from the "localization" rule as on fibroblasts/endothelial cells and human neutrophils, TLR3 and TLR9 respectively, are expressed also as surface receptors (Lindau et al. 2013; Miyake and Onji 2013; Pohar et al. 2013).
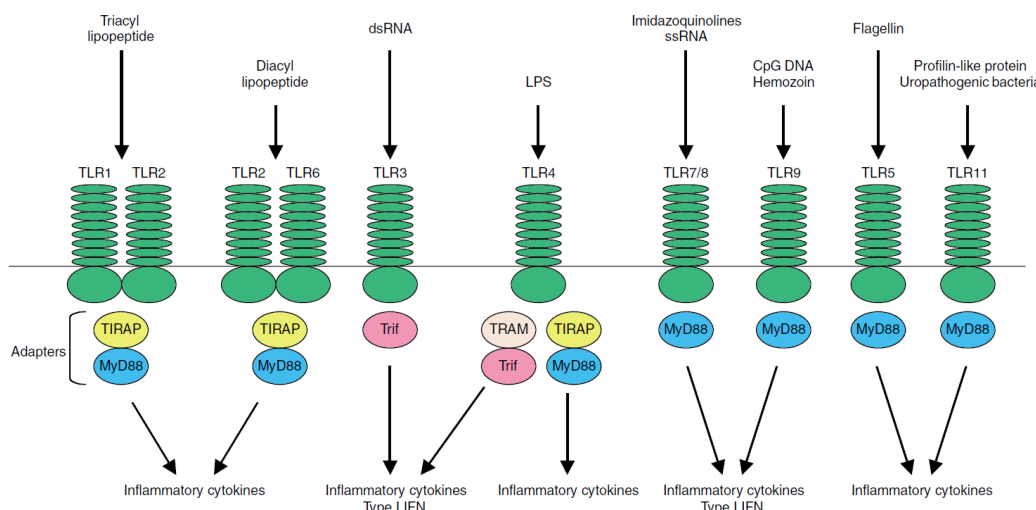
Figure 1. TLR-mediated immune responses; taken from (Kawai and Akira 2006).
TLR2 in concert with TLR1 or TLR6 discriminates between the molecular patterns of triacyl and diacyl lipopeptide, respectively. TLR3 recognizes dsRNA. TLR4 recognizes bacterial LPS. TLR7/8 mediates recognition of imidazoquinolines and ssRNA. TLR9 recognizes CpG DNA of bacteria and viruses. TLR5 recognizes flagellin and mouse TLR11 recognizes components of uropathogenic bacteria and profilin-like molecule of the Toxoplasma gondii. TLR1/2 and TLR2/6 utilize MyD88 and TIRAP/MAL as essential adapters. TLR3 utilizes Trif. TLR4 utilizes MyD88, TIRAP/MAL, Trif and TRAM. TLR7/8, TLR9, TLR5 and TLR11 use only MyD88.

1.1.3. TLR signaling pathways

Upon ligand binding, TLRs dimerise and recruit proximal TIR-domain containing adaptor proteins initiating downstream signaling leading to the activation of transcription factors such as NF-κB, IRFs and AP-1. The outcome of the response is dependent on the type of adaptor protein or their combination used. So far, five TLR adaptor proteins, acting alone or in combination, have been described: MyD88, MAL, TRIF, TRAM and SARM, reviewed in (Dunne and O'Neill 2003; Kawai and Akira 2010) (Figure 2, (Kawai and Akira 2011). MyD88 is utilized by all TLRs (with the exception of TLR3) and members of IL-1R family and transmits signals culminating in NF-kB and MAP kinase activation and the induction of inflammatory cytokines. TLR3 and TLR4 use TRIF to activate an alternative pathway leading to the activation of NF-kB and IRF3 and the induction of type I IFN and inflammatory cytokine productions. TLR2 and TLR4 use TIRAP as an additional adaptor to recruit MyD88. TRAM acts as a bridge between TLR4 and TRIF (Kawai and Akira 2011). TLR4 is the solely TLR that activates two distinct signaling pathways involving MyD88 or TRIF adaptors with a different kinetics. Initially, surface TLR4 recruits TIRAP and MyD88. Subsequently, MyD88 recruits IRAKs, TRAF6, and the TAK1 complex, leading to early-phase activation of NF-kB and MAP kinases (Kawai and Akira 2010). TLR4 is then endocytosed and delivered to intracellular vesicles to form a complex with TRAM and TRIF, which then recruits TRAF3 and the protein kinases TBK1 and IKKi, which catalyze the phosphorylation of IRF3, leading to the expression of type I IFN (Barton and Kagan 2009). TRAM-TRIF also recruits TRAF6 and TAK1 to mediate late-phase activation of NF-kB and MAP kinases. Whereas type I IFN response is elicited upon TRIF recruitment, the robust NF-kB and MAP kinase activation followed by the induction of inflammatory response demands utilization of both MyD88 and TRIF. Accordingly, TLR2-TLR1 and TLR2-TLR6 heterodimers that signal through TIRAP and MyD88, are recruited to the phagosome during phagocytosis of zymosan or *Staphylococcus aureus* to induce the production of inflammatory cytokines (Kawai and Akira 2011). In addition, TLR2 is capable to induce type I IFN in inflammatory monocytes infected with vaccinia viruses (Barbalat et al. 2009). TLR7 and TLR9 are exclusively expressed in plasmacytoid DCs (pDCs), which have the capacity to secrete vast amounts of type I IFN rapidly in response to viral infection in a MyD88 dependent manner (Gilliet et al. 2008; Reizis et al. 2011). One recent study suggests that TLR5, which normally signals from the surface through MyD88 to elicit inflammatory cytokine production, in intestinal epithelial cells recruits TRIF in addition to MyD88, which leads to the activation of NF-kB rather than IRF3 (Choi et al. 2010).

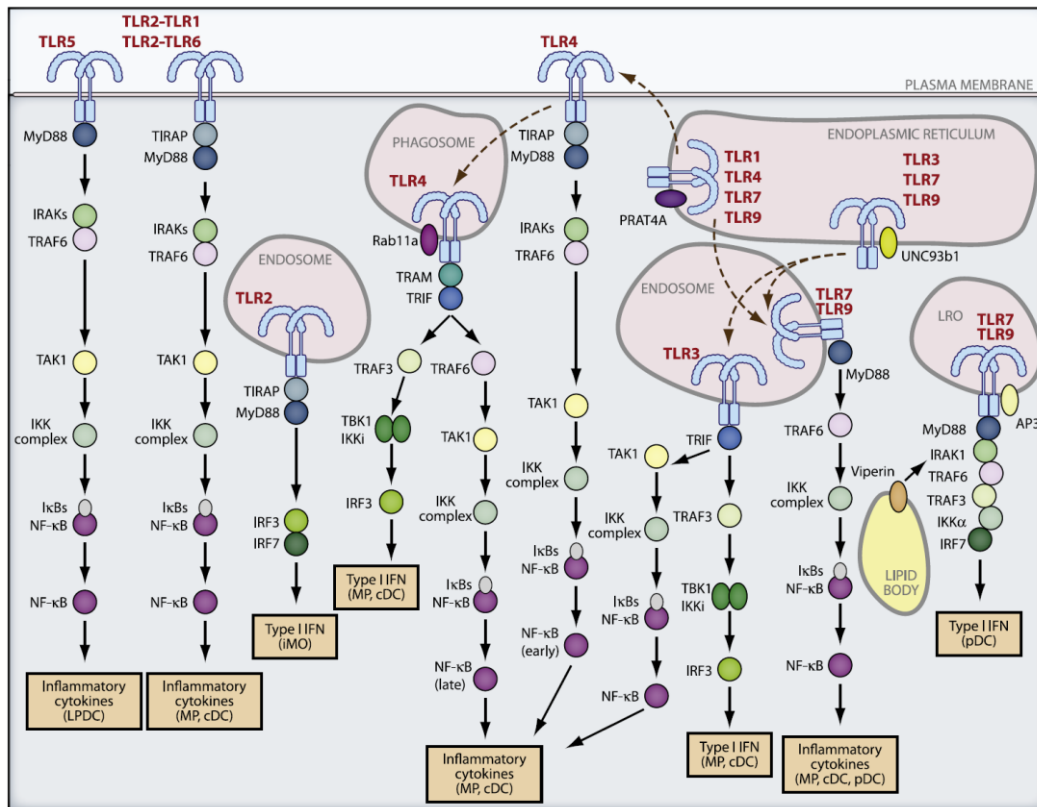*Figure 2. TLR-mediated immune response; taken from (Kawai and Akira 2011).*

Individual TLRs initiate overlapping and distinct signaling pathways in various cell types such as macrophages (MP), conventinal DC (cDC), plasmacytoid DC (pDC), lamina propria DC (LPDC), and inflammatory monocytes (iMO). PAMP engagement induces conformational changes of TLRs that allow homo- or heterophilic interactions of TLRs and recruitment of adaptor proteins (MyD88, TIRAP, TRIF, and TRAM). TLR5, highly expressed on the cell surface of LPDC, uses MyD88 and activates NF-kB through IRAKs, TRAF6, TAK1, and IKK complex, resulting in induction of inflammatory cytokines. Heterodimers of TLR1- TLR2 and TLR2-TLR6 are also expressed on the cell surface and induce NF-kB activation through recruitment of TIRAP and MyD88 in MPs and cDCs. In iMO, TLR2 is found to be expressed within the endosome and induce type I IFN via IRF3 and IRF7 in response to viruses. TLR4, which is expressed on the cell surface, initially transmits signals for the early-phase activation of NF-kB by recruiting TIRAP and MyD88. TLR4 is then transported into Rab11a$^+$ phagosomes that contain bacteria, where it recruits TRAM and TRIF and activates TRAF3-TBK1-IRF3 axis as well as late-phase NF-kB activation for the induction of type I IFN. Both early- and late-phase activation of NF-kB is required for the induction of inflammatory cytokines. TLR3, TLR7, and TLR9 are localized mainly to the ER in the steady state and traffic to the endosomal compartment, where they engage with their ligands. TLR3 activates the TRIF-dependent pathway to induce type I IFN and inflammatory cytokines in MPs and cDCs. In pDCs, TLR7and TLR9 activate NF-kB and IRF7 via MyD88 to induce inflammatory cytokines and type I interferon, respectively. The activation of NF-kB during TLR7 and TLR9 signaling is initiated from the endosome whereas IRF7 activation is initiated from the lysosome-related organelle (LRO) after TLR7 and TLR9 are transported from the endosome to this vesicle in a manner dependent on AP3. MyD88-dependent IRF7 activation in pDCs is mediated by activation of IRAK1, TRAF6, TRAF3, and IKKa and is facilitated by IFN-inducible Viperin expressed in the lipid body. In cDCs and MPs, TLR7 and TLR9 induce inflammatory responses by activating NF-kB via MyD88 but fail to activate IRF7.

18

1.1.4. TLR expression

Recognized as the sensors for danger signals, TLRs are expressed mainly by innate immune cells such as macrophages, monocytes, dendritic cells, granulocytes and NK cells (Hornung et al. 2002; Sabroe et al. 2002; Nagase et al. 2003), but also by other, more specialized types of immune and nonimmune cells – B and T lymphocytes (Bourke et al. 2003; Caramalho et al. 2003), keratinocytes and other epithelial cells (Gewirtz et al. 2001; Saint André et al. 2002; Wolfs et al. 2002; Pivarcsi et al. 2003).

Recently, hematopoietic stem cells (HSCs) and hematopoietic progenitors have been shown to express TLRs allowing them to directly sense the presence of infections (Nagai et al. 2006; Sioud et al. 2006; De Luca et al. 2009). While in unperturbed physiological circumstances bone marrow (BM) hematopoiesis is driven by a lineage specific combination of endogenous cytokines and growth factors secreted *in situ* by cells residing in the hematopoietic niche or from a remote site (Alexander 1998), it has been demonstrated that TLR stimulation can nudge the BM hematopoiesis towards the increased production of granulocytes, monocytes and monocytic dendritic cells (Ueda et al. 2005; Nagai et al. 2006; Sioud et al. 2006). For the first time, in 2006, Nagai and colleagues have shown that HSCs and hematopoietic progenitors express TLRs, the immune system triggers. According to their findings, TLR ligands drove normal but not MyD88-deficient HSCs and multipotent progenitors (MPPs) to proliferate and increased their output of differentiated progeny and supported the common lymphoid progenitors (CLPs) to preferentially differentiate into CD11c^{+} dendritic cells (Figure 3). Shortly after, the expression of TLRs and TLR-signaling driven instruction for a myeloid cell fate were described for human BM CD34^{+} cells (Sioud et al. 2006) and human HSCs (De Luca et al. 2009).

Thus sensing of danger signals by TLRs expressed on HSCs and hematopoietic progenitors serves as an important back-up mechanism operating during the course of infection when rapid replenishment of short-lived myeloid cells is crucial for the maintenance of adult immune homeostasis (Holl and Kelsoe 2006; Welner and Kincade 2007).
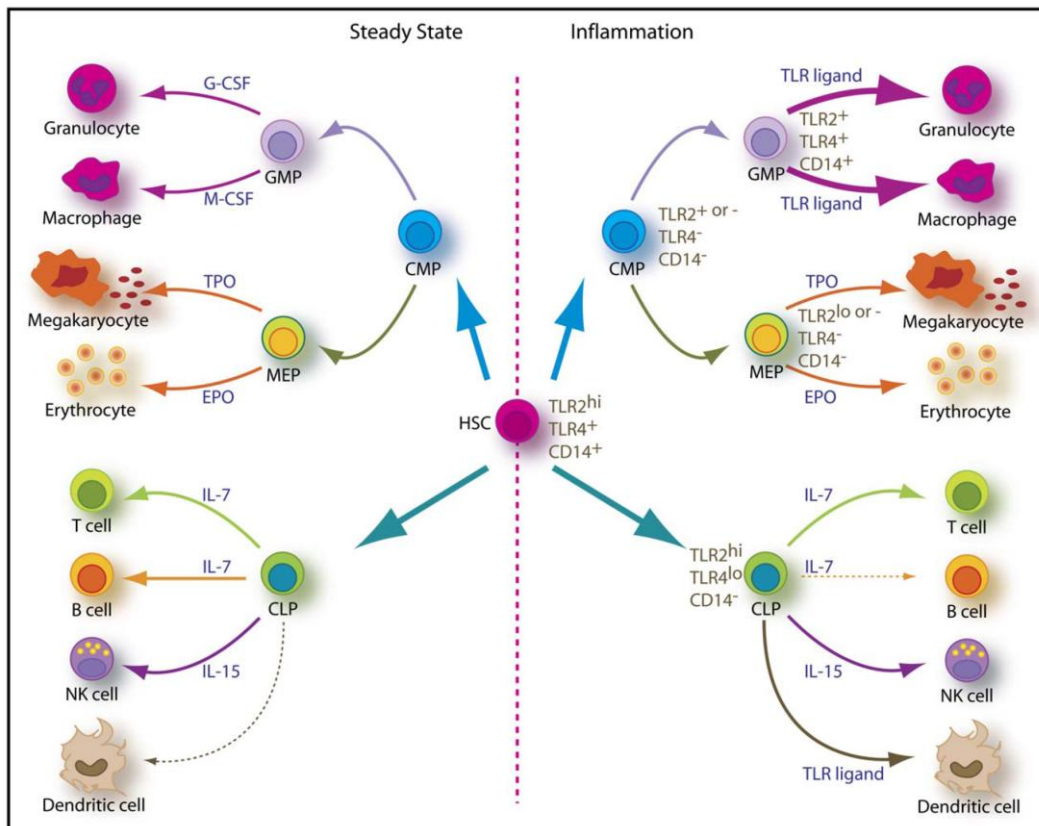
Figure 3. Hematopoiesis under steady-state and inflammatory conditions; taken from (Holl and Kelsoe 2006).

All hematopoietic lineages arise from a common ancestor, the hematopoietic stem cell (HSC). In turn, the self-renewing HSC gives rise to progenitor cells with more limited developmental plasticity through asymmetric division. Committed myeloid progenitors (CMPs) and committed lymphoid progenitors (CLPs) are multipotent cells incapable of self-renewal but under normal, steady-state conditions (left) generate all differentiated myeloid and erythroid (CMP) or lymphoid (CLP) cell types. CLPs differentiate to B or T lymphocytes under the influence of IL-7, to NK cells with IL-15, or to DCs. CMPs produce even more differentiated granulocyte and monocyte progenitors (GMP) that respond to granulocyte colony stimulating factor (G-CSF) or macrophage colony stimulating factor (M-CSF) by differentiating to granulocytes or macrophages, respectively. Megakaryocyte and erythroid progenitors (MEPs) are driven by thrombopoietin (TPO) or erythropoietin (EPO) to form, respectively, megakaryocytes or erythrocytes. In the presence of the TLR ligands LPS and Pam3CSK4 (right), HSC and more differentiated progenitors bearing TLR2 and/or TLR4 respond by altering hematopoietic output. GMPs become capable of producing granulocytes and macrophages in the absence of G-CSF or M-CSF, and while lymphocyte production by CLPs is reduced, DC output becomes increased. Generation of megakaryocytes and erythrocytes by MEPs is little affected.

While it was generally accepted, that HSCs are sheltered from the danger signals by their BM niches, several groups have recently shown that HSCs and hematopoietic stem and progenitor cells *(*HSPCs) are constitutively circulating though the blood stream between the BM and peripheral organs (Figure 4)(Wright et al. 2001). This process is believed to be critical in the maintenance of normal hematopoietic homeostasis in dispersed BM cavities (Wright et al. 2001), but also enables the pathogen recognition receptors-bearing HSPCs to patrol the immune periphery (Massberg et al. 2007). Indeed, the migratory pool of HSPCs might act as a source of highly versatile stem and progenitor cells that can respond to danger signals locally within tissues before the information is spread to the BM (Nagai et al. 2006; Massberg et al. 2007). Notably, TLR stimulation also prevents HSPCs to exit from inflamed tissues (Massberg et al. 2007).
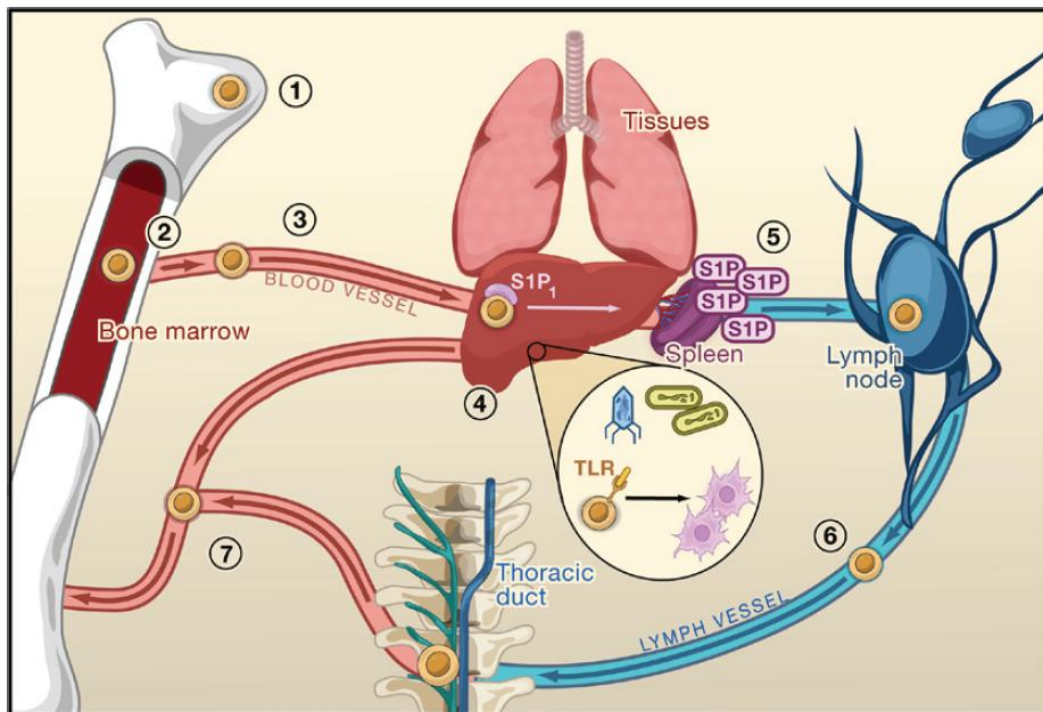
Figure 4. Migration of Hematopoietic Stem and Progenitor Cells; taken from (Welner and Kincade 2007).
(1) Many stem cells reside in association with osteoblasts in trabecular bone. (2) An even greater number are close to centrally located vascular sinuses, but little is known about exchange between these two locations. (3) PAMPs and cytokines released during infection can mobilize hematopoietic stem and progenitor cells (HSPCs), which migrate out of the BM into blood, but small numbers exit under normal circumstances. HSPCs remain in the circulation for only seconds but reside in tissues such as the lungs, liver, and spleen for at least 36 hr. (4) Their stay is extended by recognition of PAMPs by TLRs that they express. Myeloid cells are produced locally from HSPCs in response to particular TLR ligands, and these effectors of the innate immune system presumably fight infections and promote tissue repair. (5) Unstimulated HSPCs use their sphingosine-1-phosphate receptors to recognize steep gradients of sphingosine-1-phosphate and to enter the lymph (blue). (6) HSPCs quickly transit through one or more lymph nodes before returning to the blood via the thoracic duct. (7) At least some stem cells return to BM niches, but it is not known if they are affected by the journey.

1.2. Hematopoietic stem cells

During the lifetime, all blood cells, including red blood cells, megakaryocytes, myeloid cells (monocyte/macrophage and neutrophil) and lymphocytes are continually produced in the BM through the expansion and differentiation of progenitors that originate from a scarce cell population, the long-term hematopoietic stem cells (LT-HSCs). LT-HSCs, that sit atop a hierarchy of hematopoietic progenitors, are capable of extensive self-renewal capacity and ability to differentiate to short-term HSCs and lineage restricted progenitors (Orkin and Zon 2008). Under steady-state conditions, HSCs divide infrequently and are found mainly in the G0 phase of cell cycle (Trumpp et al. 2010).

Initially, HSCs were identified based on their ability to form colonies in the spleens of lethally irradiated mice upon BM transfer (Till and McCulloch 1961). With contemporary methods, HSCs may be highly purified such that as few as one cell may provide long-term hematopoietic reconstitution in a recipient. All functional HSCs are found among the lineage (Lin) negative, stem-cell antigen 1 (Sca1) and c-kit positive (LSK) fraction of BM cells.

However, there is a consensus that no *ex vivo* functional assays can replace *in vivo* transplantation for measuring biological activity of HSCs. Similarly, the characterization of LT-HSC cell populations, based solely on the expression profile of cell surface markers, cannot be considered synonymous with determining their function. In this respect, LT-HSCs are defined on the basis of their functional ability to provide a long-term hematopoietic reconstitution in myeloablated hosts. A sustained output of ≥ 1% of all the circulating white blood cells for ≥ 4 months is considered as a „gold standard" to define multipotency of LT-HSCs (Purton and Scadden 2007).

As HSCs divide and pass developmental branch points they become more restricted and ultimately yield unipotent progenitor cells. The lineage restriction, which occurs at each branch point, is also referred to as "cell fate decision" or "lineage commitment". Visualization of these branching events via a cartoon map provides essential information about the relationships between these lineages. According to a textbook model, formulated approximately 30 years ago, HSCs generate the common myeloid-erythroid progenitors (CMEP) and a common lymphoid progenitors (CLP), which produce myeloid or erythroid cells and T or B cells, respectively. Apart from this "classical model" of lineage commitment, in 2001, the so-called "myeloid-based" model was proposed by Kawamoto and colleagues (Katsura and Kawamoto 2001). It posits that HSCs first diverge into the CMEPs and the common myelo-lymphoid progenitors (CMLPs), which generate T and B cell progenitors through a bipotential myeloid-T progenitor and a

myeloid-B progenitor stage. Thus the potential to generate myeloid cells is retained in all, erythroid, T and B lineage branches (Figure 5).
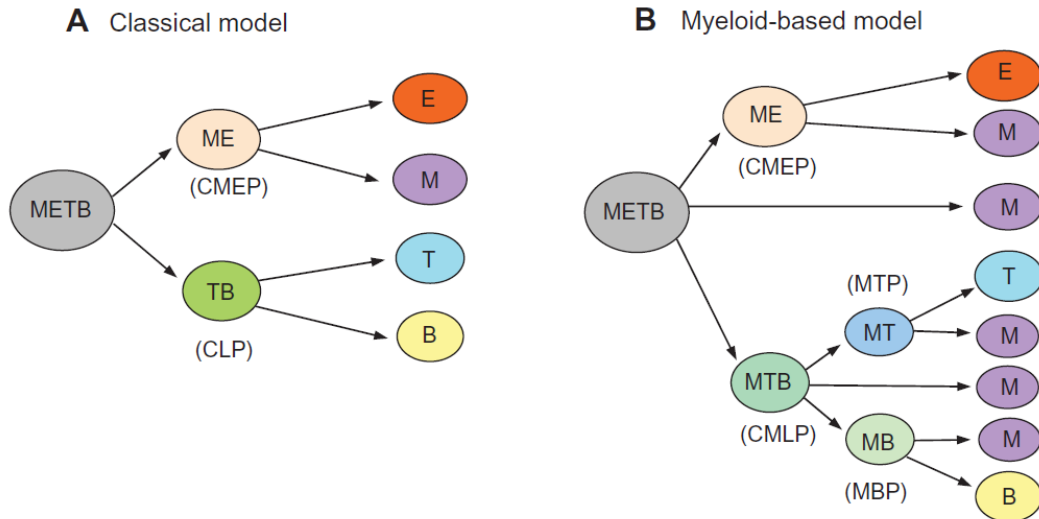
Figure 5. Representative models of hematopoiesis; taken from (Kawamoto et al. 2010).
(A) This model proposes that the HSC firstly diverges into a CMEP and a CLP. Note that CMEPs are sometimes referred to as common myeloid progenitors (CMPs). E, M, T and B represent the progenitor potential for erythroid, myeloid, T and B cells, respectively. (B) In this model, the first branch point generates CMEPs and CMLPs, and the myeloid potential persists in the T and B cell branches even after these lineages have diverged.

1.2.1. The ontogeny of mammalian hematopoiesis

The mammalian hematopoiesis is established during embryonic development via a successive passage of hematopoietic cells through several anatomic niches where they originate, expand or differentiate (Figure 6)(Costa et al. 2012).

The onset of hematopoiesis is tightly coupled with gastrulation, a morphogenetic event through which the three definitive germ layers, ectoderm, mesoderm and endoderm, are established (Tam and Beddington 1987; Ferkowicz and Yoder 2005). During this process, the formation of the yolk sac (YS) is initiated from the primitive streak, a region of epiblast in close proximity to extra-embryonic ectoderm around E6.5 (Gardner and Rossant 1979; Lawson et al. 1991). Developmentally, the YS is established by the contribution of extra-embryonic visceral endoderm and extra-embryonic mesoderm generated by ingression of the most posterior epiblast cells located close to extra-embryonic ectoderm (Smith et al. 1994). Later, cells ingressing from the middle and anterior streak regions form intra-embryonic mesoderm including the future aorta gonad mesonephros (AGM) region (Tam and Beddington 1987). The very first blood cells are detected between E7.0-E7.5 in the YS blood island, with a predominant emergence of

primitive nucleated erythroblasts expressing embryonic and fetal forms of hemoglobin (Silver and Palis 1997). This first wave of hematopoiesis is generally called primitive hematopoiesis/erythropoiesis (Golub and Cumano 2013). In addition, differentiated macrophages and megakaryocytes start to appear in the YS blood island, arising probably from the hemangioblast precursor migrating from the posterior primitive streak around E7.25 (Moore and Metcalf 1970; Palis et al. 1999; Xu et al. 2001; Huber et al. 2004; Ferkowicz and Yoder 2005).

However, these YS-derived precursors are not considered HSCs as they are incapable of long term multi-lineage reconstitution (LTML) of irradiated adult host unless conditioned in appropriate environment (the co-culture with AGM-derived cell lines, remnants of fetal liver (FL) in newborn animals) (Yoder et al. 1997; Cumano et al. 2001; Matsuoka et al. 2001).

The first *bona fide* HSCs emerge from the hemogenic endothelium of the AGM at E10.5 (Muller et al. 1994; Medvinsky and Dzierzak 1996; de Bruijn et al. 2000; Cumano et al. 2001; Dzierzak and Medvinsky 2008). There is a growing body of evidence that the hemogenic endothelium derives from hemangioblast cells (Lancrin et al. 2009). Subsequently, AGM-derived HSCs start to successively colonize the sites of definitive hematopoiesis: fetal liver, spleen, thymus, and eventually bone marrow where they expand and differentiate (Moore and Metcalf 1970). Importantly, and in contrast to the YS-derived early hematopoietic precursors, their E10.5 AGM counterparts can engraft adult host in LTML reconstitution manner. In addition it has been recently shown, that after E10.5, the placenta, chorion, allantois as well as vitelline and umbilical arteries can provide a niche suitable for HSCs emergence (de Bruijn et al. 2000; Zeigler et al. 2006; Rhodes et al. 2008) (Figure 6).

Hematopoietic organs in the mouse embryo
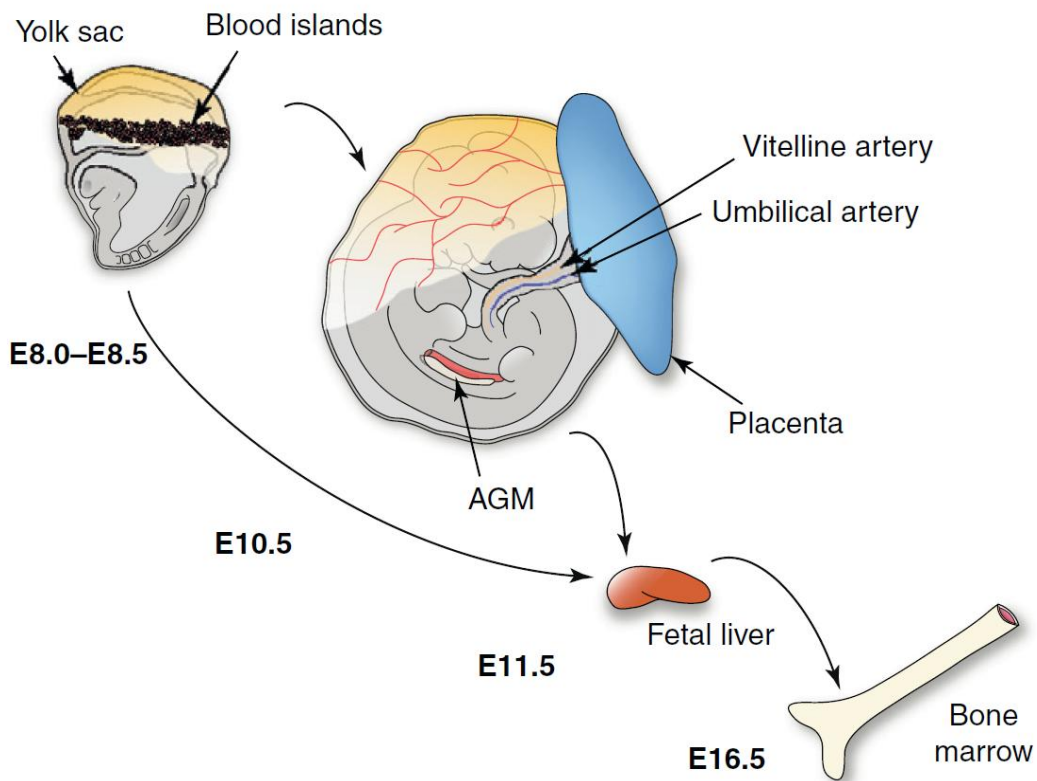
Figure 6. Embryonic sites of blood development; taken from (Costa et al. 2012).
In murine embryos, hematopoiesis takes place in several tissues where blood cells are generated and/or undergo maturation. The first hematopoietic progenitors are found extra-embryonically at E8.0–E8.5, in the YS blood islands in close proximity to emerging endothelial cells. Once circulation is established, blood cells colonize other developing hematopoietic organs. Around E10.5, the AGM, placenta, umbilical artery and vitelline artery initiate the generation of blood precursors that, together with YS cells, colonize to the FL rudiment around E11.5. The FL is the major hematopoietic site where blood progenitors expand and/or mature. Finally, the BM is colonized by precursors from the FL before birth and remains the main hematopoietic niche throughout adult life.

What remains uncertain is the origin and developmental path leading to HSCs appearance in AGM (Ueno and Weissman 2007; Medvinsky et al. 2011). One model suggests that this process is independent from the hematopoiesis occurring in the visceral YS (Medvinsky and Dzierzak 1996; Cumano et al. 2001; Bertrand et al. 2005a). According to this view, the YS precursors, emerging at ~E7.5, provide only a transient and lineage-limited supply of hematopoietic progenitors (Muller et al. 1994; Medvinsky and Dzierzak 1996; de Bruijn et al. 2000; Cumano et al. 2001). In contrast, the second model posits the existence of a common founder of hematopoiesis, that emerges either from the YS (Moore and Metcalf 1970; Samokhvalov et al. 2007; Tanaka et al. 2012) or, alternatively, from mesoderm precursors in posterior primitive streak, so called hemangioblast, migrating concurrently towards the YS as well as para-aortic splanchnopleura (PSp), future AGM (Figure 7)(Huber et al. 2004).
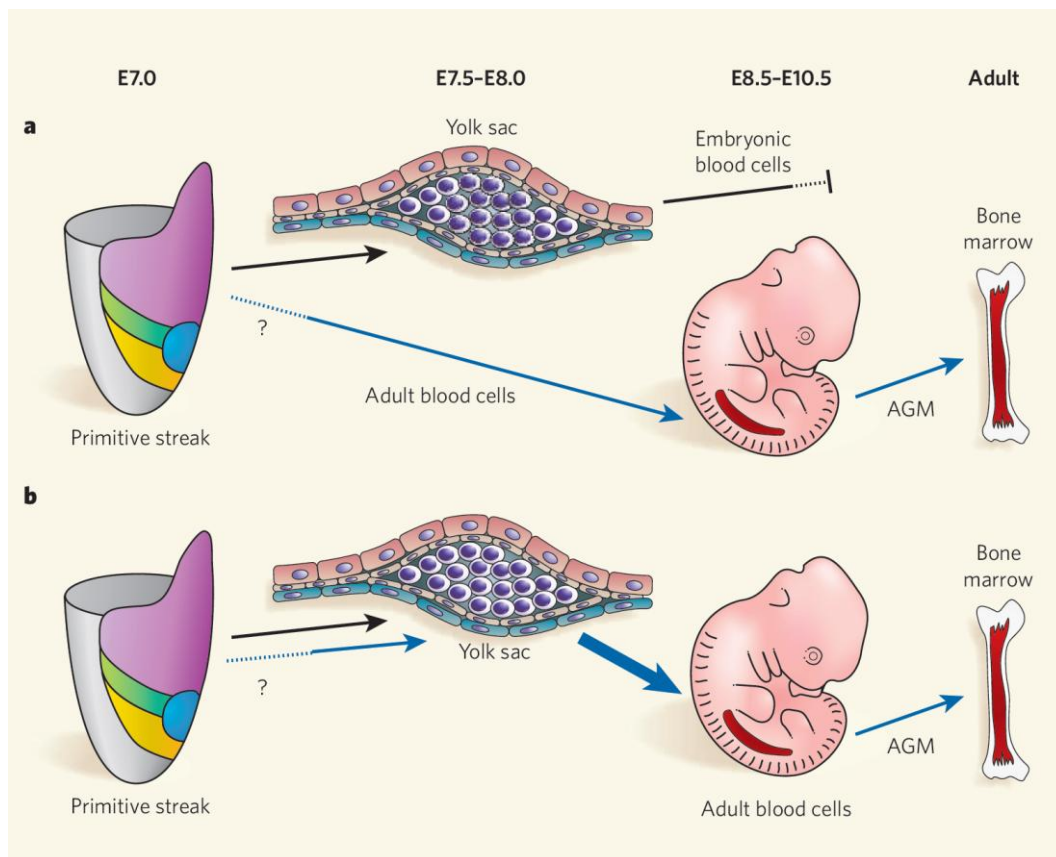
Figure 7. Two models of embryonic and adult blood formation; taken from (Ueno and Weissman 2007).
a, The 'separate' model. Embryonic blood-forming cells, generated in a region called the 'primitive streak', proliferate in the yolk sac, migrate to the embryo proper, but eventually die out. The adult blood-forming cells, whose origin in the early-stage embryo is unknown, are separately generated in the aorta–gonad–mesonephros (AGM) region and later seed the adult bone marrow. b, The 'common' model. Adult blood-forming cells in the AGM regions at least partly originate from Runx1-positive progenitors in the yolk sac. Black and blue arrows show pathways of embryonic and adult blood-forming cells, respectively; bold blue arrow is the pathway described by Samokhvalov and colleague (Samokhvalov et al. 2007). Regions of cells at the primitive-streak stage: notochord (blue); somites (yellow); heart and cranial mesoderm (green); extra-embryonic mesoderm (pink)(Kinder et al. 1999).

Specifically, the concept of intra-embryonic AGM as a unique and independent source of HSCs has been challenged by a recent genetic cell-lineage tracing study showing that YS-derived hematopoietic precursors can contribute to the pool of HSCs that give rise to adult hematopoietic cells (Samokhvalov et al. 2007). In this study the authors used a non-invasive pulse–labeling system based on Cre/*loxP* recombination to track *Runx1* expressing cells *in vivo* to raise the possibility that at least a certain pool of HSCs originates from YS precursors. Upon genetic labeling, induced at E7.5, Runx1^{+} YS cells were found in E10.5 circulating primitive erythroid (Ter119^{+}) and CD45^{+} lineages. Later, at E16.5, Runx1 positive cells were found among fetal (E16.5) erythro-myeloid and lymphoid (B and T) lineages, whereas the contribution to E12.5 YS VE-cadherin^{+} CD45^{−} Ter119^{−} endothelial cells was negligible. Moreover, the analysis of peripheral blood of 9-12 month old mice revealed the contribution of E7.5 induced Runx1^{+} YS cells to the

hematopoietic system of adult mice, proving their long term repopulating capacity (1-10%). In addition, when genetically labeled at E9.5, virtually all cells of every major blood cell lineage were present among labeled descendants of tagged embryonic cells. In sharp contrast, no embryonic or adult hematopoietic lineage was susceptible to genetic labeling induced at E6.5. Based on these data, the authors proposed that, by E9.5, the HSC lineage is fully committed and completely segregated from Runx1$^-$ mesodermal precursors, i.e. *de novo* generation of the adult HSC lineage is completed and thus, a new HSCs recruitment thereafter is unlikely. Hence, it is reasonable to assume, that the YS contributes to normal adult hematopoiesis (Samokhvalov et al. 2007).

Because the accurate assessment of the site of origin of hematopoietic cells is obscured by extreme mobility of blood cells upon development of cardiac function, Lux and his colleagues used Ncx1$^{-/-}$ mice that lack heartbeat but their hematopoiesis is intact to determine the role of blood circulation on distribution of hematopoietic precursors in developing embryos (Ncx1$^{-/-}$ embryos die by E11.5). Using this model, they showed, that while the number of primitive erythrocytes (EryP) and definitive hematopoietic progenitor cells (HPC) emerging from the YS is similar among Ncx1$^{+/-}$ and Ncx1$^{-/-}$ embryos, the PSp region of Ncx1$^{-/-}$ embryos completely lacked hematopoietic cells from E8.25-9.5, suggesting that EryP and definitive HPC that seed the liver are ultimately derived from the YS (Lux et al. 2008).

The lineage tracing data were further developed by Yosuke Tanaka from Samokhvalov's group in 2012. To deconvolute the origin of hematopoiesis they designed an embryo-rescue system in which *Runx1* can be reactivated in Runx1$^{-/-}$ concepti at desired developmental stages. In this system, only the reactivation of *Runx1* expression at E6.5-E7.5 led to the lethal phenotype rescue, suggesting the critical ontogenetic function of *Runx1* at this time point. Restoration of Runx1 function at E7.5 led to the full recovery of adult-type HSCs and entire hematopoiesis. Thus, these *in vivo* and *ex vivo* experiments provided compelling evidence that definitive hematopoiesis and adult type HSCs originate predominantly from the nascent extra-embryonic mesoderm and suggested that while the YS operates as a primary and sufficient source of adult type hematopoiesis, the AGM region is redundant for *de novo* blood generation and may represent a transitory niche for developing HSCs (Tanaka et al. 2012).

Similarly, several studies have documented the occurrence of YS-derived adult myeloid cells independent of AGM origin (Alliot et al. 1999; Ginhoux et al. 2010; Schulz et al. 2012). Moreover, LTML reconstitution capacity of AGM precursors is largely compromised if isolated from embryo <E10.5. This engraftment incompetence can be

regained by co-culturing them with AGM-derived stromal cells, what strongly attest to the importance of AGM environment in maturation of these hematopoietic precursors (Yoder et al. 1997; Cumano et al. 2001; Matsuoka et al. 2001). Surprisingly, it has been demonstrated that subjecting the YS-derived hematopoietic precursors from a precirculation embryo (≤E8.0) to the same co-culture system also endows them with LTML reconstitution capacity (Matsuoka et al. 2001). Given that embryonic blood circulation is gradually established from around E8.25 (McGrath et al. 2003), the cross-migration of hematopoietic precursors from the YS to AGM, where they mature to HSCs, cannot be ruled out (Cumano et al. 2001; Lux et al. 2008). Taken together these studies further support the notion that not only AGM, but also YS-derived precursors could display HSC potential and thus, at least a fraction of adult HSCs could be of YS origin (Matsuoka et al. 2001; Samokhvalov et al. 2007; Tanaka et al. 2012).

1.3. Myeloid cells in development and disease

1.3.1. The biology of myeloid cells

While there is probably a certain level of functional plasticity shared in all hematopoietic cells, there is no doubt that, except HSCs, myeloid cells are endowed with the highest level of plasticity (Galli et al. 2011). Adult type myeloid cells that represent the major leukocytes in the peripheral blood originate in the BM through the granulocyte-monocyte progenitor (GMP) (reviewed in (Iwasaki and Akashi 2007)).

Based on integrin β7 expression GMP can be divided into two fractions. While integrin β7 negative GMP give rise to monocytes, DCs, neutrophils and eosinophils, β7^{LOW} GMPs generate mast cell and basophil precursors. The developmental scheme describing the generation of adult type myeloid cells is shown in Figure 8.

Granulocytes (neutrophils, eosinophils and basophils) are the first cells to be recruited to the local sites upon pathogen invasion, providing an immediate immune response to infections (Kawamoto and Minato 2004).

Monocytes differentiate into macrophages in peripheral tissues, where they show unique, tissue specific functions, but they may also differentiate to dendritic cells (DCs) in lymphoid organs and Langerhans cells in skin as well. DCs are professional antigen-presenting cells that ultimately control immunity and tolerance and their complex biology is beyond the scope of this thesis (for review see (Ueno et al. 2007)).
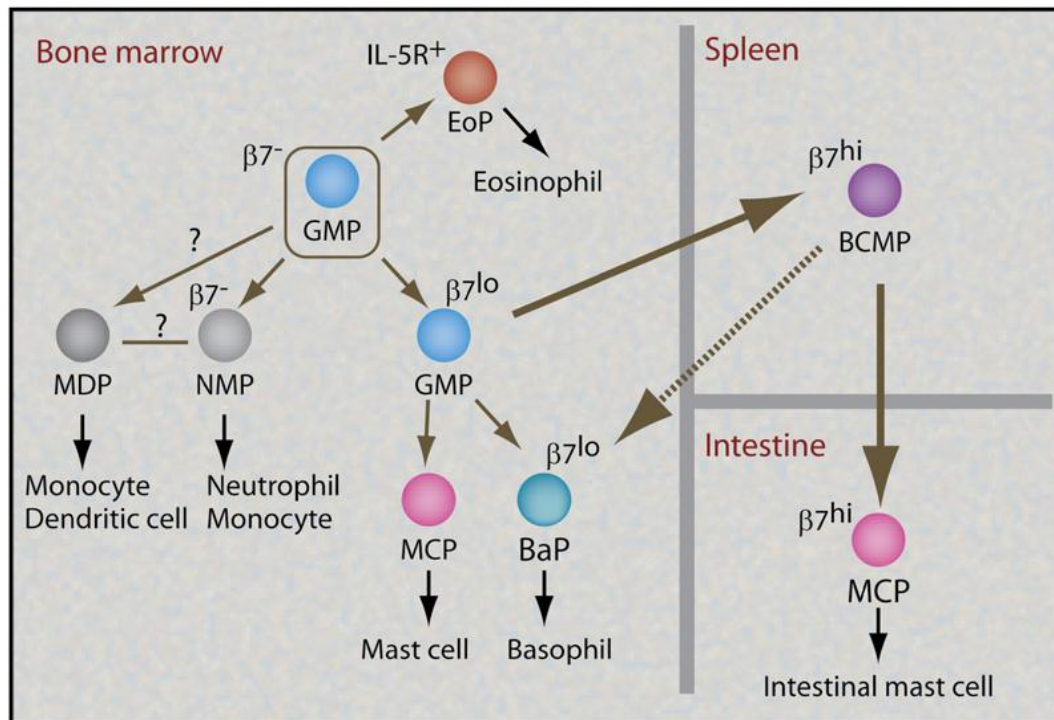
Figure 8. Developmental Pathways downstream of GMP (taken from (Iwasaki and Akashi 2007)).
Isolatable progenitors for each granulocyte lineage are shown. The GMP is divided into integrin $\beta7^-$ and $\beta7^{lo}$ populations. The latter is primed to the basophil and the mast-cell lineages: $\beta7^{lo}$ GMP presumably migrate into the spleen to become $\beta7^{hi}$ BMCP that give rise to $\beta7^{hi}$ intestinal MCP. $\beta7^{lo}$ GMP may also give rise to $\beta7^{lo}$ BaPs and $\beta7^{hi}$ MCP in the BM. $\beta7^-$ GMP differentiate into $\beta7^-$ EoP as well as MDP or putative NMP. The lineal relationships among these progenitor populations remain unclear. MCP, mast-cell progenitor; BaP, basophil progenitor; BMCP, basophil/mast-cell progenitor; EoP, eosinophil progenitor; NMP, neutrophil-monocyte progenitor; and MDP, macrophage-dendritic-cell progenitor.

1.3.2. Tissue-resident macrophages

During embryogenesis, macrophages are among the first hematopoietic cells to appear. Starting E9.5 in the mouse, they are already dispersed throughout the embryo to contribute to the tissue integrity maintenance. It is now widely accepted, that under a steady state, major tissue-resident macrophage populations, including microglia, Kupffer cells of the liver, lung alveolar, splenic, and peritoneal macrophages, are established prenatally either from the YS or AGM/FL hematopoiesis and in adults are replenished independently of the BM (Ginhoux et al. 2010; Yona et al. 2013). Under inflammatory conditions, however, resident macrophages can be transiently complemented by Ly6C+ monocytes recruited from the BM (Ajami et al. 2011; Leuschner et al. 2012). Interestingly, it has been recently shown that two major adult tissue resident macrophage populations established during embryogenesis that coexist during lifetime, i.e. YS derived (F4/80BRIGHT) and AGM/FL derived (F4/80LOW) fractions differ in their dependency on Myb transcription factor and have a distinct replenishment capacity. Notably, in contrast to F4/80LOW Myb-dependent macrophages, the YS derived Myb-independent F4/80BRIGHT lineage persists in adult mice independently of HSCs and cannot be continuously renewed from the BM (Schulz et al. 2012).

Originally described by Gordon and Hume, resident macrophages represent an incredible diverse set of cells employed in every aspect of organism's biology from development, homeostasis, repair and immune responses (Hume et al. 1984; Wynn et al. 2013). The individual expression profiles of macrophages resident to particular tissues overlap only marginally, suggesting that they represent many unique classes of macrophages equipped with a transcriptome tailored to the given tissue demands (Gautier et al. 2012). During development they are responsible for tissue patterning, including osteogenesis and branching morphogenesis (mammary gland, kidney and pancreas) (Rae et al. 2007; Pollard 2009; Stefater Iii et al. 2011). In the BM stem cell niche, macrophages modulate the dynamics of hematopoietic cell release (Chow et al. 2011). As professional phagocytes, macrophages are involved in tissue remodeling not only during embryogenesis, but also in adults. Adult-type erythropoiesis is dependent on macrophages surrounding enucleating erythroblasts that engulf excluded erythrocyte nuclei (Kawane et al. 2001). Macrophages also tightly regulate angiogenesis by secreting angiopoietic factors as well as instructing vascular endothelial cells to apoptosis when not placed properly (Rao et al. 2007). Microglia shape the brain architecture as they promote neuron viability, modulate neuron activity and prune synapses during development (Pollard 2009; Paolicelli et al. 2011; Li et al. 2012b). Moreover resident macrophages are involved in the metabolic homeostasis by facilitating metabolic adaptation to cold (adipose) or increased caloric uptake (liver) and modulating insulin resistance upon inflammatory insult (Odegaard et al. 2007; Nguyen et al. 2011; Samuel and Shulman 2012).

However the reparative and homeostatic functions of macrophages can be subverted by chronic insults, resulting in relatively common association of macrophages with disease states (Wynn et al. 2013). Although inflammatory macrophages are initially beneficial to the infected tissue, they also trigger collateral tissue damage. Moreover, if the control mechanism of immune response failed, macrophages can contribute to disease progression as seen in many chronic inflammatory or autoimmune conditions (Nathan and Ding 2010). Specifically, direct involvement of macrophages has been shown in atherosclerosis, asthma, inflammatory bowel disease, rheumatoid arthritis and diabetes (Marée et al. 2005; Kamada et al. 2008; Hansson and Hermansson 2011; Murray and Wynn 2011). In addition, macrophages have been shown to promote tumor initiation, progression and metastasis (Qian and Pollard 2010).

1.3.3. Granulocytes

Granulocytes are relatively short lived effector innate immune cells characterized by the presence of intracellular granules and segmented nucleus. In the absence of pro-survival factors, they die by apoptosis shortly after maturation (Geering et al. 2013). Based on their effector functions, granule content and appearance of histological staining, three types of granulocytes can be distinguished: neutrophils, eosinophils and basophils.

Neutrophils, the most abundant granulocytes in the blood, are equipped to kill pathogens in several ways. Most importantly they are capable to engulf smaller pathogens in the phagolysosomes and destroy them upon fusion with granules containing reactive oxygen species (ROS) generated by NADPH oxidase and myeloperoxidase together with proteolytic enzymes, cytotoxins (lysozyme) and antimicrobial peptides (defensins) (Borregaard et al. 2007). They are also able to release pro-inflammatory cytokines and pro-resolving mediators, modulate immune responses and generate neutrophil extracellular traps (NET) to capture extracellular pathogens (Brinkmann et al. 2004; Mantovani et al. 2011). Once neutrophils enter the bloodstream they are destined to rapidly die by apoptosis in the absence of exogenous signals. However their survival can be prolonged under inflammatory conditions (Summers et al. 2010). Anti-apoptotic signals can be delivered to neutrophils by PRRs. Specifically it has been demonstrated, that neutrophils express a wide spectrum of TLRs, and that their triggering leads to prolongation of cell lifespan (Francois et al. 2005). TLR signaling has been shown to have multiple effects in neutrophils, including cytokine production, ROS generation, receptor expression and phagocytosis (Hayashi et al. 2003).

Eosinophils are characterized by a bi-lobed nucleus with highly condensed chromatin and the presence of granules containing eosinophil peroxidase, eosinophil lysophospholipase and cationic proteins (Yousefi et al. 2012). They spend only a short time in the blood stream before they localize to the thymus, spleen, lymph nodes or gastro-intestinal tract where they home under physiological conditions. In response to inflammatory signals, eosinophils migrate to peripheral tissues where their survival is prolonged and they start to secrete their products into the surrounding tissue, thereby triggering local inflammation and tissue remodeling (Weller 1994; Gleich 2000). Although not being "professional" antigen presenting cells, eosinophils can process antigens, and stimulate T cells in an antigen specific manner (Wang et al. 2007). They are also able to shape T_H1/T_H2 T cell differentiation (Spencer et al. 2009). In comparison to neutrophils, eosinophils express fewer TLRs and their responsiveness has been so far demonstrated only to TLR2, TLR5 and TLR7 ligands. In eosinophils, TLR triggering can lead to the induction of adhesion molecules and pro-inflammatory cytokine expression as

well as ROS generation, suggesting that they can participate in the recognition and killing of pathogens (Wong et al. 2007). A tightly controlled degranulation (piecemeal degranulation) is a prominent eosinophil function, enabling the release of bactericidal cationic proteins in the extracellular space (Lehrer et al. 1989). Another bactericidal mechanism employed by eosinophils is the formation of eosinophil extracellular traps containing bactericidal granule proteins and mitochondrial DNA (Yousefi et al. 2008). However, the function of eosinophils in health and disease remains elusive. Although eosinophils are often found in some tissue pathologies (asthma, eosinophilic oesophagitis, helmint infections), whether and how they are involved in the onset or outcome of these diseases is largely unknown (Rosenberg et al. 2013).

Basophils represent the rarest population of granulocytes. Like eosinophils, they contain bi-lobular nucleus and basophilic granules. Their granules contain biologically active molecules as histamine and heparin. While they share many common features with mast cells (histamine, high affinity IgE receptor) they differ in lack of c-kit on their surface, their maturation pathway in the BM and shorter lifespan. Like eosinophils, basophils play a role in parasitic infections, allergies and induction of T_H2 responses (Min et al. 2012; Suurmond et al. 2014). They are usually found in tissues where allergic reactions occur and thus likely contribute to the severity of these reactions. Basophils also represent a substantial source of a T_H2 promoting cytokines IL-4 and IL-13, both of which are critical in the pathogenesis of allergies. However, it seems unlikely, that basophils serve as antigen presenting cells (Schroeder et al. 2001; Suurmond et al. 2014). Several reports have identified TLRs expressed in basophils, suggesting that specific ligands for these receptors play a role in modulating mediator release and cytokine secretion. While basophil viability or adhesion molecule induction is not influenced by TLR triggering (Komiya et al. 2006), TLR2/6 ligand, peptidoglycan, was shown to induce secretion of IL-4 and IL-13 from basophils although in lower levels than upon IgE/FcεRI cross-linking (Bieneman et al. 2005). Recently, the cytokine production upon TLR triggering has been observed for human TLR1-9). Moreover, TLR mediated basophil responses can enhance the IgE mediated degranulation. These findings suggest that basophils may function as accessory cells skewing naïve T cells, in the presence of APCs, towards T_H2 response (Suurmond et al. 2014).

1.3.4. Emergency myelopoieis

Upon pathogen invasion, myeloid cells migrate to local tissues employing navigation capability of their chemokine receptors and are primed for phagocytosis as well as secretion of inflammatory cytokines, thereby playing key roles in innate immunity.

Since myeloid cells represent the first line of defense against invading pathogens, there is no wonder that these cells are capable to rapidly mobilize from the BM upon acute infection. This process is commonly referred to as "emergency myelopoiesis". Accompanied by increased proliferation and differentiation of HSPCs in the BM induced by infection, myelopoiesis becomes the predominant form of cellular production on expense of the production of lymphoid and erythroid cells (Takizawa et al. 2012). It is generally accepted, that HSCs and HSPCs are induced to proliferate and differentiate by two distinct mechanisms. First, mature cells are depleted form the BM as they differentiate and are released to the periphery thereby exerting a "pull" signal on HSCs and progenitors. The second "push" signal is generated by cytokines and colony stimulating factors produced by differentiated cells of hematopoietic (e.g. tissue macrophages) or nonhematopoietic (e.g. endothelial cells) origin triggered by infection (King and Goodell 2011).

1.3.5. TLR mediated autophagy in myeloid cells

Recently, the list of processes, leading to eventual elimination of infection, triggered by TLRs has been broadened to include the induction of autophagy (Sanjuan et al. 2007; Delgado et al. 2008; Shi and Kehrl 2008). Autophagy is an evolutionary conserved survival mechanism enabling the recycling of cytoplasmic components during starvation. This process involves the formation of double membrane organelles, called autophagosomes to sequester portions of the cytosol including long-lived proteins and damaged organelles. Autophagosomes then fuse with lysosomes do degrade their contents (Mizushima et al. 2002; Levine and Deretic 2007).

Apart from its role in keeping cytoplasmic homeostasis during aging and development (Mizushima et al. 2002) the importance of autophagy in immunity becomes obvious (Levine and Deretic 2007; Lunemann and Munz 2008). Autophagy can not only contribute to intracellular pathogen elimination (Gutierrez et al. 2004; Nakagawa et al. 2004) but also contribute to MHCII-restricted endogenous antigen presentation (Dengjel et al. 2005; Paludan et al. 2005), immune cell survival (Pua and He 2007; Miller et al. 2008), T_H1/T_H2 polarization (Harris et al. 2007) and influence central tolerance (Nedjic et al. 2008). It has been shown that TLR (TLR3, TLR4, TLR7/8) triggering can induce autophagy in a mouse macrophage cell line RAW264.7. However, these studies suggested

that autophagy is largely a MyD88-independent process (Sanjuan et al. 2007; Xu et al. 2007; Delgado et al. 2008).

1.3.6. TLRs in immune disorders

The initiation of emergency myelopoiesis is critically dependent on the recognition of pathogen that is achieved by pattern recognition receptors including TLRs (Takizawa et al. 2012). However the potent immune response triggered by TLRs represents a potential risk when induced inappropriately. Several studies have already emphasized the significance of tight control of TLR signaling and its breaks in disease pathogenesis.

So far TLRs have been implicated in a plethora of inflammatory and autoimmune conditions including asthma, atherosclerosis, rheumatoid arthritis, multiple sclerosis, systemic lupus erythematosus and diabetes as well as tumor growth progression and metastasis (Pandey and Agrawal 2006; Kim et al. 2009). However, the evidence for the role of TLRs in development of some of these conditions is conflicting (Keogh and Parker 2011). First TLR targeting drugs are currently undergoing pre-clinical or early-clinical phase evaluations and the upcoming results of these studies will provide insight in the potential of their therapeutical use. Nevertheless further research is needed to elucidate the roles of TLRs in disease.

2. Thesis Aims

The main aims of the thesis were to

(i) reveal the expression pattern of TLRs during murine early embryonic development

(ii) identify the TLR expressing cells

(iii) test whether TLRs are functional during embryonic development

(iv) develop transgenic mouse models enabling the visualization and lineage tracing of cells with active *Tlr2* promoter

(v) identify differetially expressed proteins in detergent resistant microdomains of *Francisella tularensis* infected macrophages

(vi) reveal the source of myeloid α-defensins in peripheral blood of type 1 diabetes patients

3. Methods

3.1. Flow cytometry and cell sorting

Embryonic cell suspensions were prepared using dispase treatment. After Fc receptor blocking by rat anti-mouse CD16/32 antibody (2.4G2; Biolegend), single cell suspensions were stained with directly conjugated monoclonal antibodies. Fluorescence data were acquired using LSRII flow cytometer (BD Biosciences). Flow cytometry analyses were performed using FlowJo software (Tree Star). Cell debris and dead cells were excluded from the analysis based on scatter signals and Hoechst 33258 (Sigma-Aldrich) fluorescence. The intracellular staining procedure is described in section 4.4. Materials and Methods. Cell sorting was performed with the Influx cell sorter (BD Biosciences).

3.2. Gene expression analysis

Total RNA was isolated using the RNeasy Plus Micro Kit (Qiagen) and reverse transcribed using Premium RevertAid (Fermentas) and random hexamers (Fermentas). Quantitative RT-PCR (qRT-PCR) was performed using the LightCycler 480 SYBR Green I Master mix on a LigthCycler 480 (Roche). Each sample was tested in triplicate. The relative gene expression was calculated using LightCycler 480 1.5 software and normalized to a housekeeping gene mRNA level. Primers were designed using UPL software (Roche). Intron-spanning primers were used whenever possible. Primer efficiencies were calculated using LightCycler 480 1.5 software. Data were analyzed using Prism 5.03 software (GraphPad). Microarrays were performed using MouseWG-6 v1 and MouseWG-6 v2 Expression BeadChips (Illumina) as specified in section 4.3. Materials and Methods.

3.3. *In vitro* assays

Following *in vitro* assays were used in this study:

Differentiation of embryonic hematopoietic cells on OP-9 stroma (see section 4.1.3.6.)

Proliferation of embryonic hematopoietic cells on OP-9 stroma (see section 4.1.3.6.)

Colony forming cell assay (see section 4.1.3.7.)

Phagocytosis assay (see section 4.3. Materials and Methods)

Infection Assay: Synchronized Phagocytosis (see section 4.4. Materials and Methods)

Cholesterol Depletion and Survival Test (see section 4.4. Materials and Methods)

3.4. Cytokine antibody array, ELISA

Changes in cytokine secretion were assessed using semiquantitative Mouse Cytokine Antibody Array G3 according to the manufacturer's instructions (RayBiotech). Levels of TNF-α in supernatants were assessed using mouse TNFα ELISA Ready-SET-Go! kit (eBioscience). The serum levels of DEFA1-3 were measured using an ELISA kit (Hycult Biotech) in accordance with the supplier's recommendation. Each sample was tested in triplicate.

3.5. Determination of intracellular calcein-AM chelatable iron level

Intracellular iron levels were measured using the fluorescent probe calcein-AM as specified in section 4.3. Materials and Methods.

3.6. Immunohistochemistry and imaging

Immunohistochemistry was performed as specified in section 4.1.3.8. Confocal microscopy images were acquired using Leica SP5 equipped with HCX PL APO 63.0 × 1.40 Oil UV objective. Whole mount immunohistochemistry was performed as specified in section 4.1.3.8. Signals were visualized and digital images were obtained by using a Zeiss LSM 780 equipped with two photon, argon and helium–neon lasers. For 3D image, individual confocal planes (25-30 planes in 1-2 μm intervals) were projected to generate a single stacked 3D-reconstructed image using Imaris 7.3 (Bitplane).

3.7. Quantitative image analyses

Images were acquired with Olympus Scan[R] Screening Station for Life Science equipped with LUCPLFLN 20× PH objective. The data were analyzed by Scan[R] Analysis 1.3.0.3 software (Olympus Imaging Solutions GmbH). Dead cells and debris were excluded from the analysis based on DAPI intensity value.

3.8. BAC cloning

(for details see section 4.2.2.)

For cloning, restriction analyses, PCR verifying or transformation of electro-competent bacteria BAC DNA was isolated by alkaline lysis followed by phenol-chloroform extraction. Verified BACs were electroporated to EL250 bacteria equipped with the recombination machinery. The cassette was electroporated do BAC containing EL250 bacteria and the recombination was induced by a heat shock. The neomycin cassette flanked by Frt sites was excluded by flipase. Upon validation performed by diagnostic restriction enzyme digest and sequencing, the BAC construct was electroporated to DH10B strain, and isolated by Qiagen® Large-Construct Kit. The quality of obtained BAC DNA was analyzed by Pulse Field Gel Electrophoresis and the sequence was validated by PCR followed by sequencing. BAC DNA was diluted to 1 ng/μl in injection buffer (10mM Tris HCl, pH 7.0, 100 μM EDTA) and the pronuclear injection (PNI) was carried out at the Transgenic Unit of IMG.

3.9. Tamoxifen administration

2 mg of tamoxifen (T5648, Sigma) was diluted in ethanol and sunflower oil and administered to pregnant dams by oral gavage. For details see section 4.2.2.)

3.10. Proteomic analyses

SILAC labeling of J774.2 macrophages was performed as specified in section 4.4. Materials and Methods. Following SILAC labeling, DRMs were isolated as described in section 4.4. Materials and Methods. 2D Liquid Chromatography of triptic peptides was performed as described in section 4.4. Materials and Methods. The mass spectrometric analysis was performed on a 4800 MALDI TOF/ TOF Analyzer (AB Sciex) as described in section 4.4. Materials and Methods. Data acquisition and processing were carried out using 4000 Series Explorer software v3.5 (AB Sciex). Protein identification and quantification was conducted using ProteinPilot software v2.0.1 (AB Sciex) equipped with a Paragon searching algorithm, Pro Group algorithm (AB Sciex) and a PSPEP script that permits false discovery rate estimation as described in section 4.4. Materials and Methods.

3.11. Small hairpin RNA (shRNA) treatment

The J774.2 macrophages were spin-infected with p62-shRNA or control shRNA encoding lentiviral particles produced in HEK293T cells. 72 hours after lentiviral transduction, the J774.2 cells were either subjected to puromycin selection for 2 weeks or used directly for bacterial infection experiments.

3.12. Western blot

Samples were boiled in sample loading buffer for 10 min, loaded into 16% Tricine-SDS-Urea-PAGE gel and run under reducing conditions (see section 4.5. of Materials and Methods). Resolved proteins were transferred onto 0.2 µm PVDF membrane (Biorad), blocked in 3% BSA, incubated with specific Ab and detected with secondary anti-mouse HRP-labeled antibodies. GAPDH housekeeping protein was used as a loading control. The reaction was visualized by the West Dura ECL system (Pierce/Thermo Scientific).

3.13. May-Grünwald-Giemsa (MGG) staining

Sorted cells were stained according to MGG staining protocol (Penta). Leica DMI6000 microscope was used for bright field imaging.

3.14. Statistical analysis

Statistical analyses were applied to the data and used statistical methods are indicated in each respective Figure or particular "Materials and Methods" section. Statistical analysis calculations were performed using the GraphPad Prism software http://www.graphpad.com.

4. Results and Discussion

4.1. Toll-like receptor 2 tracks the emergence of earliest erythro-myeloid progenitors in precirculation embryo

In this study we show that TLRs are expressed during early embryonic development. We determined that the source of TLR expression are maternal cells invading embryonic tissues as well as embryo-derived cells. We described a population of early postgastrulation embryonic hematopoietic progenitors that express TLR2 and posses a myelo-erythroid differentiation potential. TLR2 triggering enhanced the proliferation rate as well as myeloid differentiation of these hematopoietic precursors in a MyD88-dependent manner. TLR2$^+$ progenitors appeared in the embryo as early as at E6.5 and at E7.5 localized mainly to the extra-embryonic yolk sac. We conclude that expression of TLR2 marks the emergence of common embryonic hematopoietic progenitors of early erythro-myeloid lineages and endows them with the capacity to boost the production of myeloid cells.

The manuscript has been submitted to the Genes and Development journal and is currently in revision.

Toll-like receptor 2 tracks the emergence of earliest erythro-myeloid progenitors in precirculation embryo

Jana Balounová[1,3], Tereza Vavrochová[1,3], Martina Benešová[1], Meritxell Alberich-Jordà[2], Andrea Jurisicova[4], Hoon-ki Sung[4] and Dominik Filipp[1]

[1]Laboratory of Immunobiology, Institute of Molecular Genetics AS CR, Prague, Czech Republic
[2]Laboratory of Molecular Immunobiology, Institute of Molecular Genetics AS CR, Prague, Czech Republic
[3]Department of Cell Biology, Faculty of Science, Charles University in Prague, Prague, Czech Republic
[4]Samuel Lunenfeld Research Institute, Mount Sinai Hospital, Toronto, Ontario, Canada

4.1.1.Abstract

The discovery of mammalian Toll-like receptors (TLRs) unearthed the fundamental mechanisms that govern immunity to pathogens. Nevertheless, the biology of TLRs during embryonic development has been overlooked. Here, we show that all TLRs are expressed during early embryogenesis. Using a transgenic model to trace cells of embryonic origin, we provide evidence that hematopoietic precursors expressing TLR2 preferentially differentiate into myeloid lineage cells *in vivo* and *in vitro*, and TLR2 triggering enhances their proliferation rate as well as myeloid differentiation in MyD88-dependent manner. In the presence of erythropoietin, TLR2+ precursors display the capacity to mature into primitive erythroid cells. The appearance of TLR2+ precursors in pre/early primitive streak embryo at E6.5 coincides with the onset of gastrulation, and these cells persist in both the yolk sac (YS) and the embryo proper before the establishment of circulation. However, only a subset of YS-derived TLR2+ckit+ progenitors coexpresses CD41, CD150 and Runx1, markers of primitive as well as definitive hematopoiesis. Taken together, the expression of TLR2 marks the emergence of common embryonic hematopoietic progenitors of early erythro-myeloid lineages and endows them with the capacity to boost the production of myeloid cells.

4.1.2. Introduction

Despite extensive research, the understanding of the origin and developmental path of hematopoietic cells in an embryo is still incomplete (Ueno and Weissman 2007; Medvinsky et al. 2011). Conventionally, two main hematopoietic sites are considered in the developing embryo: the yolk sac and aorta gonad mesonephros region. The YS formation is at around E6.5-7.5 initiated by the association of extra-embryonic visceral endoderm and an inner layer of extra-embryonic mesoderm derived from the posterior primitive streak, which is formed shortly after the onset of gastrulation (E6.25-6.5) (Smith et al. 1994; Palis and Yoder 2001; McGrath and Palis 2005; Palis 2006). Later, cells ingressing from middle and anterior streak regions form an intra-embryonic mesoderm that gives rise to an additional hematopoietic site, the para-aortic splanchnopleura which later develops to the AGM (Tam and Beddington 1987; Kinder et al. 1999).

The first hematopoietic cells emerge from the hemangioblast precursors in the forming YS around E7.25 (Moore and Metcalf 1970; Shalaby et al. 1997; Choi et al. 1998; Palis et al. 1999; Palis and Yoder 2001; Huber et al. 2004). It is believed that these differentiated cells, including primitive erythrocytes, macrophages and megakaryocytes, surrounded by a layer of endothelial cells and thus forming a cluster of cells called the blood island, provide only a transient and lineage-limited supply of hematopoietic progenitors (Palis et al. 1999; Xu et al. 2001). The first *bona fide* hematopoietic stem cells develop independently in AGM at around E10.5 (Muller et al. 1994; Dzierzak and Medvinsky 1995; Medvinsky and Dzierzak 1996; Cumano et al. 2001). In addition, it has been recently shown that other developing hematopoietic tissues such as the chorion, allantois, placenta as well as vitelline and umbilical arteries can provide niche for an independent development of HSCs (de Bruijn et al. 2000; Zeigler et al. 2006; Rhodes et al. 2008).

The yolk sac is the first embryonic tissue where macrophages appear during early ontogenesis. However, due to a limited number of molecular and cellular markers, the original studies were unable to make any assertion of their differentiation pathway. Recently, three different myeloid cell populations have been shown to successively populate the mouse YS region. The first population is of maternal origin and displays a mature ckit$^-$ CD45$^+$ phenotype, while the other two develop from ckit$^+$ CD45$^-$ embryonic progenitors with macrophage and then erythro-myeloid differentiation potential (Bertrand et al. 2005b). Accumulated data also provided evidence that YS-derived myeloid precursors represent a specific lineage of cells capable of differentiating into adult tissue resident macrophages independently of HSCs (Alliot et al. 1999; Ginhoux et

al. 2010; Schulz et al. 2012). What remains uncertain is the nature of the immediate precursors of embryonic macrophage populations and their pathway of differentiation.

Toll-like receptors (TLRs) recognize conserved microbial structures and are critically important for triggering immune responses to infections. In addition, the interaction of TLRs with their ligands also initiates several distinct signaling pathways that lead to the regulated development of antigen-specific immunity (reviewed in (Akira et al. 2001; Medzhitov 2007). Adult HSCs have been shown to express TLRs, allowing them to directly sense the presence of infections (Nagai et al. 2006; Sioud et al. 2006; De Luca et al. 2009). Notably, while TLR-independent BM hematopoiesis is driven by a combination of endogenous cytokines and growth factors (Ueda et al. 2005) , TLR stimulation can nudge this process towards increased production of myeloid cells (Nagai et al. 2006; Sioud et al. 2006; Boiko and Borghesi 2011). This serves as an important back-up mechanism when the rapid replenishment of short-lived myeloid cells is crucial for the maintenance of adult immune homeostasis (Holl and Kelsoe 2006; Welner and Kincade 2007). So far, the biology of TLRs during early mammalian embryonic development has been overlooked and only a few studies have provided a limited set of data related to the expression levels of selected TLRs in developing murine placenta, lung, liver and brain starting from E10.0-13.0 (Harju et al. 2001; Kaul et al. 2012). Arguably, due to the absence of distinguishable developmental phenotype in all the murine TLR knockouts, it seems that their defects are solely immune related. Thus, whether TLRs are expressed and how can TLR signaling affect the development of hematopoietic lineages and/or their maturation in an early embryo (E6.5-10.5), was the main objective of this study.

Here, we investigated not only the expression of TLRs in early embryonic hematopoietic precursors but also their capacity to employ TLR signaling to regulate embryonic hematopoiesis during an infectious assault. We demonstrated that a full complement of TLRs and their adaptor proteins are expressed during early embryogenesis. Using a transgenic model that allowed us to distinguish between cells of maternal and embryonic origin, we provided phenotypic and functional evidence that TLR2+ cells represent the earliest precursors of embryonic myelo- and erythropoiesis and that their engagement of TLR2 receptor is functionally coupled to the enhanced production of embryonic myeloid cells.

4.1.3. Materials and Methods

4.1.3.1. Mice

CD1 and C57Bl/6J mice were maintained in the animal facility of the Institute of Molecular Genetics in Prague. pCAGEGFPMos3 mice expressing EGFP under the control of the β-actin promoter, here referred to as TgEGFP mice were obtained from Petr Svoboda (Nejepinska et al. 2012). MyD88$^{-/-}$ mice (B6.129P2(SJL)-*Myd88$^{tm1.1Defr}$*/J), derived from MyD88^{fl} mice (Hou et al. 2008), were obtained from The Jackson Laboratory. All experiments were approved by the ethical committee of the IMG.

4.1.3.2. Cell suspension preparation

Time pregnant females (the day that the vaginal plug was observed was designated as E0.5) were sacrificed by cervical dislocation and embryos from different stages of development were dissected from uteri. E6.5-8.5 embryos were carefully stripped of maternal decidua, Reichart's membrane and the ectoplacental cone and were maintained intact, unless indicated otherwise. For FACS and mRNA analyses, cells from E7.5-E8.5 dissected embryos were pooled from one litter. For the assessment of gene expression shown in Figure 1, later stage embryos, E9.5-12.5, were separated from extra-embryonic membranes (YS and amnion) and single embryos were analyzed. Due to their small size, for FACS analyses of E6.5 embryos, several litters were pooled. For cell sorting experiments, E6.5, 7.5, or E8.5 embryos from several litters were pooled as well. Embryos were washed in phosphate buffered saline (PBS) and dissociated using 1 mg/ml dispase (Invitrogen) in PBS for 10 min at 37 °C with occasional gentle pipetting. The reaction was stopped by the addition of 1% fetal calf serum (FCS) and a subsequent wash in 1% FCS in PBS. Embryonic suspensions were then passed through a 50μm cell strainer.

4.1.3.3. Flow cytometry and cell sorting

After Fc receptor blocking by rat anti mouse CD16/32 antibody (2.4G2; Biolegend) single cell suspensions were stained with the following directly conjugated monoclonal antibodies: anti-CD11b-PE (M1/70; eBioscience), anti-CD31-APC (MEC13.3; Biolegend), anti-CD41-APC (MWReg30; eBioscience), anti-CD45-PerCP (30-F11; BD PharMingen), anti-CD93- PECy7 (AA4.1; eBioscience), anti-CD144-A647 (VECD1; Biolegend), anti-CD150-PECy7 (TC15-12F12.2; Biolegend), anti-B220-A647 (RA3-6B2; Biolegend), anti-ckit-PE (ACK2; eBioscience), anti-F4/80-PECy7 (BM8; eBioscience), anti-Gr1-A647 (RB6-8C5; Biolegend), anti-Ter119-PECy7 (TER-119; Biolegend), anti-Sca1-PerCP (D7; Biolegend) and anti-mouse Lineage Cocktail-Pacific Blue (Biolegend). Biotin conjugated anti-TLR2 antibody (6C2; eBioscience) was detected with streptavidin (SA)-APC or SA-PECy7 (eBioscience). Fluorescence data were acquired using LSRII flow cytometer (BD

Biosciences). Flow cytometry analyses were performed using FlowJo software (Tree Star). Cell debris and dead cells were excluded from the analysis based on scatter signals and Hoechst 33258 (Sigma-Aldrich) fluorescence. Cell sorting was performed with the Influx cell sorter (BD Biosciences).

4.1.3.4. Gene expression analysis

Total RNA from whole embryos or sorted cells was isolated using a RNeasy Plus Micro Kit (Qiagen) and was reverse transcribed using Premium RevertAid (Fermentas) and random hexamers (Fermentas). Quantitative RT-PCR (qRT-PCR) was performed using the LightCycler 480 SYBR Green I Master mix on a LigthCycler 480 (Roche). Each sample was tested in triplicate. The relative amounts of mRNA were calculated using LightCycler 480 1.5 software with Casc3 mRNA levels as the control. Primers were designed using UPL software (Roche). Intron-spanning primers were used whenever possible. Primer efficiencies were calculated using LightCycler 480 1.5 software. Primer sequences are listed in Table S1. Data were analyzed using Prism 5.03 software (GraphPad). The expression level of different TLRs and their adaptors highlighted in Figure 1 precluded the effect of primer efficiency factor.

4.1.3.5. Tracking cells of maternal and embryonic origin

To follow the cells of embryonic origin, we crossed the wild type (wt) CD1 females with heterozygous TgEGFP males. Only EGFP+ embryos were included in subsequent analysis. Due to paternal inheritance, all EGFP+ cells were considered to be of embryonic origin (Fig. S1A). To follow maternal cells, heterozygous TgEGFP females were crossed with wt CD1 males. Maternally derived EGFP-expressing cells were evaluated in wt embryos that did not inherit the maternal EGFP allele (~50%) (Fig. S1B).

4.1.3.6. *In vitro* assays

Distinct subpopulations of E6.5, E7.5 or E8.5 embryonic EGFP+ cells were sorted based on their TLR2, ckit and CD45 surface expression, plated on a semi-confluent layer of OP-9 cells (gift from J.C. Zuniga-Pflucker) and cultured in RPMI containing 10% FCS (Sigma-Aldrich). E6.5 and E7.5 sorted cells were supplemented with recombinant cytokines IL-3 (1 ng/ml), SCF (50 ng/ml) GM-CSF (3 ng/ml) and M-CSF (10 ng/ml) (Biolegend). A thousand cells from each E8.5 sorted EGFP+ population were co-cultured with OP-9 cells in the presence or absence of Pam3CSK4 (Invivogen) for 72 hours. Total numbers of surviving EGFP+ cells were normalized to 10000 events obtained by FACS analysis. The proliferation history of EGFP+ TLR2+ cells was determined by the dilution of Cell Proliferation Dye eFluor 670 (eBioscience) according to manufacturer's instructions.

4.1.3.7. Colony forming cell assay

Sorted E7.5 cells were plated in methylcellulose medium M3434 (Stem Cell Technologies) according to manufacturer's instructions. Cultures were maintained at 37 °C in humidified air with 5% CO_2. Hematopoietic colonies were counted at day 2-3 and harvested at day 10 for FACS analysis. Microscopic images were acquired using Nikon Diaphot 300 equipped with 10x/0.25 or Plan 20x/0.4 objectives.

4.1.3.8. Whole mount embryo immunohistochemistry and imaging

E7.5 embryos were dissected from decidua washed several times in ice cold PBS, fixed overnight in PHEM fixative (80 mM PIPES, 5 mM EGTA, 1 mM $MgCl_2$, 25 mM HEPES at pH of 7.2, 3.7% formaldehyde, purified 0.1% Triton X-100) at 4°C and then rinsed three times in PBS. Embryos were blocked in PBS supplemented with 10% of goat serum for 1h. The primary antibody, purified rat anti-mouse TLR2 (clone 6C2, eBioscience) was added to a final concentration of 5 µg/ml for overnight at 4°C and developed with the secondary goat anti-rat IgG labeled with Alexa 488. The isotype control antibody produced no specific staining (data not shown). Embryos were then embedded with Vectashield mounting medium with 4',6-diamino-2-phentlindole (DAPI) (Vector Laboratories) and prepared for scanning. Signals were visualized and digital images were obtained by using a Zeiss LSM 780 equipped with two photon, argon and helium–neon lasers. For 3D images, individual confocal planes (25-30 planes in 1-2 µm intervals) were projected to generate a single stacked 3D-reconstructed image using Imaris 7.3 (Bitplane).

4.1.4. Results

4.1.4.1. Tlr and Tlr adaptor mRNAs are expressed in early stages of mouse embryonic development

Twelve functional *Tlrs* and five *Tlr* adaptor proteins, namely *MyD88, Mal, Trif, Tram* and *Sarm1*, have been described in the mouse (Dunne and O'Neill 2003; Kawai and Akira 2010). To obtain an overall picture of *Tlr* and *Tlr* adaptor protein expression during mouse early embryonic development from E7.5 to E12.5, we first determined their expression in whole embryos isolated as described in the Materials and Methods. We observed two distinguishable trends in the kinetics of expression patterns. Despite some subtle variations, *Tlr1, Tlr4, Tlr5, Tlr6, Tlr11, Tlr12, Mal* and *Sarm1* expression showed a gradual increase during embryonic development, with *Tlr1, Tlr6* and *Mal* expression slightly diminished at day E12.5 and *Tlr11* displaying a unique pattern (Fig. 1A). In contrast, *Tlr2, Tlr3, Tlr7, Tlr8, Tlr9, Tlr13, MyD88, Trif* and *Tram* showed a convex-like expression profile, with a substantial decline at E9.5 (Fig. 1B). These data revealed expression profiles of genes postulated to play an essential role in innate immunity and suggested their involvement in immune and/or non-immune homeostatic processes during early embryonic development.
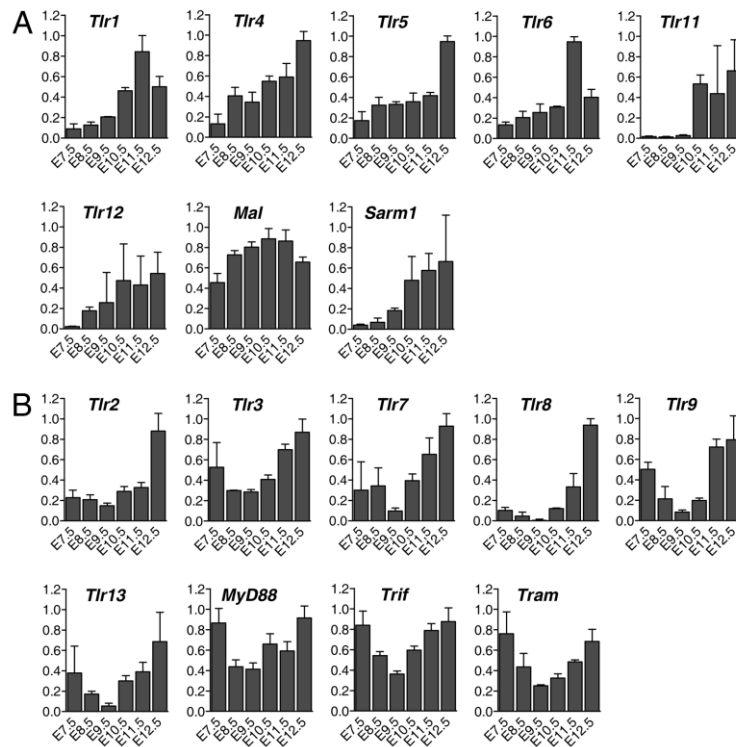
Figure 1. Tlr and Tlr adaptor mRNA expression during murine early embryonic development.
Expression levels of Tlrs and Tlr adaptor proteins genes were quantified by qRT-PCR in isolated embryos in different stages of murine embryonic development (E7.5-E12.5). The observed signal was normalized to Casc3 mRNA levels. For each gene, the highest level of expression was set to an arbitrary value "1". The kinetics of expression profiles of individual Tlrs and Tlr adaptor proteins were classified either as increasing (A) or convex (B). Error bars represent mean ± SD (n=3).

4.1.4.2. Myeloid TLR2+ CD11b+ cells appear in the embryo before E10.5

The early embryonic expression of *Tlr* genes strongly suggested that these receptors could be used to track the origin and developmental stages of embryonic hematopoiesis. Due to the commercial availability of specific antibodies, we analyzed surface expression of TLR2, along with other well-established hematopoietic and myeloid markers, at different stages of embryonic development. Notably, we detected the coexpression of CD11b on TLR2+ cells at as early as E7.5 (Fig. 2A). At this developmental time point, TLR2+ CD11b+ cells represented approximately 0.5% of total embryonic cells. Their frequency then dropped to 0.15-0.18% at E8.5-E9.5 and rose again to almost 1% at E10.5. Moreover, as illustrated in Figure 2, E7.5 TLR2+ cells were TLR2^{LOW} CD11b^{HIGH} and F4/80$^{-/LOW}$, whereas E10.5 TLR2+ cells were predominantly TLR2^{HIGH} CD11b^{LOW} and F4/80+. We hypothesized that these changes in the cellularity and phenotype of TLR2+ cells reflected developmentally regulated processes that were associated with the rapid turnover of distinct phagocyte populations during early embryonic development.
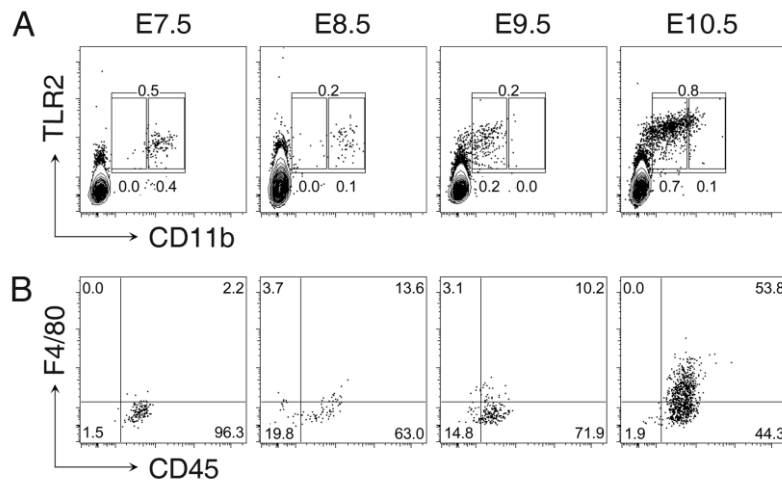
Figure 2. Early appearance of TLR2$^+$ CD11b$^+$ cells during mouse embryonic development.
Embryos at different stages of development (E7.5-E10.5) were dissociated and single cell suspensions were stained for TLR2, CD11b, CD45 and F4/80 and analyzed by FACS. (A) Surface expression of TLR2 and CD11b. Cell subsets with the low and high expression of CD11b are distinguished by separate gates. (B) Surface expression of CD45 and F4/80, gated on the entire TLR2$^+$ CD11b$^+$ subset. Representative data from at least three independent experiments are shown.

4.1.4.3. Maternal TLR2$^+$ CD11b$^+$ cells were replaced by embryonic TLR2$^+$ CD11b$^+$ cells during early embryonic development

The differences in the level of TLR2, CD11b and F4/80 positivity prompted us to search for the source of TLR2$^+$ cells in the embryo. We employed a transgenic mouse model suitable for the tracking of cells of maternal or embryonic origin (Fig. S1). These experiments revealed the existence of two different cell populations expressing the surface marker TLR2 at the early embryonic development (E7.5-8.5). As illustrated in Figure S1B, the first TLR2$^+$ population represented maternal CD11b^{HIGH} CD45$^+$ cells that appeared early (E7.5), diminished gradually, and was barely detectable at E10.5. The other TLR2$^+$ population was of embryonic origin and at E7.5 was devoid of hematopoietic markers such as CD45, CD11b (Fig. S1A). However, the expression of these markers gradually increased starting at E8.5. Together, these data demonstrated that the presence of maternal macrophages was of a transient nature and that at ~E8.5-9.5 these cells were gradually replaced by embryo-derived macrophages.

4.1.4.4. Embryonic TLR2+ progenitor cells differentiated to TLR2+ CD45+ myeloid cells at E9.75-10.5

The presence of TLR2 positive, but otherwise lineage negative (CD3−, Gr-1−, CD11b−, B220− and Ter119−) cells (Fig. S2) within E7.5 embryos suggested that this population could represent early progenitors that posses the potential for lineage commitment. Using an approach for tracking EGFP+ cells of embryonic origin (Fig. S1A), we gated on either TLR2+ or TLR2− cells (Fig. 3A) and analyzed their ckit and CD45 expression using a previously described labeling scheme (Bertrand et al. 2005b). As illustrated in Figure 3A, top panels, there were two phenotypically distinguishable stages during the specification of TLR2+ subset towards CD45+ hematopoietic lineage: (i) at E9.75, TLR2+ ckit+ CD45− cells acquired the surface expression of CD45, and (ii) the subsequent loss of ckit expression limited to the E9.75-10.5 time window of development. In this context, the prior accumulation of high levels of *Cd45* mRNA at E7.5-9.5 strongly correlated with the capacity of these cells to undergo the developmental transition from TLR2+ ckit+ CD45− to TLR2+ ckit+ CD45+ subset (Fig. 3B). In contrast, a subset of TLR2− ckit+ cells, which remained CD45 negative between E7.5-10.5, failed to commit to the CD45+ hematopoietic developmental path (Fig. 3A, bottom right panels). These findings suggested that only TLR2+ ckit+ and not TLR2− ckit+ progenitor cells were endowed with the capacity to gain CD45 expression *in vivo*.

The distinct developmental fate of the TLR2+ ckit+ and TLR2− ckit+ subsets correlated with their differential expression of relevant endothelial, hematopoietic and myeloid markers. To quantify these markers, we chose to look at embryonic cells isolated from E8.5, when the difference in *Cd45* mRNA expression between TLR2+ and TLR2− subsets had reached its maximum (~110 fold) (Fig. 3B). As the TLR2+ ckit+ CD45+ stage represented a developmental progression towards myeloid specification, the gene expression levels of this TLR2+ subset served as a positive control for myeloid markers. All expression levels were normalized to the TLR2− ckit− CD45− population. As illustrated in Figure 3C, TLR2+ ckit+ cells showed considerable expression of early endothelial/hematopoietic markers and transcription factors expressed in hemogenic endothelium (*Flk1*, *Tie2*, *Cd31*, *Cd34*, *Cd41*, *Cd93*, *Cd105*, *Cd144*, *Cd150*, *Gata1*, *Gata2* and *Lmo2*), as well as myeloid markers (*Csf1R*, *Cd11b*, *Mpo*, *Tlr4*, *Tlr9* and *MyD88*). As expected, during their maturation to the CD45+ stage, these cells tended to increase expression of myeloid markers while downregulating markers typically associated with transition from the hemangioblast to hemogenic endothelium and to early hematopoietic cells. Thus, due to its expression of both endothelial and hematopoietic markers (Huber et al. 2004) the TLR2+ ckit+ population could represent the hemogenic progenitor cells that, upon entry into the YS, display an early commitment to hematopoietic fate during normal mouse ontogeny.
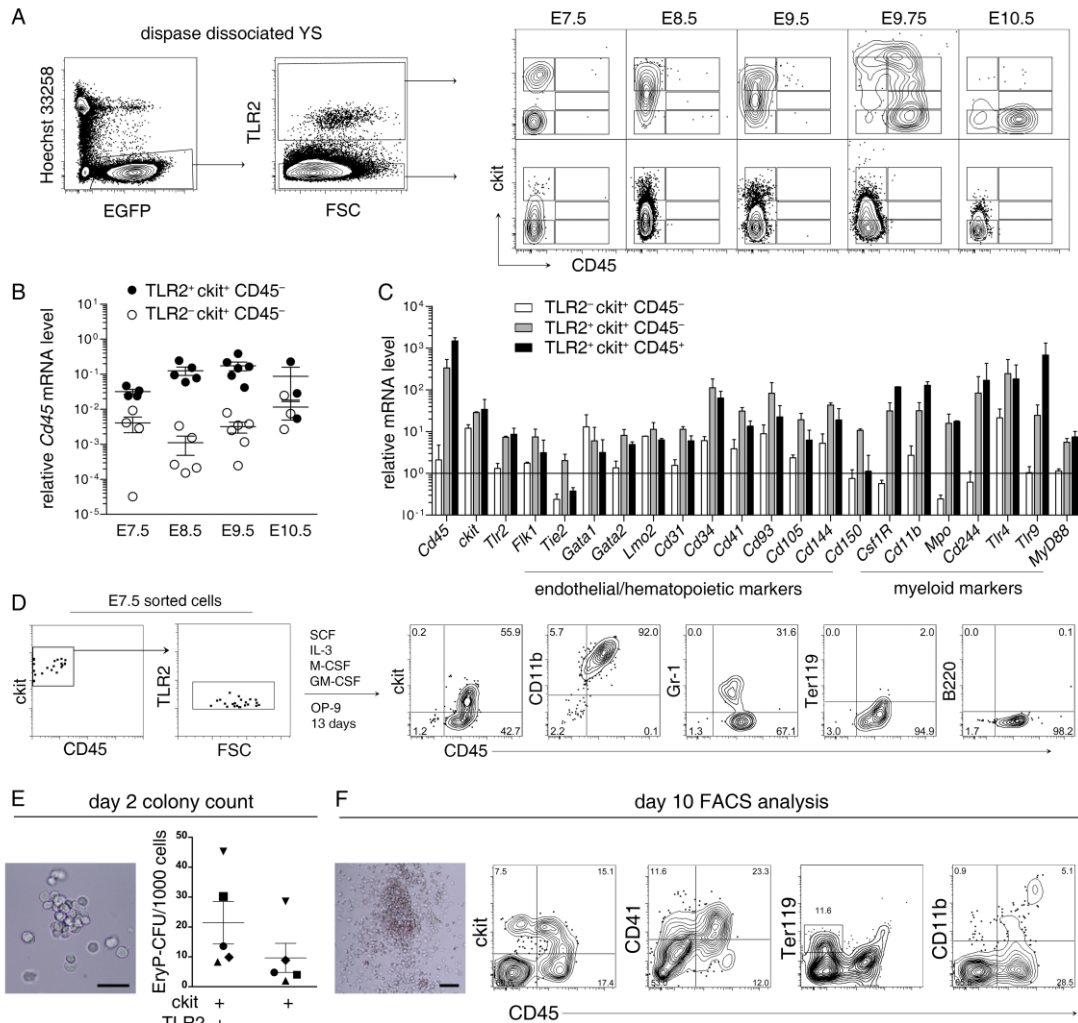
Figure 3. Embryonic TLR2+ progenitor cells differentiate to TLR2+ CD45+ myeloid cells in vivo and in vitro.

(A-F) Wt females were crossed with TgEGFP males to discriminate EGFP+ embryonic cells.

(A) Live EGFP+ cells of either the TLR2+ or TLR2− phenotype isolated from the YS were analyzed for expression of ckit and CD45 during different stages of development (E7.5- E10.5) using FACS. (B) Cd45 mRNA expression in embryonic TLR2+ ckit+ CD45− cells and TLR2− ckit+ CD45− cells during different stages of development (E7.5-E10.5). Data are representative of 3-5 independent experiments (mean ± SEM). (C) mRNA expression of endothelial/hematopoietic progenitor- and macrophage-associated genes was analyzed in sorted E8.5 embryonic cells and normalized to the levels in the TLR2− ckit− CD45− population, which served as a negative control. Error bars represent mean ± SD (n=3). (D) E7.5 EGFP+ TLR2+ ckit+ CD45− cells were sorted (two left panels), grown on OP-9 stromal cells in the presence of myeloid cytokine cocktail for 13 days and analyzed by FACS. (E, F) E7.5 TLR2+ ckit+ CD45− and E7.5 TLR2− ckit+ CD45− cells were sorted and plated in methylcellulose medium M3434 (Stem Cell Technologies) according to manufacturer's instructions. (E) Hematopoietic colonies were counted at day 2-3 (left panel; 20x magnification; scale bar 50µm) and harvested at day 10 for FACS analysis (right panel; 10x magnification; scale bar 100µm). Microscopic images were acquired using Diaphot 300 equipped with 10x/0.25 or Plan 20x/0.4 objectives. Representative data from three independent experiments are shown.

4.1.4.5. TLR2$^+$ ckit$^+$ CD45$^-$ progenitors differentiated into TLR2$^+$ ckit$^-$ CD45$^+$ cells *in vitro*

To directly follow the fate of TLR2$^+$ ckit$^+$ progenitors, their hematopoietic potential was assessed *in vitro*. Using crosses between wild-type females (CD1 strain) and TgEGFP males (Fig. S1A), we sorted TLR2$^+$ ckit$^+$ cells from E7.5 embryos (Fig. 3D, left panels) and cultured them on a monolayer of OP-9 stromal cells in the presence of a myeloid differentiation cocktail containing SCF, IL-3, M-CSF and GM-CSF. As illustrated in Figure 3D, right panels, after 13 days the entire population of TLR2$^+$ cells attained surface expression of CD45 and CD11b and gradually lost ckit expression. Approximately one third of the cells gained Gr-1 expression. In contrast, neither Ter119$^+$ nor B220$^+$ cells were detected. It is of note that neither the TLR2$^-$ ckit$^-$ CD45$^-$ nor the TLR2$^-$ ckit$^+$ CD45$^-$ populations were able to survive or differentiate in this culture system, even when a higher number of sorted cells was plated (data not shown).

However, the hematopoietic potential of E7.5 TLR2$^+$ ckit$^+$ embryonic hematopoietic progenitors was not restricted to the myeloid lineage. When these cells were plated for 48-72 hours in methylcellulose colony assay supporting the growth of erythroid as well as myeloid colonies, the presence of small and compact colonies formed by relatively large cells that morphologically resembled those described previously as primitive erythroid cells (EryP-CFU; Erythroid^{primitive}-colony forming unit) (Ferkowicz et al. 2003) was microscopically detectable (Fig. 3E, left panel). Counting these colonies derived from sorted E7.5 TLR2$^+$ ckit$^+$ or TLR2$^-$ ckit$^+$ cells demonstrated the enhanced erythroid potential of the former (Fig. 3E, right panel). When these cultures were inspected at day 10, we observed absence of colonies in the plates seeded with TLR2$^-$ ckit$^+$ cells, whereas plates seeded with TLR2$^+$ ckit$^+$ cells demonstrated the presence of relatively large colonies morphologically resembling CFU-GM (Granulocyte, Macrophage) and CFU-GEMM (Granulocyte, Erythroid, Macrophage, Megakaryocyte) (Fig. 3F, left panel). As evident from FACS analysis shown in right panels in Figure 3F, the cells forming these colonies were (i) undergoing differentiation towards CD45$^+$ ckit$^-$ stage; (ii) expressed the earliest marker of primitive erythroid and early macrophage progenitors, CD41; and contained a mixture of differentiated Ter119^{DIM} CD45$^-$ cells (iii), as well as CD45$^+$ CD11b$^+$ myeloid cells (iv). This provided evidence that E7.5 TLR2$^+$ ckit$^+$ cells, in the presence of erythropoietin, possess the capacity to differentiate towards Ter119^{DIM} CD45$^-$ primitive erythroblasts (Ferkowicz et al. 2003). On contrary, when adult BM cells were tested for erythro-myeloid differentiation potential on OP-9 stroma cultures, only Lin$^-$ TLR2$^-$ ckit$^+$ progenitors displayed appreciable erythropoietic potential (Fig. S3). Together, the data presented in Figure 3, strongly support the view that E7.5 TLR2$^+$ ckit$^+$ cells represent

common hematopoietic progenitors that can produce CD45^{+} CD11b^{+} myeloid cells both *in vivo* and *in vitro* as well as primitive erythroid lineages.

4.1.4.6. TLR2 stimulation promoted TLR2^{+} ckit^{+} precursor cell proliferation and myeloid differentiation

The functional significance of TLR2 expression on ckit^{+} embryonic cells was assessed through stimulation with the TLR2 agonist Pam3CSK4. TLR2^{+} ckit[+], TLR2^{-} ckit[+] and TLR2^{-} ckit^{-} cells were sorted from E8.5 EGFP[+] embryos and co-cultured with the OP-9 stromal cells without cytokine or growth factor supplements in the presence or absence of Pam3CSK4 for 72 hours. As illustrated in Figure 4A and Figure S4A, the recovery of both TLR2^{-} populations was ineffective whether stimulated with TLR2 agonist or not. In sharp contrast, approximately 24% (SD=11.5; n=3) and 39% (SD=8.6; n=3) of EGFP^{+} cells were recovered from cultures that were seeded with TLR2^{+} ckit[+] embryonic precursors either unstimulated or stimulated with Pam3CSK4, respectively. The increased recovery rate observed upon TLR2 agonist treatment correlated with their higher rate of proliferation (Fig. 4B, middle panel; Fig. S4B, C). This effect was ameliorated in TLR2^{+} ckit^{+} progenitor cells derived from MyD88 deficient mice (Fig. 4B, right panel), formally demonstrating the involvement of TLR signaling in this process. The quantification of this assay is presented in Figures S3B and S3C. Moreover, following 72 hours in culture, Pam3SCK4 stimulated cells showed enhanced expression of the macrophage marker CD11b, suggesting a more efficient myeloid differentiation rate upon TLR2 stimulation (Fig. 4C). These data suggested that TLR2 engagement endowed embryonic hematopoietic cells with enhanced potential for the production of CD11b myeloid leukocytes.
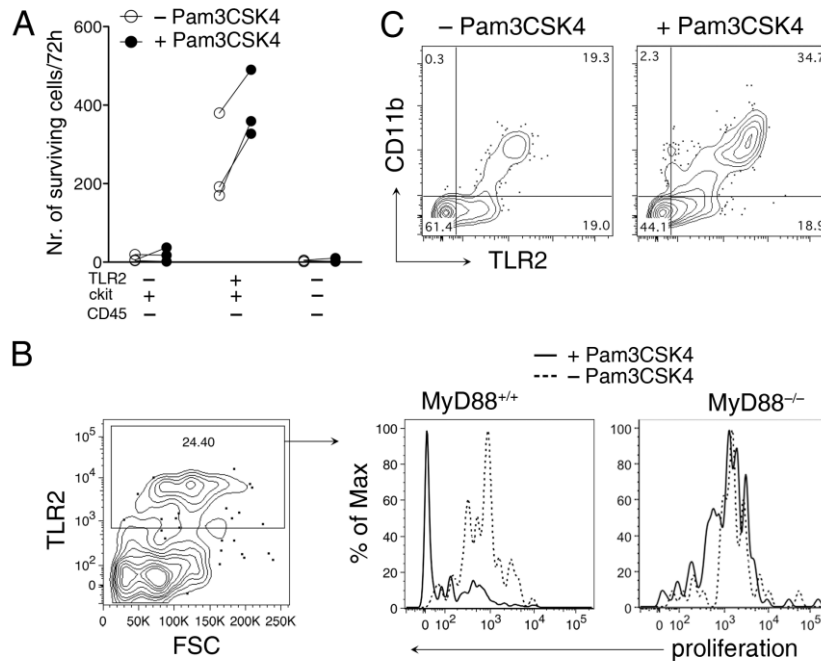
Figure 4. TLR2 stimulation enhances the proliferation and myeloid differentiation of E8.5 embryonic TLR2⁺ ckit⁺ CD45⁻ cells.

Wt females were crossed with TgEGFP males to identify EGFP⁺ embryonic-derived cells. E8.5 TLR2⁺ ckit⁺ CD45⁻, TLR2⁻ ckit⁺ CD45⁻ and TLR2⁻ ckit⁻ CD45⁻ cells were sorted and plated on OP-9 stromal cells in the presence or absence of TLR2 agonist Pam3CSK4. After 72 hours of co-culture, cells were harvested and analyzed by FACS. Data are representative from three independent experiments. (A) Survival analysis of sorted TLR2⁻ ckit⁺ CD45⁻, TLR2⁺ ckit⁺ CD45⁻ and TLR2⁻ ckit⁻ CD45⁻ cells either unstimulated or stimulated with Pam3CSK4 (1 µg/ml). (B) The proliferation history of TLR2⁺ ckit⁺ CD45⁻ cells cultured in the presence or absence of Pam3CSK4 was assessed in MyD88⁺/⁺ (middle panel) and MyD88⁻/⁻ mice (right panel) by the dilution of Cell Proliferation Dye eFlour® 670 in TLR2⁺ cells (left panel) as measured by FACS. See also Figure S4. (C) Surface expression of TLR2 and CD11b on cells derived from TLR2⁺ ckit⁺ CD45⁻ cells grown on OP-9 cells in the presence or absence of Pam3CSK4 as determined by FACS.

4.1.4.7. The presence of TLR2⁺ ckit⁺ CD45⁻ hematopoietic progenitor at E6.5 coincided with the onset of gastrulation

Given the relative abundance of hematopoietic embryonic progenitor cells at E7.5, we assessed their presence during an earlier stage of development, before the formation of the blood island at E6.5. As illustrated in Figure 5A, ckit was coexpressed exclusively on a fraction of TLR2⁺ embryonic cells. The existence of an embryonic TLR2⁺ ckit⁻ cell population suggested that TLR2 expression might precede the expression of ckit. This notion correlated with the data shown in Figure 3A (E7.5-E9.75, top panels), where apparently the majority of TLR2⁺ ckit⁻ progenitors gradually acquired ckit expression before they become CD45 positive. Importantly, and as illustrated in Figure 5B, when E6.5 TLR2⁺ CD45⁻ embryonic progenitors were FACS sorted and co-cultured for 10 days with OP-9 stroma in the presence of a myeloid differentiation cocktail, a sizeable fraction (>10%) of these cells differentiated to CD11b⁺ TLR2⁺ ckit⁻ CD45⁺ myeloid cells. In contrast, the TLR2⁻ CD45⁻ population, gated as indicated in the left panel of Figure 5B,

was not able to survive or differentiate in this culture system (data not shown). Together, these data suggested that the initiation of embryonic myelopoiesis was concomitant with the onset of gastrulation, and the initial TLR2+ hematopoietic precursor cells were generated before the appearance of the YS blood island.
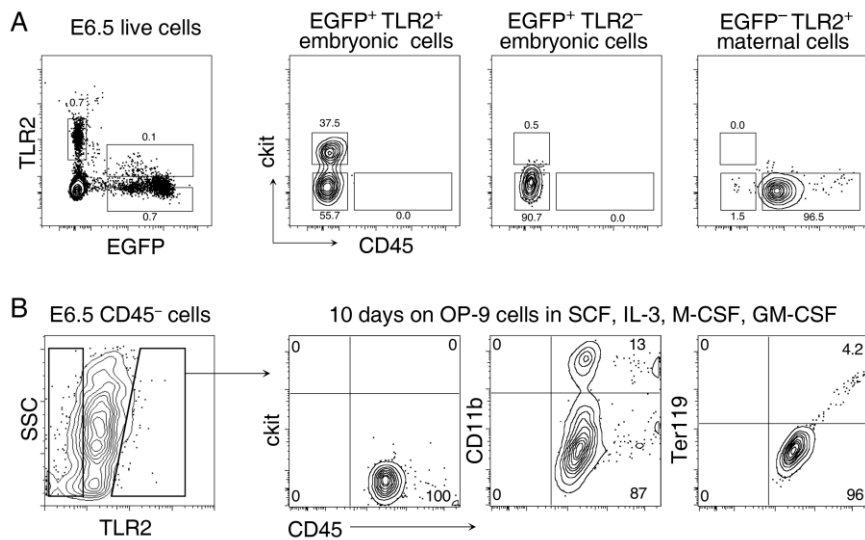

Figure 5. Myeloid cells differentiate from E6.5 TLR2$^+$ cells in vitro.
(A) E6.5 embryonic cells obtained from the crosses described in Figure S1A were analyzed for EGFP and TLR2 expression (left panel). Three distinct subsets were readily identified: two EGFP$^+$ embryonic populations, either positive or negative for TLR2 expression, and the maternally derived EGFP$^-$ TLR2$^+$ cells. Each of them was further analyzed for ckit and CD45 expression (three right panels). (B) E6.5 TLR2$^+$ CD45$^-$ cells were sorted (left panel), grown on OP-9 stromal cells in the presence of myeloid cytokine cocktail for 10 days and analyzed by FACS for indicated markers. Representative data from three independent experiments are shown.

4.1.4.8. E7.5 TLR2+ckit+ hematopoietic progenitors populated both extra- and intra- embryonic structures but displayed distinct phenotypes

Next, we examined the spatial distribution of TLR2+ cells in the neural plate stage embryo (E7.5) using confocal microscopy. As illustrated in Figure 6, TLR2+ cells occupied the space between the most proximal and the distal edge of the YS which approaches the embryo proper. In addition, detail examination of confocal as well as 3D-reconstructed images revealed the presence of TLR2LOW cells in the area from the level of the EP to the more proximal region of the YS (Fig. 6, white box, two right panels, and Movie S1). This is consistent with the expression of this marker on a small population of differentiating mesodermal cells migrating from the primitive streak into developing YS and their early commitment to hematopoietic fate. Importantly, it also correlates with the low expression TLR2 on E7.5 embryonic-derived hematopoietic precursors determined by FACS analysis (Fig. 2A, left panel).
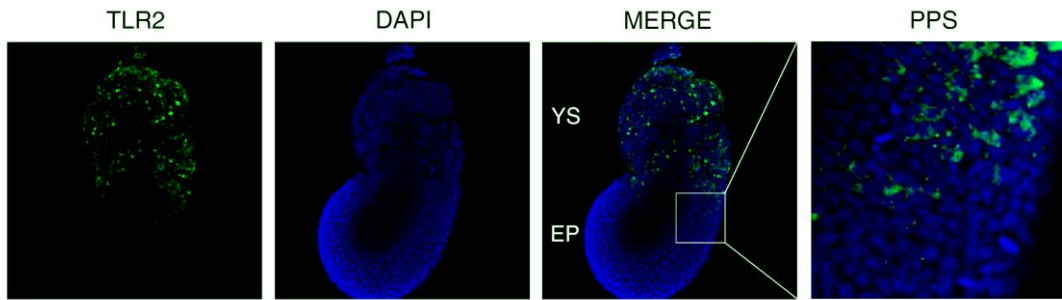
Figure 6. TLR2⁺ cells localize mainly in the forming YS in E7.5 embryos.
The whole mount embryos probed with anti-TLR2 (green) and DAPI (blue) revealed the presence of TLR2+ cells predominantly in the forming YS of the embryo. At this point of development, 90-95% of these cells were maternally-derived macrophages expressing higher levels of this antigen (Fig. 2). While some TLR2LOW progenitors of embryonic origin were also detectable in the YS structure, their exclusive presence in the region corresponding to the posterior primitive streak (PPS) (white box and its magnification in right panel) was consistent with TLR2 expression on the earliest hematopoietic progenitors migrating from this region into the developing YS. Signals were visualized and digital images were obtained by using a Zeiss LSM 780 equipped with two photon, argon and helium–neon lasers.

To validate these data by FACS analysis, we assessed the spatial distribution of TLR2⁺ ckit⁺ CD45⁻ cells at E7.5, when the YS and embryo proper (EP) structures became separable (Fig. 7A). Single cell suspensions prepared from either the YS or EP were stained for TLR2 and ckit, and the numbers of EGFP⁺ TLR2⁺ ckit⁺ cells per embryo as well as their relative proportion to total cell mass were enumerated (Fig. 7B). These data confirmed that hematopoietic progenitors were not restricted to the YS, since EGFP⁺ TLR2⁺ ckit⁺ CD45⁻ progenitors were readily detected in low but reproducible numbers in EP structures as well.

Additional staining revealed that a large proportion of the YS-derived TLR2⁺ ckit⁺ progenitors were positive for the surface expression of one of the earliest markers of primitive and definitive hematopoiesis, CD41 (Integrin alpha 2b) (Mitjavila-Garcia et al. 2002; Mikkola et al. 2003), as well as CD150 (SLAM), the marker of adult long term (LT)-HSCs (Kiel et al. 2005) (Fig. 7C). Similarly, while expression of the endothelial marker CD31 (PECAM1) (Baumann et al. 2004) was also detectable on a fraction of TLR2⁻ ckit⁺ CD45⁻ cells, we observed approximately a 10-fold higher proportion of TLR2⁺ ckit⁺ CD45⁻ CD31⁺ progenitors from the YS compared to EP (Fig. 7C and Fig. S5A). At E7.5 the surface expression of CD93 (AA4.1) (Petrenko et al. 1999) (Fig. 7C), Sca1 (Taoudi et al. 2005) (Fig. S5A) and CD144 (VE-cadherin) (Breier et al. 1996; Nishikawa et al. 1998) (Fig. S5) was not detectable on any embryonic population.

In addition, TLR2$^+$ ckit$^+$ cells isolated from YS, but not EP, were positive for mRNA coding for the transcription factor *Runx1* which is required for blood cell specification (Fig. 7D). Similar levels of *Runx1* were also expressed by the YS-derived TLR2$^-$ ckit$^+$ population, a fraction of which was also positive for CD31, CD41 and CD150 (Fig. 7D). It is of note that a substantial difference observed in the expression of *Runx1* between TLR2$^+$ ckit$^+$ cells isolated from separated YS and EP and the absence of TLR2$^+$ CD41$^+$ and TLR2$^+$CD150$^+$ cells in the separated EP (Fig. 7C) advocated for an insignificant level of cross-contamination during the embryonic dissection. Together, our data presented in Figures 6 and 7 strongly suggested that distinct cell environments could affect the differentiation and/or specification process of the TLR2$^+$ ckit$^+$ hematopoietic precursors prior to the establishment of embryonic circulation and that molecular processes underlying these events are initiated upon the migration of these cells to the YS environment which then supports a full development of their early hematopoietic potential.
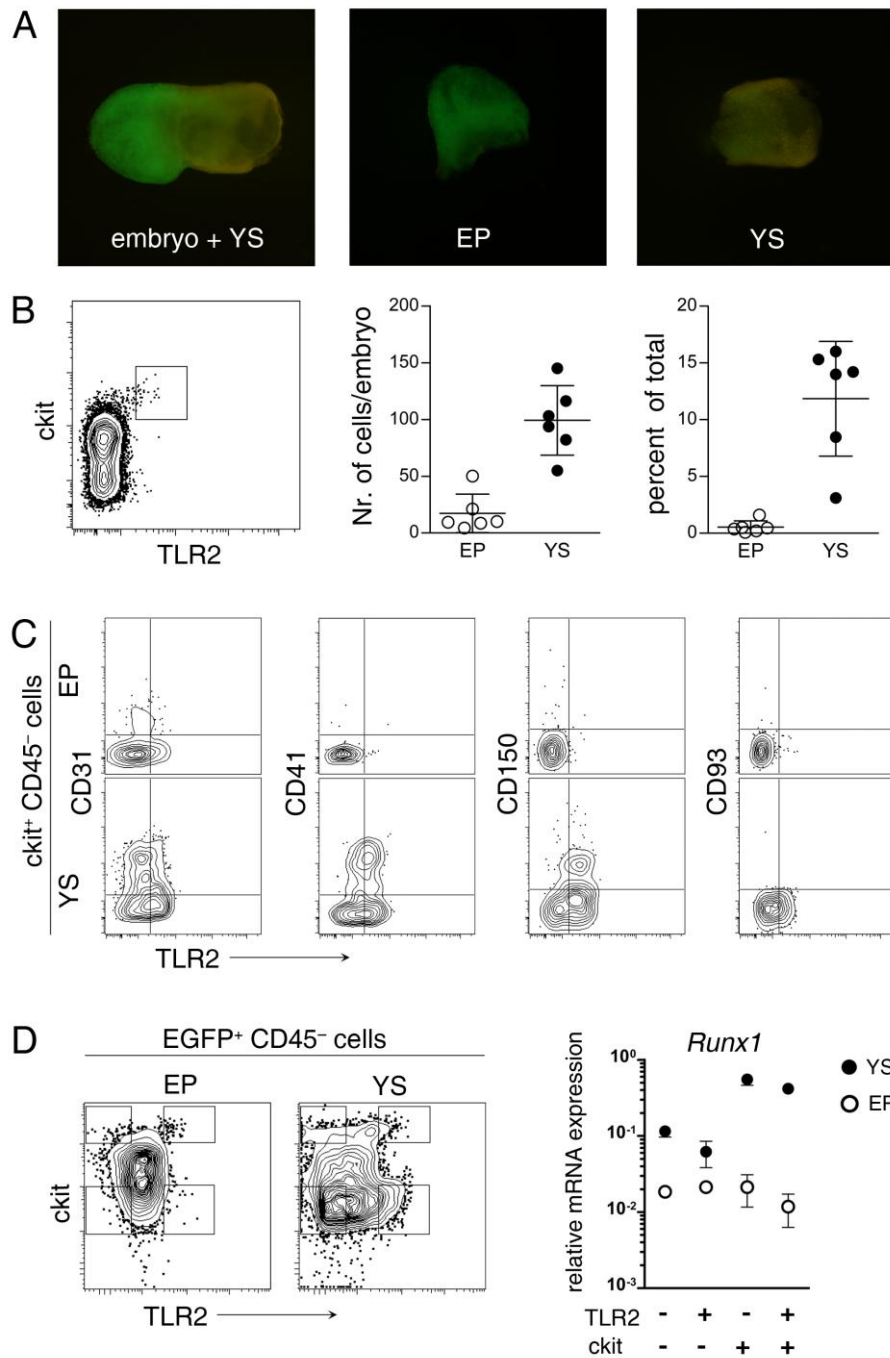
Figure 7. The appearance of early hematopoietic markers CD41 and CD150 on E7.5 YS-derived TLR2+ ckit+ cells, but not on those from the EP, correlates with Runx1 expression.

(A-D) Wt females were crossed with TgEGFP males to identify EGFP+ embryonic cells. (A) The separation of E7.5 embryo into the embryo proper (EP) and the yolk sac (YS). (B) TLR2+ ckit+ CD45− cells were enriched in the YS compared to the EP. (C) Surface coexpression of TLR2 with CD31, CD41, CD150 and CD93 on the YS- and EP-derived ckit+ CD45− cells was determined by FACS. (D) Runx1 mRNA expression in sorted subsets of embryonic EGFP+ CD45− cells with combinatorial expression of ckit and TLR2 markers. Representative data from three independent experiments are shown. See also Figure S5.

4.1.5. Discussion

Thus far, the expression and function of TLRs have been investigated almost exclusively in the context of adult immune cells. To the best of our knowledge, this is the first study where the spatio-temporal expression profile of TLRs in a post-gastrulation embryo has been evaluated on a cellular level. Specifically, we have demonstrated that, during embryonic development, TLR2 is expressed by an early-appearing transient population of maternal CD11b^{+} CD45^{+} macrophages, which at E9.5-E10.5 is replaced by newly generated embryonic cells of similar phenotype. This ontogenetically regulated phenomenon is also reflected by a drop in mRNA expression of several TLRs and their adaptor proteins (*Tlr2, Tlr3, Tlr7, Tlr8, Tlr9, Tlr13, MyD88, Trif* and *Tram)* around E8.5-9.5. This finding is consistent with recent studies that suggest that an early embryo is colonized by sequential waves of maternally and then yolk sac-derived phagocytes (Bertrand et al. 2005b). Our data demonstrating the timely coordinated replacement of maternal phagocytes by embryonic phagocytes support the notion of their vital role in early embryonic developmental processes likely related to tissue remodeling and the secretion of trophic factors (Rae et al. 2007).

We report here that, due to surface expression of TLR2, the first appearance of precursors of myeloid cells were traceable in the early streak embryo at E6.5. The hematopoietic commitment of E6.5-7.5 TLR2^{+} ckit[+], but not TLR2^{−} ckit^{+} cells, was marked by gradual transcript accumulation and at E9.5 by surface expression of CD45. We also determined that at E6.5 many TLR2^{+} cells coexpressed ckit and subsequently (E7.5-E8.5) started to express a set of molecular markers that are closely associated with the specification of the hemangioblast and its transition to the earliest hematopoietic progenitors. Notably, the coexpression of *Flk1* with other relevant hematopoietic and endothelial markers on E8.5 TLR2^{+} ckit[+] progenitors was consistent with the notion that Flk1^{+} hemangioblasts represent the earliest commitment towards the hematopoietic and endothelial lineages (Eichmann et al. 1997; Faloon et al. 2000; Huber et al. 2004; Lancrin et al. 2009). Our data also demonstrated that, between E9.5 and E10.5, the surface expression of TLR2 became largely restricted to CD45^{+} embryonic myeloid progenitors. Thus, the timing of the appearance of an embryonic TLR2 single positive population correlated with previously published data in which the presence of hematopoietic progenitors for both primitive erythroid and macrophage lineages was first detected in the yolk sac during the transition from the mid-streak stage at E7.0 to the neural plate stage at E7.5 (Palis et al. 1999). In this respect, TLR2 represents one of the earliest molecular signatures marking the specification of early embryonic hematopoietic precursors from nascent mesodermal cells shortly after their appearance at E6.25. These data imply that the onset of mammalian hematopoiesis is nearly concomitant with the

process of gastrulation (Smith et al. 1994; Kinder et al. 1999; Ferkowicz and Yoder 2005; Furuta et al. 2006).

Moreover, and analogous to the situation in the adult bone marrow described by Nagai and colleagues (Nagai et al. 2006), the stimulation of E8.5 TLR2^{+} progenitors by Pam3CSK4 ligand enhanced their proliferation rate and differentiation to myeloid cells. As expected, this effect was not observed in progenitors derived from MyD88 deficient animals. However, as the proliferation and differentiation of TLR2^{+} embryonic progenitors proceeded at the basal level also without Pam3CSK4 stimulation, TLR2-generated signals seemed dispensable for normal embryonic myelopoiesis under non-inflammatory conditions. In agreement with our finding, no evidence for the impaired development of myeloid cells in TLR2 or MyD88 knockout mice has been reported (Adachi et al. 1998; Takeuchi et al. 1999).

In the developmental context, TLR2 expression seems to endow cells with a predisposition to preferentially differentiate into myeloid cells. This notion fits well into the myeloid-based model of hematopoietic lineage restriction proposed by Kawamoto and colleagues. It posits that myeloid cells represent a prototype of hematopoietic cells and, as such, their myeloid developmental potential is retained during the early stages of branching out toward erythroid, T-cell, and B-cell lineages (Kawamoto and Katsura 2009). The finding that TLR2 stimulation of early TLR2^{+} ckit^{+} CD45^{−} precursors augmented their myeloid fate strongly supports this concept and demonstrates that (i) the mechanism of TLR driven hematopoiesis is operational not only in adults (Nagai et al. 2006) but also in embryonic hematopoietic progenitors, and can thus be utilized continuously during the ontogenetic development as an evolutionary conserved "emergency" backup mechanism adopted for the rapid replenishment of circulating innate immune cells during infectious insult; and (ii) in this scenario, the expression of TLRs on hematopoietic precursors serves as a direct molecular link conveying microbial environmental cues to the genetically controlled myeloid-based differentiation program.

Our data are consistent with the current paradigm positing that the first hematopoietic cells in the mouse embryo emerge from hemangioblast precursors that migrate from the posterior primitive streak to the forming YS around E7.25, where they give rise to differentiated cells including nucleated erythrocytes, macrophages and megakaryocytes (Moore and Metcalf 1970; Eichmann et al. 1997; Palis et al. 1999; Xu et al. 2001; Huber et al. 2004). However, while our data also demonstrated that E7.5 TLR2^{+} ckit^{+} CD45^{−} hematopoietic progenitors reside mainly in the developing YS and only 5-10% of these cells can be found in the EP, only the former coexpress CD41, the marker indicative of a

commitment to early hematopoietic development (Ferkowicz et al. 2003; Mikkola et al. 2003) and CD150, the marker of adult LT-HSCs (Kiel et al. 2005). Given the fact that only one third of mesodermal cells traversing the primitive streak emigrate to extraembryonic sites while the remaining cells colonize the EP and contribute to generate various derivates of intraembryonic mesoderm (Palis 2006), such phenotypic divergence between the YS- and EP-derived TLR2^{+} progenitors, caused either by their interaction with the environment in distinct regions of the embryo (Matsuoka et al. 2001; Nishikawa et al. 2001; Sugiyama et al. 2007) or, alternatively, by a regionalization of cell fates during their allocation along the anterioposterior axis (Tam and Beddington 1987; Kinder et al. 1999; Ueno and Weissman 2010) suggests their separate developmental paths and most likely distinct contribution to embryonic hematopoiesis. Further experimentation is needed to resolve this issue.

Importantly, the above described phenotypic distinction between the extra- and intra-embryonic populations of E7.5 TLR2^{+} ckit^{+} cells is also paralleled by the expression profile of *Runx1*, a transcription factor that is essential for the primitive erythropoiesis as well as definitive hematopoiesis (Okuda et al. 1996; North et al. 1999; Lacaud et al. 2002; Yokomizo et al. 2008; Lancrin et al. 2009; Tanaka et al. 2012). The expression of *Runx1* and CD41 in TLR2^{+} ckit[+] early progenitors around E7.5 is also likely regulated by cues from within the YS environment, as these markers are absent in their TLR2^{+} ckit[+] counterparts residing in the EP. This further strengthens the notion that the YS could act as an essential site for the initiation of primitive and definitive hematopoiesis (North et al. 1999; Lacaud et al. 2002; Ferkowicz et al. 2003; Li et al. 2006).

Interestingly, recent genetic cell tracking experiments have demonstrated the essential contribution of E6.5-7.5 Runx1^{+} CD144^{+} YS-derived cells to the emergence of adult HSCs (Samokhvalov et al. 2007; Tanaka et al. 2012). Based on these data, it is tempting to speculate that definitive HSCs could also originate among these early TLR2^{+} hematopoietic ancestors. While further evaluation of this proposal is needed using a lineage tracing approach, the recently reported discovery of very slowly engrafting, adult CD150[HIGH] myeloid-biased HSCs whose full potential can be seen only after secondary transplantation supports this notion (Morita et al. 2010). Similarly, several studies have documented the occurrence of YS-derived adult myeloid cells independent of AGM origin (Alliot et al. 1999; Ginhoux et al. 2010; Schulz et al. 2012).

In this study, we also documented the existence of a TLR2^{-} YS population which is ckit^{+} CD41^{+} CD150^{+} and *Runx1*^{+}, thus also fulfilling critical requirements for being considered a progenitor of hematopoiesis. However, because this thus far enigmatic population was

not able to survive and/or proliferate in the presence of OP-9 cells conditioned with either a myelo- or lympho-cytokine cocktail (Bertrand et al. 2005b; Tanaka et al. 2012) and did not express CD45 before E10.5, its hematopoietic potential remains uncertain.

Taken together, our data illustrated the utility of TLR2 as a cellular marker of common embryonic precursors with an early commitment (E6.5) to primitive and definitive hematopoiesis and revealed a much broader complexity and dynamics of hematopoietic subpopulations at this stage of ontogenetic development. Herein, the described data also provided further evidence supporting the current paradigm that the YS serves as an important niche from where the mesodermal ancestors acquire the competence to initiate hematopoietic development.

4.1.6. Acknowledgments

4.1.7. Supporting Information
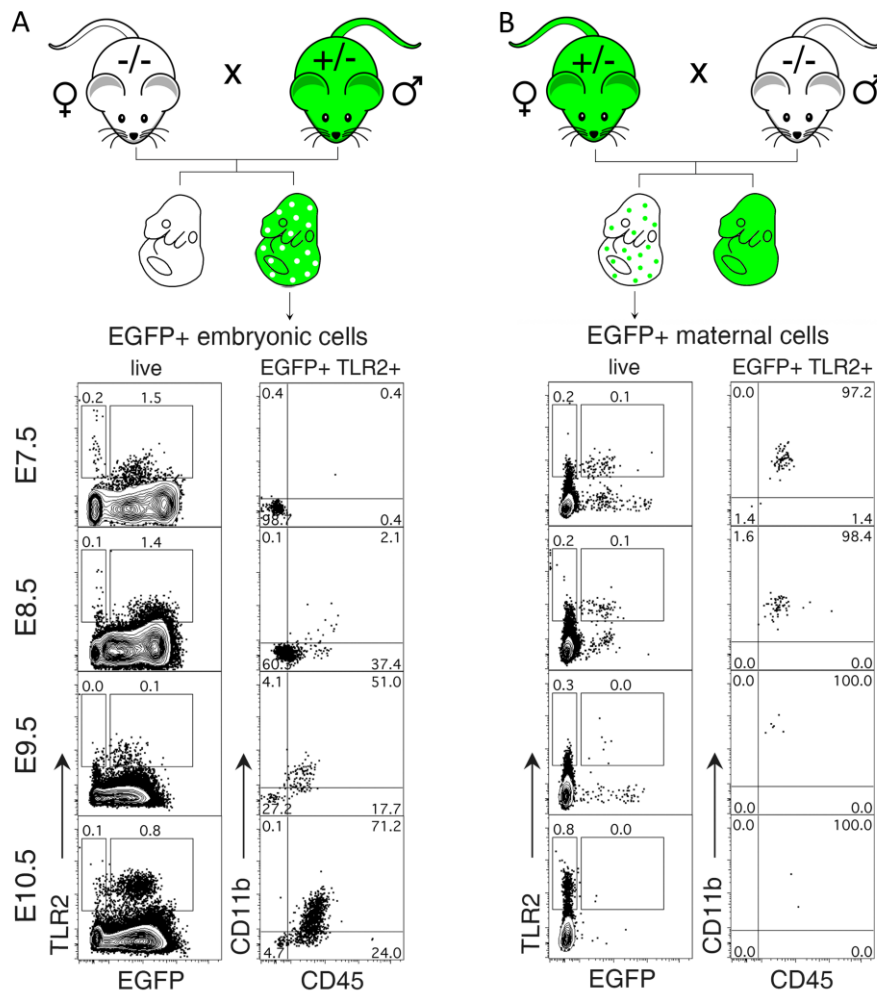
Figure S1, Breeding schemes enabling tracking of embryonic and maternal cells, related to Figures 3-5 and 7.

(A) Tracking of embryonic cells. Wt females were crossed with heterozygous TgEGFP males expressing EGFP under the control of the β-actin promoter. Only EGFP$^+$ embryos were further analyzed. Based on EGFP expression, embryonic cells were discriminated from EGFP$^-$ maternal cells (white dots). EGFP positive heterozygous embryos (E7.5-E10.5) were analyzed for TLR2, CD11b and CD45 expression. The right side panels show the expression of CD45 and CD11b on gated EGFP$^+$ TLR2$^+$ embryonic cells.

(B) Tracking of maternal cells. Heterozygous TgEGFP females expressing EGFP under the control of β-actin promoter were crossed with wt males. Only wt embryos were further analyzed for the presence of EGFP$^+$ maternal cells (green dots) transiently colonizing embryo at early developmental stages. Wt embryos (E7.5-E10.5) were analyzed for TLR2, CD11b and CD45 expression. The right side panels show the expression of CD45 and CD11b on gated EGFP$^+$ TLR2$^+$ maternal cells. Representative data from at least three independent experiments are shown.
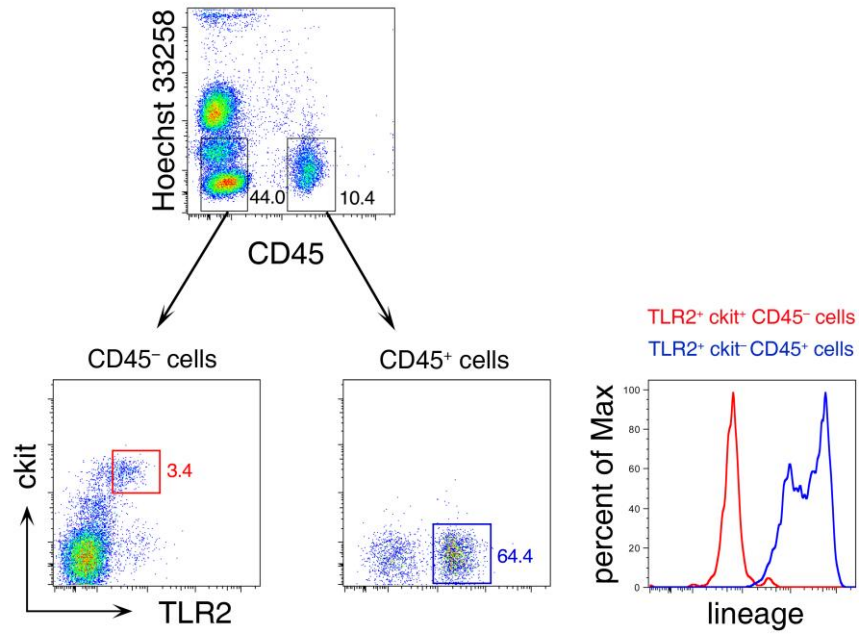
Figure S2, E7.5 TLR2$^+$ ckit$^+$ CD45$^-$ embryonic progenitors are lineage negative, related to Figure 3. E7.5 TLR2$^+$ ckit$^+$ CD45$^-$ embryonic cells were analyzed for the presence of lineage markers (CD3, Gr-1, CD11b, B220 and Ter119) by FACS. Live TLR2$^+$ ckit$^+$ CD45$^-$ cells were gated and their surface expression of lineage markers was compared to TLR2$^+$ ckit$^-$ CD45$^+$ maternal hematopoietic cells. Representative data from three independent experiments are shown.
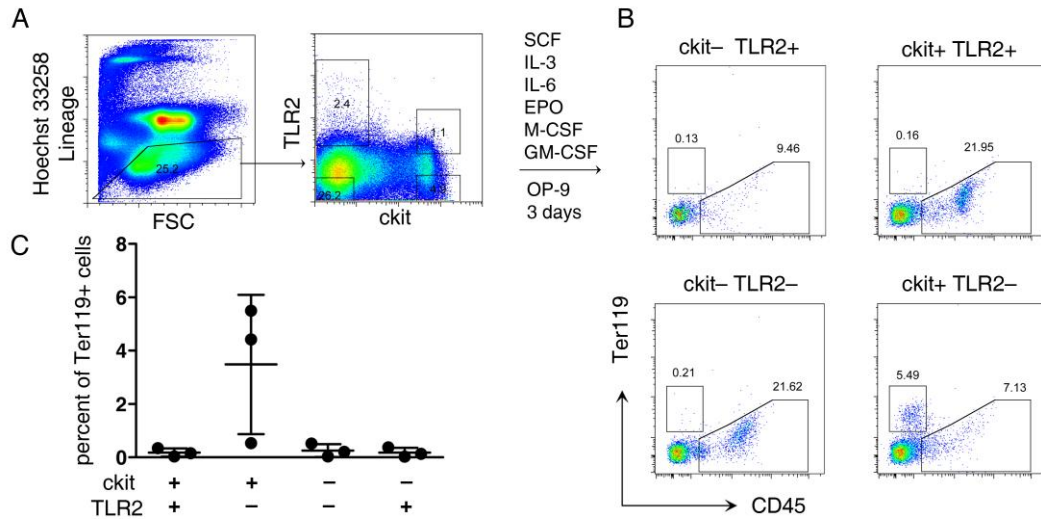
Figure S3. In the adult BM, the highest erythroid differentiation potential is found in the Lin⁻ ckit⁺ TLR2⁻ fraction, related to Figure 3.

Adult BM cells were depleted for erythrocytes by ACK lysis. Differentiated progenitors and dead cells were excluded using lineage antibody cocktail and Hoechst 33258 viability dye respectively. Four populations of lineage⁻ cells were sorted based on their ckit and TLR2 surface expression (A) and cultured on OP-9 stroma in the presence of a myelo-erythroid differentiation cocktail (SCF, IL-3, IL-6, EPO, M-CSF, GM-CSF). (B, C) After 3 days of co-culture the expression of Ter119 and CD45 was measured by FACS. Data represent mean +/- SD; n=3.
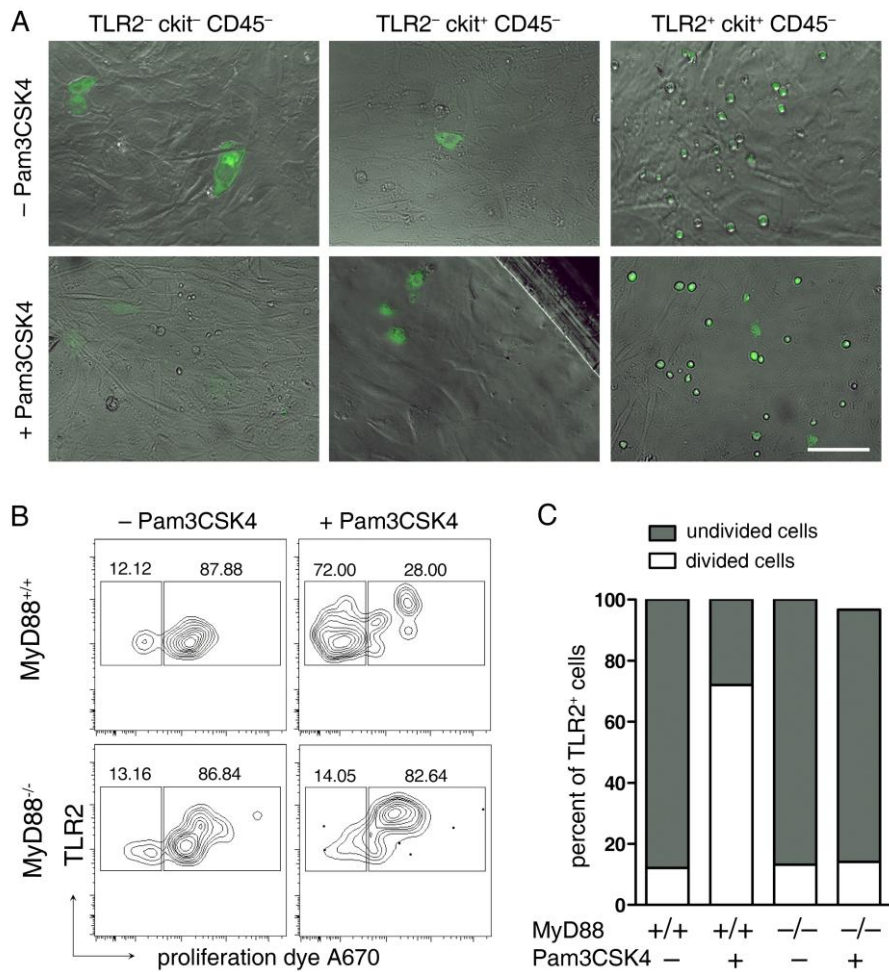
Figure S4, Proliferation of E8.5 TLR2+ ckit+ CD45− cells in vitro, related to Figure 4.

(A) E8.5 TLR2+ ckit+ CD45−cells survive in culture with or without TLR2 stimulation

E8.5 embryonic EGFP+ TLR2− ckit− CD45−, EGFP+ TLR2− ckit+ CD45− or EGFP+ TLR2+ ckit+ CD45− cells were plated on OP-9 cells and co-cultured in the presence or absence of Pam3CSK4 for 72 hours. Olympus Cell^R, magnification 20x, scale bar represents 100µm.

(B, C) TLR2 triggered proliferation of E8.5 embryonic TLR2+ ckit+ CD45− cells is MyD88 dependent.

(B) Proliferation of E8.5 embryonic TLR2+ ckit+ CD45− cells derived from wt (MyD88+/+) or MyD88 deficient (MyD88−/−) mice grown in the absence or presence of Pam3CSK4 for 72 hours measured by FACS. Live TLR2+ cells were included in the analysis.

(C) Quantification of proliferation rate of E8.5 embryonic TLR2+ ckit+ CD45− cells derived from wt (MyD88+/+) or MyD88 deficient (MyD88−/−) mice.

Representative data from three independent experiments are shown.
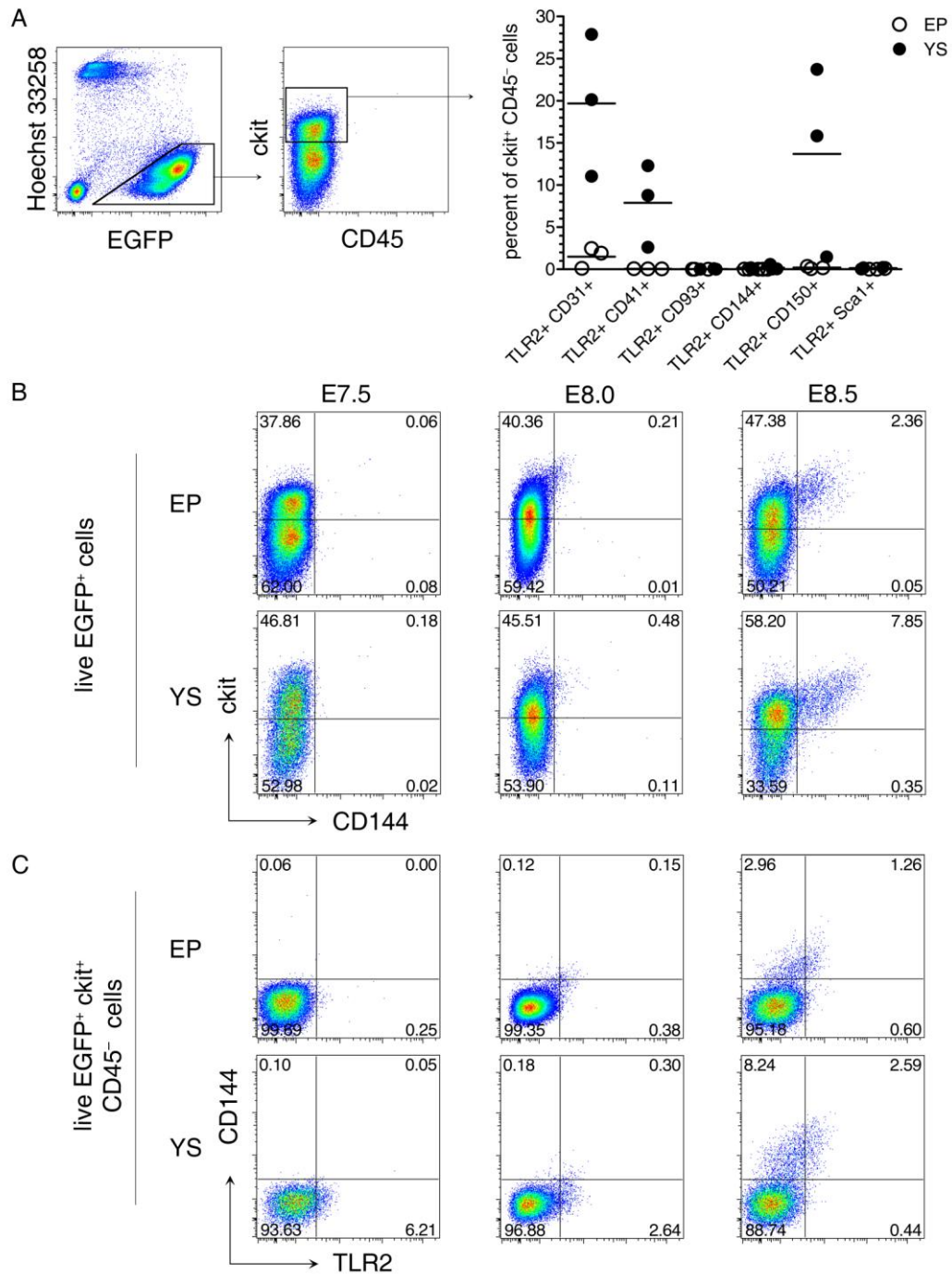
Figure S5, Expression of hematopoietic and endothelial markers on early embryos, related to Figure 7
(A-C) Wt females were crossed with TgEGFP males to discriminate EGFP$^+$ embryonic cells. (A)
Coexpression of TLR2 and hematopoietic/ endothelial markers on E7.5 ckit$^+$ CD45$^-$ cells isolated from
the EP and the YS. Live, EGFP$^+$ ckit$^+$ CD45$^-$ cells were gated and the percentage of cells positive for TLR2
and the indicated maker was enumerated (mean ± SD; n=3).
(B, C) Surface expression of CD144 starts at E8.0 in the YS. Single cell suspensions isolated from the EP
or YS portion of embryos at different stages of development (E7.5-E8.5) were analyzed for the surface
expression of CD144. (B) The expression of ckit and CD144 on live embryonic (EGFP$^+$) cells isolated from
the EP (upper panel) and the YS (lower panel) respectively. (C) Coexpression of TLR2 and CD144 on
EGFP$^+$ ckit$^+$ CD45$^-$ cells isolated from the EP (upper panel) and the YS (lower panel) respectively.
Representative data from three independent experiments are shown.

66

Supplemental Movie S1, Anatomical location of TLR2$^+$ cells in an early embryo, related to Figure 6.
3D reconstructed image of E7.5 embryo stained with anti-TLR2 antibody (green) and counterstained with DAPI (blue) was generated by optical sectioning and projecting individual confocal planes (25-30 planes in 1-2 μm intervals) using Imaris software 7.3 (Bitplane).

Gene	Forward primer 5'– 3'	Reverse primer 5'– 3'
CasC3	TTCGAGGTGTGCCTAACCA	GCTTAGCTCGACCACTCTGG
Cd11b	CAATAGCCAGCCTCAGTGC	GAGCCCAGGGGAGAAGTG
Cd31	GCTGGTGCTCTATGCAAGC	ATGGATGCTGTTGATGGTGA
Cd34	GGGTAGCTCTCTGCCTGATG	TCCGTGGTAGCAGAAGTCAA
Cd41	TGCTGCTGACCCTGCTAGT	GTCGATTCCGCTTGAAGAAG
Cd45	AGTAGGAAACTTGCTCCCCATCTGA	TGGAGATCAGCTGTGCCCCT
Cd93	GAGAATCAGTACAGCCCAACACCAG	TGCCTATCCCAAGCCACCAGGT
Cd105	CGTTCTCTTCCTGGATTTTCC	ATTTTGCTTGGATGCCTGAA
Cd144	GTTCAAGTTTGCCCTGAAGAA	GTGATGTTGGCGGTGTTGT
Cd150	GACCCCTGCACAACCATT	TGTGGTGGGGTTTGGTTC
Cd244	TTGTACCGTGTACGAGGAGGT	CAAAGTTCTCCAGCTCTCTGC
ckit	GGAGCCCACAATAGATTGGTAT	CACTGGTGAGACAGGAGTGG
Csf1r	CGAGGGAGACTCCAGCTACA	GACTGGAGAAGCCACTGTCC
Flk1	CCCCAAATTCCATTATGACAA	CGGCTCTTTCGCTTACTGTT
Gata1	TCCCAGTCCTTTCTTCTCTCC	TCACACACTCTCTGGCCTCA
Gata2	GCTTCACCCCTAAGCAGAGA	TGGCACCACAGTTGACACA
Lmo2	CGAAAGGAAGAGCCTGGAC	CGGTCCCCTATGTTCTGCT
Mal	CTGCACTATGGCTTCATCCTC	AGAGCCTGCCTGAACCAGT
Mpo	GGAAGGAGACCTAGAGGTTGG	TAGCACAGGAAGGCCAATG
MyD88	TGGCCTTGTTAGACCGTGA	AAGTATTTCTGGCAGTCCTCCTC
Runx1	CTCCGTGCTACCCACTCACT	GCACTCTGGTCACCGTCAT
Sarm1	GCTTGCTGGAGCAGATCCT	TCACGCCTAGACCGATGC
Tie2	GGCCAGGTACATAGGAGGAA	CCCACTTCTGAGCTTCACATC
Tlr1	GGCGAGCAGAGGCAATTGTGGA	TTCTTCAGAGCATTGCCACATGGG
Tlr2	GTTCATCTCTGGAGCATCCG	ACTCCTGAGCAGAACAGCGT
Tlr3	ATACAGGGATTGCACCCATA	CCCCCAAAGGAGTACATTAGA
Tlr4	GGACTCTGATCATGGCACTG	CTGATCCATGCATTGGTAGGT
Tlr5	ACGCACCACACTTCAGCA	AGCCTCGGAAAAAGGCTATC
Tlr6	GTCAGTGCTGGAAATAGAGC	CCACGATGGGTTTTCTGTCT
Tlr7	ACTCTCTTCTCCTCCACCAGACCT	GAGGCCACTTGTCTGTCACACTG
Tlr8	CAAACGTTTTACCTTCCTTTGTC	ATGGAAGATGGCACTGGTTC
Tlr9	CGCCCAGTTTGTCAGAGGGAGC	GGTGCAGAGTCCTTCGACGGAG
Tlr11	ATGGGGCTTTATCCCTTTTG	AGATGTTATTGCCACTCAACCA
Tlr12	TTTCAAGCACTGGCCTAACC	GAAGCCTAGGCATGGCAGT
Tlr13	CTATGTGCTAGGAGCTTCTGAGAG	AGGAAGCAGAGAACCAGGAA
Tram	TGGTCAAGCAGTACCACTTCC	GAGACGCCTTAGCCTCCAGT
Trif	ACCAGGGACCGGGAGATCTACCA	CAAAGATGCTGGAGGGCGGCA

Table S1, List of primer sequences used for qRT-PCR analysis of selected genes.

4.2. Generation of *Tlr2* reporter mice

This chapter describes the process of generation of two transgenic reporter mouse strains suitable for visualization and fate mapping of cells with active *Tlr2* promoter and their progeny. In addition, so far unpublished data, that confirmed that our attempt to generate *Tlr2* reporter strains was successful, are included in this chapter to illustrate the benefits of the use of these transgenic mouse lines in hematopoiesis research.

4.2.1. Introduction

Since no unique surface marker of HSCs has been identified so far, the only way how to probe a cell to have HSC features is a successful reconstitution of adult irradiated host (Boisset and Robin 2012). However, probably due to lack of environmental cues and inability to express a proper set of homing receptors, these features posses only embryonic cells isolated after E10.5. Since TLR2+ precursors of appear way before E10.5, the only option to assess their differentiation potential *in vivo* and to reveal their full hematopoietic potential is the lineage tracing approach. For this purpose it was necessary to establish constitutive and inducible *Tlr2* reporter mouse lines.

In order to generate the transgenic mice we employed the Bacterial Artificial Chromosome (BAC) recombineering (recombination-mediated genetic engineering) strategy (Lee et al. 2001). Due to its simplicity and precisely defined methodological steps it allowed us to create transgenic mice in few months. BAC genomic clones often contain genomic segments that include most if not all of the extragenic cis-acting regulatory elements of a gene of interest. For this reason, BAC technology is suitable for generating transgenic mice because the relatively large insert size allows the expression of a gene under the control of its own regulatory elements, mimicking the endogenous expression pattern (Sharan et al. 2009).

We have generated two mouse strains expressing constitutive and inducible Cyclic recombinase (*Cre*) under the control of *Tlr2* promoter and its regulatory elements respectively. Cre is a tyrosine recombinase derived from the P1 bacteriophage that utilizes a topoisomerase I like mechanism to carry out site specific recombination events between two DNA recognition sites (loxP sites) (Hamilton and Abremski 1984). The bacteriophage uses Cre-lox recombination to circularize and facilitate replication of its genomic DNA when reproducing. Since being discovered, the bacteriophage's recombination strategy has been developed as a technology for genome manipulation in many organisms (Araki et al. 1997). The orientation and location of the genetically introduced loxP sites determine whether Cre recombination induces a deletion, inversion, or chromosomal translocation. If the loxP sites are oriented in the same

direction on a chromosome segment, Cre recombinase mediates a deletion of the loxP flanked (floxed) DNA segment. Typically, *Cre* and *loxP* mouse strains are developed separately and only thereafter crossed to produce a *Cre-lox* strain (Nagy 2000). The expression of *Cre* can be further controlled in inducible *Cre* strains that express a modified form of *Cre* that is non-functional until an inducing agent is administered at a desired time point in embryonic development or adult life. In the presence of synthetic ligand, the Cre fusion protein translocates into the nucleus where it exerts its function.

In order to visualize cells with active *Tlr2* locus, we decided to use Rosa26-YFP reporter strain, where EYFP is expressed from a very effective ubiquitous Rosa26 promoter after the floxed transcriptional termination sequence is removed by Cre recombinase (Srinivas et al. 2001). Upon recombination in F1 generation of these mice, EYFP is permanently expressed in all cells with active *Tlr2* locus and their progeny (Figure 1). In addition to constitutive *Tlr2-Cre* mouse strain, we have generated *Tlr2-CreER^{T2}* strain, where the Cre recombinase is fused to a mutated ligand-binding domain of human estrogen receptor (ER) that lost its ability to bind endogenous estrogen, but binds tamoxifen. Due to this modification, CreER^{T2} protein, although constitutively expressed, is retained in the cytoplasm and cannot translocate to the nucleus to execute its function unless it binds tamoxifen.
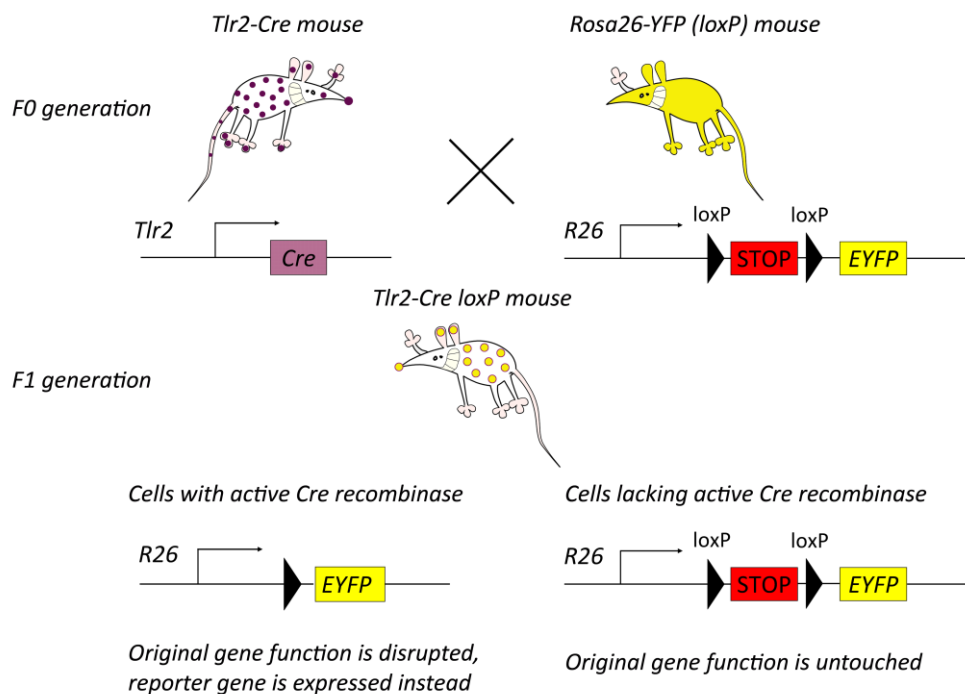

Figure 1. Diagram describing a model genetic experiment,where Tlr2-Cre and Rosa26-YFP mice are crossed to visualize cells with active Tlr2 locus in their F1 progeny.

4.2.2. Materials and Methods

4.2.2.1. Isolation of BAC DNA

For cloning, restriction analyses, PCR verifying or transformation of electro-competent bacteria BAC DNA was isolated by alkaline lysis followed by phenol-chloroform extraction. BAC clones were grown in 50 ml LB media containing chloramphenicol (12.5 μg/ml) overnight (ON) in a shaker incubator at 37 °C (DH10B strain) or 32°C (EL250 strain) and 200 RPM. Bacterial pellets were lysed in 4 ml buffer P1 (50 mM Tris, pH 8.0, 10 mM EDTA, 100 mg/ml RNase A). Then, 4 ml of P2 buffer (200 mM NaOH, 1% SDS) was added, the tube was inverted two to three times to mix, and incubated for 5 min. Finally, 4 ml of 2 M potassium acetate were added and the tube was inverted two to three times to mix. Upon chilling on ice for 15 min followed by centrifuging at 12,000 × g, the supernatant was transferred into a new tube and the phenol/chloroform extractions were carried out. Finally the BAC DNA was precipitated by adding an equal volume of isopropanol and chilling on ice for 15 minutes followed by centrifugation for 30 min at 12,000 × g. The pellet was washed with 1 ml of 70% ethanol and centrifuged for 5 min at 3,000 × g. Upon air drying, the pellet was resuspended in 100 μl of water. For PNI BAC DNA was isolated using X-Large DNA isolation kit (Qiagen).

4.2.2.2. Diagnostic restriction enzyme digestion of BAC clones

Restriction enzymes that cut two to four times in the BAC sequence were selected and 10 μl of BAC DNA from mini-prep was digested with 0.5 μl of enzyme, 2 μl of 10× buffer, and 8 μl of H_2O at 37 °C for 1-4 hours.

4.2.2.3. Polymerase chain reaction (PCR)

For detection of endogenous *Tlr2* in the BAC, following PCR reaction was set up:

DNA	2 μl
10× Taq buffer	2.5 μl
25 mM $MgCl_2$	2 μl
dNTP (10 mM each)	0.5 μl
primer Tlr2_i2-i3_F	1 μl
primer Tlr2_e2-300_R	1 μl
Taq (1 U/μl)	1 μl
H_2O	15 μl

PCR program

95 °C   5′ 00′′
[95 °C   0′ 30′′
57 °C   0′ 30′′
72 °C   1′ 20′′] 33x
72 °C   5′ 00′′

Primer sequences

primer Tlr2_i2-i3_F   GCGTGATAATAATGATATGTC

primer Tlr2_e3-300_R   CCAGAGAATAAAAGGCGTCTCC

For cloning of homology arm in the *Cre* cassette following PCR reaction was set up:

DNA	1 µl	
5× Q5 buffer	5 µl	
2.5 mM betain	10 µl	
dNTP (10 mM each)	0.5 µl	
primer F	0.5 µl	
primer R	0.5 µl	
Q5 polymerase (2 U/µl)	0.25 µl	
H₂O	7.25 µl	

PCR program

98 °C   0′ 30″
[98 °C   0′ 10″
66 °C   0′ 30″
72 °C   2′ 30″] 30x
72 °C   2′ 00″

Primer sequences

Tlr2_Cre_F

CAGATACACTCACTCACATGAGCGTCATTTGTTTTAAGGTCAAATCTCAGACC**ATG**TCCAATT
TACTGACCGTACA

Tlr2_Cre_R

GAACTGGGGGATATGCAACCTCCGGATAGTGACTGTTTCTACTTTACCCAGGCTATTCCAGAA
GTAGTGAG

Tlr2_CreERT2_R

CACAAAGACCTTAGTTAAGGAAGTCAGGAACTGGGTGGAGAACCTAGGACTTTATGCCGCTCT
AGAACTAGTGGATC

For detection of recombined *Cre* allele and endogenous *Tlr2* allele following PCR reaction was set up:

DNA	2 µl
10× Taq buffer	2.5 µl
25 mM MgCl$_2$	3 µl
dNTP (10 mM each)	0.5 µl
primer Tlr2_F	1 µl
primer Tlr2_R	1 µl
primer Cre_R	1 µl
Taq (1 U/µl)	0.5 µl
H$_2$O	13.5 µl

PCR program

95 °C 5′ 00′′
[95 °C 0′ 30′′
57 °C 0′ 30′′
72 °C 1′ 20′′] 33x
72 °C 5′ 00′′

Primer sequences

primer Tlr2_F	GAGACATCCTTGGTGAGCGT
primer Tlr2_R	CCAGAGAATAAAAGGCGTCTCC
primer Cre_R	TGCGAACCTCATCACTCGTT

4.2.2.4. Transformation of electrocompetent bacteria (EL250)

An isolated colony of EL250 bacteria was grown in 2 ml of LB/chloramphenicol (LB/CH) at 32°C ON. Next morning, 2 ml of starter culture was diluted in 100 ml of LB/CH and grown until it reached OD$_{600}$=0.5-0.6. The cultures were than centrifuged for 5 min at 3000 × g at 4°C. The pellet was then washed 2 times in 20 ml of ice cold H$_2$O and resuspended in 100 µl of ice cold H$_2$O. 3 µl of BAC DNA was mixed with 50 µl of bacteria and chilled on ice for 5 minutes. Upon transfer to a 0.2 cm cuvette, cells were electroporated (2.5 kV, 25 µF, 200 Ω). The transformed bacteria were transferred to 1 ml of LB and incubated at 32°C for 1 hour and then plated on a LB/CH plate and incubated for 20 hours at 32°C.

4.2.2.5. Homologous recombination in bacteria

EL250 bacteria containing the verified BAC clone were inoculated in 100 ml of LB/CH media and grown until the culture reached OD$_{600}$=0.5-0.6. Then the cultures were split to two halves and each 50 ml of culture was incubated in inducing (42°C) or non-inducing (0°C) conditions for 15 minutes. Electrocompetent bacteria were prepared as described earlier. Induced and noniduced cell were transformed with 1.5 µl of *Cre* and *Tlr2* homologous arms containing cassette. Colonies generated from induced transformed cultures were PCR screened for the presence of the recombined allele. Positive colonies were used to inoculate 50 ml LB/CHK cultures for BAC DNA isolation.

4.2.2.6. Exclusion of *Neo* cassette flanked by Frt sites

Colonies of the recombinant strain containing the correct insertion of the transgene with its selectable marker (Neo/K) flanked by Frt sites were grown at 32°C overnight in 3 ml of LB/CHK. 1 ml of the culture was diluted into 10 ml of LB/CHK and grown at 32°C until it reached an OD_{600}=0.6. Then, 100 µl of 10% filter-sterilized arabinose were added to a final concentration of 0.1% to induce the *flp* gene in EL250 strain. The culture was grown at 32°C for 1 hour and 100 µl of 10^{-3} and 10^{-4} dilutions were plated on LB/CH and LB/CHK plates and incubated at 32°C ON to reveal the efficiency of *Neo* cassette exclusion. The clones that lost the selectable marker by site-specific recombination were screened for antibiotic sensitivity by simultaneous plating on LB/CH and LB/CHK plates. The loss of *Neo* cassette was further validated by PCR.

4.2.2.7. Preparation of BAC DNA for pronuclear injection

Upon validation by diagnostic restriction enzyme digest and sequencing, the BAC construct was electoporated to DH10B strain, again validated and a large scale culture was set up for BAC DNA isolation using the Qiagen® Large-Construct Kit. The quality of obtained BAC DNA was analyzed by Pulse Field Gel Electrophoresis (PFGE) in 1% agarose gel (6 kV/cm, 120 °, 16 hours, 14°C) and the sequence was validated by PCR followed by sequencing. BAC DNA was diluted to 1 ng/µl in injection buffer (10mM Tris HCl, pH 7.0, 100 µM EDTA) and the pronuclear injection (PNI) was carried out at the Transgenic Unit of IMG.

4.2.2.8. Cell suspension preparation

Time pregnant females (the day that the vaginal plug was observed was designated as E0.5) were sacrificed by cervical dislocation and embryos from different stages of development were dissected from uteri. For FACS analysis, cells from E7.5-E8.5 dissected embryos were pooled from one litter. Embryos were washed in phosphate buffered saline (PBS) and dissociated using 1 mg/ml dispase (Invitrogen) in PBS for 10 min at 37°C with occasional gentle pipetting. Dispase was removed from cell suspensions by centrifugation of the cells followed by washing of the cells with 1% FCS in PBS. Embryonic suspensions were then passed through a 50 µm cell strainer.

4.2.2.9. Flow cytometry and cell sorting

After Fc receptor blocking by rat anti mouse CD16/32 antibody (2.4G2; Biolegend) single cell suspensions were stained with the following directly conjugated monoclonal antibodies: anti-CD11b-PE (M1/70; eBioscience), anti-CD45-PerCP or anti-CD45-A450 (30-F11; BD PharMingen), anti-B220-A647 (RA3-6B2; Biolegend), anti-ckit-PE (ACK2; eBioscience), anti-Ter119-PECy7 (TER-119; Biolegend). Biotin conjugated anti-TLR2

antibody (6C2; eBioscience) was detected with streptavidin (SA)-APC, SA-PECy7 or SA-Qdot605 (eBioscience). Fluorescence data were acquired using LSRII flow cytometer (BD Biosciences). Flow cytometry analyses were performed using FlowJo software (Tree Star). When possible, cell debris and dead cells were excluded from the analysis based on scatter signals and Hoechst 33258 (Sigma-Aldrich) fluorescence.

4.2.2.10. Tamoxifen administration

Tamoxifen solution was prepared as follows, for one dose, 2 mg of tamoxifen (T5648, Sigma) was resuspended in 80 μl ethanol and further dissolved in 320 μl sunflower oil (S5007, Sigma). This 1 mg/100 μl tamoxifen solution was shaken rigorously at 55°C. 200 μl of tamoxifen solution (1 mg/100 μl) was administered to time pregnant ROSA-YFP females crossed with *Tlr2-CreER^{T2}* males by oral gavage.

4.2.3. Results

4.2.3.1. Generation of *Tlr2 Cre* reporter mice

The workflow of this procedure is depicted in Figure 2. First step in this approach was the selection of BAC clones carrying the entire *Tlr2* gene and its regulatory elements from publically available repository (Children's Hospital Oakland Research Institute; CHORI, USA). A 180kb long BAC clone encompassing *Tlr2* gene with extensive upstream (46 kb) and downstream (123 kb) sequences (RP23-455F23) was obtained from BAC resource depository at CHORI.
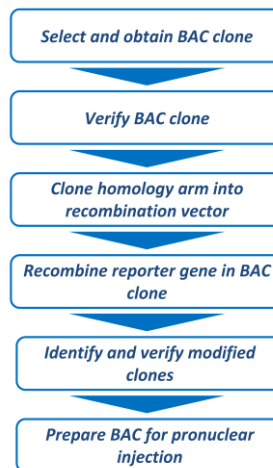
Figure 2. Diagram describing the process of generation of a BAC reporter, adopted from (Fu and Maye 2011).

Upon BAC clone verification (PCR, diagnostic restriction enzyme digest), the generation of recombinant construct with a selected type of reporter gene followed. To insert the reporter gene in the sequence of *Tlr2*, homology arms located a few nucleotides upstream of *Tlr2* gene translation start site and 3'downstream sequence were PCR-cloned into the reporter cassette *Cre-FRT-Neo-FRT* (gift from Dr. Kozmik) and *CreER^{T2}-FRT-Neo-FRT* (gift from Dr. Kořínek) respectively (Figure 3).
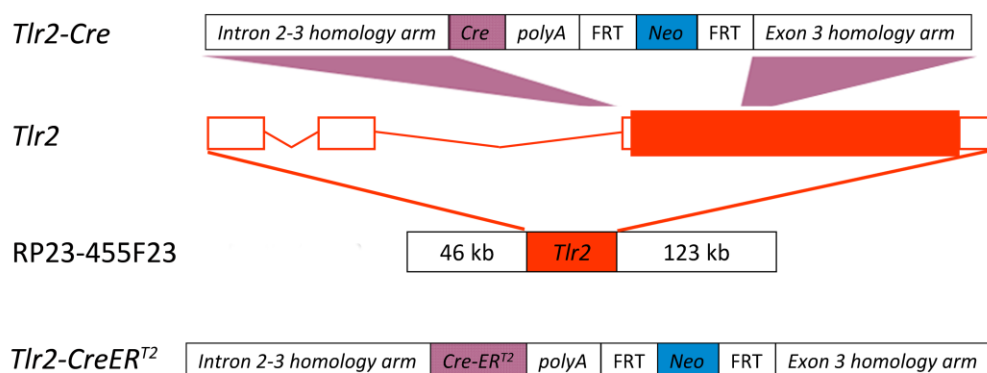
Figure 3. The schematic illustration of Tlr2-Cre and Tlr2-CreER^{T2} construct generation.
Cre and CreER^{T2} replaced the fist and only coding exon (exon3) of Tlr2 gene respectively.

This enabled its homology recombination in a bacterial strain where the gene recombination event was heat induced (strain EL250). Subsequently the selection marker (neomycin resistance (*Neo*), flanked with Frt sites), included in the cloning cassette, was removed by flipase (*flp*) the expression of which was induced by the addition of arabinose. The resulting transgenic BAC was then isolated and its integrity and quality verified (PCR, diagnostic restriction enzyme digest, sequencing, pulse field gel electrophoresis) before the pronuclear injection (PNI) (Sharan et al. 2009). The PNI (Figure 4) was carried out by the Transgenic Unit of the IMG, headed by Dr. Sedláček. In case of *Tlr2-Cre* construct, 3 PCR positive founders were found among 39 born mice and the transgene was transmitted to F1 progeny from 2 out of 3 founders. In case of *Tlr2-CreER^{T2}* construct, also 3 PCR positive founders were identified among 24 pups obtained. The *Tlr2-CreER^{T2}* transgene was transmitted to F1 progeny from two of these founders, the third founder being sterile. All founders were backcrossed to C57Bl/6N background.

The phenotype of F1 progeny was analyzed upon mating with reporter strains.
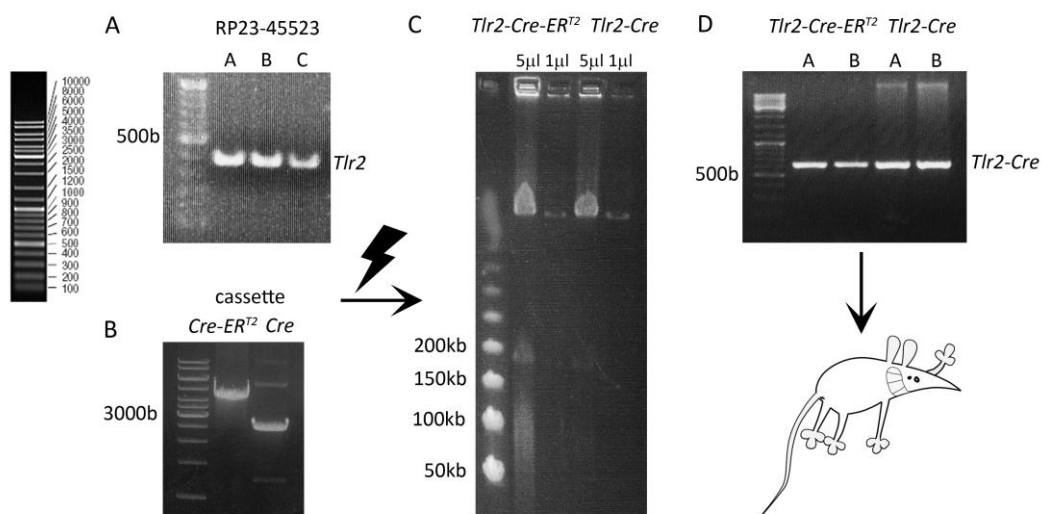
Figure 4. Generation of Tlr2 Cre recombinase constructs.
(A) The presence of Tlr2 gene in BAC RP23-45523 was verified by PCR. (B) To insert Cre recombinase in the sequence of Tlr2, homology arms located a few nucleotides upstream of Tlr2 gene translation start site and 3'downstream sequence were PCR-cloned into reporter cassettes CreER^{T2}-FRT-Neo-FRT and Cre-FRT-Neo-FRT respectively. This enabled its homology recombination in a bacterial strain where the gene recombination event was heat induced (strain EL250). (C, D) The resulting transgenic BAC was then isolated and its integrity and quality verified by pulse field gel electrophoresis and PCR before the pronuclear injection.

4.2.3.2. Visualization of TLR2 expression in *Tlr2-Cre* reporter strain

One of the crucial questions concerning the ontogenesis of hematopoietic system is whether HSCs or their progenitors originate from the EP or the YS. To visualize emerging cells with active *Tlr2* locus, we crossed the *Tlr2-Cre* males, where *Cre* recombinase is expressed under the control of *Tlr2* promoter and its regulatory elements, with *Rosa26-YFP* females (Srinivas et al. 2001). As a result, EYFP (hereafter referred to as YFP) fluorescence was detected in the cells where recombination occurred as well as in all their progeny (Figure 5).
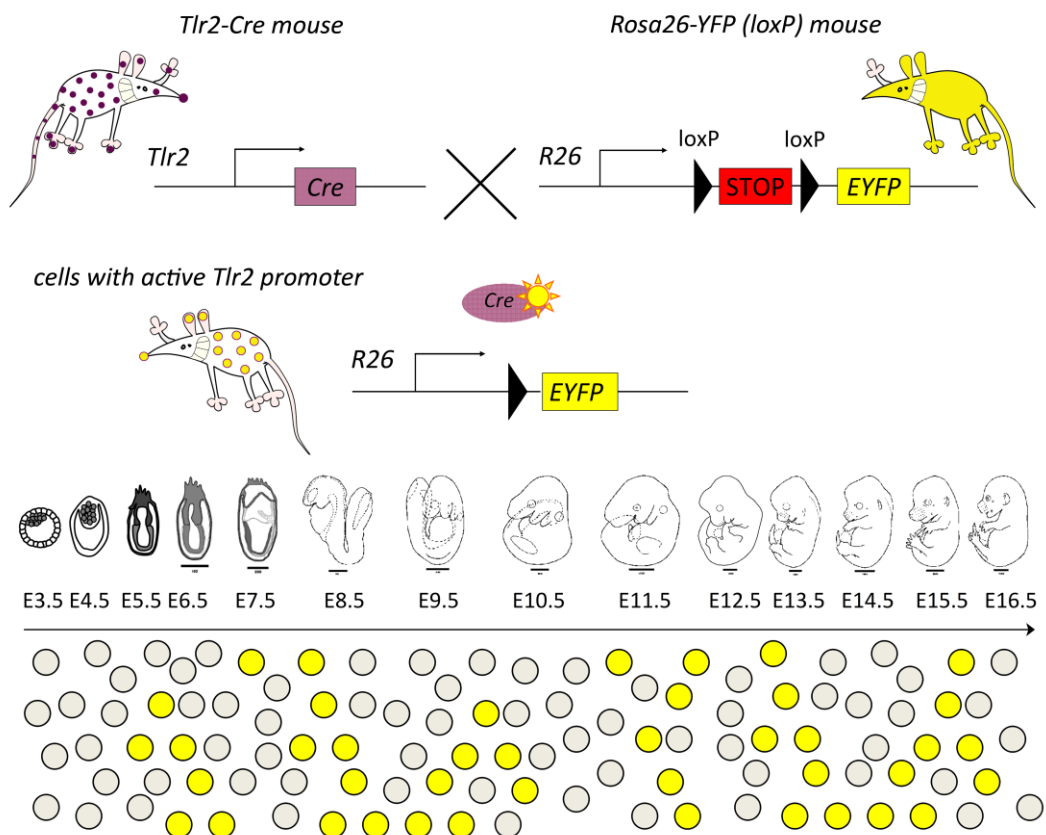
Figure 5. Visualization of cells with active Tlr2 locus using Tlr2-Cre mouse strain.
In Tlr2-Cre mice the Cre recombinase is expressed under the control of Tlr2 promoter. Upon breeding of Tlr2-Cre mouse with Rosa26-YFP mouse, Cre excises a transcription terminator preceeding EYFP flanked by loxP sites, thus allowing the expression of EYFP in cells with active Tlr2 promoter and all their progeny.

Indeed YFP positive cells were detectable as early as at E7.5 (Figure 6). At E7.5 most of the YFP+ cells were localized to the YS–EP boundary, close to the posterior primitive streak region. At E8.75, YFP+ cells showed a more disperse pattern, however a significant number of these cells localized to the head/brain region. In the context of previously published data describing that microglia derive from YS myeloid precursors and appear in the brain at E9.5 (Ginhoux et al. 2010), the head/brain localization of YFP+ cells suggests that these cell could represent microglia precursors.
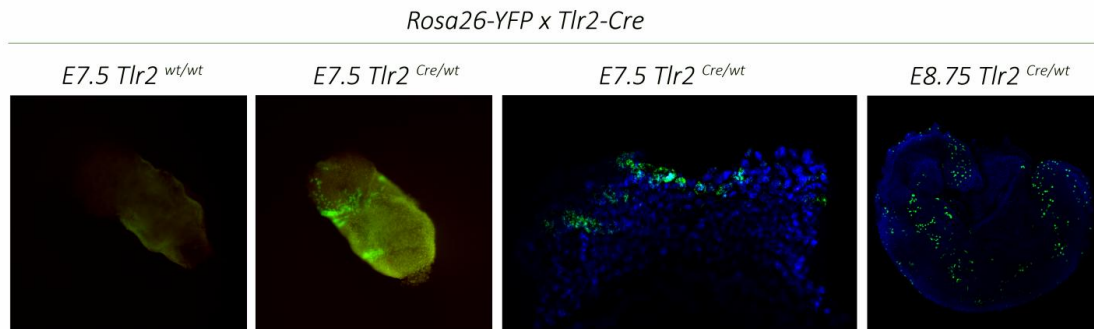
Figure 6. Visualization of cells with active Tlr2 promoter during embryogenesis.
Rosa26-YFP females were crossed to Tlr2-Cre males. YFP fluorescence in E7.5 and E8.75 F1 embryos was detected using Olympus SZX9 (zoom 6.3-57.0 x) fluorescence stereomicroscope (two left panels) or Nikon AZC1 confocal macroscope (two right panels). The magnification of middle left panel is shown in middle right panel. Scale bar represents 200 μm.

FACS analysis of E7.5-E8.5 YFP positive cells revealed that only less than 1% of them co-expressed TLR2 on their surface. Interestingly, most of YFP+ cells expressed the prototypical progenitor marker, c-kit. In addition to c-kit, most of E8.5 YFP+ cells coepressed the erythroid lineage marker Ter119 (Figure 7A). In the peripheral blood of adult animals all three main hematopoietic lineages (erythroid, myeloid and lymphoid) were identified in the pool of YFP+ cells with minor contribution to the erythroid lineage, suggesting the involvement of *Tlr2* promoter region activation in uncommitted hematopoietic precursors (Figure 7B). In peripheral blood of adult animals, YFP+ cells represented 11.6% (SD=4.9 n=3) of all viable cells and the majority of them coexpressed TLR2 on their surface (mean = 82.9%, SD= 6.2, n=3). The highest level of TLR2 surface expression was detected in the pool of CD11b+ myeloid cells, whereas lymphoid cells showed only low TLR2 expression (data not shown). Interestingly, when the distribution of individual hematopoietic lineages was compared in YFP+ and YFP- cells from the same sample, it appeared that in the pool of YFP+ cells, erythroid cells were much less abundant than CD45+ cells. Additionally, while myeloid cells were significantly enriched in the YFP+ fraction as compared to YFP- cells, no difference was found in the proportion of lymphoid cells (Figure 7C). These data suggest that the commitment of cells with active *Tlr2* locus is shifted towards the myeloid fate.
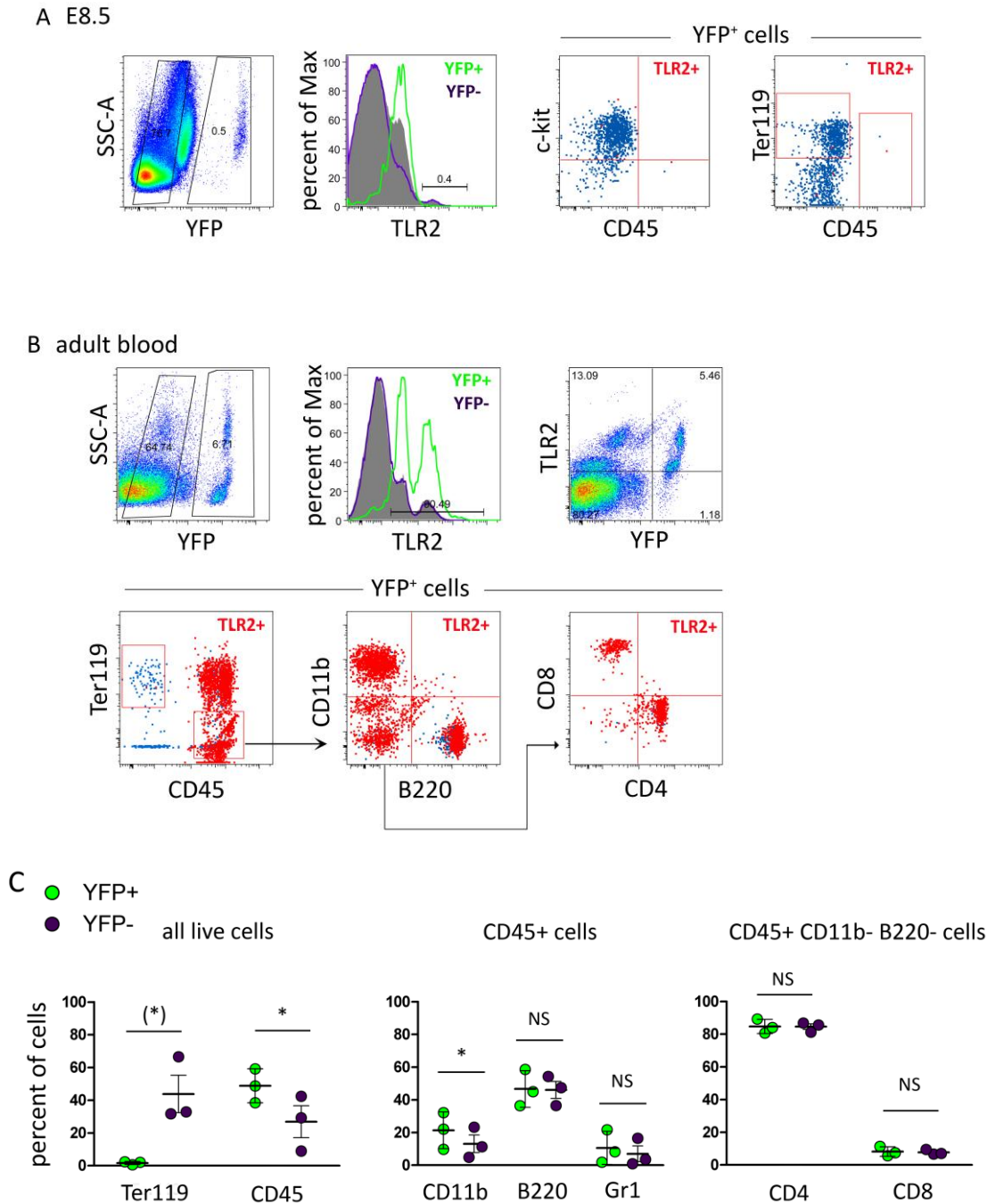
Figure 7. Phenotypic analysis of YFP⁺ cells derived fromF1 progeny of ROSA26-YFP mice crossed with Tlr2-Cre mice .

*Rosa26-YFP females were crossed to Tlr2-Cre males. The phenotype of YFP⁺ cells isolated from (A) E8.5 embryos or (B) peripheral blood of F1 adult mice was determined by FACS. The histogram shows surface expression of TLR2 in YFP⁺ cells (open green histogram) and YFP⁻ cells (open violet histogram) as compared to the signal derived from secondary reagent only (closed grey histogram). In double color dotplots, TLR2⁺ cells are highlighted in red color. (C) The relative abundanies of individual cell populations in Tlr2^{Cre/wt} (YFP⁺) cells as well as Tlr2^{wt/wt} (YFP⁻) cells were calculated based on FACS data. Percentage of Ter119⁺ and CD45⁺ cells among all live cells is shown in left panel, percentage of CD11b⁺, B220⁺ and Gr1⁺ cells in all CD45⁺ cells is shown in middle panel and percentage of CD4 and CD8 cells among all CD45⁺ CD11b⁻ B220⁻ cells is shown in right panel. p values were calculated using two tailed paired t-test; * pval ≤ 0.05, (*)pval ≤ 0.1.*

4.2.3.3. TLR2 lineage tracing using *Tlr2-CreER^T2* reporter strain

To track the developmental fate of embryonic TLR2+ cells, *Tlr2-CreER^T2* males were crossed with *Rosa26-YFP* females and the recombination in F1 progeny was induced by tamoxifen administration to pregnant dams by oral gavage at specific time points. In these experiments, YFP was expressed only in cells which at the time of induction attained active *Tlr2* promoter and transcribed the *Tlr2-CreER^T2* construct. This enabled genetic labeling (YFP expression) of cells with active *Tlr2* locus into a narrowly defined time-window of early embryonic development. Importantly, since all progenies of these cells retained YFP expression throughout entire lifespan, their lineage identity could be easily determined by FACS (Figure 8).
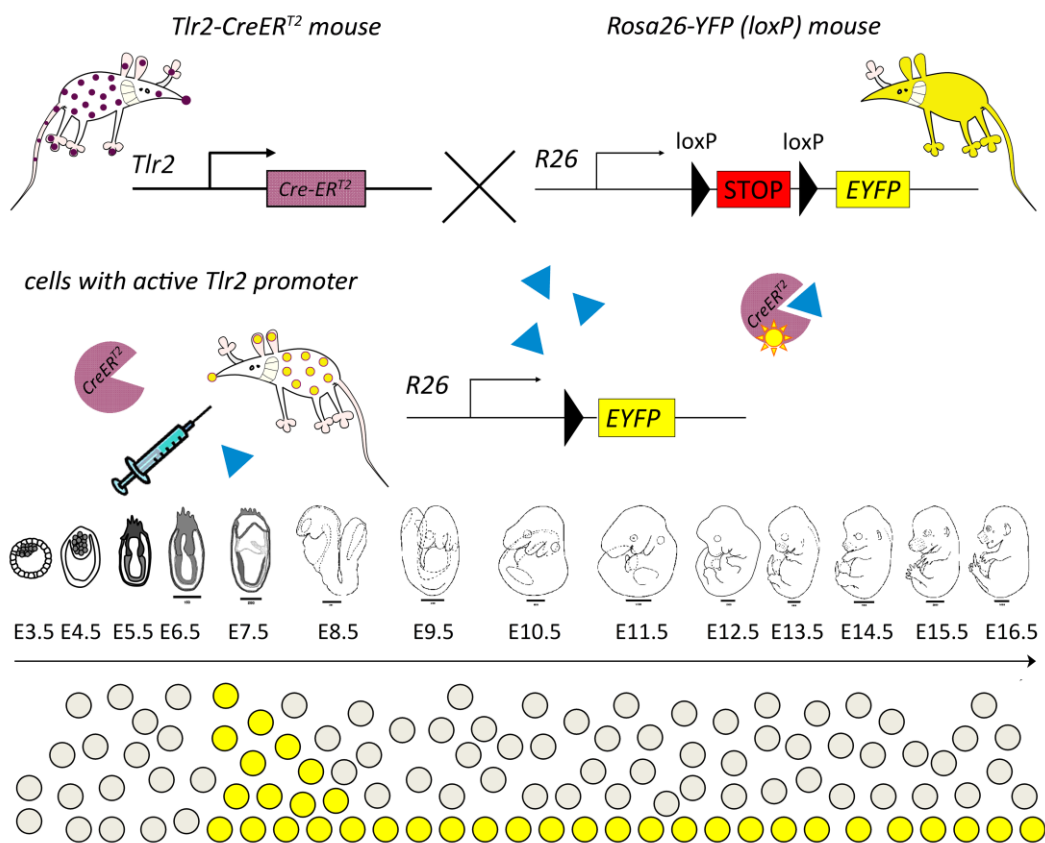
Figure 8. Lineage tracing of cells with active Tlr2 locus using Tlr2-CreER^T2 mouse strain.
In Tlr2-CreER^T2 mice the inactive Cre recombinase is expressed under the control of Tlr2 promoter. Upon breeding of Tlr2- CreER^T2 mouse with Rosa26-YFP mouse, the modified Cre is expressed in cells with active Tlr2 promoter and is retained in cytoplasm untill tamoxifen is administered. Only upon tamoxifen binding CreER^T2 translocates to the nucleus and removes a transcription terminator preceeding EYFP flanked by loxP sites allowing the expression of EYFP in cells with active Tlr2 locus and all their progeny.

In a pilot experiment, to test the efficiency of the inducible model, we crossed a Rosa26-YFP female with a Tlr2-CreER^{T2} male, induced the recombination in the pregnant dam by 5 mg of tamoxifen at E10.5 and assayed the recombination efficiency in the E12.5 fetal liver (Figure 9). 48 hours after tamoxifen treatment, 0.2% of E12.5 FL cells expressed YFP and thus represented the recombined cells. Additionally, more than 50% of YFP+ cells coexpressed TLR2 on their surface. In the pool of YFP+ cells we have identified myeloid cells (TLR2+ CD45+ CD11b+) as well as hematopoietic progenitors (TLR2+/− c-kit+ CD45−).
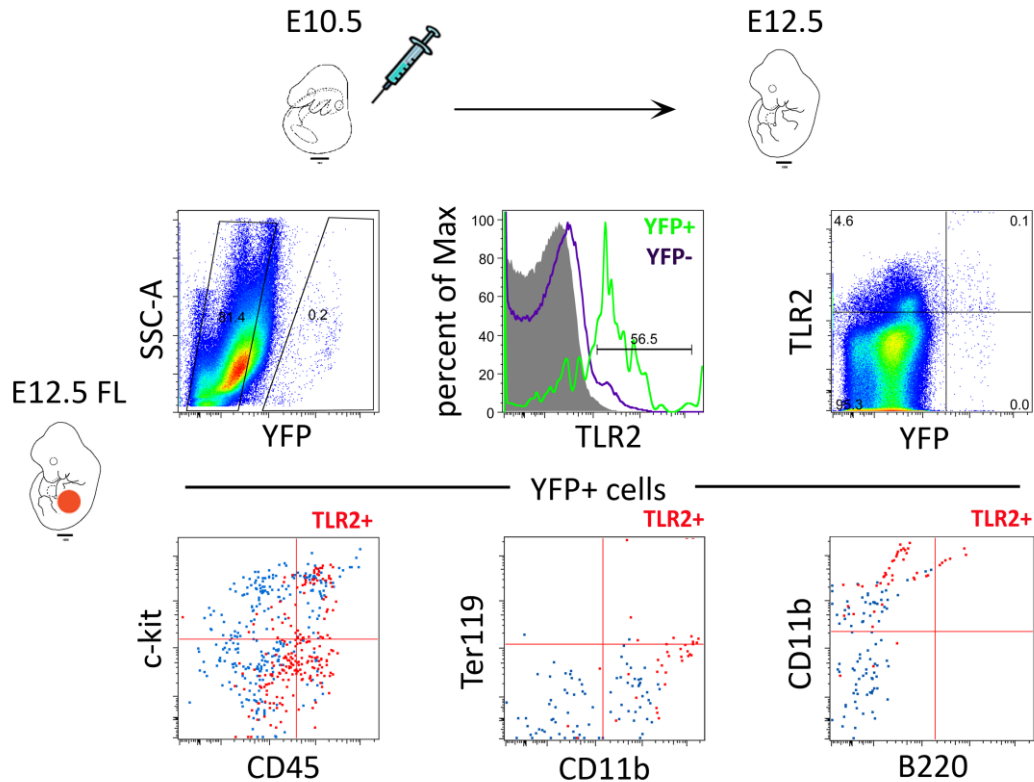
Figure 9. Tamoxifen induced Tlr2-dependent cell tagging at E10.5 analyzed after 48 hours.
Rosa26-YFP female was crossed with Tlr2-CreER^{T2} male. Tamoxifen was administered in a single dose (5 mg) at E10.5 to the pregnant dam by oral gavage. After 48 hours, embryos were harvested and fetal livers (FL) analyzed for the presence of YFP^{+} cells. The histogram shows surface expression of TLR2 in YFP^{+} cells (open green histogram) and YFP$^{−}$ cells (open violet histogram) as compared to the signal derived from secondary reagent only (closed grey histogram). In double color dotplots, TLR2^{+} cells are highlighted in red color.

When recombination was induced at E9.5 and embryos were analyzed at E16.5, we detected all main hematopoietic lineages (erythroid, myeloid and B-lymphoid) in the pool of YFP+ cells isolated from the FL (Figure 10). In contrast to the cells isolated from the FL, YFP+ cells found in peripheral tissues represented mainly differentiated CD45+ CD11b+ myeloid cells, resembling the phenotype of tissue macrophages.
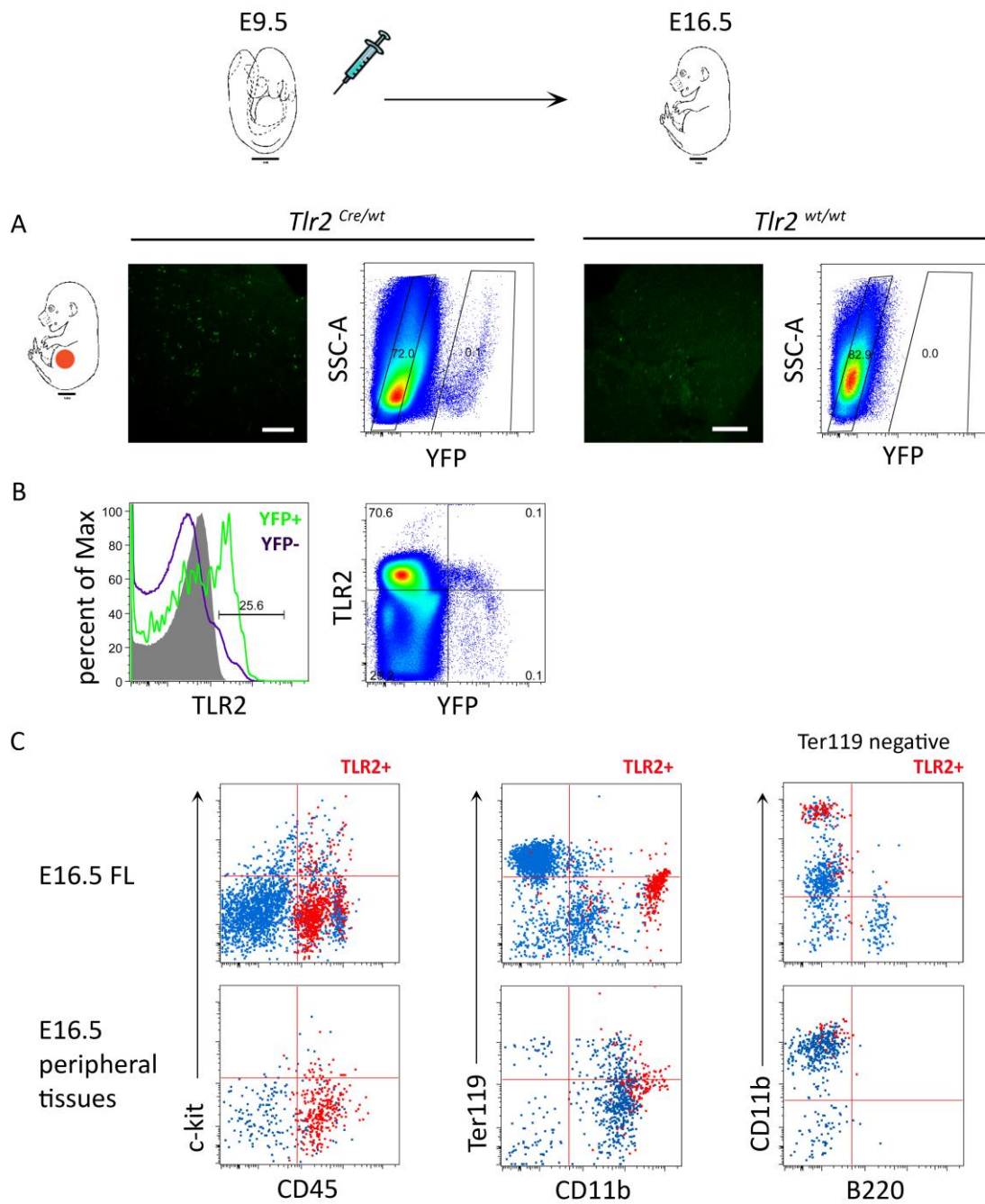
Figure 10. Tamoxifen induced Tlr2-dependent cell tagging at E9.5 marks all main hematopoietic lineages in E16.5 fetal liver.

Rosa26-YFP female was crossed with Tlr2-CreER^{T2} male. Tamoxifen was administered in a single dose (2 mg) at E9.5 to the pregnant dam by oral gavage. At E16.5 embryos were harvested and fetal livers analyzed for the presence of YFP$^+$ cells. (A) Confocal macroscope image and FACS analysis of E16.5 FL dissected from Tlr2$^{Cre/wt}$ and Tlr2$^{wt/wt}$ embryos. Scale bar 200 µm). (B) The histogram shows surface expression of TLR2 in YFP$^+$ cells (open green histogram) and YFP$^-$ cells (open violet histogram) as compared to the signal derived from secondary reagent only (closed grey histogram). (C) FACS analysis of expression of differentiation markers c-kit, CD45, Ter119, CD11b and B220 in E16.5 YFP$^+$ cells isolated from the FL or peripheral tissues. In double color dotplots, TLR2$^+$ cells are highlighted in red color.

Interestingly, induction of recombination at E6.75 resulted in similar amount of YFP labeled cells in the E16.5 FL. YFP$^+$ cells in the FL represented mainly TLR2$^-$ erythroid cells and TLR2$^+$ myeloid cells. In the E16.5 fetal thymus, YFP marked, apart from very few erythroid, myeloid and B-lymphoid cells, almost exclusively CD8$^+$CD4$^+$ thymocytes that should appear in the fetal thymus after E16.0 (Figure 11) (Zuniga-Pflucker and Lenardo 1996). These data suggest that early post-gastrulation cells with active *Tlr2* regulatory elements can contribute to all hematopoietic lineages.
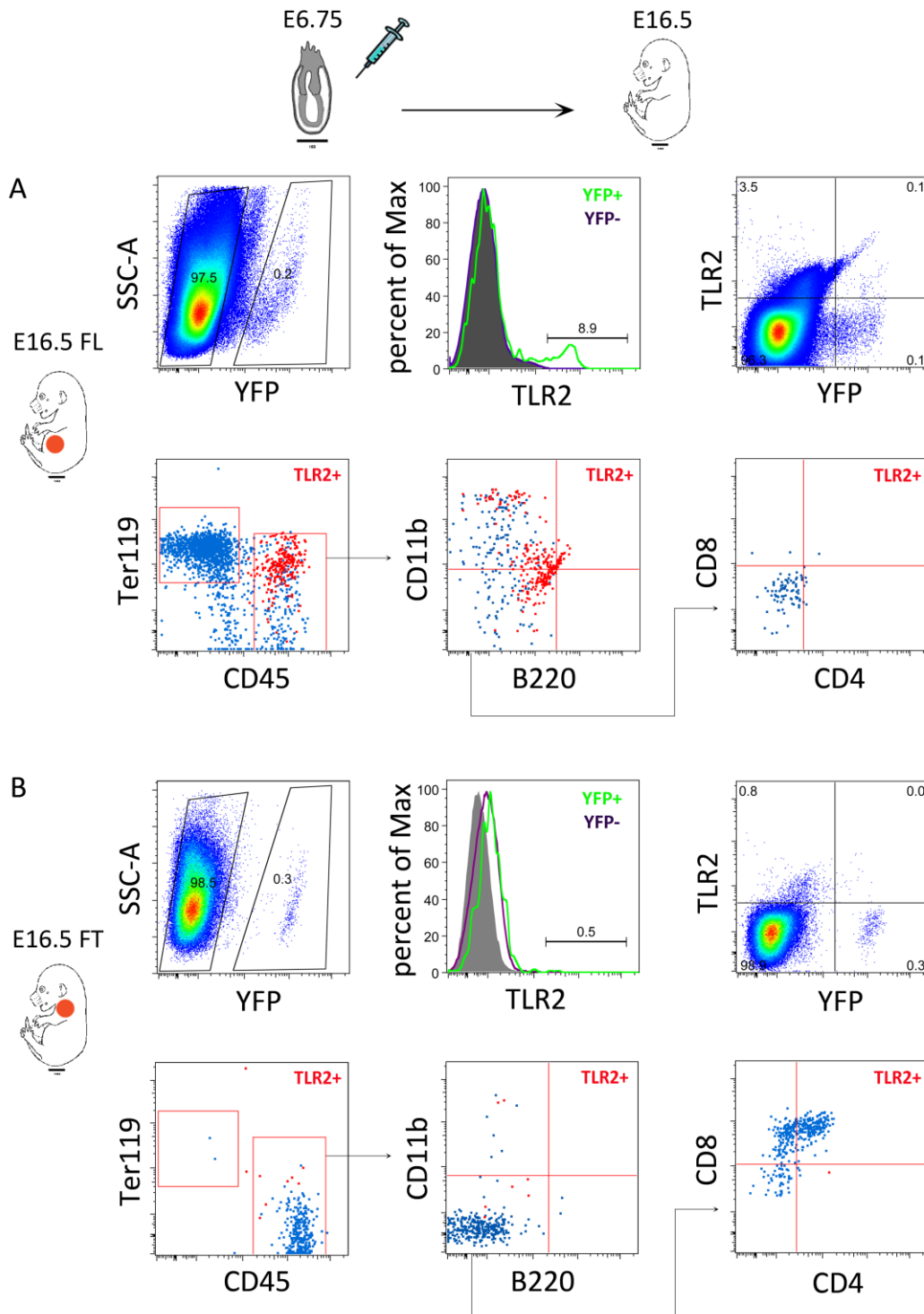
Figure 11. Tamoxifen induced Tlr2-dependent cell tagging at E6.75 marks all main hematopoietic lineages in E16.5 fetal liver and T cells in the fetal thymus.

Rosa26-YFP female was crossed with Tlr2-CreER^{T2} male. Tamoxifen was administered in a single dose (2 mg) at E6.75 to the pregnant dam. E16.5 embryos were harvested and fetal livers (FL, A) and thymi (FT, B) analyzed for the presence of YFP$^+$ cells. The surface expression of TLR2 as well as all main hematopoietic differentiation markers was analyzed in YFP$^+$ cells. The histogram shows surface expression of TLR2 in YFP$^+$ cells (open green histogram) and YFP$^-$ cells (open violet histogram) as compared to the signal derived from secondary reagent only (closed grey histogram). In double color dotplots, TLR2$^+$ cells are highlighted in red color.

4.2.4. Discussion

The generation of inducible TLR2 reporter mouse strain represents a unique and so far the only effective tool to reveal whether TLR2 expressing cells posses the potential to develop into *bona fide* HSCs and which developmental path they choose to follow. In addition the development of a mouse line expressing *Cre* recombinase under the control of endogenous promoter enabled us to visualize all cells with active *Tlr2* locus, including progenitors which have not yet started or just started to express TLR2. The selection of BAC recombineering as a method of choice enabled us a rapid development of two transgenic mouse strains. It took only 2 months for the first transgenic animals to be born since BAC stub receiving. The implementation of this method in our laboratory allowed us to widen the scope of our research. Moreover the *Cre* recombinase system enables specific *Tlr2*-promoter driven deletion of a number of genes upon breeding with transgenic mice where the gene of interest is flanked by *lox P* sites. Thus important transcription factors involved in early hematopoietic commitment like *Runx1* can be specifically deleted in the progeny of *Tlr2-Cre* mice bred with *Runx1tm3.1Spe* mice available from The Jackson Laboratory (Bar Harbor, ME, USA).

Using the constitutive *Tlr2-Cre* strain we were able to localize emerging recombined cells with active *Tlr2* locus to the E7.5 EP and EP-YS boundary. It is of note, that in three independent experiments performed so far at E7.5, YFP$^+$ cells were detected only in one litter and YFP was expressed only in one embryo out of three *Tlr-Cre* PCR positive embryos. These data suggest that E7.5 could be the earliest time point for detection of recombined cells and thus YFP fluorescence might not be detected at this time point. The one day delay in appearance of these cells in comparison to TLR2$^+$ cells detected at E6.5 embryo by FACS, likely reflects the time needed for the production of active *Cre* recombinase followed by rearrangement of STOP cassette, YFP synthesis and folding. Such a delay in YFP expression has been previously observed in another study with similar setup and was further prolonged when inducible *Cre* was used (Yona et al. 2013).

While E7.5-E8.5 YFP$^+$ cells represented mainly erythroid cells and c-kit$^+$ hematopoietic precursors, the progeny of these cells repopulated all main hematopoietic lineages in the adult peripheral blood (erythroid, myeloid and lymphoid). These data revealed an unexpected involvement of *Tlr2* locus activation in hematopoietic lineages that either don't express or express very low levels of surface TLR2 (erythroid and lymphoid cells). However, when proportions of distinct hematopoietic lineages were compared in YFP$^+$ and YFP$^-$ cells in the adult blood, myeloid cells clearly dominated the pool of YFP$^+$ cells upon endogenous *Tlr2* dependent recombination. In addition, myeloid YFP$^+$ cells expressed the highest levels of surface TLR2. Together these data confirmed our *in vitro*

data which suggest that hematopoietic progenitors with an active *Tlr2* locus exhibited enhanced myeloid differentiation.

Lineage tracing experiments performed with the inducible *Tlr2-CreER^T2* strain revealed that cells with active *Tlr2* regulatory elements contribute to all hematopoietic lineages and hence suggest their importance at the onset of hematopoiesis. When *Cre* recombination was induced in early post-gastrulation embryos at E6.75, YFP+ cells were traced not only in E16.5 FL erythroid and myeloid lineages but also in double positive fetal thymocytes. This finding points to the enormous plasticity of early post-gastrulation hematopoietic progenitors. While additional experiments, such as the engraftment of E6.5 induced hematopoietic progenitors in adult irradiated host, are required to bring more information on this issue, our data provide the very first evidence that early hematopoietic progenitors with an active *Tlr2* locus can contribute to the pool of hematopoietic stem cells. Alternatively, cells with an active *Tlr2* locus could overlap with lymphomyeloid-restricted progenitors undergoing extensive lymphoid transcription priming in the E9.5 YS, before the emergence of definitive HSCs and establishment of FL hematopoiesis (Yoshimoto et al. 2012; Böiers et al. 2013). While the lymphoid priming of these HSC-independent progenitors was so far back-traced to E9.5 (Böiers et al. 2013), our data suggest that progenitors at ~ E7.5, irrespective of their localization, could be already committed to this fate.

What remains to be determined is the kinetics of embryonic hematopoietic and peripheral tissues colonization of *Tlr2*-tagged cells starting at E6.5 and their single cell profiling that could elucidate the role of these progenitors at the onset of hematopoiesis.

4.3. Toll-like receptors expressed on embryonic macrophages couple inflammatory signals to iron metabolism during early ontogenesis.

In this study we have, for the very first time, shown that a full spectrum of Toll like receptors is expressed in E10.5 embryonic macrophages. We have also demonstrated that TLRs on the surface of E10.5 macrophages are fully functional and respond to triggering by production of inflammatory cytokines in a *MyD88*- and *Trif*-dependent manner. Using a comparative mRNA microarray, we have determined differences in the expression pattern between E10.5 embryonic macrophages and adult peritoneal macrophages as well as embryonic non-macrophage cells. Based on our original data and their comparison with recent results published by Schulz at al. (Schulz et al. 2012), we have concluded, that the general transcription profile of *Tlrs* and their adaptors (with few exceptions) in all macrophage populations analyzed is largely independent of their origin, location and developmental stage and thus is common for all myeloid cells tested. We have also shown that E10.5 embryonic macrophages are equipped with protein machinery essential for iron recycling. Additionally, iron metabolism in embryonic macrophages can be directly controlled by *Tlr* engagement in a *MyD88*-dependent manner.

Toll-like receptors expressed on embryonic macrophages couple inflammatory signals to iron metabolism during early ontogenesis

Jana Balounová[1,2], Tereza Vavrochová[1,2], Martina Benešová[1], Ondřej Ballek[1,2], Michal Kolář[3] and Dominik Filipp[1]

[1] Laboratory of Immunobiology, Institute of Molecular Genetics AS CR, Prague, Czech Republic
[2] Department of Cell Biology, Faculty of Science, Charles University in Prague, Prague, Czech Republic
[3] Laboratory of Genomics and Bioinformatics, Institute of Molecular Genetics, Czech Academy of Science, Prague, Czech Republic

Mammalian TLRs in adult animals serve indispensable functions in establishing innate and adaptive immunity and contributing to the homeostasis of surrounding tissues. However, the expression and function of TLRs during mammalian embryonic development has not been studied so far. Here, we show that CD45$^+$ CD11b$^+$ F4/80$^+$ macrophages from 10.5-day embryo (E10.5) co-express TLRs and CD14. These macrophages, which have the capability to engulf both apoptotic cells and bacteria, secrete a broad spectrum of proinflammatory cytokines and chemokines upon TLR stimulation, demonstrating that their TLRs are functional. Comparative microarray analysis revealed an additional set of genes that were significantly upregulated in E10.5 TLR2$^+$ CD11b$^+$ macrophages. This analysis, together with our genetic, microscopic, and biochemical evidence, showed that embryonic phagocytes express protein machinery that is essential for the recycling of cellular iron and that this expression can be regulated by TLR engagement in a MyD88-dependent manner, leading to typical inflammatory M1 responses. These results characterize the utility of TLRs as suitable markers for early embryonic phagocytes as well as molecular triggers of cellular responses, the latter being demonstrated by the involvement of TLRs in an inflammation-mediated regulation of embryonic homeostasis via iron metabolism.

Keywords: Embryonic macrophages · Ferroportin · Gene expression microarray · Iron metabolism · TLR stimulation

▣ Additional supporting information may be found in the online version of this article at the publisher's web-site

Introduction

Macrophages are evolutionarily the oldest and most critically important immune cells, yet the understanding of their role during embryonic development is still incomplete. There is evidence that embryonic macrophages engulf effete cells and secrete a wide range of growth factors, cytokines, and chemokines, thus promoting tissue remodeling and organogenesis [1]. Consistent with these data, gene expression profiling of fetal macrophages revealed their phenotype associated with homeostatic and trophic functions in developing organs [2].

Correspondence: Dr. Dominik Filipp
e-mail: dominik.filipp@img.cas.cz

www.eji-journal.eu

Recent studies have suggested that an early embryo is colonized by three major waves of macrophages that differ in their origin. The first population of macrophages, which appears in the extraembryonic yolk sac (YS) at embryonal day 7.5 (E7.5) are maternally derived CD45$^+$ ckit$^-$ phagocytes [3]. This population is only transient and at E8.5–9.5 is replaced by the first wave of embryonic CD45$^-$ ckit$^+$ macrophage progenitors developing in the YS [3]. These macrophages, together with primitive erythrocytes and megakaryocytes, are derived from hematopoietic cells that emerge from hemangioblast precursors in the YS around E7.25 [4–6]. Although YS hematopoiesis is transient and limited to the embryonic stage, recent data have demonstrated that YS-derived myeloid precursors differentiate into tissue resident macrophages and persist throughout adulthood [7–9]. Lastly, as definitive hematopoiesis from hematopoietic stem cells is established in the aorta-gonad-mesonephros (AGM) region in the embryo proper, a third wave of distinct adult AGM-derived macrophages subsequently develops in the niches of fetal liver and spleen after E12.5 [9–12].

This origin-related heterogeneity among early embryonic phagocyte subpopulations makes it challenging to assess their roles in early development. However, due to the transient nature and early disappearance of maternally derived macrophages at E9.5 on one hand and only a relatively late appearance of AGM-derived macrophages (≥E12.5) on the other, the presence of a single, YS-derived population of macrophages in E10.5 embryo makes this population an attractive and readily accessible model of early embryonic macrophage development and function. Despite some advances, there is only a limited amount of information about the role of YS-derived macrophages in the regulation of homeostasis in a developing embryo. It is also uncertain if the molecular structures and signaling modules described as essential for the function of adult macrophages are also expressed and involved in these homeostatic processes.

TLRs are critically important in triggering immune responses to infections [13]. Upon interaction with their ligands, which are derived from conserved microbial structures, several signaling pathways are initiated resulting in global changes in gene expression [14]. This, in turn, leads to effective innate immune responses and regulated development of Ag-specific immunity [15]. In addition, there is a growing body of evidence that TLRs can also sense the presence of endogenous ligands, which are induced by stress, necrosis, aseptic injury, and irritation, implicating their involvement in sterile physiological inflammation [16, 17]. All TLRs signal through the intracellular adaptor protein MyD88 which, in general, induces the expression of proinflammatory cytokines [18]. The exceptions is TLR3 that signals solely via the adaptor protein Trif, and TLR4 that uses Trif in the combination with MyD88, to elicit IFNs as well as proinflammatory cytokines [19, 20]. Macrophages, which express the greatest variety of TLRs, can in peripheral tissues polarize into classically activated (M1) and alternatively activated (M2) phenotypes [21]. By sensing environmental cues associated with infection and inflammation, TLR signaling can trigger this polarization program toward the M1 phenotype associated with their capacity to store

iron, thus exhibiting bacteriostatic properties [22–26]. Conversely, in M2 macrophages, due to the efficient recycling of iron and its release into the microenvironment, its intracellular levels are kept at low levels.

Whether early embryonic macrophages also express TLRs and if so, what is their potential function, have not been explored so far. Here, we investigated the expression and cellular distribution of TLRs in E10.5 embryos and assessed their signaling competence. Our data also provide insight into the contribution of YS-derived embryonic macrophages to organismal homeostasis where TLRs could play a regulatory role in the integration of immune-related signals with the essential metabolic needs of developing embryos.

Results

Embryonic macrophages express TLRs

Flow cytometric analysis of E10.5 embryos revealed that TLR2 and TLR4 were almost exclusively expressed on the surface of CD11b$^+$ CD14$^+$ F4/80$^+$ CD45$^+$ cells of the macrophage phenotype (Fig. 1A), which represent approximately 1% of the total mass of embryonic cells. While CD11b is recognized as a prominent surface marker of embryonic macrophages [27], additional expression of CD14 on these cells has not been previously shown. It is of note that E10.5 TLR2$^+$ CD11b$^+$ cells do not express the granulocyte surface marker Gr-1 (Supporting Information Fig. 1A). These results demonstrated that at this developmental stage, nearly all cells expressing the hematopoietic marker CD45 represent TLR2$^+$ TLR4$^+$ CD11b$^+$ F4/80$^+$ CD14$^+$ embryonic macrophages. Importantly, strict gating on CD11b and TLR2 markers (Supporting Information Fig. 1B) resulted in a subset where ≥99% of cells co-expressed all macrophage markers tested, thus providing an efficient sorting strategy to distinguish embryonic macrophages.

E10.5 TLR2$^+$ CD11b$^+$ macrophages express a full spectrum of *Tlrs* and *Tlr* adaptor proteins

To evaluate whether the expression of all *Tlrs* and their adaptors is restricted to embryonic macrophages, we quantified their mRNA expression. qRT-PCR analysis of FACS-sorted E10.5 TLR2$^+$ CD11b$^+$ (double positive, DP; Supporting Information Fig. 1C) and TLR2$^-$CD11b$^-$ cells (double negative, DN; Supporting Information Fig. 1C) revealed that *Tlr* transcripts were significantly enriched in the former. Notably, as shown in Figure 1B, the expression of *Tlr1, 2, 4, 6, 7, 8,* and *9* was approximately 30–3000 times higher in DP than in DN cells. A three- and tenfold difference in expression levels was revealed for two other receptors, *Tlr5* and *Tlr3*, respectively. The expression of *Tlr12* was roughly equal in DP and DN cells. The only exception was *Tlr11*, which exhibited higher expression in DN cells, however, barely detectable levels were found in both types of cells (Supporting Information Fig. 1E). Importantly, as demonstrated in Figure 1A, a 50- to 100-fold
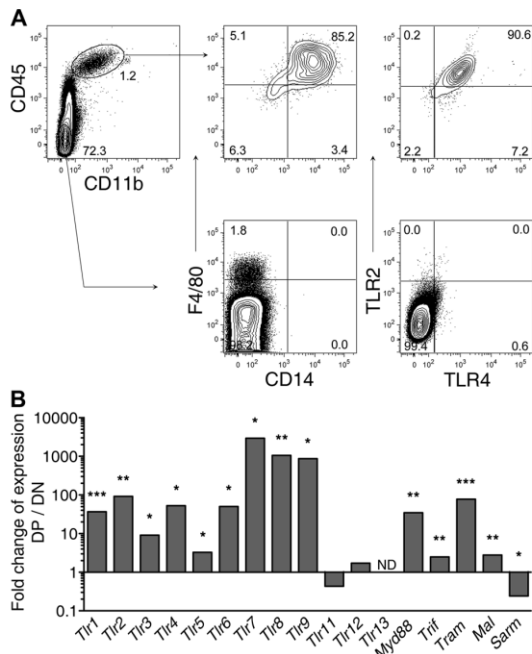
Figure 1. E10.5 TLR2^{+} CD11b^{+} macrophages express a full spectrum of *Tlrs* and *Tlr* adaptor proteins. (A) E10.5 embryonic macrophages express TLR2 and TLR4. A cell suspension from whole E10.5 embryos was stained for the panhematopoietic marker CD45, macrophage markers CD11b, CD14, F4/80, TLR2, and TLR4 and analyzed by flow cytometry. Analyzed gates are indicated. (B) The expression of *Tlrs* and *Tlr* adaptor protein mRNAs was analyzed in double positive (DP) E10.5 TLR2^{+} CD11b^{+} and double negative (DN) TLR2^{−} CD11b^{−} populations by qRT-PCR, normalized to *Casc3* mRNA levels, and plotted as fold change of expression (DP/DN). Data are representative of three independent experiments. *$p < 0.05$, **$p < 0.001$, ***$p < 0.001$, Student's paired *t*-test with Welch approximation; ND: under detection limit.

difference in *Tlr2* and *Tlr4* transcript levels was sufficient to distinguish TLR-positive DP from DN cells on the protein level.

Similarly, the adaptor proteins *Tram* and *Myd88* displayed approximately 80- and 35-fold higher expression in DP versus DN cells, respectively. The expression of *Trif* and *Mal* in DP seemed to be only three times higher than in DN. In contrast, the expression of the adaptor protein *Sarm*, previously shown to be associated with a nonimmune function in neuronal cells [28, 29], was increased about five times in DN cells. The normalized relative expression of all TLRs and their adaptors in DP versus DN cells is summarized in Supporting Information Fig. 1E.

TLRs expressed on E10.5 embryonic macrophages are signaling competent

To confirm the phagocytic nature of embryonic DP cells, we confirmed their capacity to engulf apoptotic as well as bacterial cells in vitro (Fig. 2A and B, and Supporting Information Fig. 2A and B). Furthermore, we tested whether TLRs expressed on these cells
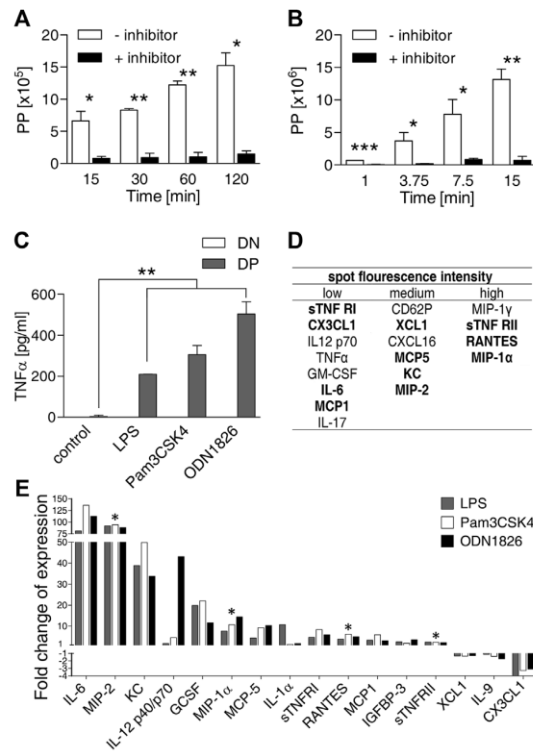
Figure 2. Embryonic TLR2^{+} CD11b^{+} (DP) cells engulf both apoptotic cells and bacteria and produce proinflammatory cytokines upon TLR stimulation in vitro. (A, B) The phagocytosis product of E10.5 TLR2^{+} CD11b^{+} cells was measured by flow cytometry after the addition of (A) opsonized CFSE-labeled apoptotic cells or (B) tdTomato expressing *E. coli* for the indicated time in the presence or absence of phagocytosis inhibitor cytochalasin D. Data are shown as mean + SD of three samples and are from a single experiment representative of three independent experiments. *$p \leq 0.05$, **$p \leq 0.01$, ***$p \leq 0.001$, Student's paired *t*-test with Welch approximation. (C) TNF-α secretion was measured by ELISA in supernatants harvested from FACS-sorted E10.5 DP and TLR2^{−} CD11b^{−} (DN) cells cultured in the presence or absence of LPS, Pam3CSK4, or ODN1826 for 18 h. Data are shown as mean + SD of three samples and are from one experiment representative of two independent experiments performed. **$p \leq 0.01$, Welch two-sample *t*-test. (D, E) E10.5 DP cells were cultured in the presence or absence of TLR1/2, TLR4, and TLR9 agonists for 18 h. Supernatants were analyzed for the presence of a broad range of cytokines using RayBio Mouse Cytokine Antibody Array. Data are from one experiment and are representative of two independent experiments performed. (D) The basal level of cytokine secretion in unstimulated cells is categorized as low (less than 1%), medium (1–10%), or high (more than 10% of the highest intensity signal on the chip after stimulation). Cytokines differentially secreted by stimulated cells are printed in bold. (E) Fold change in protein secretion after stimulation with TLR ligands. Cytokines highly secreted by unstimulated cells are marked by an asterisk.

are functionally wired by assessing their cytokine response to TLR stimulation. Notably, using ELISA, we determined the amount of TNF-α in supernatants of FACS-sorted E10.5 DP and DN cells after stimulation with TLR1/2, TLR4, and TLR9 ligands. Only the activation of the DP population, irrespective of the ligand used, led to a significant increase in the production of TNF-α compared

with that in unstimulated controls; the secretion of this cytokine was undetectable in DN cells regardless of the type of TLR stimulation (Fig. 2C). This finding led us to investigate the cytokine response of E10.5 DP phagocytes in response to various MyD88-dependent TLR ligands using a semiquantitative cytokine Ab array. As shown in Fig. 2D, several cytokines such as MIP-1α, MIP-1γ, RANTES, and sTNFRII were produced in relatively large quantities even in unstimulated cells. In addition, stimulation with TLR1/2, TLR4, and TLR9 ligands resulted in the enhanced secretion of IL-6, MIP-2, KC, IL-12, GCSF, MIP-1α, MCP-5, IL-1α, sTNFRI, RANTES, and MCP1 (Fig. 2E). In contrast, the production of lymphotactin (XCL1), IL-9, and fractalkine (CX3CL1) was slightly reduced in TLR agonist-treated cells.

When E10.5 TLR2$^+$ CD11b$^+$ macrophages derived from WT or MyD88-deficient animals were stimulated with polyI:C ligand, which acts exclusively via TLR3-Trif pathway, the significant upregulation of *Tnfα* and *Ifnβ* mRNA expression was found to be independent of MyD88 (Supporting Information Fig. 2C). However, and consistent with previously published data [30], the production of these cytokines mediated by TLR2-MyD88 signaling, was ameliorated on a MyD88-deficient background. Thus, Trif-dependent TLR signaling in E10.5 DP cells is also fully operational. Together, these results demonstrated that TLRs expressed on early embryonic phagocytes are functional and their engagement leads to the secretion of a set of cytokines and chemokines.

Comparative microarray analyses of E10.5 TLR2$^+$ CD11b$^+$ embryonic phagocytes

To identify distinct molecular determinants of E10.5 DP macrophages, their mRNA profile was independently compared with that of adult TLR2$^+$ CD11b$^+$ peritoneal macrophages (peritoneal macrophage DP) and to embryonic nonphagocytic E10.5 DN cells. The gating strategy for peritoneal macrophage DP is shown in Supporting Information Fig. 1D. According to selected criteria (FC > 2 and false discovery rate less than 0.1), 1302 and 1017 transcripts were significantly enriched in E10.5 DP versus peritoneal macrophage DP and E10.5 DP versus E10.5 DN cells, respectively (Fig. 3). The lists of these upregulated, as well as downregulated genes (not analyzed in this study) are provided in Supporting Information Table 2 (E10.5 DP versus peritoneal macrophage DP) and Supporting Information Table 3 (E10.5 DP versus E10.5 DN). Among these transcripts, 159 genes were found to be upregulated in embryonic DP cells in both comparisons (Fig. 3). Based on available information related to the ontology of each gene, that is, its function, localization, and biological process (NCBI Entrez Gene database (http://www.ncbi.nlm.nih.gov/gene) and the software DAVID [31, 32]) we chose 47 genes for further qRT-PCR validation. As a result, 16 genes, namely *Cx3cr1, Mpo, Slco2b1, Mrc1, Gas6, P2ry13, Coro1a, Msr2, Stab1, Gm4980, Gpr84, Tnni2, Fpn1, Gpr114, Maf,* and *Dab2* (Table 1), were confirmed to display an enhanced expression in embryonic DP macrophages as compared
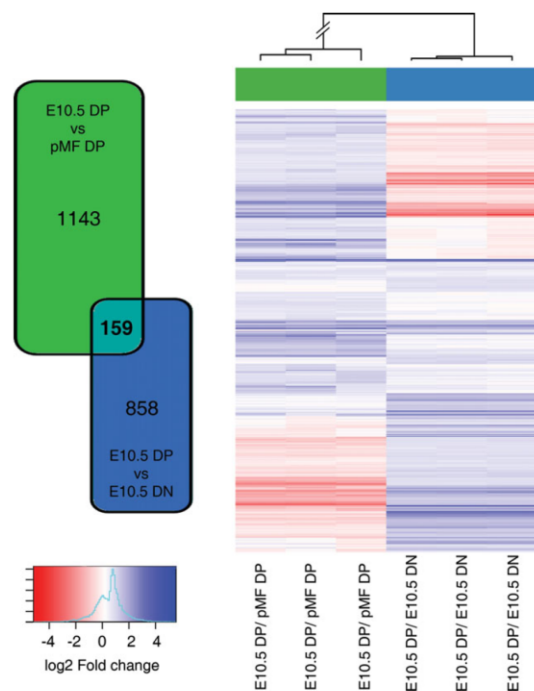
Figure 3. The identification of genes upregulated in E10.5 TLR2$^+$ CD11b$^+$ macrophages. Expression profiles of E10.5 TLR2$^+$ CD11b$^+$ cells (DP) were compared with that of TLR2$^+$ CD11b$^+$ peritoneal macrophages (pMF DP) or to E10.5 TLR2$^-$ CD11b$^-$ cells (DN). In total, 1302 and 1017 transcripts were significantly enriched in DP cells as compared with peritoneal macrophage DP (green) and DN cells (blue), respectively. Overlapping 159 genes were found to be upregulated in both analyses. Color scale denotes log$_2$ FC in the respective experiments, where three independent samples in each group were analyzed.

with that in embryonic DN cells and adult peritoneal macrophage DP cells (Supporting Information Fig. 3A).

Among these 16 genes, six encode surface proteins, notably *Fpn1, Stab1, Cx3cr1, Mrc1, Slco2b1,* and *Msr2*. We tested first four of these Ags and demonstrated that their surface expression was considerably higher on E10.5 DP cells in comparison to adult peritoneal macrophage (Fig. 4A).

Since the gene *Fpn1* (*Slc40a1, Ireg1, Mtp1*), encoding for ferroportin, is critically important for the metabolism of iron [33] and its expression on embryonic macrophages has not been reported so far, we looked at the subcellular distribution of ferroportin in E10.5 macrophages using confocal microscopy. As illustrated in Fig. 4B, upper panel, the accumulation of the *Fpn1* gene product in DP cells, observed preferentially associated with intracellular vesicles but also, albeit less intensively, on the plasma membrane, is consistent with its active role in iron recycling, as previously reported [33–35]. In agreement with flow cytometric data, *Fpn1* expression in peritoneal macrophages was barely detectable (Fig. 4B, bottom panel).

To assess whether and how the continuity of *Fpn1* expression is maintained during the earlier stages of embryonic

Table 1. Selected genes upregulated both in E10.5 DP cells compared to pMF and in E10.5 DP cells compared to E10.5 DN cells.

Entrez gene ID	Symbol	Definition	E10.5 DP versus pMF			E10.5 DP versus E10.5 DN			Rank[a]
			$\log_2$ FC	p-Value	q-Value (FDR)	$\log_2$ FC	p-Value	q-Value (FDR)	
13051	Cx3cr1	Chemokine (C-X3-C) receptor 1	8.49	3.03×10^{-9}	2.72×10^{-6}	7.67	1.03×10^{-5}	0.00025	1
17523	Mpo	Myeloperoxidase	8.21	1.67×10^{-8}	6.97×10^{-6}	6.92	6.27×10^{-7}	7.69×10^{-5}	2
101488	Slco2b1	Solute carrier organic anion transporter family, member 2b1	7.85	3.06×10^{-9}	2.72×10^{-6}	6.08	8.63×10^{-7}	8.43×10^{-5}	3
17533	Mrc1	Mannose receptor, C type 1	4.46	0.0002	0.00106	7.76	1.22×10^{-5}	0.00028	4
14456	Gas6	Growth arrest specific 6	6.58	3.50×10^{-7}	2.66×10^{-5}	4.64	1.71×10^{-7}	4.25×10^{-5}	5
74191	P2ry13	Purinergic receptor P2Y, G-protein coupled 13	4.6	0.00057	0.00225	6.09	1.05×10^{-7}	3.90×10^{-5}	6
12721	Coro1a	Coronin, actin binding protein 1A	4.17	6.92×10^{-5}	0.00052	5.71	7.19×10^{-6}	0.00021	7
80891	Msr2	Fc receptor-like S, scavenger receptor	3.93	7.32×10^{-5}	0.00054	5.6	2.43×10^{-6}	0.00012	8
192187	Stab1	Stabilin 1	4.18	0.00122	0.00387	5.11	2.20×10^{-6}	0.00012	9
100503386	Gm4980	Predicted gene 4980	4.33	3.69×10^{-5}	0.00034	4.64	3.66×10^{-5}	0.00053	10
80910	Gpr84	G-protein coupled receptor 84	3.9	3.11×10^{-6}	8.25×10^{-5}	4.59	1.45×10^{-9}	1.66×10^{-5}	11
21953	Tnni2	Troponin I, skeletal, fast 2	4.1	3.21×10^{-7}	2.54×10^{-5}	3.88	1.32×10^{-5}	0.00029	12
53945	Fpn1	Solute carrier family 40 (iron-regulated transporter), member 1	4.23	1.59×10^{-7}	2.08×10^{-5}	2.87	6.42×10^{-7}	7.69×10^{-5}	13
382045	Gpr114	G-protein coupled receptor 114	3.06	1.45×10^{-6}	5.20×10^{-5}	3.1	5.12×10^{-7}	7.21×10^{-5}	14
17132	Maf	Avian musculoaponeurotic fibrosarcoma (v-maf) AS42 oncogene homolog	2.84	4.03×10^{-6}	9.38×10^{-5}	2.68	9.88×10^{-7}	8.95×10^{-5}	15
13132	Dab2	Disabled 2, mitogen-responsive phosphoprotein	1.6	0.00039	0.00169	2.38	4.9×10^{-6}	0.00018	16

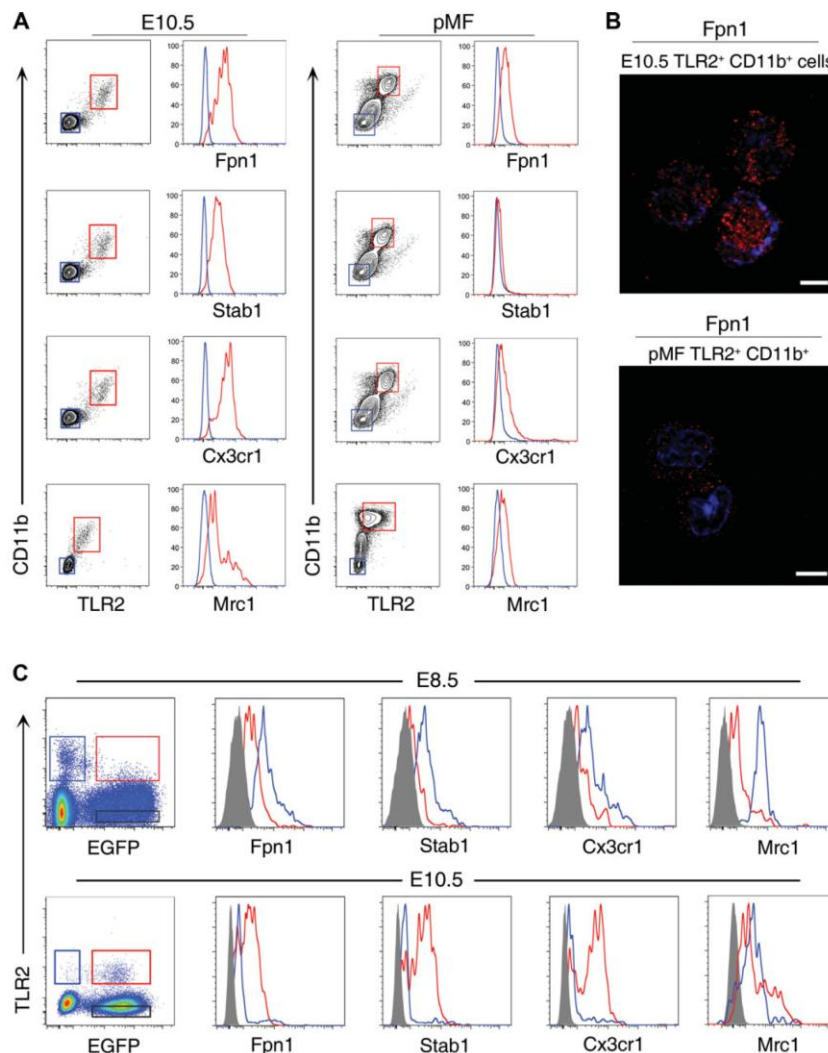[a]Rank = $\log_2$ FC (E10.5 DP versus pMF) × $\log_2$ FC (E10.5 DP versus E10.5 DN).

Figure 4. E10.5 TLR2$^+$ CD11b$^+$ (DP) cells express high levels of surface Fpn1, Stab1, Cx3cr1, and Mrc1. (A) Cell suspensions prepared from E10.5 embryos (left two panels) or by a lavage of adult mouse peritoneal cavity (right two panels) were stained for TLR2 and CD11b and analyzed for the surface expression of Fpn1, Stab1, Cx3cr1, and Mrc1 by FACS. Each histogram shows the comparison of surface expression of the indicated protein on gated DP (red) and E10.5 TLR2$^-$ CD11b$^-$ (DN, blue) populations. (B) Expression of Fpn1 (red) in DP cells (upper panel) and adult TLR2$^+$ CD11b$^+$ peritoneal macrophages (lower panel) was determined by confocal microscopy; scale bar represents 5 μm. Nuclei were stained with DAPI (blue). Images shown are representative of those taken from three experiments. (C) Continuity of expression of Fpn1, Stab1, Cx3cr1, and Mrc1 on maternally derived and then embryonic macrophages. To distinguish cells of embryonic and maternal origin, WT females were crossed with transgenic males expressing EGFP under the control of a β-actin promoter. Based on EGFP expression, embryonic cells were distinguished from EGFP$^-$ maternally derived cells. Expression of Fpn1, Stab1, Cx3cr1, and Mrc1 was determined in E8.5 (upper panel) or E10.5 embryos (lower panel) in EGFP$^+$ TLR2$^+$ embryonic phagocytes (red), EGFP$^-$ TLR2$^+$ maternal cells (blue), and EGFP$^+$ TLR2$^-$ embryonic nonmyeloid cells (gray). All data are from one experiment and are representative of at least three independent experiments performed.

development, we took advantage of a mouse transgenic system where EGFP expression in embryonic-derived cells allowed us to track the expression of this gene on either embryonic or maternal cells [36]. As illustrated in Figure 4C, the *Fpn1* gene was first expressed on early-appearing EGFP$^-$ maternally derived TLR2$^+$ CD11b$^+$ macrophages detected in E8.5 embryo (upper two left panels; blue line). Soon afterwards, at E10.5, these cells were replaced by EGFP$^+$ embryonic-derived, predominantly *Fpn1* co-expressing myeloid cells (Fig. 4C, bottom two left panels; red line). A similar pattern of cellular distribution and kinetics of expression described above for *Fpn1* was also observed for *Stab1*, *Cx3cr1*, and *Mrc1* (Fig. 4C, upper and bottom two right panels).
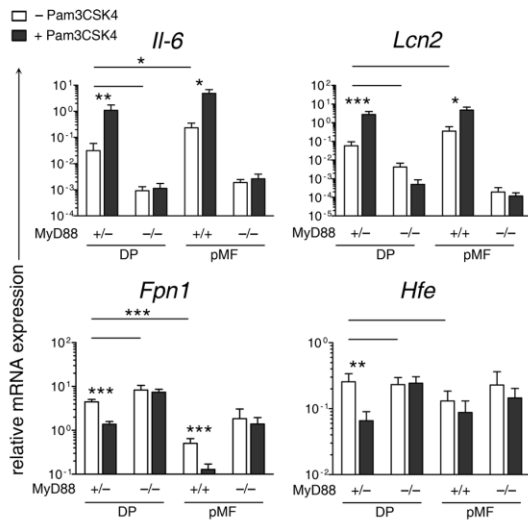

Figure 5. TLR signaling regulates iron metabolism in embryonic macrophages. FACS-sorted E10.5 TLR2$^+$ CD11b$^+$ (DP) and TLR2$^+$ CD11b$^+$ peritoneal macrophages (pMF) isolated from WT or MyD88$^{-/-}$ mice were stimulated with TLR2-specific ligand Pam3CSK4 (black bars) or left unstimulated (open bars). The transcript level of indicated genes was determined 18 h later by qRT-PCR after the normalization to *Casc3* mRNA. Data are shown as mean + SD of three pooled independent experiments performed in triplicates. $^*p \leq 0.05$, $^{**}p \leq 0.01$, $^{***}p \leq 0.001$, two-way ANOVA with interactions followed by Tukey post hoc tests.

Regulation of iron metabolism via TLR signaling

Since previous studies on adult mice suggested that TLRs are involved in the induction of hypoferremia, a marked reduction in the levels of circulating iron [26, 37, 38], we tested whether TLRs can affect the expression profile of genes regulating iron metabolism in an embryo. As illustrated in Figure 5, E10.5 DP macrophages expressed relatively high levels of the iron exporter *Fpn1* as well as hemochromatosis (*Hfe*), the gene that regulates the import of iron inside the cell. At the same time, the expression of lipocalin-2 (*Lcn2*), which is important for iron sequestration during an inflammatory insult, was rather low. Thus, these data are consistent with the previously reported M2 phenotype of embryonic macrophages [2] whereby the effective iron recycling exhibits a high capacity to internalize (*Hfe*) and release (*Fpn1*) iron [22].

Upon treatment of embryonic macrophages with the TLR2 agonist, Pam3CSK4, accompanied by a significant increase in the expression of the proinflammatory cytokine *Il-6* (Fig. 5, upper left panel) and *Tnfα* (not shown), the expression of *Fpn1* and *Hfe* was significantly downregulated (3.2 and 3.9 times, respectively), while *Lcn2* levels were increased approximately 35 times. Importantly, TLR2 agonist-induced changes in the expression of these genes were dependent on the presence of the TLR adaptor protein MyD88, formally demonstrating the involvement of TLR signaling in this event. In addition, upon TLR2 stimulation of E10.5 DP macrophages, the downregulation of *Fpn1* transcript levels translated into significantly diminished intracellular levels

of this protein compared with those in the unstimulated population (Fig. 6A). Consistent with *Fpn1* functioning as a cellular exporter responsible for pumping iron out of cells, we measured significantly increased intracellular free iron levels in E10.5 DP macrophages treated with Pam3CSK4 compared with those in unstimulated ones. Notably, due to the capacity of iron to bind to and consequently quench calcein fluorescence, we detected a significantly reduced fluorescence emission from calcein-labeled E10.5 DP macrophages treated with Pam3CSK4 compared with the unstimulated control sample (Fig. 6B). Thus, concordant with a TLR-mediated proinflammatory condition-induced polarization toward the M1 phenotype, the gene and protein expression profile was altered in favor of the mechanism supporting cellular iron sequestration [23].

Discussion

Phagocytes came into focus in studies conducted by Elie Metchnikoff more than a century ago, yet the understanding of their origin, developmental path, and function in the early developing embryo is still incomplete [39]. It was Metchnikoff who proposed that phagocytes are central for establishing embryonic homeostasis via the process of inflammation [40]. Since TLRs have been viewed as the main mediators of inflammatory processes in adult organisms, the main goal of our investigation was to determine whether TLRs are also expressed on early embryonic macrophages and to delineate developmental processes through which they can, at least partly, exert their homeostatic function. For our analyses, we have chosen E10.5 macrophages since embryonically derived hematopoietic cells attained the expression of CD45 only after E9.75 [3]. While we observed that most of TLRs and their adaptors were highly enriched in E10.5 CD45$^+$ CD11b$^+$ F4/80$^+$ CD14$^+$ TLR2$^+$ myeloid cells, these cells were not their exclusive source in the developing embryo. Surprisingly, nonphagocytic cells also expressed these molecules, albeit at very low levels. However, because these cells represent ∼99% of the total population of embryo, their contribution to the total pool of TLRs and adaptors is not negligible. Whether their low expression is characteristic for all nonphagocytic cells or it is restricted only to certain type of cells, remains to be determined. It is of note that the expression of TLRs on macrophages in later stages of embryonic development (E10.5-E14.5) remained consistent or even slightly increased over time (data not shown).

Here, we also demonstrated that TLRs expressed on embryonic macrophages are functionally wired to cytokine signaling pathways. This suggests that embryonic TLRs could play a role in microbe recognition, similar to that observed in adults. In the case of infection by transplacental transmission, TLRs would trigger signaling pathways leading to the expression of molecules that support local inflammation, thus curbing infection. In addition to the presence of TLRs, microarray analysis of E10.5 TLR2$^+$CD11b$^+$ macrophages revealed several significantly upregulated genes, which can potentially serve as novel markers for detection and
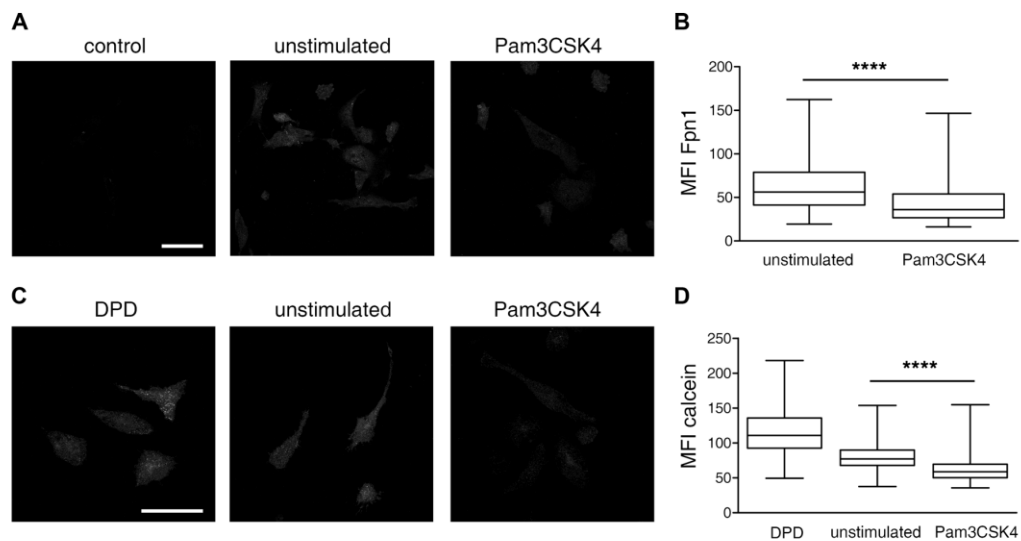
Figure 6. Embryonic macrophages downregulate Fpn1 to sequester iron upon inflammatory insult. (A) E10.5 TLR2$^+$ CD11b$^+$ cells treated (right panel) or not (middle panel) with TLR2 ligand Pam3CSK4 for 18 h were stained for Fpn1. Left panel shows staining with the secondary Ab only. (B) Fpn1 levels were quantified using Olympus ScanR microscope. All data shown are from one experiment performed with n(unstimulated) = 1945 and n(Pam3CSK4) = 2058 cells, which is representative of three independent experiments and are depicted as box-and-whisker graphs (min to max, the line represents median); Mann–Whitney test, ****$p \leq 0.0001$. (C) Intracellular free iron levels were monitored in E10.5 TLR2$^+$ CD11b$^+$ cells treated (right panel) or not (middle panel) with Pam3CSK4 for 18 h, using the cell permeable fluorescent probe calcein (CA-AM), which is quenched upon iron binding. Treatment with a cell permeable iron chelator, 2,2′-dipyridyl (DPD; 5 mM) served as the control of probe iron specificity (left panel). (D) Iron levels were quantified using an Olympus ScanR microscope. All data shown are from one experiment performed with n(DPD) = 678, n(unstimulated) = 3460, n(Pam3CSK4) = 5105 cells, which is representative of three independent experiments and depicted as box-and-whisker graphs (min to max, line represents median); Mann–Whitney test, ****$p \leq 0.0001$. Confocal microscopy images were acquired using the Leica SP5 equipped with HCX PL APO 63.0 × 1.40 Oil UV; scale bar represents 50 μm.

isolation of embryonic macrophages and provide a valuable insight into the role of these cells in early ontogenesis.

The maintenance of optimal iron levels is absolutely critical for the regulation of embryonic homeostasis, organogenesis, and hematopoiesis. Fast growing embryos can acquire iron from two sources: (i) by uptake from the maternal surrounding that is mediated mainly by cells of the extraembryonic visceral endoderm, and (ii) from old and senescent red blood cells [33]. In both scenarios, *Fpn1*, which is in eukaryotes the sole iron cellular exporter pumping iron out of cells, thus makes this essential nutrient available for the systemic uptake by other cells. The critical role of *Fpn1* in embryogenesis has been demonstrated by ablation of its expression that resulted in embryonic lethality before E7.5 [33]. Unexpectedly, our microarray, microscopic, and biochemical data pointed to the existence of an embryonic macrophage-dependent mechanism of iron recycling that could be vital for sustaining iron metabolism during early stages of embryogenesis.

Specifically, we detected in E10.5 embryonic macrophages relatively high mRNA expression levels of *Fpn1* (ten times higher than in peritoneal macrophages). So far, embryonic macrophages have not been implicated in the process of iron recycling. Our data suggest that similar to adult macrophages, embryonic ones could participate in iron recovery after erythrophagocytosis and in iron recycling in a *Fpn1*-dependent fashion [41]. We showed here that embryonic macrophages are fully capable of phagocytosing

bacteria and apoptotic cells with an efficiency similar to that of peritoneal macrophages (data not shown). Moreover, using the method of tracking cells of maternal or embryonic origin, our data demonstrated that *Fpn1* function is provided by the timely coordinated replacement of maternally derived myeloid cells by their counterparts of embryonic origin.

The capacity of TLRs expressed on embryonic macrophages to regulate genes involved in the control of iron levels upon inflammatory insult demonstrates that this function is not restricted to adult macrophages as described previously [26, 37, 42]. In adult mice, the iron limiting bacteriostatic mechanism that leads to the withdrawal of iron from blood circulation and its retention in macrophages is largely dependent on two genes: *Fpn1* and hepcidin (*Hpc*). Hpc, an acute phase protein secreted by the liver and macrophages, is induced by inflammatory cytokines, such as IL-6 and is able to bind to surface Fpn1, causing its internalization and degradation, thus preventing iron release from macrophages [43, 44]. The bacteriostatic mechanism is also supported by the macrophage-secreted protein Lcn2, which targets certain siderophores, thus further limiting iron acquisition by pathogens [45]. Our data showing a dramatic increase of *Lcn2* expression upon TLR2 stimulation are in full agreement with the previous report that demonstrated the binding of p50-IκBζ heterodimer to the NFκB binding site present in the *Lcn2* promoter [46]. On the other hand, measuring its expression in the spleen of

LPS-treated mice, there is evidence that TLR-mediated downregulation of *Fpn1* is independent of MyD88 and p50 subunit-mediated NFκB signaling [26]. Contrary to these data, we have shown that TLR2-mediated suppression of *Fpn1* in embryonic macrophages, as well as peritoneal macrophages, is MyD88-dependent (Fig. 5). These results warrant further investigation into the regulation of iron metabolism via TLR signaling and suggest the existence of its distinct cell- or tissue-specific regulatory circuits that operate during infection.

Interestingly, using qRT-PCR, we were unable to detect the expression of the *Hpc* transcript in E10.5 embryonic macrophages either before or after stimulation (data not shown). An analogous situation has been recently described for microglia, resident macrophages in the CNS, which express a broad repertoire of TLRs and thus are able to function as mediators of neuroinflammation [47]. Since the microglia originate from YS-derived macrophage precursors that seed the nervous system during early embryonic development [8] it would be intuitive to suggest that embryonic macrophages and microglial cells might share a common Hpc-independent control of iron homeostasis during infection.

In a recent study using microarray analysis and genetic approach, Schulz et al. [9] provided evidence that YS-derived F4/80^{bright} hematopoietic precursors give rise to populations of F4/80^{bright} fetal and adult tissue macrophages in *Myb* transcription factor-independent fashion. In contrast, *Myb*-dependent F4/80^{low}CD11b^{high} macrophages originate from hematopoietic stem cell precursors and represent a distinct lineage of macrophages [9]. To gain further insight into the macrophage type specific gene expression, we downloaded microarray data from Shulz et al. and compared it with the expression profiles of cells analyzed in our study (Supporting Information Fig. 3B–D). The data showed that (i) E10.5 DP macrophage cluster with F4/80^{bright} lineages of macrophages (Supporting Information Fig. 3B), thus supporting the YS origin of E10.5 DP macrophages; (ii) the expression profile of the most upregulated genes identified in the present study showed clustering among E10.5 DP, E10.5 YS-F4/80^{bright}, and E16.5 F4/80^{bright} tissue macrophages, attesting to their direct developmental relationship (Supporting Information Fig. 3C); (iii) importantly, and in contrast to the set of upregulated genes, the expression profile of TLRs and their adaptors among various types of macrophages showed no particular pattern of clustering (Supporting Information Fig. 3D). This suggests that the expression of TLRs could be a basic event specified by the process of myelopoiesis, which equips myeloid cells with the molecular machinery that is required for host defenses. This prototypic expression of TLRs thus represents rather a generic feature of all macrophage populations independent of their tissue location, stage of development, and ontogenetic origin.

An intriguing question remains, whether the stimulation of embryonic macrophages by potential endogenous TLR ligands can regulate iron metabolism in developing embryos under normal noninflammatory conditions. However, the fact that the expression levels of *Lcn2*, *Fpn1*, and *Hfe* that are regulated by TLR-MyD88 signaling pathway were in freshly isolated E10.5 embryonic DP

macrophages from WT and MyD88$^{-/-}$ comparable (Fig. 5) argues against this scenario.

Taken together, TLRs can contribute to organismal homeostasis during its entire ontogenetic development, embryonic as well as postnatal, in several ways. Upon their engagement, TLRs are able to nudge the hematopoiesis toward myelo/granulopoieis [48] and in parallel, activate the mechanisms of iron sequestration to limit its access to embryo-invading microbes. In this sense, macrophages that are in a developing embryo could be the main cellular force to impose complex homeostatic mechanisms that are triggered upon infection. Future experiments with embryonic macrophage-specific deletion of *Fpn1*, *Hfe*, and genes critical for TLR signaling will address their role in maintaining the embryonic homeostasis during unperturbed or inflammatory conditions.

Materials and methods

Animals

CD1 mice were maintained in the animal facility of the Institute of Molecular Genetics in Prague. pCAGEGFPMos3 mice expressing EGFP under the control of a β-actin promoter, here referred to as TgEGFP mice, were obtained from Petr Svoboda [49]. MyD88$^{-/-}$ mice (B6.129P2(SJL)-*Myd88tm1.1Defr*/J), derived from Myd88^{fl} mice [50], were obtained from The Jackson Laboratory. All experiments were approved by the ethical committee of the IMG.

Cell suspension preparation

Time pregnant females (the day of vaginal plug presence was designated as E0.5) were sacrificed by cervical dislocation. Embryos were dissected from uteri and all extra embryonic tissues were removed. Embryos were dissociated using 1 mg/ml Dispase (Life Technologies) in PBS for 10 min at 37°C, washed in PBS + 1% FCS, and cell suspensions were passed through a 50 μm cell strainer.

Fluorescence immunodetection and cell sorting

Cell suspensions were preincubated for 10 min with anti-CD16 and anti-CD32 antibodies to block Fc receptors and then were stained with the primary antibodies and secondary reagents listed in Supporting Information Table 1A and B, respectively. Fluorescence data were acquired using LSRII cytometer (BD) and analyzed using FlowJo software (Tree Star). Cell debris and dead cells were excluded from the analysis based on scatter signals and Hoechst 33258 fluorescence. This general gating strategy is presented in Supporting Information Fig. 1C and D. Cell sorting was performed with FACS Vantage or Influx cell sorter (BD). For microscopic analyses, sorted cells were immobilized overnight on glass coverslips, fixed with 3.7% paraformaldehyde in PBS (pH 7.4),

permeabilized in methanol for 10 min at $-20°C$, then blocked in 1% BSA in 0.1% PBS-Tween 20 (PBT), and stained with indicated antibodies in BSA-PBT. The coverslips were mounted using Vectashield containing DAPI (Vector Laboratories). Confocal microscopy images were acquired using Leica SP5 equipped with HCX PL APO 63.0×1.40 Oil UV objective.

Gene expression analysis

Total RNA from sorted cells was isolated using RNeasy Plus Micro Kit (Qiagen) and reverse transcribed using Premium RevertAid and random hexamers (Fermentas). qRT-PCR was performed using LightCycler 480 SYBR Green I Master mix on a LightCycler 480 (Roche). Each sample was tested in triplicate. The relative amount of mRNA was calculated by LightCycler 480 1.5 software using *Casc3* mRNA level as a control. Intron-spanning primer sequences (when possible) were designed using UPL software (Roche) and are available upon request. Primer efficiencies were calculated using LightCycler 480 1.5 software. Data were analyzed using Prism 5.03 software (GraphPad).

Microarrays were performed using MouseWG-6 v1 and MouseWG-6 v2 Expression BeadChips (Illumina). The integrity of mRNA samples was quantified spectrophotometrically (Agilent). Each pairwise comparison was performed in three biological replicates. The raw data were analyzed using GenomeStudio software (Illumina). After quantile normalization and variance stabilization by base 2 logarithmic transformation, differentially expressed genes were identified using moderated *t*-test as implemented in *limma* package of *Bioconductor* [51, 52]. Genes with twofold change of gene expression intensity and false discovery rate less than 0.1 were considered significantly deregulated. To combine the data from the two Illumina platforms, two separate gene lists were created for the comparisons (E10.5 DP versus peritoneal macrophage DP) and (E10.5 DP versus E10.5 DN) and their overlap was evaluated. The expression data from the resulting gene list were validated by qRT-PCR. The MIAME compliant microarray data were deposited in ArrayExpress database (https://www.ebi.ac.uk/arrayexpress/) under the accession number E-MTAB-1537.

Phagocytosis assay

Apoptosis was induced in thymocytes of CD1 mice by 1 μM dexamethasone. Target cells (apoptotic cells or bacteria) were opsonized by inactivated normal mouse serum. E10.5 cells were allowed to engulf CFSE-labeled apoptotic cells or tdTomato expressing *Escherichia coli* BL-21 in the presence or absence of the inhibitor of phagocytosis, cytochalasin D, for indicated period of time. Each sample was tested in triplicate. Phagocytosis product calculated as MFI $\times$ percentage of phagocytosing cells was assessed by FACS after vigorous washing and staining with anti-TLR2 Ab.

ELISA, cytokine Ab assay, and TLR-mediated regulation of iron metabolism genes

E10.5 TLR2$^+$ CD11b$^+$ and TLR2$^-$ CD11b$^-$ cells were sorted and grown in RPMI 1640 medium supplemented with 2 mM L-glutamine, 10 mM HEPES, and 50 μM 2-ME in the presence or absence of 100 ng/mL LPS (from *E. coli* K12 strain), or 1 μg/mL Pam3CSK4, or 5 μM ODN1826 (all Invivogen) for 18 h. Changes in cytokine secretion were assessed using semiquantitative Mouse Cytokine Antibody Array G3 according to the manufacturer's instructions (RayBiotech). Levels of TNF-α in supernatants were assessed using mouse TNFα ELISA Ready-SET-Go! kit (eBioscience). Each sample was tested in triplicate. The expression of TLR-regulated iron metabolism genes in sorted cells was determined 18 h after stimulation with 1 μg/mL Pam3CSK4 by qRT-PCR, as described above.

Determination of intracellular calcein-AM chelatable iron level

Intracellular iron levels were measured using the fluorescent probe calcein-AM (CA-AM; Life Technologies) [53] as previously described [54]. Briefly, after washing with HBSS (pH 7.4), the cells grown on cover slips were incubated with 2 μM CA-AM in HBSS in 37°C for 10 min, washed with HBSS, and fixed in 3.7% paraformaldehyde (pH 7.4). Cells that were prior to incubation with CA-AM treated with 2,2′-dipyridyl (DPD, Sigma), a well characterized iron chelator, were used as a negative control.

Quantitative image analyses

For quantitative analyses of Fpn1 protein and iron levels in macrophages, fixed and stained as described above, were mounted in Vectashield with DAPI and fluorescence images were acquired with Olympus ScanR Screening Station for Life Science equipped with LUCPLFLN 20$\times$ PH objective. The data were analyzed by ScanR Analysis 1.3.0.3 software (Olympus Imaging Solutions GmbH). Dead cells and debris were excluded from the analysis based on DAPI intensity value.

References

1 Ovchinnikov, D. A., Macrophages in the embryo and beyond: much more than just giant phagocytes. *Genesis* 2008. **46**: 447–462.

2 Rae, F., Woods, K., Sasmono, T., Campanale, N., Taylor, D., Ovchinnikov, D. A., Grimmond, S. M. et al., Characterisation and trophic functions of murine embryonic macrophages based upon the use of a Csf1r–EGFP transgene reporter. *Dev. Biol.* 2007. **308**: 232–246.

3 Bertrand, J. Y., Jalil, A., Klaine, M., Jung, S., Cumano, A. and Godin, I., Three pathways to mature macrophages in the early mouse yolk sac. *Blood* 2005. **106**: 3004–3011.

4 Moore, M. and Metcalf, D., Ontogeny of the haemopoietic system: yolk sac origin of in vivo and in vitro colony forming cells in the developing mouse embryo. *Br. J. Haematol.* 1970. **18**: 279–296.

5 Palis, J., Robertson, S., Kennedy, M., Wall, C. and Keller, G., Development of erythroid and myeloid progenitors in the yolk sac and embryo proper of the mouse. *Development* 1999. **126**: 5073–5084.

6 Ferkowicz, M. J. and Yoder, M. C., Blood island formation: longstanding observations and modern interpretations. *Exp. Hematol.* 2005. **33**: 1041–1047.

7 Alliot, F., Godin, I. and Pessac, B., Microglia derive from progenitors, originating from the yolk sac, and which proliferate in the brain. *Dev. Brain Res.* 1999. **117**: 145–152.

8 Ginhoux, F., Greter, M., Leboeuf, M., Nandi, S., See, P., Gokhan, S., Mehler, M. F. et al., Fate mapping analysis reveals that adult microglia derive from primitive macrophages. *Science* 2010. **330**: 841–845.

9 Schulz, C., Perdiguero, E. G., Chorro, L., Szabo-Rogers, H., Cagnard, N., Kierdorf, K., Prinz, M. et al., A lineage of myeloid cells independent of Myb and hematopoietic stem cells. *Science* 2012. **336**: 86–90.

10 Muller, A. M., Medvinsky, A., Strouboulis, J., Grosveld, F. and Dzierzakt, E., Development of hematopoietic stem cell activity in the mouse embryo. *Immunity* 1994. **1**: 291–301.

11 Bertrand, J. Y., Giroux, S., Golub, R., Klaine, M. l., Jalil, A., Boucontet, L., Godin, I. and Cumano, A., Characterization of purified intraembryonic hematopoietic stem cells as a tool to define their site of origin. *Proc. Natl. Acad. Sci. USA* 2005. **102**: 134–139.

12 Bertrand, J. Y., Desanti, G. E., Lo-Man, R., Leclerc, C., Cumano, A. and Golub, R., Fetal spleen stroma drives macrophage commitment. *Development* 2006. **133**: 3619–3628.

13 Kumar, H., Kawai, T. and Akira, S., Pathogen recognition by the innate immune system. *Int. Rev. Immunol.* 2011. **30**: 16–34.

14 Akira, S., Takeda, K. and Kaisho, T., Toll-like receptors: critical proteins linking innate and acquired immunity. *Nat. Immunol.* 2001. **2**: 675–680.

15 Medzhitov, R., Recognition of microorganisms and activation of the immune response. *Nature* 2007. **449**: 819–826.

16 Yu, L., Wang, L. and Chen, S., Endogenous Toll-like receptor ligands and their biological significance. *J. Cell. Mol. Med.* 2010. **14**: 2592–2603.

17 Beutler, B., Inferences, questions and possibilities in Toll-like receptor signalling. *Nature* 2004. **430**: 257–263.

18 McGettrick, A. F. and O'Neill, L. A. J., Toll-like receptors: key activators of leucocytes and regulator of haematopoiesis. *Br. J. Haematol.* 2007. **139**: 185–193.

19 Zhang, S.-Y., Herman, M., Ciancanelli, M. J., Pérez de Diego, R., Sancho-Shimizu, V., Abel, L. and Casanova, J.-L., TLR3 immunity to infection in mice and humans. *Curr. Opin. Immunol.* 2013. **25**: 19–33.

20 Jack, C. S., Arbour, N., Manusow, J., Montgrain, V., Blain, M., McCrea, E., Shapiro, A. and Antel, J. P., TLR signaling tailors innate immune responses in human microglia and astrocytes. *J. Immunol.* 2005. **175**: 4320–4330.

21 Sica, A. and Mantovani, A., Macrophage plasticity and polarization: in vivo veritas. *J. Clin. Invest.* 2012. **122**: 787–795.

22 Corna, G., Campana, L., Pignatti, E., Castiglioni, A., Tagliafico, E., Bosurgi, L., Campanella, A. et al., Polarization dictates iron handling by inflammatory and alternatively activated macrophages. *Haematologica* 2010. **95**: 1814–1822.

23 Gaetano, C., Massimo, L. and Alberto, M., Control of iron homeostasis as a key component of macrophage polarization. *Haematologica* 2010. **95**: 1801–1803.

24 Recalcati, S., Locati, M. and Cairo, G., Systemic and cellular consequences of macrophage control of iron metabolism. *Semin. Immunol.* 2012. **24**: 393–398.

25 Nguyen, N.-B., Callaghan, K. D., Ghio, A. J., Haile, D. J. and Yang, F., Hepcidin expression and iron transport in alveolar macrophages. *Am. J. Physiol. Lung Cell. Mol. Physiol.* 2006. **291**: L417-L425.

26 Liu, X.-B., Nguyen, N.-B. H., Marquess, K. D., Yang, F. and Haile, D. J., Regulation of hepcidin and ferroportin expression by lipopolysaccharide in splenic macrophages. *Blood Cells Mol. Dis.* 2005. **35**: 47–56.

27 Hughes, D. A. and Gordon, S., Expression and function of the type 3 complement receptor in tissues of the developing mouse. *J. Immunol.* 1998. **160**: 4543–4552.

28 Kim, Y., Zhou, P., Qian, L., Chuang, J. Z., Lee, J., Li, C., Iadecola, C. et al., MyD88-5 links mitochondria, microtubules, and JNK3 in neurons and regulates neuronal survival. *J. Exp. Med.* 2007. **204**: 2063–2074.

29 Molday, L. L., Wu, W. W. and Molday, R. S., Retinoschisin (RS1), the protein encoded by the X-linked retinoschisis gene, is anchored to the surface of retinal photoreceptor and bipolar cells through its interactions with a Na/K ATPase-SARM1 complex. *J. Biol. Chem.* 2007. **282**: 32792–32801.

30 Barbalat, R., Lau, L., Locksley, R. M. and Barton, G. M., Toll-like receptor 2 on inflammatory monocytes induces type I interferon in response to viral but not bacterial ligands. *Nat. Immunol.* 2009. **10**: 1200–1207.

31 Huang, D. W., Sherman, B. T. and Lempicki, R. A., Systematic and integrative analysis of large gene lists using DAVID bioinformatics resources. *Nat. Protoc.* 2008. **4**: 44–57.

32 Huang, D. W., Sherman, B. T. and Lempicki, R. A., Bioinformatics enrichment tools: paths toward the comprehensive functional analysis of large gene lists. *Nucleic Acids Res.* 2009. **37**: 1–13.

33 Donovan, A., Lima, C. A., Pinkus, J. L., Pinkus, G. S., Zon, L. I., Robine, S. and Andrews, N. C., The iron exporter ferroportin/Slc40a1 is essential for iron homeostasis. *Cell Metab.* 2005. **1**: 191–200.

34 Pietrangelo, A., The ferroportin disease. *Blood Cells Mol. Dis.* 2004. **32**: 131–138.

35 Van Zandt, K. E., Sow, F. B., Florence, W. C., Zwilling, B. S., Satoskar, A. R., Schlesinger, L. S. and Lafuse, W. P., The iron export protein ferroportin 1 is differentially expressed in mouse macrophage populations and is present in the mycobacterial-containing phagosome. *J. Leukoc. Biol.* 2008. **84**: 689–700.

36 Zhou, L., Yoshimura, Y., Huang, Y. Y., Suzuki, R., Yokoyama, M., Okabe, M. and Shimamura, M., Two independent pathways of maternal cell transmission to offspring: through placenta during pregnancy and by breast-feeding after birth. *Immunology* 2000. **101**: 570–580.

37 Flo, T. H., Smith, K. D., Sato, S., Rodriguez, D. J., Holmes, M. A., Strong, R. K., Akira, S. and Aderem, A., Lipocalin 2 mediates an innate immune response to bacterial infection by sequestrating iron. *Nature* 2004. **432**: 917–921.

38 Layoun, A., Huang, H., Calvé, A. and Santos, M. M., Toll-like receptor signal adaptor protein MyD88 is required for sustained endotoxin-induced acute hypoferremic response in mice. *Am. J. Pathol.* 2012. **180**: 2340–2350.

39 Stefater, J. A., Ren, S., Lang, R. A. and Duffield, J. S., Metchnikoff's policemen: macrophages in development, homeostasis and regeneration. *Trends Mol. Med.* 2011. **17**: 743–752.

40 Tauber, A. I., The immune self: theory or metaphor? *Immunol. Today* 1994. **15**: 134–136.

41 Hentze, M. W., Muckenthaler, M. U., Galy, B. and Camaschella, C., Two to tango: regulation of mammalian iron metabolism. *Cell* 2010. **142**: 24–38.

42 Peyssonnaux, C., Zinkernagel, A. S., Datta, V., Lauth, X., Johnson, R. S. and Nizet, V., TLR4-dependent hepcidin expression by myeloid cells in response to bacterial pathogens. *Blood* 2006. **107**: 3727–3732.

43 Nemeth, E., Rivera, S., Gabayan, V., Keller, C., Taudorf, S., Pedersen, B. K. and Ganz, T., IL-6 mediates hypoferremia of inflammation by inducing the synthesis of the iron regulatory hormone hepcidin. *J. Clin. Invest.* 2004. **113**: 1271–1276.

44 Ganz, T. and Nemeth, E., Iron imports. IV. Hepcidin and regulation of body iron metabolism. *Am. J. Physiol. Gastrointest. Liver Physiol.* 2006. **290**: G199–G203.

45 Goetz, D. H., Holmes, M. A., Borregaard, N., Bluhm, M. E., Raymond, K. N. and Strong, R. K., The neutrophil lipocalin NGAL is a bacteriostatic agent that interferes with siderophore-mediated iron acquisition. *Mol. Cell* 2002. **10**: 1033–1043.

46 Yamamoto, M., Yamazaki, S., Uematsu, S., Sato, S., Hemmi, H., Hoshino, K., Kaisho, T. et al., Regulation of Toll/IL-1-receptor-mediated gene expression by the inducible nuclear protein I[kappa]B[zeta]. *Nature* 2004. **430**: 218–222.

47 Ward, R., Crichton, R., Taylor, D., Corte, L., Srai, S. and Dexter, D., Iron and the immune system. *J. Neural Transm.* 2011. **118**: 315–328.

48 Nagai, Y., Garrett, K. P., Ohta, S., Bahrun, U., Kouro, T., Akira, S., Takatsu, K. and Kincade, P. W., Toll-like receptors on hematopoietic progenitor cells stimulate innate immune system replenishment. *Immunity* 2006. **24**: 801–812.

49 Nejepinska, J., Malik, R., Filkowski, J., Flemr, M., Filipowicz, W. and Svoboda, P., dsRNA expression in the mouse elicits RNAi in oocytes and low adenosine deamination in somatic cells. *Nucleic Acids Res.* 2012. **40**: 399–413.

50 Hou, B., Reizis, B. and DeFranco, A. L., Toll-like receptors activate innate and adaptive immunity by using dendritic cell-intrinsic and -extrinsic mechanisms. *Immunity* 2008. **29**: 272–282.

51 Smyth, G. K., Limma: linear models for microarray data. In Gentleman, R., Carey, V., Dudoit, S., Irizarry, R. and Huber, W. (Eds.) *Bioinformatics and computational biology solutions using R and bioconductor*, Springer, New York, 2005, pp 397–420.

52 Gentleman, R. C., Carey, V. J., Bates, D. M., Bolstad, B., Dettling, M., Dudoit, S., Ellis, B. et al., Bioconductor: open software development for computational biology and bioinformatics. *Genome Biol.* 2004. 5: R80.

53 Epsztejn, S., Kakhlon, O., Glickstein, H., Breuer, W. and Cabantchik, Z. I., Fluorescence analysis of the labile iron pool of mammalian cells. *Anal. Biochem.* 1997. **248**: 31–40.

54 Xu, G., Ahn, J., Chang, S., Eguchi, M., Ogier, A., Han, S., Park, Y. et al., Lipocalin-2 induces cardiomyocyte apoptosis by increasing intracellular iron accumulation. *J. Biol. Chem.* 2012. **287**: 4808–4817.

Full correspondence: Dr. Dominik Filipp, Laboratory of Immunobiology, Institute of Molecular Genetics AS CR, Vídeňská 1083, CZ-142 20 Prague 4, Czech Republic
Fax: +420-224-310-955
e-mail: dominik.filipp@img.cas.cz

4.4. Quantitative Proteomics Analysis of Macrophage Rafts Reveals Induction of Autophagy Pathway at the Early Time of *Francisella tularensis* LVS infection.

In this study we provided evidence that infection of macrophages with *F. tularensis* leads to changes in protein composition of detergent-resistant membranes (DRMs). Using SILAC-based quantitative proteomic approach, we observed the recruitment of autophagic adaptor protein p62 to DRMs at early stages of microbe–host cell interaction. Using confocal microscopy, we visualized the colocalization of p62 with ubiquitinated, LC3 decorated, intracellular *F. tularensis* microbes peaking at 1 h postinfection. Furthermore, *F. tularensis* infection of p62-knockdown macrophages led to a transient increase in the intracellular number of microbes up to 4 h after *in vitro* infection. While there no direct evidence for it yet, we propose, that TLR2 triggering could activate autophagy to inhibit the bacterial growth as described by Sanjuan et al. (Sanjuan et al. 2007).

Together, our data suggested that the activation of autophagy pathway in *F. tularensis* infected macrophages, which impacts the early phase of microbial proliferation, is subsequently circumvented by ongoing infection.

Authors contribution: Silencing of p62 protein expression using siRNA followed by CFU assay

Quantitative Proteomics Analysis of Macrophage-Derived Lipid Rafts Reveals Induction of Autophagy Pathway at the Early Time of *Francisella tularensis* LVS Infection

Anetta Härtlova,[†,‡] Marek Link,[§] Jana Balounova,[⊥] Martina Benesova,[⊥] Ulrike Resch,[‡] Adela Straskova,[†] Margarita Sobol,[¶] Anatoly Philimonenko,[¶] Pavel Hozak,[¶] Zuzana Krocova,[§] Nelson Gekara,[‡] Dominik Filipp,[⊥] and Jiri Stulik*,[§]

[†]Centre of Advanced Studies, Faculty of Military Health Sciences, Trebesska 1575, Hradec Kralove 500 01, Czech Republic

[‡]Department of Molecular Biology, The Laboratory for Molecular Infection Medicine Sweden (MIMS), Umeå University, SE-901 85 Umeå, Sweden

[§]Institute of Molecular Pathology, Faculty of Military Health Sciences, Trebesska 1575, Hradec Kralove 500 01, Czech Republic

[⊥]Laboratory of Immunobiology, Institute of Molecular Genetics of the ASCR, Videnska, 1083 Prague, Czech Republic

[¶]Laboratory of Biology of the Cell Nucleus, Institute of Molecular Genetics of the AS CR, Videnska, 1083 Prague, Czech Republic

ⓢ *Supporting Information*

ABSTRACT: *Francisella tularensis* is a highly infectious intracellular pathogen that has evolved an efficient strategy to subvert host defense response to survive inside the host. The molecular mechanisms regulating these host−pathogen interactions and especially those that are initiated at the time of the bacterial entry via its attachment to the host plasma membrane likely predetermine the intracellular fate of pathogen. Here, we provide the evidence that infection of macrophages with *F. tularensis* leads to changes in protein composition of macrophage-derived lipid rafts, isolated as detergent-resistant membranes (DRMs). Using SILAC-based quantitative proteomic approach, we observed the accumulation of autophagic adaptor protein p62 at the early stages of microbe−host cell interaction. We confirmed the colocalization of the p62 with ubiquitinated and LC3-decorated intracellular *F. tularensis* microbes with its maximum at 1 h postinfection. Furthermore, the infection of p62-knockdown host cells led to the transient increase in the intracellular number of microbes up to 4 h after in vitro infection. Together, these data suggest that the activation of the autophagy pathway in *F. tularensis* infected macrophages, which impacts the early phase of microbial proliferation, is subsequently circumvented by ongoing infection.

KEYWORDS: *innate immune response, bacterial infection, lipid rafts, Francisella tularensis, phagocytosis, autophagy*
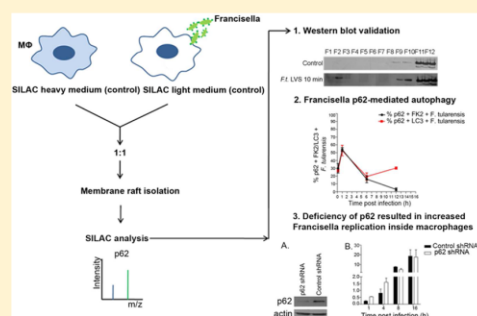
■ INTRODUCTION

Francisella tularensis is a causative agent of tularemia, a zoonotic disease, that has received special attention because of its extreme virulence, its ease of aerosol transmission, and its ability to cause severe illness and death.[1] As few as ten bacteria of this highly virulent strain can cause lethal disease in humans.[2] For this reason, *F. tularensis* is classified as a category A agent by the Center for Disease Control and Prevention (CDC).[3] Its ability to cause the disease is associated with its ability to enter and replicate inside host cells, mostly in phagocytes.[4,5] However, the precise molecular mechanisms supporting its phagocytosis and intracellular retention are not fully understood. Uptake of *F. tularensis* into macrophages is facilitated by complement opsonization.[6] In the absence of complement, *F. tularensis* enters macrophages through the Fc receptor,[7] mannose receptor,[8] or scavenger receptor.[9] Once inside host cells, *F. tularensis* transiently resides in a vacuole that is acidified

by the proton vATPase pump, which is essential for *Francisella* containing vacuole (FCV) disruption and subsequent escape of *F. tularensis* into the host cell cytoplasm,[10] where it further proliferates.[11,12] The avoidance of phagosome−lysosomal fusion and escape into the cytosol is a hallmark of *F. tularensis* infection because escape-defective mutants are attenuated in their virulence.[13−16] After cytoplasmic replication, during the late stage of infection, *F. tularensis* re-enters the endocytic compartment via autophagy-mediated processes.[17]

Recent studies have demonstrated an important role of cholesterol in *F. tularensis* internalization into macrophages[18] and nonphagocytic hepatocytes.[19] Cholesterol is considered to be the key structural and regulatory element of the integrity of cholesterol-rich membrane domains, so-called lipid rafts.[20]

A

Lipid rafts are liquid-ordered membrane domains enriched in cholesterol and sphingolipids, acting as spatiotemporal regulators of signal transduction by concentrating or excluding signaling molecules.[21] A wide variety of bacterial pathogens, including *Salmonella* spp.,[22] *Shigella* spp.,[23] and *Mycobacterium* spp.,[24] have been shown to preferentially interact with the signaling molecules within lipid rafts to successfully invade host cells. Exploiting lipid rafts, bacteria can manipulate host signaling pathways and vesicular trafficking to create a survival- and growth-sustainable niche inside host cells.[25,26] However, the molecular mechanisms linking raft-associated molecules with the intracellular pathogen's evading strategy is still lacking.

Cholesterol-rich domains were shown to be important for *Francisella* entry into macrophages; therefore, we investigated the protein composition of these domains during *F. tularensis* live vaccine strain (LVS)[27] internalization by quantitative, SILAC-based proteomic analysis of highly purified detergent-resistant membranes (DRMs). We found that upon its entry, *Francisella* induces the recruitment of the autophagic adaptor protein, sequestosome-1/p62 (hereafter referred to as p62), and demonstrated that p62 plays a regulatory role in LC3-mediated autophagy pathway induced at early stages of *F. tularensis* LVS infection.

■ MATERIALS AND METHODS

Cell Culture Conditions

The murine macrophage-like cell line J774.2, derived from J774.1 solid tumor cell line, was obtained from the European Collection of Cell Culture (EACC, ref No. 85011428). The J774.2 were cultured in high glucose DMEM (hyclone), containing 10% (v/v) FBS and 2 mM glutamine at 37 °C in a 5% CO_2 humidified atmosphere.

Bacterial Strains and Growth Conditions

The attenuated LVS bacterial strain of *Francisella tularensis* subsp. *holarctica* (*F. tularensis* LVS) was obtained from the American Type Culture Collection, ref no. ATCC29684. Although *F. tularensis* LVS is attenuated for humans, it is fully virulent for mice.[27]

Infection Assay: Synchronized Phagocytosis

Macrophage infection was performed using synchronized phagocytosis with minor modifications to the previously published method.[28] For all assays, we used J774.2 murine macrophage cell line, which faithfully reproduces the infection of murine macrophages with *F. tularensis* LVS.[11] Briefly, J774.2 macrophages were infected at multiplicity of infection (MOI) 500 by centrifuging microbes onto adherent macrophages at 400*g* for 4 min at 25 °C in all experiments. For lipid raft isolation, macrophages were incubated with bacteria for 10 min at 37 °C under a 5% CO_2 atmosphere to allow the induction of coalescence of clustered lipid rafts followed by extensive washing with PBS. To evaluate the intracellular replication of *F. tularensis* LVS in J774.2 cells, macrophages were incubated with bacteria for 30 min at 37 °C under 5% CO_2 atmosphere to let bacteria enter macrophages. After 30 min of incubating the macrophages with bacteria, 5 μg/mL gentamicin was added to kill any remaining extracellular bacteria.

Cholesterol Depletion and Survival Test

For cholesterol depletion, J774.2 macrophages were treated with 10 mM methyl-β-cyclodextrin (MβCD) or 5 μg/mL filipin for 30 min prior to infection. After infection, cells were lysed in PBS containing 0.1% sodium deoxycholate (w/v). Intracellular

vital bacterial count (CFU) was assessed by titrating cell lysates on McLeod's plates. The results were expressed as the number of intracellular bacteria per cell relative to the control. Results are the mean values of at least three independent experiments.

SILAC Labeling

Metabolic labeling of J774.2 macrophages by stable isotope labeling by amino acids in cell culture (SILAC) was achieved by culturing cells in lysine- and arginine-deficient DMEM medium supplemented with 10% dialyzed FBS, 2 mM glutamine with either 100 mg/L of L-lysine−HCl (MW = 146.1055) and L-arginine (MW = 174.1117) ("light medium") or heavy L-lysine−HCl [$^{13}C_6$] (MW = 152.1259) and L-arginine [$^{15}N_4^{13}C_6$] (MW = 184.1241) ("heavy medium").[29] Complete incorporation of heavy L-lysine and L-arginine was typically achieved after six cell divisions and confirmed by MS analysis of a tryptic digest from a whole protein lysate (data not shown).

Detergent-Resistant Membranes (DRMs) Preparation and Western Blot Analysis

Following SILAC labeling, DRMs were isolated as described previously with minor modifications.[28] Briefly, J774.2 macro-phages were lysed in a buffer containing 0.5% TX-100 (v/v), 25 mM Tris−HCl pH 7.5, 150 mM NaCl, 10 mM glycerophosphate, and 5 mM EDTA. Quantification was performed using a Pierce BCA protein kit. Equal amounts of protein lysates obtained from noninfected J774.2 cells grown in heavy medium and *F. tularensis*-infected J774.2 cells grown in light medium were combined and mixed with an equal volume of 80% ice cold sucrose (w/v) in MES buffer (25 mM MES pH 6.5, 150 mM NaCl, 5 mM EDTA). The combined lysate was overlaid with 5 mL of ice cold 30% sucrose (w/v) solution in MES buffer and 2 mL of ice cold 5% sucrose (w/v) solution in MES buffer and centrifuged for 17 h at 200 000*g* at 4 °C using a swing-out rotor (SW41). The DRMs fraction, separating as a white light-scattering band between 30% and 5% sucrose interface after centrifugation, was isolated, pelleted by centrifugation, and washed twice with PBS. The DRMs protein pellet was solubilized in 0.2% RapiGest SF in 100 mM ammonium bicarbonate (pH 7.8), reduced and alkylated, and digested by trypsin overnight at a protease:protein ratio of 1:50.

For Western blot analysis, 12 fractions of equal volume from top to bottom were collected from the sucrose gradient and probed with primary antibodies for Caveolin-1 (BD Biosciences; Sigma, Santa Cruz), Flotillin-1 (BD Biosciences), Flotillin-2 (Cell Signaling Technology), Caveolin-2 (BD Biosciences), Fyn (Cell Signaling Technology), Lyn (Cell Signaling Technology), or Tfr (Zymed). Horseradish-perox-idase-conjugatated antibodies (Dako Cytomation) were used as secondary antibodies, and proteins were detected by enhanced chemiluminiscence detection on X-ray films (Agfa).

2D Liquid Chromatography

2D (RP × RP) liquid chromatography separation of tryptic peptides employing different pH in both RP separation dimensions[30] was performed. The first dimension of separation was performed on a Gemini C18 3 μm, 110 Å, 2.0 × 150 mm column (Phenomenex) at high-pH mobile phase conditions using an Alliance 2695 liquid chromatograph (Waters). The mobile phases were A−water, B−acetonitrile (ACN), and C−200 mM ammonium formate buffer, pH 10. Peptides were separated by a linear gradient formed by mobile phase A and mobile phase B, from 5 to 55% of mobile phase B in 50 min at a flow rate of 0.16 mL/min. Mobile phase C proportioning was

10% throughout the separation. Column temperature was kept constant at 40 °C and the separation was monitored at 215 nm. In total, 11 fractions were collected into microcentrifuge tubes and evaporated to dryness. Second dimension RP-LC was performed on an Ultimate 3000 liquid chromatograph (Dionex). The trap-column configuration was used for separation of the first four collected fractions. Here, the peptides were separated on an Atlantis dC18 3 μm, 100 Å, 0.1 × 150 mm column in combination with a C18 PepMap100, 5 μm, 100 Å, 0.3 × 5 mm trap column (Dionex). Column temperature was kept constant at 25 °C, and the separation was monitored at 215 nm. The mobile phases were A, 5% ACN, 95% water, and 0.1% TFA (v/v) and B, 80% ACN, 20% water, and 0.1% TFA (v/v). The sample was loaded for 5 min with 2% ACN, 98% water, and 0.1% TFA (v/v) onto the trap column at a flow rate of 20 μL/min. The peptide separation was performed by a step linear gradient formed by mobile phase A and mobile phase B, from 0 to 35% B in 62 min, and from 35 to 50% of mobile phase B, in 15 min at a flow rate of 0.36 μL/min. The direct injection configuration was used for separation of the remaining collected fractions to improve analysis of hydrophobic peptides. The peptides were separated on a Zorbax 300SB C18 3.5 μm, 300 Å, 0.1 × 150 mm column (Agilent). Column temperature was kept constant at 45 °C, and the separation was monitored at 215 nm. The mobile phases were A, 3% ACN, 97% water, and 0.1% TFA (v/v) and B, 80% ACN, 20% water, and 0.1% TFA (v/v). The peptide separation was performed by a linear gradient formed by mobile phase A and mobile phase B, from 0 to 60% of mobile phase B in 93 min at a flow rate of 0.45 μL/min.

Mass Spectrometry Analysis: MALDI TOF/TOF

The Probot (Dionex) was used for online fraction collection and MALDI matrix addition. The eluent was mixed with the MALDI matrix solution using a microtee union. The final concentration of the α-cyano-4-hydroxycinnamic acid (Laser-Bio Laboratories) in the spotting solution was 2.3 mg/mL. The frequency of fraction collection was five fractions per minute and the volume of each fraction was 0.25 μL. The mass spectrometric analysis was performed on a 4800 MALDI TOF/TOF Analyzer (AB Sciex). Mass spectra were acquired from 800 to 4000 m/z window in the reflector positive ion mode. One spectrum was accumulated from 1250 laser shots. Tandem mass spectra of automatically selected precursor ions were acquired using a 1 kV MS/MS reflector positive ion mode. The quality of each tandem mass spectrum was monitored on-the-fly by stop conditions criteria with a maximum of 1800 laser shots per spectrum. For automatic selection of precursor ions, the exclusion of ±6.02 and ±10.01 Da precursor ion adducts was set up to ensure nonredundant acquisition and selection of the most intense precursor ion for each isotopically labeled peptide pair. Data acquisition and processing were carried out using 4000 Series Explorer software v3.5 (AB Sciex).

Protein Database Search and Criteria for Protein Quantification

Protein identification and quantification was conducted using ProteinPilot software v2.0.1 (AB Sciex) equipped with a Paragon searching algorithm,[31] Pro Group algorithm (AB Sciex) and a PSPEP script that permits false discovery rate estimation.[32] Searches were conducted against a concatenated target-decoy protein sequences database.[33] The target protein database was composed of mouse (*Mus musculus*) sequences (UniProt/KB; reference proteome; downloaded January, 2013;

50 517 sequences, including canonical and isoform sequences) and contaminant sequences (113 sequences, maintained in house). The decoy database was obtained by reversing the target protein database. The raw peptide identification results from the Paragon algorithm searches were further processed by the Pro Group algorithm within the ProteinPilot software before final display. The global FDR, defined as $FDR_{Global} = 2 \times$ (number of decoy hits/total number of hits) was calculated by PSPEP software.[32] Mouse proteins detected with the protein level global FDR < 1% were accepted. For quantification, the ProteinPilot software included peptides meeting all of the following criteria: complete labeling, peptides carrying at the most three labeled residues, peptides identified from spectra uniquely awarded to that peptide sequence, peptides not shared between different proteins, and peptides with the spectral level global FDR < 1%. The protein ratios, standard deviations, and p values employed to estimate the statistical significance of the protein changes were calculated by ProteinPilot. To filter out the proteins that displayed significant changes in the DRMs proteome upon infection, we performed a three-step data processing. First, only proteins identified and quantified in all three replicates with at least two unique peptides were considered. Second, only proteins with a 1.35-fold ratio in all three biological replicates were included. Third, only protein ratios with a p value $p \leq 0.01$ were accepted.

Immunolabeling and Fluorescence Microscopy

For immunofluorescence analysis, J774.2 macrophages were seeded on glass coverslips, infected, and afterward fixed for 20 min in 3.8% PFA (w/v) at room temperature. The PFA fixation was quenched with 50 mM NH_4Cl in PBS, and then the coverslips were washed in PBS and blocked in PBS, 3% BSA. The samples were permeabilized in 0.1% TX-100 (v/v) in PBS for 5 min followed by PFA fixation and incubated in primary antibodies diluted in blocking buffer for 1 h. The primary antibodies used were antitularemia serum (in house), anti-p62 (ProgenBiotik), and antiubiquitin (FK-2) (Callbiochem). The samples were then washed in PBS and incubated with secondary antibodies (Alexa Fluor 405, Molecular Probes) and biotin/Alexa Fluor 488/594 (Molecular Probes). Stained, washed, and dried coverslips were mounted on glass slides using mowiol mounting medium. Images of the samples were acquired using either the Eclipse E2 Nikon fluorescence microscope or Eclipse TE2000-E confocal laser scanning microscope.

Small Hairpin RNA (shRNA) Treatment

The J774.2 macrophages were spin-infected with p62-shRNA or control shRNA-encoding lentiviral particles produced in HEK293 T cells after cotransfection of respective transfer vectors (pLKO.1-shp62, sh control, Sigma) along with the second generation packaging vector psPAX2 and the envelope pMD2.G obtained from Addgene. After 72 h lentiviral transduction, the J774.2 cells were either subjected to puromycin selection (5 μg/mL) for 2 weeks or used directly for bacterial infection experiments.

Statistical Analysis

Statistical analysis calculations were performed using the GraphPad Prism software http://www.graphpad.com. Statistical analysis was performed using the Mann−Whitney test when comparing two groups and ANOVA test with Dunn's post-test for multiple comparisons when comparing three groups. Significance was defined as $p < 0.05$. Results are presented as

mean ± SD. Nonparametric tests were used when we compared groups with small sample sizes ($n = 3$).

RESULTS

Quantitative Proteomic Analysis of Macrophage-Derived Lipid Rafts after *Francisella tularensis* LVS Entry

A recent report showed the cholesterol-dependent entry of *Francisella tularensis* into macrophages.[18] We confirmed this finding in our in vitro infectious model system. In agreement with the published data, we found that treatment of macrophages with the cholesterol-depleting agent, MβCD, and cholesterol-binding agent, filipin, strongly reduced *F. tularensis* uptake into macrophages by more than 60% and 30%, respectively, within the first 60 min of postinfection (p.i.) (Supporting Information Figure S1). Because cholesterol is a key structural component of lipid rafts, it can be anticipated that *F. tularensis* entry induces raft aggregation, resulting in signaling molecule accumulation which, in turn, is important for its internalization and intracellular retention.

The purity of our lipid raft preparations was verified by the Western blot analysis of raft-associated proteins including flotillin-1, flotillin-2, acylated nonreceptor tyrosine kinases (Fyn and Lyn), caveolin-1, and caveolin-2 as well as the nonraft marker, transferrin receptor (Tfr). The raft markers, flotillin-1 and flotillin-2, as well as Fyn and Lyn, were detected in the DRMs fractions 2−5,[34] whereas the nonraft marker transferrin receptor (Tfr) was distributed within the non-DRMs fractions (Figure 1). Surprisingly, another typical raft marker, caveolin-1,
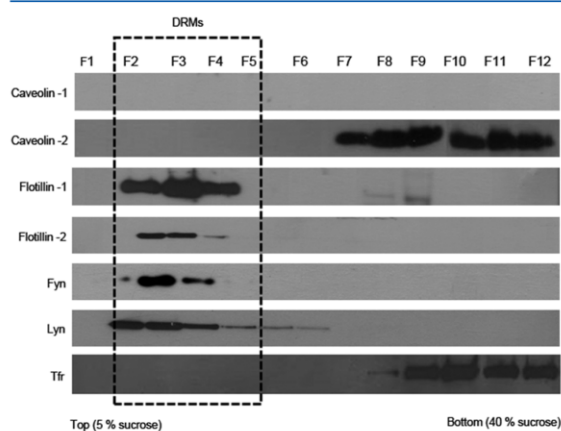

Figure 1. Distribution of DRMs-associated and detergent-soluble proteins within flotation density gradient. After ultracentrifugation, the sucrose gradient was divided into 12 fractions; the fraction 1 is the lightest, and the fraction 12 is the heaviest. Equal volumes of each fraction were separated by SDS-PAGE, transferred to a PVDF membrane, and probed for caveolin-1, caveolin-2, flotillin-1, flotillin-2, Fyn, Lyn, or transferrin receptor (TfR). Representative blots of three independent experiments are shown.

was not detected in any DRMs fractions using different antibodies. Gargalovic and Dory studied the expression of caveolin-1 and caveolin-2 in murine peritoneal macrophages and in different macrophage-like cell lines like Raw, J774.2, THP-1 using RT-PCR, immunoblotting, and immunofluorescence approaches.[35] Consistent with our data, caveolin-1 was expressed only in the THP-1 cell line. Caveolin-2 is considered to be an accessory protein for the caveolin-1-mediated

formation of caveolae.[36] In the absence of caveolin-1, as exemplified in J774 macrophages, caveolin-2 is not present at the cell surface but in the Golgi apparatus, detectable in detergent-soluble fractions.[37] In agreement with this notion, we observed the accumulation of caveolin-2 in detergent-soluble fractions of sucrose gradient and, thus, confirmed the previous findings.

We used the quantitative MS-based proteomic approach to specifically identify changes in protein composition of lipid rafts in response to *Francisella* infection (Figure 2). A total of 262
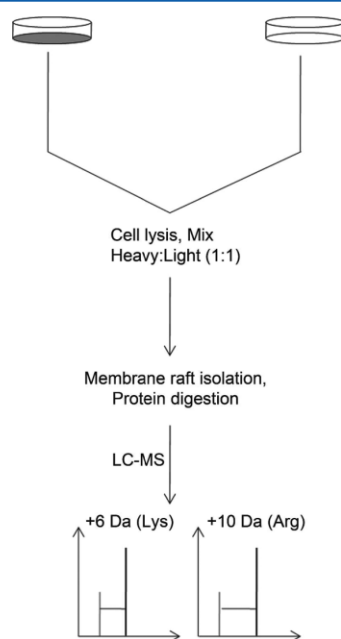

Figure 2. Experimental design: SILAC-based quantitative proteomic analysis of macrophage-derived lipid rafts upon *Francisella tularensis* LVS-stimulation. Light or heavy isotopic labeled cells were left untreated or stimulated with *Francisella tularensis* LVS for 10 min. Afterward, control and stimulated cell lysates were mixed at equal amounts. The lipid rafts were isolated using the low density detergent-resistant fractionation. The proteins were digested by trypsin, and the resulting peptides were fractionated and analyzed on LC/MS.

unique raft-associated proteins were identified reproducibly in three biological replicates at the false discovery rate of 1% (Supporting Information Table S1−S6). Only one protein, p62, was specifically recruited into the membrane raft region upon *Francisella* internalization in all three biological replicates. The recruitment of this protein was very specific (Table 1), and no other protein showed consistent significant quantitative change in all three biological replicates (Supporting Information Table S7).

Confirmation of *F. tularensis* LVS-Induced p62 Recruitment into Macrophage-Derived Lipid Rafts

To validate the *Francisella*-induced recruitment of p62 into lipid rafts, we performed Western blot analysis. As shown in Figure 3, p62 partitioned to detergent-soluble fractions under control conditions, but upon *Francisella* internalization, it was found redistributed to lipid rafts. Thus, this finding confirmed the SILAC proteomics data.

D

Table 1. Quantitative Analysis of Macrophage-Derive Lipid Rafts upon *F. tularensis* LVS Entry

|	Uniprot ID	protein name	peptide ID confidence	peptide sequence	peptide ratio (Ft control)	protein ratio (Ft control)	protein *p* value
biological replicate I	sp|Q64337| SQSTM_MOUSE	p62	99	EHRPPCAQEAFR	3.3	2.85	0.000 009 85
			99	FSFCTSPEAEAQAAAGPGPCER	2.89		
			99	IFPNPFGHLSDSFSHSR	2.14		
			99	LIFPNPFGHLSDSFSHSR	2.11		
			99	NMVHPNVICDGCNGPVVGTR	1.53		
			99	NYDIGAALDTIQYSK	2.2		
			99	REHRPPCAQEAPR	3.72		
			99	YKCSVCPDYDLCSVCEGK	1.85		
biological replicate II	sp|Q64337| SQSTM_MOUSE	p62	99	AGDGRPCPTAESASAPPEDPNVNFLK	4.78	4.49	2.393 840 459 191 67 ×10^{-9}
			99	CSVCPDYDLCSVCEGK	2.79		
			99	EHRPPCAQEAPR	4.39		
			99	FPNPFGHLSDSFSHSR	3.95		
			99	FSFCFSPEPEAEAQAAAGPGPCER	5.21		
			99	LIFPNPFGHLSDSFSHSR	5.19		
			99	NMVHPNVICDGCNGPVVGTR	2.21		
			99	REHRPPCAQEAPR	5.94		
biological replicate III	sp|Q64337| SQSTM_MOUSE	p62	99	AGDGRPCPTAESASAPPEDPNVNFLK	1.63	1.37	0.00436378316953778
			99	CFSPEPEAEAQAAAGPGPCER	1.37		
			99	CPDYDLCSVCEGK	1.1		
			99	EAALYPHLPPEADPR	1.26		
			99	FPNPFGHLSDSFSHSR	1.3		
			99	FPTLRPGGF	1.00		
			99	FPTLRPGGFQAH	1.10		
			99	FPTLRPGGFQAHYR	1.33		
			99	FSFCFSPEPEAEAQAAAGPGPCER	1.39		
			99	IALESVGQPEEQMESGNCSGGDDDWTHLSSK	1.36		
			99	NMVHPNVICDGCNGPVVGTR	1.35		
			99	RPPCAQEAPR	1.50		
			99	SFCFSPEPEAEAQAAAGPGPCER	1.52		
			99	SNTQPSSCSSEVSKPDGAGEGPAQSLTEQM	1.36		
			99	SNTQPSSCSSEVSKPDGAGEGPAQSLTEQMK	1.34		
			99	WPGWEMGPPGNWSPRPPR	2.10		
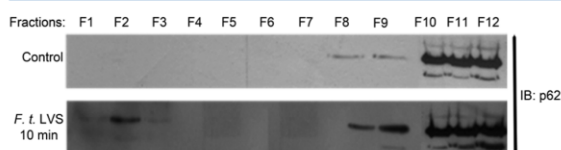
Figure 3. *F. tularensis* LVS-induced recruitment of p62 protein into macrophage-derived lipid rafts. Each fraction (fractions 1−12) of the sucrose gradient from control or *F. tularensis* LVS-stimulated J774.2 macrophages was analyzed by immunoblotting with anti-p62 antibody. Representative blots of two independent experiments are shown.

p62 Links Ubiquitinated *F. tularensis* LVS with Autophagy Machinery

The protein p62 is known to be a cytoplasmic multimodule adaptor protein. It is comprised of several domains that enable the interaction with diverse group of proteins as well as the regulation of a variety of cellular processes. The C-terminal end harbors an ubiquitin-associated domain (UBA) that interacts with polyubiquitinated molecules.[38] Adjacent to the UBA domain is a LC3-interacting region (LIR) that is able to interact with the autophagosomal marker, LC3. Thus, p62 can function

as a linker coordinating the degradation of polyubiquitinated protein aggregates with the process of autophagy.[39] In this context, we investigated whether p62 plays a role in the activation of early autophagy of *F. tularensis* LVS. Using confocal microscopy, we observed a transient colocalization of p62 with ubiquitinated proteins around *F. tularensis* LVS microbes (Figure. 4A). Time-course experiments revealed that this colocalization peaked at 1 h p.i. and gradually dropped under ~5% within 12 h p.i. (Figure. 4C). Approximately 50% of the ubiquitinated bacteria colocalized with the p62. Next, we focused on the association of p62 with the intracellular population of bacteria targeted by autophagy. Toward this end, the J774.2 macrophages expressing the autophagy marker GFP-LC3 were infected by *F. tularensis* LVS and the localization of both the p62 and GFP-LC3 was analyzed (Figure 4B). Similar to ubiquitinated bacteria, the colocalization of the p62 with GFP-LC3$^+$ bacteria was up to 50% at 1 h p.i. (Figure 4C).

To determine the biological relevance of the p62 in the autophagic process during *F. tularensis* LVS infection, we knocked down the p62 expression in J774.2 macrophages by shRNA-mediated silencing (Figure 5A). Subsequent infection
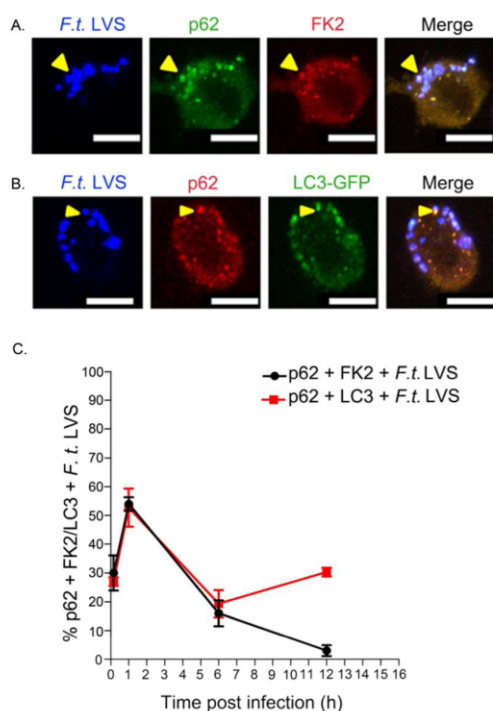
E

Figure 4. *F. tularensis* LVS is targeted by autophagy at an early stage after microbial invasion. The p62 colocalization with Ub positive (Ub +) or GFP-LC3 positive (GFP-LC3+) *F. tularensis* microbes. (A) J774.2 cells were infected with *F. tularensis* LVS, fixed, and processed for labeling with *F. tularensis* LVS antibody (in blue), the p62 antibody (in green), and the ubiquitin antibody (FK2, in red). Scale bar, 10 μm. Arrowheads indicate Ub+ or GFP-LC3+ bacteria. (B) J774.2 cells were infected with *F. tularensis* LVS, fixed, and processed for labeling with *F. tularensis* LVS antibody (in blue) and the p62 antibody (in red). Scale bar, 10 μm. Arrowheads indicate GFP-LC3+ bacteria. (C) Kinetics of generation of ubiquitin-positive or GFP-LC3 positive *F. tularensis* LVS. The percentage of Ub+ or GFP-LC3+ bacteria colocalizing with p62 was enumerated by fluorescence microscopy. Data are mean ± SD, and at least 100 bacteria were counted for each condition. The data are presented as the average ± SD for three independent experiments.
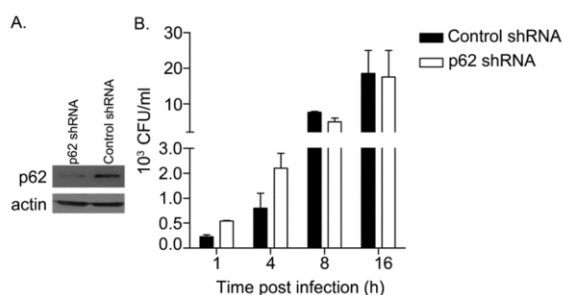

Figure 5. Deficiency of p62 resulted in increased *F. tularensis* LVS replication inside macrophages. (A) Knockdown of p62 expression was verified by immunoblotting. (B) Intracellular growth of *F. tularensis* LVS in the wild-type and p62 knockdown cells was determined by CFU analysis. Data shown are representative of results obtained in three independent experiments.

of the p62 knockdown macrophages with *F. tularensis* LVS led to an increase in bacterial load during the first 4 h of infection compared to that of the control cells. However, there was no significant difference in bacterial number between wild type and knockdown cells at later time points, indicating that the inhibition of the early autophagic process did not affect the final fate of bacterial invasion (Figure 5B).

■ DISCUSSION

F. tularensis is a bacterium with an intracellular lifestyle that has developed the efficient strategy to exploit endogenous host pathways in order to dampen the pro-inflammatory pathway.[40] However, much less is known about the host–pathogen interaction at the time of entry and about the subsequent behavior of *F. tularensis* inside host cells. For example, a recent study highlighted the impact of *F. tularensis* entry mode on the speed and extent of phagosomal escape, which limits intracellular replication in the cytosol.[41] Consistent with the previous finding,[18] we found that *F. tularensis* LVS requires intact cholesterol-rich lipid rafts to enter J774.2 macrophages. Disruption of their integrity using MβCD or filipin led to the significant inhibition of bacterial entry. The extent of the inhibition reflected different mechanisms of action of the drugs.[42]

To investigate whether the bacterial entry can induce the plasma membrane signaling events that influence the intracellular fate of bacteria, we performed an unbiased quantitative proteomics analysis of the lipid rafts isolated from *F. tularensis* infected macrophages. Taking advantage of the DRMs isolation on the buoyant density gradient, it is possible to identify proteins enriched in lipid rafts by MS-based proteomic approach.

Our analysis identified, in total, 262 proteins enriched in DRMs fractions. The identification included membrane raft-associated proteins such as flotillin-1, flotillin-2, PAG, NTAL, GTP binding proteins, both small GTP-binding proteins involved in cytoskeleton rearrangements and heterotrimeric G proteins involved in signal transduction, and acylated tyrosine kinases as well as proteins harboring putative post-translational modifications that direct these proteins into the environment of lipid rafts.[43] As expected, similar to other lipid rafts studies, we also copurified nonrafts proteins in our DRMs fraction due to the nature of biochemical isolation technique itself. However, the SILAC quantitative proteomics approach allowed us to selectively focus on those proteins exhibiting significant dynamic changes in their partitioning upon *F. tularensis* LVS internalization.[44]

Our proteomic analysis unveiled that only one protein, the p62, was significantly recruited into the macrophage-derived lipid rafts region upon *F. tularensis* LVS entry. As an autophagy adaptor protein, p62 serves as a link between ubiquitinated proteins and the autophagy pathway.[45] We showed that the interaction of *F. tularensis* LVS with p62, ubiquitin, and LC3 autophagy component occurs very early and peaks at 1 h p.i. On the contrary, the previous data described the activation of LC3-mediated *Francisella* autophagy at later time of the infection, after bacteria replication in the cytosol.[17] However, in the study by Checroun and colleagues, the conclusions that *Francisella* induces autophagy in the late stage of the infection was based on the examination of replicating cytosolic bacteria at 24 h p.i., a different time window compared to our experimental set up. Both of these findings are consistent with the observations of Chiu et al. describing the antibacterial effect

of AR-12 autophagy-inducing small molecule on *Francisella* replication inside human THP-1 macrophages. The kinetic study revealed that AR-12 can induce autophagy-based anti-*F. tularensis* activity in human macrophages at 2.5 and 24 h p.i.[46] Furthermore, a similar early autophagy induction was described for *Salmonella typhimurium*[47] and *Listeria monocytogenes* infections.[48] Thus, this early autophagic response to pathogen invasion seems to be a more general phenomenon.

A growing body of evidence indicates that the p62 serves as an autophagy adaptor protein for delivering cytosolic bacteria into autophagosome.[49,50] The importance of *Francisella*-p62 interaction for microbial survival inside host cells was verified by CFU counting of the intracellular bacteria in the p62 knockdown macrophages. The CFU analysis revealed an increase in the number of intracellular *F. tularensis* LVS microbes in the p62 knockdown cells in the early stage of infection. This increase, however, was not permanent, and the number of microbes in both the wild type and the p62 knockdown host cells reached similar levels at 8 h p.i., suggesting that *F. tularensis* LVS must overcome the early stage of the autophagic process to successfully multiply inside the host macrophages. Consistently, the inhibitory effect of AR-12-induced autophagy on intracellular survival was abolished 12 h p.i.[46] This assumption is further corroborated by the microarray data showing that both highly virulent *F. tularensis* SchuS4 and *F. novicida* can downregulate genes required for both autophagosome nucleation and for elongation of autophagic vesicles.[51]

However, it is not clear how the autophagy process is activated. A recent study demonstrated the TLR2-dependent activation of autophagy. It has been shown that the triggering of TLR2 signaling pathway during phagocytosis recruits the autophagy protein LC3 to phagosomes and promotes their acidification and microbial killing. Interestingly, translocation of LC3 to the phagosome was not associated with the formation of double-membrane vacuole.[52] Similarly to TLR2-induced autophagy, we also did not observe the formation of double-membrane vacuoles around phagocytosed *Francisella* microbes at 1 h p.i. when the interaction between p62 and GFP-LC3 decorated bacteria reaches its maximum (data not shown).

In summary, our study shows for the first time the early activation of autophagic process in macrophages invaded by *F. tularensis* LVS microbes. This process is mediated by p62 adaptor protein, which accumulates in lipid rafts at the time of bacterial entry. The effect of autophagy on inhibition of bacterial growth is only transient because *F. tularensis* can apparently overcome this inhibition.

Table 1. J774.2 macrophages were either nonstimulated or stimulated with *F. tularensis* LVS for 10 min. Autophagy protein p62 showed consistent recruitment into membrane raft upon *F. tularensis* LVS entry. The peptide confidence, identified peptides, peptide ratios, protein ratios, and *p* values from ProteinPilot are presented in the table.

■ ASSOCIATED CONTENT

Ⓢ Supporting Information

Identified DRMs associated proteins in Biological Replicate 1 (BR01) generated by Protein Pilot, identified and quantified DRMs associated proteins in Biological Replicate 2 (BR02) generated by Protein Pilot, identified and quantified DRMs associated proteins in Biological Replicate 3 (BR03) generated by Protein Pilot, identified and quantified DRMs associated peptides in BR01 generated by Protein Pilot, identified and quantified DRMs associated peptides in BR02 generated by Protein Pilot, identified and quantified DRMs associated peptides in BR03 generated by Protein Pilot, identified and quantified DRMs associated proteins by three biological replicates. This material is available free of charge via the Internet at http://pubs.acs.org.

■ AUTHOR INFORMATION

Corresponding Author

*J. Stulik. E-mail: jstulik@pmfhk.cz. Phone: +42 097 325 3220. Fax: +42 049 551 2451.

Author Contributions

The manuscript was written through contributions of all authors. All authors have given approval to the final version of the manuscript.

Notes

The authors declare no competing financial interest.

■ ABBREVIATONS

ANOVA, analysis of variance; ATCC, American type culture collection; CDC, Centers for Disease Control and Prevention; CFU, colony forming units; DMEM, , Dulbecco's modified eagle's medium; DRMs, detergent resistant membranes; DsBA, disulfide oxidoreductase; EACC, European collection of cell Culture; F. tularensis, francisellatularensis; Ft, francisellatularensis; FBS, fetal bovine serum; FDR, false discovery rate; GTP, guanosine-5′-triphosphate; LIR, LC3-interacting region; LVS, live vaccine strain; MOI, multiplicity of infection; MβCD, methyl-β-cyclodextrin; MΦ, macrophages; NaCl, natrium chloride; OD, optical density; PBS, phosphate buffered saline; PFA, paraformaldehyde; PI, post-infection; RP, reversed phase; RT, room temperature; SD, standard deviations; shRNA, small hairpin RNA; SILAC, stable isotope labeling with amino acids in cell culture; Sqstm-1, sequestosome-1; TCEP, tris(2-carboxyethyl)phosphine; Tfr, transferrin receptor; TLR, toll like receptor; TX-100, Triton X-100; UBA, ubiquitin associated domains

■ REFERENCES

(1) Tarnvik, A.; Berglund, L. Tularaemia. *Eur. Respir. J.* **2003**, *21* (2), 361−373.

(2) Saslaw, S.; Eigelsbach, H. T.; Prior, J. A.; Wilson, H. E.; Carhart, S. Tularemia vaccine study. II. Respiratory challenge. *Arch. Intern. Med.* **1961**, *107*, 702−714.

(3) Dennis, D. T.; Inglesby, T. V.; Henderson, D. A.; Bartlett, J. G.; Ascher, M. S.; Eitzen, E.; Fine, A. D.; Friedlander, A. M.; Hauer, J.; Layton, M.; Lillibridge, S. R.; McDade, J. E.; Osterholm, M. T.; O'Toole, T.; Parker, G.; Perl, T. M.; Russell, P. K.; Tonat, K.. Tularemia as a biological weapon: medical and public health management. *JAMA* **2001**, *285* (21), 2763−2773.

(4) Bosio, C. M.; Dow, S. W. Francisella tularensis induces aberrant activation of pulmonary dendritic cells. *J. Immunol.* **2005**, *175* (10), 6792−6801.

(5) Hall, J. D.; Woolard, M. D.; Gunn, B. M.; Craven, R. R.; Taft-Benz, S.; Frelinger, J. A.; Kawula, T. H.. Infected-host-cell repertoire and cellular response in the lung following inhalation of Francisella tularensis Schu S4, LVS, or U112. *Infect. Immun.* **2008**, *76* (12), 5843−5852.

(6) Clemens, D. L.; Lee, B. Y.; Horwitz, M. A. Francisella tularensis enters macrophages via a novel process involving pseudopod loops. *Infect. Immun.* **2005**, *73* (9), 5892−5902.

(7) Balagopal, A.; MacFarlane, A. S.; Mohapatra, N.; Soni, S.; Gunn, J. S.; Schlesinger, L. S. Characterization of the receptor-ligand pathways important for entry and survival of Francisella tularensis in human macrophages. *Infect. Immun.* **2006**, *74* (9), 5114−5125.

(8) Schulert, G. S.; Allen, L. A. Differential infection of mononuclear phagocytes by Francisella tularensis: role of the macrophage mannose receptor. *J. Leukocyte Biol.* **2006**, *80* (3), 563−571.

(9) Pierini, L. M. Uptake of serum-opsonized Francisella tularensis by macrophages can be mediated by class A scavenger receptors. *Cell Microbiol.* **2006**, *8* (8), 1361−1370.

(10) Santic, M.; Asare, R.; Skrobonja, I.; Jones, S.; Abu Kwaik, Y. Acquisition of the vacuolar ATPase proton pump and phagosome acidification are essential for escape of Francisella tularensis into the macrophage cytosol. *Infect. Immun.* **2008**, *76* (6), 2671−2677.

(11) Golovliov, I.; Baranov, V.; Krocova, Z.; Kovarova, H.; Sjostedt, A. An attenuated strain of the facultative intracellular bacterium Francisella tularensis can escape the phagosome of monocytic cells. *Infect. Immun.* **2003**, *71* (10), 5940−5950.

(12) Clemens, D. L.; Lee, B. Y.; Horwitz, M. A. Virulent and avirulent strains of Francisella tularensis prevent acidification and maturation of their phagosomes and escape into the cytoplasm in human macrophages. *Infect. Immun.* **2004**, *72* (6), 3204−3217.

(13) Straskova, A.; Pavkova, I.; Link, M.; Forslund, A. L.; Kuoppa, K.; Noppa, L.; Kroca, M.; Fucikova, A.; Klimentova, J.; Krocova, Z.; Forsberg, A.; Stulik, J. Proteome analysis of an attenuated Francisella tularensis dsbA mutant: identification of potential DsbA substrate proteins. *J. Proteome Res.* **2009**, *8* (11), 5336−5346.

(14) Lindgren, H.; Golovliov, I.; Baranov, V.; Ernst, R. K.; Telepnev, M.; Sjostedt, A. Factors affecting the escape of Francisella tularensis from the phagolysosome. *J. Med. Microbiol.* **2004**, *53* (Pt 10), 953−958.

(15) Santic, M.; Molmeret, M.; Klose, K. E.; Jones, S.; Kwaik, Y. A. The Francisella tularensis pathogenicity island protein IglC and its regulator MglA are essential for modulating phagosome biogenesis and subsequent bacterial escape into the cytoplasm. *Cell Microbiol.* **2005**, *7* (7), 969−979.

(16) Bonquist, L.; Lindgren, H.; Golovliov, I.; Guina, T.; Sjostedt, A. MglA and Igl proteins contribute to the modulation of Francisella tularensis live vaccine strain-containing phagosomes in murine macrophages. *Infect. Immun.* **2008**, *76* (8), 3502−3510.

(17) Checroun, C.; Wehrly, T. D.; Fischer, E. R.; Hayes, S. F.; Celli, J. Autophagy-mediated reentry of Francisella tularensis into the endocytic compartment after cytoplasmic replication. *Proc. Natl. Acad. Sci. U. S. A.* **2006**, *103* (39), 14578−14583.

(18) Tamilselvam, B.; Daefler, S. Francisella targets cholesterol-rich host cell membrane domains for entry into macrophages. *J. Immunol.* **2008**, *180* (12), 8262−8271.

(19) Law, H. T.; Lin, A. E.; Kim, Y.; Quach, B.; Nano, F. E.; Guttman, J. A. Francisella tularensis uses cholesterol and clathrin-based endocytic mechanisms to invade hepatocytes. *Sci. Rep.* **2011**, *1*, 192.

(20) Simons, K.; Ikonen, E. How cells handle cholesterol. *Science* **2000**, *290* (5497), 1721−1726.

(21) Simons, K.; Ikonen, E. Functional rafts in cell membranes. *Nature* **1997**, *387* (6633), 569−572.

(22) Knodler, L. A.; Vallance, B. A.; Hensel, M.; Jackel, D.; Finlay, B. B.; Steele-Mortimer, O. Salmonella type III effectors PipB and PipB2 are targeted to detergent-resistant microdomains on internal host cell membranes. *Mol. Microbiol.* **2003**, *49* (3), 685−704.

(23) Lafont, F.; Tran Van Nhieu, G.; Hanada, K.; Sansonetti, P.; van der Goot, F. G. Initial steps of Shigella infection depend on the cholesterol/sphingolipid raft-mediated CD44-IpaB interaction. *EMBO J.* **2002**, *21* (17), 4449−4457.

(24) John Gatfield, J. P. Essential Role for Cholesterol in Entry of Mycobacteria into Macrophages. *Science* **2000**, *288* (5471), 1647−1651.

(25) Rosenberger, C. M.; Brumell, J. H.; Finlay, B. B. Microbial pathogenesis: lipid rafts as pathogen portals. *Curr. Biol.* **2000**, *10* (22), R823−825.

(26) Hartlova, A.; Cerveny, L.; Hubalek, M.; Krocova, Z.; Stulik, J. Membrane rafts: a potential gateway for bacterial entry into host cells. *Microbiol. Immunol.* **2010**, *54* (4), 237−245.

(27) Conlan, J. W.; KuoLee, R.; Shen, H.; Webb, A. Different host defences are required to protect mice from primary systemic vs pulmonary infection with the facultative intracellular bacterial pathogen, Francisella tularensis LVS. *Microb. Pathog.* **2002**, *32* (3), 127−134.

(28) Gupta, N.; Wollscheid, B.; Watts, J. D.; Scheer, B.; Aebersold, R.; DeFranco, A. L. Quantitative proteomic analysis of B cell lipid rafts reveals that ezrin regulates antigen receptor-mediated lipid raft dynamics. *Nat. Immunol.* **2006**, *7* (6), 625−633.

(29) Mann, M. Functional and quantitative proteomics using SILAC. *Nat. Rev. Mol. Cell Biol.* **2006**, *7* (12), 952−958.

(30) Gilar, M.; Olivova, P.; Daly, A. E.; Gebler, J. C. Orthogonality of separation in two-dimensional liquid chromatography. *Anal. Chem.* **2005**, *77* (19), 6426−6434.

(31) Shilov, I. V.; Seymour, S. L.; Patel, A. A.; Loboda, A.; Tang, W. H.; Keating, S. P.; Hunter, C. L.; Nuwaysir, L. M.; Schaeffer, D. A. The Paragon Algorithm, a next generation search engine that uses sequence temperature values and feature probabilities to identify peptides from tandem mass spectra. *Mol. Cell Proteomics* **2007**, *6* (9), 1638−1655.

(32) Tang, W. H.; Shilov, I. V.; Seymour, S. L. Nonlinear fitting method for determining local false discovery rates from decoy database searches. *J Proteome Res.* **2008**, *7* (9), 3661−3667.

(33) Elias, J. E.; Gygi, S. P. Target-decoy search strategy for mass spectrometry-based proteomics. *Methods Mol. Biol.* **2010**, *604*, 55−71.

(34) Neumann-Giesen, C.; Falkenbach, B.; Beicht, P.; Claasen, S.; Luers, G.; Stuermer, C. A.; Herzog, V.; Tikkanen, R. Membrane and raft association of reggie-1/flotillin-2: role of myristoylation, palmitoylation and oligomerization and induction of filopodia by overexpression. *Biochem. J.* **2004**, *378* (Pt 2), 509−518.

(35) Gargalovic, P.; Dory, L. Caveolins and macrophage lipid metabolism. *J. Lipid Res.* **2003**, *44* (1), 11−21.

(36) Scherer, P. E.; Lewis, R. Y.; Volonte, D.; Engelman, J. A.; Galbiati, F.; Couet, J.; Kohtz, D. S.; van Donselaar, E.; Peters, P.; Lisanti, M. P. Cell-type and tissue-specific expression of caveolin-2. Caveolins 1 and 2 co-localize and form a stable hetero-oligomeric complex in vivo. *J. Biol. Chem.* **1997**, *272* (46), 29337−29346.

(37) Gargalovic, P.; Dory, L. Caveolin-1 and caveolin-2 expression in mouse macrophages. High density lipoprotein 3-stimulated secretion and a lack of significant subcellular co-localization. *J. Biol. Chem.* **2001**, *276* (28), 26164−26170.

(38) Moscat, J.; Diaz-Meco, M. T.; Wooten, M. W. Signal integration and diversification through the p62 scaffold protein. *Trends Biochem. Sci.* **2007**, *32* (2), 95−100.

(39) Pankiv, S.; Clausen, T. H.; Lamark, T.; Brech, A.; Bruun, J. A.; Outzen, H.; Overvatn, A.; Bjorkoy, G.; Johansen, T. p62/SQSTM1 binds directly to Atg8/LC3 to facilitate degradation of ubiquitinated protein aggregates by autophagy. *J. Biol. Chem.* **2007**, *282* (33), 24131−24145.

(40) Wehrly, T. D.; Chong, A.; Virtaneva, K.; Sturdevant, D. E.; Child, R.; Edwards, J. A.; Brouwer, D.; Nair, V.; Fischer, E. R.; Wicke, L.; Curda, A. J.; Kupko, J. J., 3rd; Martens, C.; Crane, D. D.; Bosio, C. M.; Porcella, S. F.; Celli, J. Intracellular biology and virulence determinants of Francisella tularensis revealed by transcriptional profiling inside macrophages. *Cell Microbiol.* **2009**, *11* (7), 1128−1150.

(41) Geier, H.; Celli, J. Phagocytic receptors dictate phagosomal escape and intracellular proliferation of Francisella tularensis. *Infect. Immun.* **2011**, *79* (6), 2204−2214.

(42) Naroeni, A.; Porte, F. Role of cholesterol and the ganglioside GM(1) in entry and short-term survival of Brucella suis in murine macrophages. *Infect. Immun.* **2002**, *70* (3), 1640−1644.

(43) Bini, L.; Pacini, S.; Liberatori, S.; Valensin, S.; Pellegrini, M.; Raggiaschi, R.; Pallini, V.; Baldari, C. T. Extensive temporally regulated

108

reorganization of the lipid raft proteome following T-cell antigen receptor triggering. *Biochem. J.* **2003**, *369* (Pt 2), 301–309.

(44) Foster, L. J.; De Hoog, C. L.; Mann, M. Unbiased quantitative proteomics of lipid rafts reveals high specificity for signaling factors. *Proc. Natl. Acad. Sci. U. S. A.* **2003**, *100* (10), 5813–5818.

(45) Waters, S.; Marchbank, K.; Solomon, E.; Whitehouse, C. A. Autophagic receptors Nbr1 and p62 coregulate skeletal remodeling. *Autophagy* **2010**, *6* (7), 981–983.

(46) Chiu, H. C.; Soni, S.; Kulp, S. K.; Curry, H.; Wang, D.; Gunn, J. S.; Schlesinger, L. S.; Chen, C. S. Eradication of intracellular Francisella tularensis in THP-1 human macrophages with a novel autophagy inducing agent. *J. Biomed. Sci.* **2009**, *16*, 110.

(47) Zheng, Y. T.; Shahnazari, S.; Brech, A.; Lamark, T.; Johansen, T.; Brumell, J. H. The adaptor protein p62/SQSTM1 targets invading bacteria to the autophagy pathway. *J. Immunol.* **2009**, *183* (9), 5909–5916.

(48) Mostowy, S.; Sancho-Shimizu, V.; Hamon, M. A.; Simeone, R.; Brosch, R.; Johansen, T.; Cossart, P. p62 and NDP52 proteins target intracytosolic Shigella and Listeria to different autophagy pathways. *J. Biol. Chem.* **2011**, *286* (30), 26987–26995.

(49) Shaid, S.; Brandts, C. H.; Serve, H.; Dikic, I. Ubiquitination and selective autophagy. *Cell Death Differ.* **2013**, *20* (1), 21–30.

(50) Johansen, T.; Lamark, T. Selective autophagy mediated by autophagic adapter proteins. *Autophagy* **2011**, *7* (3), 279–296.

(51) Cremer, T. J.; Amer, A.; Tridandapani, S.; Butchar, J. P. Francisella tularensis regulates autophagy-related host cell signaling pathways. *Autophagy* **2009**, *5* (1), 125–128.

(52) Sanjuan, M. A.; Dillon, C. P.; Tait, S. W.; Moshiach, S.; Dorsey, F.; Connell, S.; Komatsu, M.; Tanaka, K.; Cleveland, J. L.; Withoff, S.; Green, D. R. Toll-like receptor signalling in macrophages links the autophagy pathway to phagocytosis. *Nature* **2007**, *450* (7173), 1253–1257.

4.5. Eosinophils from patients with type 1 diabetes mellitus express high level of myeloid α-defensins and myeloperoxidase.

In this study we have described enhanced expression of myeloid α-defensins in capillary blood of type 1 diabetic (T1D) patients. We have identified eosinophils as the source of myeloid α-defensin expression. Based on myeloid α-defensin mRNA expression we could distinguish two groups of patients, defensin-high-diabetics (DHD) and defensin-normal-diabetics (DND). Eosinophils of DHD patients expressed 200x higher levels of DEFA1-3 mRNA and contained significantly higher amount DEFA1-3 protein as measured by intracellular FACS than eosinophils isolated from healthy donors. We have demonstrated that myeloid α-defensins could serve as a reliable molecular signature of eosinophil cellular activation. Our results demonstrated the presence of transcriptionally active eosinophils in patients with T1D and argue for the involvement of innate immunity at the onset of T1D. While our findings did not provide the elucidation of the mechanism of eosinophil activation in patients with T1D, based on published data, we hypothesized that eosinophil activation could be a direct consequence of bacterial or viral infections. Our speculative model envisions a plausible involvement of eosinophils in the pathogenesis of T1D through their TLR-mediated activation and subsequent degranulation. This way, cytotoxic proteins released from eosinophil primary granules could cause severe tissue damage and in turn, initiate immune presentation of autoantigens linked to the pathogenic process of self-destruction. In this scenario, α-defensin expression in eosinophils could serve as a molecular readout of the progression of diabetogenic process. Moreover, we believe that this study will promote heightened interest of research community in the involvement of eosinophils in the onset of autoimmune-related diseases in general.

Authors contribution: qRT-PCR analyses, intracellular FACS

Contents lists available at SciVerse ScienceDirect

Cellular Immunology

Eosinophils from patients with type 1 diabetes mellitus express high level of myeloid alpha-defensins and myeloperoxidase

Aleš Neuwirth [a], Jan Dobeš [a], Jana Oujezdská [a], Ondřej Ballek [a], Martina Benešová [a], Zdeněk Šumník [b], Jana Včeláková [b], Stanislava Koloušková [b], Barbora Obermannová [b], Michal Kolář [c], Kateřina Štechová [b,1], Dominik Filipp [a,*,1]

[a] Laboratory of Immunobiology, Institute of Molecular Genetics AS CR, Prague, Czech Republic
[b] Department of Paediatrics, 2nd Faculty of Medicine, Charles University and University Hospital Motol, Prague, Czech Republic
[c] Laboratory of Genomics and Bioinformatics, Institute of Molecular Genetics AS CR, Prague, Czech Republic

ARTICLE INFO

ABSTRACT

Type 1 diabetes (T1D) is an autoimmune disease caused by T-cell mediated destruction of pancreatic beta cells. Recently, small cationic α-defensin molecules have been implicated in the pathogenesis of certain inflammatory and autoimmune diseases. The purpose of this study was to assess the α-defensin expression in patients with T1D and elucidate the cellular source of their production. Our results show that 30% of patients exhibit increased levels of α-defensin mRNAs in their capillary blood. Quantitative RT-PCR performed on FACS-sorted granulocytes identified CD15^{dull}/CD14^{weak} population as the cellular source of α-defensins. Surprisingly, this granulocyte subpopulation displayed augmentation of α-defensin expression in all T1D patients tested. The determination of cell surface markers, expression of cell-specific genes and confocal microscopy identified CD15^{dull}/CD14^{weak} cells as eosinophils. The presence of transcriptionally active eosinophils in diabetic patients suggests that eosinophils could be a part of an intricate innate immune cellular network involved in the development of diabetes.

© 2012 Elsevier Inc. All rights reserved.

1. Introduction

Type 1 diabetes (T1D) is an autoimmune disease characterized by a progressive destruction of insulin-producing pancreatic β-cells. The subsequent insulin deficiency is clinically recognizable only when 85–95% of pancreatic β-cells are destroyed during the so-called pre-diabetic phase [1]. Etiology of this disease is rather complex and stems from the failure of immune homeostatic mechanisms to maintain tolerance due to largely uncharacterized but obviously unfavorable interactions between genes and environmental factors in genetically predisposed individuals [2].

T-cells and other cellular and humoral components of adaptive immune system are central to the mechanism of β-cell destruction [2]. In contrast, components of the innate immune system have not been considered an integral part of cellular pathways involved in the maintenance of immune tolerance and hence were deemed

unimportant for autoimmunity. And although there is a growing evidence for the pathogenic role of innate immune cells in the initiation and destruction phases of T1D [3], the nature of innate immune mechanisms that conspire with adaptive ones to initiate the break of tolerance are largely obscure.

Myeloid alpha-defensins (m-α-defensins), an evolutionary ancient group of antimicrobial peptides, represent an essential part of the humoral branch of innate immunity [4]. They are synthesized mainly by neutrophils during their promyelocytic stage of maturation in the bone marrow and stored with other bactericidal and proteolytic proteins in peroxidase-positive, so called primary or azurophilic granules [5]. After the exit of neutrophils from bone marrow into circulation, transcription of these granule proteins including m-α-defensin ceases and stays on a very low basal level. m-α-Defensins are involved in the destruction of microbes following phagocytosis, degranulation or the formation of neutrophil extracellular traps (NETs) [6]. Additional activities of m-α-defensins include the modulation of cell signaling, chemotoxicity and wound healing [7].

Previous reports suggested that m-α-defensins could also be involved in the pathogenesis of certain inflammatory and autoimmune diseases [8–10]. In addition, our independent study in a rat model of diabetes revealed an intriguing correlation between the

tissue-specific expression of defensins and the incidence of diabetes (manuscript in preparation). These outcomes prompted us to assess the α-defensin expression pattern in patients with T1D and to identify the cellular source of their production.

2. Materials and methods

2.1. Participants

All 30 patients participating in the study were diagnosed with T1D according to ADA criteria [11] and were treated with insulin. Their mean age at the time of diagnosis was 14.4 ± SD 3.9 (range 4–38) years. The control group consisted of 30 healthy volunteers, with the mean age 21.3 ± SD 6.2 (range 11–33) years. To be included in the study, all participants or their lawful custodians had to sign an informed consent. This study was approved by the ethics committees of the Institute of Molecular Genetics and the 2nd Faculty of Medicine, Motol, Prague, Czech Republic.

2.2. qRT PCR

Total RNA from a capillary (200 μl from the finger) or a venous blood sample was isolated using RNeasy protect animal blood kit (Qiagen, Hilden, Germany). Total RNA from sorted cells was isolated using RNeasy plus micro kit (Qiagen, Hilden, Germany). RNA was reverse-transcribed using SuperScript III (Invitrogen, Carlsbad, USA). The expression of human m-α-defensins (DEFA1-3), myeloperoxidase (MPO) and eosinophilic cationic protein (ECP) was normalized to glyceraldehyde 3-phosphate dehydrogenase (GAPDH). All experiments were performed in triplicates on a Roche LC480 cycler using the Sybr green master mix (Roche, Mannheim, Germany). The following pairs of primers were used in PCR reactions: DEFA1-3: 5′-CTT GGC TCC AAA GCA TCC-3′, 5′-TCC CTG GTA GAT GCA GGT TC-3′, MPO: 5′-CCC TGT CTC CTC ACC AAC C-3′, 5′-ATC TCA CTG GAA CGG GTG TC-3′, ECP: 5′-AGC TGG ATC AGT TCT CAC AGG-3′, 5′-AGC CCT CCA CAC CCA TAA G-3′. Target gene expression was quantified using the relative quantification model with efficiency correction [12].

2.3. Flow cytometry and cell sorting

Capillary blood granulocytes were magnetically isolated by AutoMACS separator using a Whole blood CD15 microbead kit (Miltenyi Biotec, Bergisch Gladbach, Germany). Purified cells were stained with fluorescently labeled monoclonal antibodies (Ab) recognizing surface markers CD14, CD15 (Exbio, Prague, Czech Republic) and CD16 (Immunotech, Marseille, France) and analyzed on a BD-LSRII or sorted on a BD-Vantage. The intracellular staining procedure has been described elsewhere [13]. Briefly, sorted cells were fixed in 2% PFA, permeabilized with 0.01% saponin and blocked with mouse serum. The cells were then incubated with DEFA1-3 specific Ab, clone D21 (Hycult Biotech, Uden, Netherland) or isotype control (Exbio, Prague, Czech Republic), washed and stained with fluorescently labeled secondary antibodies (Invitrogen, Carlsbad, USA) and analyzed on a BD-LSRII.

2.4. Confocal immunofluorescence

Sorted cells were fixed in 4% PFA and blocked in 2.5% BSA plus 2.5% FBS in PBS. The primary antibodies specific for DEFA1-3, MPO (Hycult Biotech, Uden, Netherland) and EPX (Santa Cruz Biotechnology, Santa Cruz, USA) in combination with AF488- or AF555-conjugated secondary antibodies (Invitrogen, Carlsbad, USA) were applied. Cells were mounted using Vectashield-DAPI (Vector Laboratories, Burlingame, USA). Images were taken by Leica Sp5 confocal microscope.

2.5. May-Grünwald-Giemsa (MGG) staining

Sorted cells were stained according to MGG staining protocol (Penta, Chrudim, Czech Republic). Leica DMI6000 microscope was used for bright field imaging.

2.6. ELISA

The serum levels of DEFA1-3 were measured using an ELISA kit (Hycult Biotech, Uden, Netherland) in accordance with the supplier's recommendation.

2.7. Western blot

Freshly sorted eosinophils were lysed and boiled in sample loading buffer for 10 min, loaded into 16% Tricine-SDS-Urea-PAGE gel and run under reducing condition [14]. Resolved proteins were transferred onto 0.2 μm PVDF membrane (Biorad, Hercules, USA), blocked in 3% BSA, incubated with DEFA1-3 specific Ab (Hycult Biotech, Uden, Netherland) and revealed with secondary anti-mouse HRP-labeled antibodies. GAPDH housekeeping protein was used as a loading control. The reaction was visualized by the West Dura ECL system (Pierce/Thermo Scientific, Rockford, USA).

2.8. Statistical analysis

Statistical analysis was performed within the R environment [15] using the package mclust [16] implying Bayesian information criterion (BIC) [17] and Akaike information criterion (AIC) [18] to estimate the quality of the fit.

3. Results

3.1. m-α-Defensin levels in patients with type 1 diabetes

qRT-PCR analysis performed on mRNA isolated from blood samples determined that 9 out of 30 patients (30%) exhibited α-defensin expression levels above the relative value of 11.07, the highest expression value measured in the control group (Fig. 1A).

In the exploratory statistical analysis, the distribution of the $\log_2$-intensity of m-α-defensin expression in patients with T1D showed signs of bimodality (Fig. 1B). To test it, we fitted uni- and multimodal normal mixtures and evaluated the quality of these fits using AIC and BIC. Both criteria supported the bi-modal distribution as the best fit (Fig. 1B).

On the basis of a distinct level of defensin expression, we labeled these two groups of patients as defensin-high-diabetics (DHD) (Fig. 1B, closed circles) and defensin-normal-diabetics (DND) (Fig. 1B, open circles). The statistical analysis showed no significant differences between DHD and DND patients with respect to their sex, age, duration of disease, GHb, neutrophil and eosinophil counts and IgE levels (Table 1).

The comparative analysis of the capillary and venous blood samples collected from the same DHD donors revealed approximately 2.5-fold enrichment of m-α-defensins in the former (Fig. 1C). Daily fluctuations in the individuals' α-defensin expression, assessed in six capillary blood samples taken at different time points in the course of two consecutive days, were within the range of their respective group values (Fig. 1D). It is of note that high levels of defensin expression in DHD patients persisted during the entire course of this study (~1 year).

3.2. Cellular source of α-defensins in capillary blood

CD14/CD15 staining profile of granulocytes, known to express m-α-defensins, revealed the existence of two major subpopula-
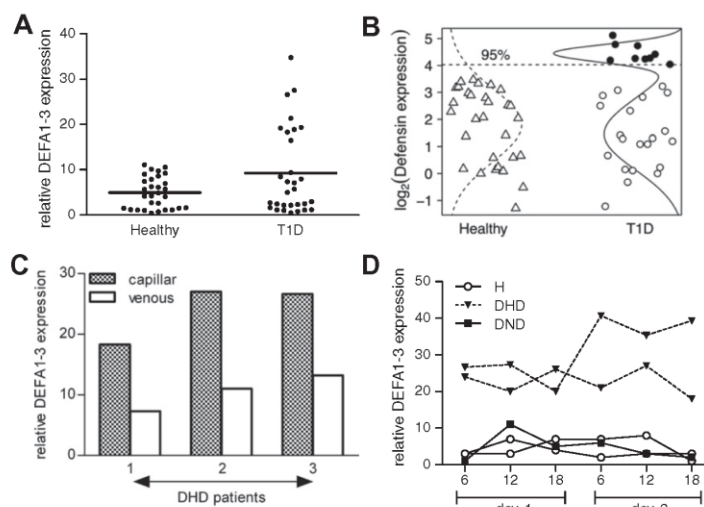
Fig. 1. Expression of m-α-defensins (DEFA1-3) in capillary blood is enhanced in 30% of patients with T1D. (A) Relative mRNA level for DEFA1-3 in the capillary blood samples of the control individuals (healthy) and the patients with T1D were analyzed using qRT-PCR. (B) The m-α-defensin values show bimodal distribution in patients with T1D. Log$_2$-relative values of α-defensin expression are plotted in arbitrary order for the healthy controls (triangles) and the patients (circles), together with the best normal (dashed curve) and bimodal normal (full line) fits for these data, respectively. The two components of bimodal fit consist of $N_1 = 21$ and $N_2 = 9$ patients (mean $\mu_1 = 1.45$ and $\mu_2 = 4.46$, standard deviations $\sigma_1 = 1.34$ and $\sigma_2 = 0.33$, respectively). Nine values (closed circles) fall above the 95th percentile of the healthy patients (horizontal dashed line). While defensin levels in the first component do not differ from those in the healthy ($N = 30$, $\mu = 1.79$, $\sigma = 1.36$) with insignificant difference in a Welsch two sample t-test (two-tailed, $p = 0.25$), the second component shows significantly higher log$_2$-intensity of defensins (two-tailed t-test, $p = 1.6 \times 10^{-11}$). (C) Comparative analysis of relative expression of DEFA1-3 in venous and capillary blood samples obtained from three DHD patients. (D) The individuals' fluctuations of DEFA1-3 mRNA levels in the capillary blood collected on two consecutive days at 6 a.m. (6), at noon (12) and at 6 p.m. (18) from healthy (H), DND and DHD subjects.

Table 1
Comparison of clinical parameters of DHD (defensin high) and DND (defensin normal) patients with type 1 diabetes.

Characteristic	No.	F/M	Age (median/range; years)	Diabetes duration (median/range; months)	HbA$_{1c}$ (IFCC; median/range)	Neu (median/range)	Eos (median/range)	IgE (median/range) IU/ml	Allergy (yes/no)	Other auto-immunity
Normal range, units					2.8–4.5%	54–62%	1–6%	0–200		
DHD	9	6/3	16 (9–37)	38.5 (7–312)	7.65 (5–12.5%)	57 (47.3–63)	1.8 (1.6–6.8)	59.9 (11.3–357)	3/9	2/9
DND	21	10/11	12 (4–18)	39 (1–156)	7.3 (5–12.4%)	51.7 (37–86.4)	2.5 (0.9–14.6)	56.9 (6.4–1717)	4/21	6/21

No, number of subjects; F, female; M, male; IFCC, International Federation of Clinical Chemistry and Laboratory Medicine.

tions: CD15^{high}/CD14$^+$, labeled here as subset A, and CD15^{dull}/CD14^{weak}, labeled here as subset B (Fig. 2A, right panel). The frequency of these two cell subsets among individuals from DHD, DND and the control group were comparable: subset A ranged between 90% and 97% and subset B between 2% and 8% of the total MACS-enriched CD15 granulocyte population.

qRT-PCR performed on mRNA samples derived from FACS-sorted subset A and B granulocytes from three randomly selected individuals in each group identified cellular subset B as the major production site of m-α-defensins in patients with T1D (Fig. 2B). Notably, subset B of DND and DHD group expressed on average 10 and 200 times more of m-α-defensin transcript, respectively, compared to the same subset in the control group. In contrast, m-α-defensin mRNA levels in the subset A from DHD, DND and the control group were comparable (Fig. 2B). In summary, the granulocyte subset B of all patients tested displayed upregulated levels of m-α-defensin genes. Moreover, its very high expression in DHD patients translated to the measurable increase in m-α-defensin mRNA levels in the whole blood capillary samples.

An enhanced expression of m-α-defensins on the protein level in the subset B granulocytes derived from the DHD group compared to those of the control group was readily detectable using confocal immunofluorescent microscopy (Fig. 2C). m-α-defensins were observed to be stored in intracellular granules where they colocalized with MPO (Fig. 2C). MPO protein and its transcript levels were also significantly elevated (Fig. 2C and D). The increased protein level of m-α-defensins was also confirmed by intracellular FACS staining (Fig. 2E). Interestingly, while the protein production of m-α-defensins in the subset B derived from DHD was significantly higher compared to those derived from the controls (Fig. 2E, left panel) and thus correlated with differences in their respective mRNA levels (Fig. 2B), m-α-defensins levels in the subset A from DHD and the controls were comparable. It is of note that even though the expression levels in the subset A from DHD and the controls were similar to that of the subset B from DHD (Fig. 2E), neither of those former two expressed elevated levels of m-α-defensin DEFA1-3 mRNA (Fig. 2B). That suggests that while the subset A from DHD and the controls retain a significant amount of m-α-defensin proteins with
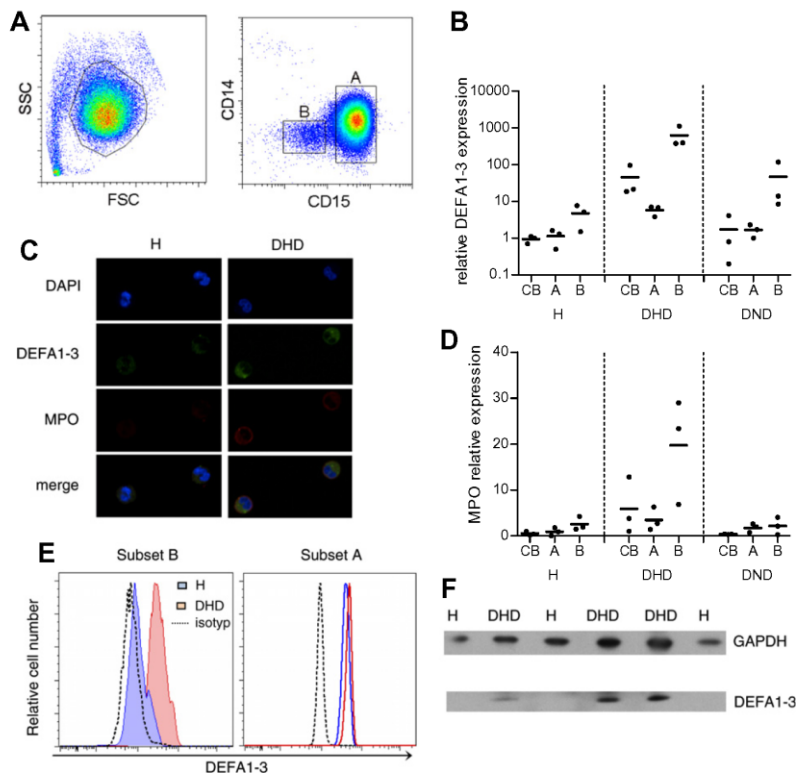
Fig. 2. High m-α-defensin expression is attributed to a distinct subpopulation of granulocytes derived from patients with T1D. (A) Flow cytometry analysis of MACS-enriched CD15$^+$ granulocyte population derived from a capillary blood sample. Within the granulocyte gate (left panel), two distinct cell subsets, CD15^{high}/CD14$^+$ (A) and CD15^{dull}/CD14^{weak} (B) are distinguished (right panel). (B) The relative m-α-defensin mRNA levels (DEFA1-3) in the total capillary blood (CB) and in the A and B subsets sorted from three individuals in each DHD, DND and healthy (H) groups. (C) Representative confocal microscopy images of immunocytochemical staining show the colocalization of m-α-defensin (DEFA1-3, green color) and myeloperoxidase (MPO, red color) in the sorted subset B from control samples (H) and the DHD patients. (D) The relative MPO mRNA levels analyzed in samples described in B. (E) FACS analyses of intracellular anti-DEFA1-3 staining performed on sorted granulocyte of subset A and B from DHD and healthy donors (H). DEFA1-3 protein levels in DHD group of subset B are significantly higher compared to those of H and the isotype control (left panel). The subset A from both DHD and H has comparable but, significantly higher levels of DEFA1-3 defensins compared to their isotype control. One representative sample of four comparative FACS analyses using granulocytes from different DHD patients and healthy controls is shown. (F) The comparative Western blot analysis of cell subsets B from healthy (H) and DHD patients confirmed elevated levels of defensin production in the latter. An aliquot of protein samples were interspersed randomly and immunoblotted with anti-DEFA1-3 antibody. GAPDH was used as a loading control. (For interpretation of the references to color in this figure legend, the reader is referred to the web version of this article.)

only a low level of their transcription, high levels of m-α-defensin proteins in the subset B from DHD directly correlate with their dramatic increase on the transcription level. As illustrated in Fig. 2F, significant differences revealed by the comparative Western blot analysis of the lysates from subset B demonstrates that m-α-defensins are readily detectable in DHD but not in healthy controls. It is worthy of mentioning that differences in the level of m-α-defensins in sera derived from capillary blood of the DHD group and the healthy controls were statistically insignificant (data not shown).

Several lines of evidence strongly suggest that the granulocytes of subset B are indeed eosinophils. First, as illustrated in Fig. 3A, cell subset B (red dots, middle panel) exhibits low FSC and high SSC phenotype (red dots, left panel), a typical feature of eosinophils in flow cytometric analyses [19]. Second, the staining profile of CD15$^+$ granulocytes with anti-CD16 antibody clearly distinguishes between the highly positive subset A and the weakly positive subset B (red dots, right panel). This pattern correlates with differential CD16 surface expression on neutrophils and eosinophils, respectively [20]. Third, MGG staining of subset B granulocytes revealed their eosinophil-specific morphological features, including bilobed nuclei and pink-colored intracellular granular structures (Fig. 3B). Subset A, on the other hand, morphologically resembles neutro-

phils. Fourthly, the comparative qRT-PCR quantification of eosinophil cationic protein expression demonstrated its cell-type restricted presence in subset B (Fig. 3C). In addition, confocal microscopy revealed that subset B also contains eosinophil peroxidase (EPX), one of the major constituents of eosinophil specific granules [21]. While we have not observed significant differences in EPX signal between the subset B from the DHD group and the healthy controls, its colocalization with defensin-enriched granular structures further attests to eosinophil identity of these cells (Fig. 3D). In aggregate, these data unambiguously identified the subset B granulocytes as eosinophils.

4. Discussion

In recent years, arguments for the involvement of innate immunity in the initiation phase of T1D are gaining experimental support. Our results demonstrate the presence of transcriptionally active eosinophils in patients with type 1 diabetes. Surprisingly, the population of neutrophils that are considered to be the primary cellular site of α-defensin production is unaffected. As the transcription of genes that encode granule proteins in blood-born granulocytes is silenced [5,21], the upregulated expression of m-α-
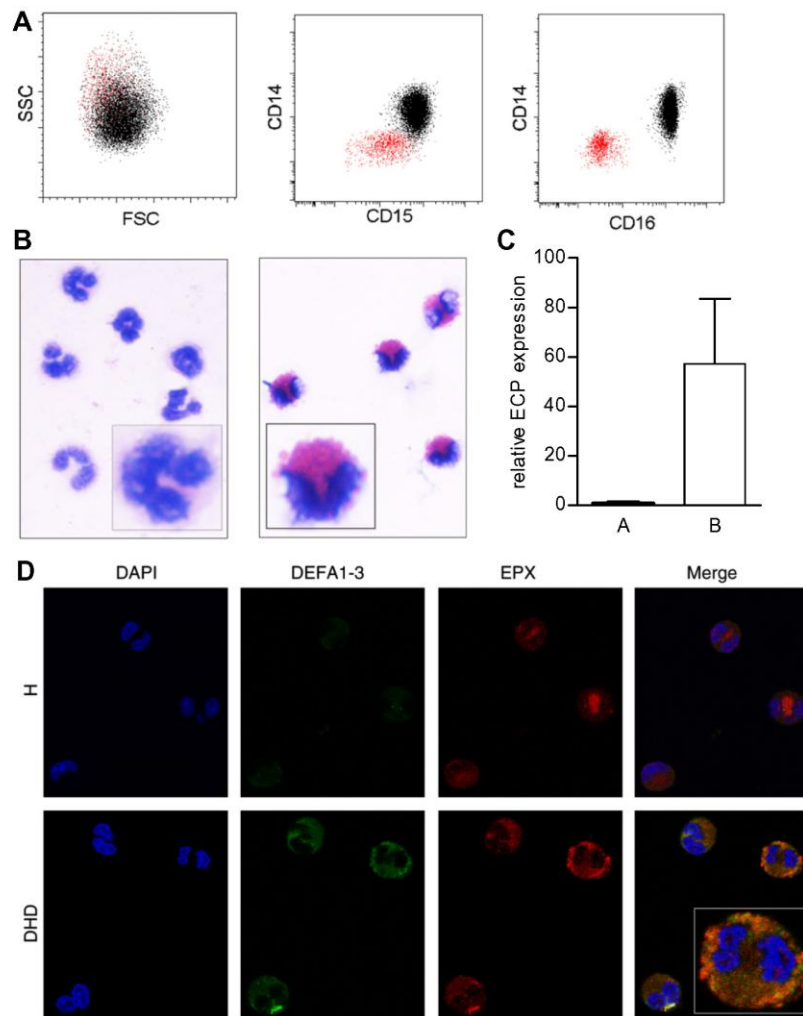
A. Neuwirth et al./Cellular Immunology 273 (2012) 158–163

Fig. 3. Eosinophils are the cellular source of m-α-defensins in patients with type 1 diabetes. (A) MACS-enriched CD15⁺ granulocyte population derived from a capillary blood sample of healthy donors was triple-stained with antibody specific for CD14, CD15 and CD16 antigens. The cell subsets A (black dots) and B (red dots) were distinguished based on CD15/CD14 staining profile (middle panel) as described in Fig. 2A. Using the same color code, FCS/SSC and CD16/CD14 profiles for each of these two subpopulations are presented in the left and right panels, respectively. (B) The cell subsets A and B were separated by FACS sorting, immobilized on a glass surface and subjected to MGG staining. Staining pattern revealed that cell subsets A and B represent neutrophils and eosinophils, respectively. (C) qRT-PCR-based comparative analysis of eosinophil cationic protein (ECP) demonstrated its principal expression in the cell subset B granulocytes. (D) The colocalization of eosinophil peroxidase (EPX) with highly expressed m-α-defensins (DEFA1-3) in the subset B of the DHD patients is confined to intracellular granular structures (see the insert in the merge image of the DHD sample). (For interpretation of the references to color in this figure legend, the reader is referred to the web version of this article.)

defensins and myeloperoxidase in eosinophils from the DHD and DND groups (Fig. 2B and D) is indicative of their cellular activation [13]. In this context, an increased expression of m-α-defensins observed in the capillary compared to the venous blood (Fig. 1C) could be explained by the enrichment of activated eosinophils due to their enhanced adhesion properties to peripheral vascular structures [22]. Thus, m-α-defensins could serve as a reliable molecular signature of eosinophil cellular activation.

Recent data from patients suffering from inflammatory diseases such as atherosclerosis [8], cardiovascular disease [9] and autoimmune lupus [10] suggest that m-α-defensins could be a useful marker for chronic low-grade inflammatory conditions that are linked to the development of autoimmune diseases. Our data support these conclusions. On the other hand, our inability to

correlate an increased intracellular production of α-defensins with their elevated serum level points to the differences in the regulation of cellular signaling network underlying various inflammatory and autoimmune diseases. Notably, whereas high levels of serum m-α-defensins in SLE patients [10] could be correlated with the impairment of NET degradation [23], it appears that eosinophil activation in patients with T1D does not affect serum levels of α-defensins.

The principal question concerns the mechanism of eosinophil activation in patients with T1D. While our findings do not provide an insight into this mechanism, published data suggest that eosinophil activation could be a direct consequence of bacterial or viral infections. Specifically, the mycobacterial lipomannan and antiviral reagent R848, ligands for TLR2 and TLR7, respectively, induced

eosinophil activation as measured by upregulation of m-α-defensin expression, superoxide generation and modulation of surface expression of adhesion molecules [13,24]. Thus, our speculative model envisions a plausible involvement of eosinophils in the pathogenesis of T1D through their TLR-mediated activation and subsequent degranulation. This way, cytotoxic proteins contained in eosinophil primary granules could cause severe injury of a targeted tissue and in turn, initiate immune presentation of autoantigens linked to the pathogenic process of self-destruction. Thus, the proposition that viral infection can precipitate genetic predisposition to β-islet autoimmunity [25] should include eosinophils as potential suspects in the initiation of inflammatory processes contributing to the diabetes pathogenesis. Remarkably, in a rat model of diabetes, genetic predisposition of β-islet cells to produce eotaxin correlates with the recruitment of eosinophils to pancreas [26]. Thus, eosinophils could function as sentinels conveying the combined effect of genetic and environmental factors to the molecular mechanisms regulating the magnitude of inflammation and β-cell destruction. In this scenario, α-defensin expression in eosinophils could serve as a molecular readout of the progression of diabetogenic process.

In general, the role of eosinophils in diabetogenesis has been largely overlooked. While our data demonstrates the eosinophil's transcriptionally activated phenotype in patients with T1D, mechanistically, we have not been able to show how this is achieved. Eosinophils from both DHD and DND patients exhibit this phenotype, i.e. they significantly upregulate levels of alpha-defensins, albeit the subjects of the DND group less dramatically those in the DHD group (Fig. 2B). Thus, the physiological differences between these two groups of patients could be very subtle and rather quantitative with no apparent distinguishing features in the clinical manifestation of diabetes. As different molecular and cellular pathways or their combination are likely to be involved in the onset of T1D, eosinophils could play a role in a subset of patients with T1D or could have more specific and/or limited involvement in this process. Moreover, we believe that this study brings an impetus for the investigation of the involvement of eosinophils in other types of autoimmune-related diseases. Definitively, more investigation into the role of eosinophils in autoimmunopathological situations is required to understand their phenotype described in this study.

5. Conclusions

Our data demonstrate that the population of capillary blood eosinophils, but not neutrophils, displayed augmentation of m-α-defensin expression in all T1D patients tested. This eosinophil-specific transcriptional activation in the patients with T1D suggests that these cells could be linked, directly or indirectly, to the pathogenesis of diabetes.

Acknowledgments

References

[1] M. von Herrath, S. Sanda, K. Herold, Type 1 diabetes as a relapsing-remitting disease?, Nat. Rev. Immunol. 7 (2007) 988–994.
[2] J.A. Todd, Etiology of type 1 diabetes, Immunity 32 (2010) 457–467.
[3] A. Lehuen, J. Diana, P. Zaccone, A. Cooke, Immune cell crosstalk in type 1 diabetes, Nat. Rev. Immunol. 10 (2010) 501–513.
[4] T. Ganz, Defensins: antimicrobial peptides of innate immunity, Nat. Rev. Immunol. 3 (2003) 710–720.
[5] N. Borregaard, O.E. Sorensen, K. Theilgaard-Monch, Neutrophil granules: a library of innate immunity proteins, Trends Immunol. 28 (2007) 340–345.
[6] V. Papayannopoulos, A. Zychlinsky, NETs: a new strategy for using old weapons, Trends Immunol. 30 (2009) 513–521.
[7] M.E. Selsted, A.J. Ouellette, Mammalian defensins in the antimicrobial immune response, Nat. Immunol. 6 (2005) 551–557.
[8] H. Nassar, E. Lavi, S. Akkawi, K. Bdeir, S.N. Heyman, P.N. Raghunath, et al., Alpha-Defensin: link between inflammation and atherosclerosis, Atherosclerosis 194 (2007) 452–457.
[9] G. Joseph, L. Tarnow, A.S. Astrup, T.K. Hansen, H.H. Parving, A. Flyvbjerg, et al., Plasma alpha-defensin is associated with cardiovascular morbidity and mortality in type 1 diabetic patients, J. Clin. Endocrinol. Metab. 93 (2008) 1470–1475.
[10] Z.M. Sthoeger, S. Bezalel, N. Chapnik, I. Asher, O. Froy, High alpha-defensin levels in patients with systemic lupus erythematosus, Immunology 127 (2009) 116–122.
[11] Diagnosis and classification of diabetes mellitus. Diabetes Care 34 (Suppl. 1) (2011) S62–S69.
[12] M.W. Pfaffl, A new mathematical model for relative quantification in real-time RT-PCR, Nucleic Acids Res. 29 (2001) e45.
[13] V. Driss, F. Legrand, E. Hermann, S. Loiseau, Y. Guerardel, L. Kremer, et al., TLR2-dependent eosinophil interactions with mycobacteria: role of alpha-defensins, Blood 113 (2009) 3235–3244.
[14] H. Schagger, Tricine-SDS-PAGE, Nat. Protoc. 1 (2006) 16–22.
[15] Team RDC, R: a language and environment for statistical computing. R Foundation for Statistical Computing, Vienna, Austria ISBN 3-900051-07-0, 2010.
[16] C. Fraley, A.E. Raftery, Model-based clustering, discriminant analysis and density estimation, J. Am. Stat. Assoc. 97 (2002) 611–631.
[17] G. Schwarz, Estimating the dimension of a model, Ann. Statist. 6 (1978) 461–464.
[18] H. Akaike, A new look at the statistical model identification, IEEE Trans. Autom. Control 19 (1974) 716–723.
[19] I. Sabroe, E.C. Jones, L.R. Usher, M.K. Whyte, S.K. Dower, Toll-like receptor (TLR)2 and TLR4 in human peripheral blood granulocytes: a critical role for monocytes in leukocyte lipopolysaccharide responses, J. Immunol. 168 (2002) 4701–4710.
[20] M. Schefzyk, M. Bruder, A. Schmiedl, M. Stephan, A. Kapp, B. Wedi, et al., Eosinophil granulocytes: functional differences of a new isolation kit compared to the isolation with anti-CD16-conjugated MicroBeads, Exp. Dermatol. 18 (2009) 653–655.
[21] V. Gruart, M.J. Truong, J. Plumas, M. Zandecki, J.P. Kusnierz, L. Prin, et al., Decreased expression of eosinophil peroxidase and major basic protein messenger RNAs during eosinophil maturation, Blood 79 (1992) 2592–2597.
[22] L. Hakansson, E. Bjornsson, C. Janson, B. Schmekel, Increased adhesion to vascular cell adhesion molecule-1 and intercellular adhesion molecule-1 of eosinophils from patients with asthma, J. Allergy Clin. Immunol. 96 (1995) 941–950.
[23] A. Hakkim, B.G. Furnrohr, K. Amann, B. Laube, U.A. Abed, V. Brinkmann, et al., Impairment of neutrophil extracellular trap degradation is associated with lupus nephritis, Proc. Natl. Acad. Sci. USA 107 (2010) 9813–9818.
[24] H. Nagase, S. Okugawa, Y. Ota, M. Yamaguchi, H. Tomizawa, K. Matsushima, et al., Expression and function of Toll-like receptors in eosinophils: activation by Toll-like receptor 7 ligand, J. Immunol. 171 (2003) 3977–3982.
[25] M. von Herrath, Can we learn from viruses how to prevent type 1 diabetes?: the role of viral infections in the pathogenesis of type 1 diabetes and the development of novel combination therapies, Diabetes 58 (2009) 2–11.
[26] M.J. Hessner, X. Wang, L. Meyer, R. Geoffrey, S. Jia, J. Fuller, et al., Involvement of eotaxin, eosinophils, and pancreatic predisposition in development of type 1 diabetes mellitus in the BioBreeding rat, J. Immunol. 173 (2004) 6993–7002.

5. General Discussion

In mammals, Toll like receptors have been most frequently associated with evolutionary conserved immune responses elicited by innate immune cells, especially, myeloid cells (Muzio et al. 2000; Hornung et al. 2002). TLRs represent a set of germline encoded pattern recognition receptors recognizing a diverse spectrum of pathogen-associated molecular patterns and probably also detect endogenous stress signals through danger-associated molecular patterns. Their prominent role has been recognized in the induction of innate immune responses, indispensable for rapid elimination of pathogens. In addition to their essential role in the first line of defense against infectious agents (Medzhitov 2001), they are critical in triggering adaptive immune responses that ultimately lead to the antigen-tailored immune response with a long-lasting memory (Akira et al. 2001).

Recently, TLRs have been discovered to be expressed on HSCs and HSPCs, where they can sense pathogens and drive their proliferation and differentiation along the myeloid lineage (reviewed in (Yanez et al. 2013)). While it was believed, that there is no phenotype alteration in hematopoiesis of TLR deficient mice, some recent findings suggest that the absence of TLR4, TLR9 or the TLR adapter protein MyD88 but not TLR2 gives HSCs an advantage in transplantation assays. This observation argues that HSCs could be vulnerable to certain TLR ligands during handling or in the damaged environment of irradiated recipients (Ichii et al. 2010). Thus, in addition to the response to "pull" and "push" signals delivered by their environment, HSCs might be able to directly respond upon ligation of their TLRs. However, the significance of this proposition has been recently challenged by a study showing that LPS-induced emergency myelopoiesis depends on TLR4-expressing nonhematopoietic cells (Boettcher et al. 2012). Undoubtedly, more studies are needed to resolve this issue.

So far, all studies investigating the role of TLR expression and function in HSPCs were conducted on adult hematopoietic cells. We have, for the first time, shown that TLR2 is expressed on hematopoietic precursor cells of embryonic origin. TLR2 triggering enhances the proliferation rate as well as differentiation of embryonic hematopoietic progenitors towards myeloid lineage in MyD88-dependent manner. Using *in vitro* and *in vivo Tlr2* lineage tracing experiments we have shown that very early embryonic hematopoietic precursors with active *Tlr2* locus could differentiate to all hematopoietic lineages and give rise to adult type hematopoietic cells. The very early emergence of these progenitors opens the question concerning the YS versus intra-embryonic origin of HSC precursors. Based on our preliminary results with constitutive *Tlr2-Cre* reporter

strain we cannot rule out, that hematopoietic precursors originate in the embryo proper from early mesodermal cells. Further, we suggest that the presence of TLRs on these progenitors could be in agreement with a proposed myeloid based model of hematopoietic cells differentiation. This model posits that myeloid differentiation potential is retained in all, erythroid, T and B lineage branches (Kawamoto et al. 2010). In this scenario, the myeloid program starts to operate very early in the development in TLR2+ progenitors and is retained in either HSCs that originate from these cells or in embryonic progenitors with mixed myelo-lymphoid potential (Böiers et al. 2013). Taking in account that the population of embryonic c-kit+ TLR2+ cells might be quite heterogeneous, additional assays analyzing the expression pattern on single cell level could address this question.

Apart from the hematopoietic precursors, the whole spectrum of TLRs is expressed in E10.5 YS-derived macrophages. While the expression of PRRs during early embryogenesis has not been described previously, we have also shown that TLRs expressed by E10.5 YS-derived macrophages are fully functional. There is no doubt that, during embryogenesis, a substantial pool of tissue resident macrophages originates either from YS or AGM/FL macrophages (Ginhoux et al. 2010; Schulz et al. 2012; Yona et al. 2013). An elegant study by Ginhoux and colleagues has shown that microglia derive from YS myeloid progenitors that arise before E8.0, seed the brain through circulation before the blood-brain barrier closes and postnataly are maintained independently of circulating adult monocytes (Ginhoux et al. 2010). Interestingly, a study aiming to reveal the transcriptional regulatory pathways underlining the identity and diversity of tissue macrophages concluded that macrophage populations from different organs are considerably diverse (Gautier et al. 2012). When we compared expression profiles of E10.5 TLR2+ embryonic and adult TLR2+ peritoneal macrophages with publically available microarray data, derived from E10.5 YS and E16.5 tissue macrophages supplied by Schulz and colleagues, we observed the gene clustering of E10.5 TLR2+ macrophages with E10.5 YS-derived F4/80+ and E16.5 F4/80BRIGHT tissue macrophages. This relationship was even further strengthened when differentially expressed genes from E10.5 TLR2+ cells were compared across these three populations. On contrary, analysis of TLRs and their adaptor proteins revealed no obvious clustering of any of the macrophage populations tested (Schulz et al. 2012). This suggests that TLR expression cannot distinguish between diverse macrophage populations. Rather, this uniform pattern of TLR expression shared by all macrophage subsets seems to represent the functional signature of prototypic myeloid program which operates in these cells. Interestingly, our RNA microarray analysis identified many differentially overexpressed genes in E10.5 TLR2+ embryonic macrophages as compared to adult TLR2+ peritoneal macrophages and

E10.5 TLR2⁻ cells. Among them four transmembrane proteins were prominent; Cx3cr1, Mrc1, Stab1 and Fpn1. While all of these proteins were described to play a role in adult tissue resident macrophages, it was rather surprising, that they were enriched in the embryonic YS-derived macrophages as compared to tissue resident peritoneal macrophages (Kzhyshkowska et al. 2006; Wentworth et al. 2010; Gautier et al. 2012). Particularly, the sole mammalian iron exporter, ferroportin (Fpn1), attracted our attention. Fpn1 is highly expressed on duodenal enterocytes, placenta, hepatocytes and tissue resident macrophages and enables the absorption of maternal and dietary iron. Apart from the materno-fetal transfer that establishes initial iron stores, the macrophage-mediated recycling of iron is probably the most potent way how to supply enough iron for erythroid precursors (Donovan et al. 2005; Recalcati et al. 2012). As a consequence, the expression of Fpn1 is tightly controlled on multiple levels. Ferroportin expression is negatively regulated by inflammatory mediators (Yang et al. 2002), particularly the acute phase protein hepcidin, that binds Fpn1 and mediates its internalization and degradation. Additionally, expression of Fpn1 is also regulated post-transriptionally by the iron regulatory protein system (IRP) (Wallander et al. 2006). Our results have shown, that in embryonic macrophages, expression of Fpn1 coupled with iron flow can be directly downregulated upon TLR2 signalling in a MyD88-dependent manner, leading to iron sequestration in M1 polarized inflammatory macrophages. Moreover the expression of Fpn1 on the surface of embryonic macrophages could attest for their role in intraembryonic iron recycling upon phagocytosis of erythroid cells. This is, in addition to Fpn1-mediated iron transport from visceral endoderm, which was, until now, considered as the only source of embryonic iron. Together, our data described a novel way to activate the prototypic M2-like embryonic macrophages towards the inflammatory M1-phenotype associated with the pro-inflammatory cytokine and chemokine expression and iron sequestration.

Next, we focused on pathogen-host interaction of intracellular bacteria *Francisella tularensis* with macrophages as their primary target. Due to its extreme virulence, ease of aerosol transmission and lethality, *F. tularensis* has been recognized as a potentially deadly biological weapon (Dennis et al. 2001; Tarnvik and Berglund 2003). The prerequisite for the pathogenicity of *F. tularensis* is its ability to invade and replicate in host cells, mostly phagocytes (Hall et al. 2008). Upon infection, macrophages engulf *F. tularensis*, and although the destiny of the phagosome is to fuse with lysosomes, *F. tularensis* escapes to the cytosol, where it can proliferate (Santic et al. 2008). Importantly, strains that fail to avoid the phago-lysosomal fusion and or cannot escape to the cytosol are attenuated in their virulence (Lindgren et al. 2004). Recently, cholesterol-rich detergent resistant microdomains (DRM) have been shown to be essential for the entry

of *F. tularensis* to macrophages (Tamilselvam and Daefler 2008). We confirmed that *F. tularensis* requires intact cholesterol-rich DRMs to enter J774.2 macrophage cell line. Therefore, we aimed to elucidate the early stages of interactions of macrophages with the bacteria by determining the protein composition of DRMs upon *F. tularensis* infection using a quantitative mass spectrometry based proteomic approach. Only one protein, Sequestosome 1 (Sqstm1/ p62), was found to be specifically recruited to DRMs upon *F. tularensis* internalization with significant reproducibility. This cytoplasmic multimodule adaptor protein contains an ubiquitin binding domain as well as a segment that interacts with autophagosomal transmembrane protein LC3. Thus p62 can directly bridge degradation of polyubiqutinated protein aggregates with the process of autophagy (Seto et al. 2013). Indeed we have observed very early colocalization of ingested bacteria covered with ubiquitinated proteins with LC3$^+$ autophagosomes peaking at 1 hour post infection. While Checroun and colleagues, who focused on later stages of infection, described autophagy induction 24 hours upon *F. tularensis* infection, our data are in agreement with observations of Chiu and colleagues describing the antibacterial effect of a small autophagy inducing molecule AR-12 at 2.5 and 24 hours postinfection. Moreover, p62 silencing led to increased bacterial load during early, but not late phases of infection (Checroun et al. 2006; Chiu et al. 2009). However, the initiation of autophagy pathway, necessary for *F. tularensis* elimination, is still enigmatic. Autophagy, an ancient cellular homeostatic process that is also involved in multiple immune pathways, including intracellular pathogen removal, endogenous antigen presentation, modulation of T_H1/T_H2 polarization and shaping of central tolerance, and they all can be induced also by TLR triggering (Nakagawa et al. 2004; Paludan et al. 2005; Harris et al. 2007; Sanjuan et al. 2007; Nedjic et al. 2008; Delgado and Deretic 2009). It has been shown, that a particle that engages TLRs on the surface of macrophages, while it is phagocytosed, guides the autophagosome marker LC3 to phagosomes using the autophagy-dependent pathway. This LC3 translocation is associated with phagosome fusion with lysosomes, leading to a rapid acidification followed by enhanced pathogen killing. Similarly to TLR2-induced autophagy, described by Sanjuan and colleagues, we could not observe the formation of double membrane vacuoles around ingested *F. tularensis* 1 hour post infection, when the interaction of p62 with LC3 peaked (Sanjuan et al. 2007). In summary, our study revealed for the first time, *F. tularensis*-driven, very early activation of autophagy pathway mediated by adaptor protein p62 that could be initiated by TLR triggering.

Finally, in the last study included to this thesis, we investigated the role of myeloid cells in type 1 diabetes (T1D) which is an autoimmune disease caused by immune-mediated destruction of insulin producing pancreatic β-cells leading to insulin deficiency and persistent hyperglycemia. Even with the current insulin substitution therapy, secondary complications such as blindness, heart disease or kidney failure may develop in T1D patients. A whole spectrum of immune cells has been associated with T1D onset or progression. Both CD4^{+} and CD8^{+} T lymphocytes have been implicated as key players in β-cells destruction, while other cells as DCs, macrophages, B cells and NK cells have regulatory roles. Myeloid cells including DCs and MFs participate in auto-antigen presentation to T cells and their priming; at the onset of the disease, insulin specific CD4^{+} T cells appear, later on, T cells specific for other pancreas specific antigens dominate. Pancreatic β-cells lack MHC class II proteins, suggesting that direct cell destruction can only be mediated by CD8^{+} cytotoxic T cells that recognize peptide antigen: MHC class I complexes displayed on β-cells (Katz et al. 1993; Bulek et al. 2012). Apart from direct cell-to-cell contact, cytotoxic T cells can mediate elimination of β-cells by releasing of pro-inflammatory cytokines, granzyme B, or perforin, and possibly by signaling through pathways of programmed cell death (Khadra et al. 2011). Regulatory T cells might be involved in protection from T1D, since the decrease in their numbers promotes a more severe disease while their adoptive transfer leads to the opposite outcome (Salomon et al. 2000; Tonkin and Haskins 2009). B cells, although not directly pathogenic to β-cells, can participate in disease progression by production of autoantibodies followed by generation of immune complexes, and possibly by antigen presentation to generate primary autoreactive T cell responses, maintenance of CD4^{+} T cell memory or production of pro-inflammatory cytokines (Cox and Silveira 2009). Accumulation of NK cells, DCs, macrophages or eosinophils in earliest islet infiltrates attests for their so far enigmatic role in T1D development (Hessner et al. 2004; Kim and Lee 2009; Brauner et al. 2010).

However, the research of the regulatory immune networks in human T1D is complicated by limited access to appropriate samples due to ethical and practical concerns (Han et al. 2012). Thus, in our study we focused on analysis of readily accessible peripheral capillary blood samples. Interestingly we detected increased level of myeloid α-defensins in approximately 30% of T1D patients (defensin high diabetic, DHD). The analysis of cell populations in peripheral blood of DHD patients identified eosinophils as the exclusive source of myeloid α-defensins. This was a surprising finding considering that under physiological conditions, neutrophils are the main source of myeloid α-defensins (Borregaard et al. 2007). Additionally, myeloid α-defensins were elevated in eosinophils isolated from the peripheral capillary blood of defensin-normal-diabetic (DND) patients with normal level of myeloid α-defensins in total blood samples. Thus, transcriptional

activation of eosinophils manifested by increased expression of myeloid α-defensins and myeloperoxidase could represent a general process linked to the pathology of T1D. The level of myeloid α-defensins expression in peripheral capillary blood eosinophils could serve as a diagnostic marker of the disease progression. In support of our data, eosinophil infiltration in pancreas and pancreatic lymph nodes has been previously associated with development of diabetes in the model of BioBreeding rat (Hessner et al. 2004).

The role of the innate immune system in triggering T1D was shown only recently. Research in this area was greatly facilitated by the discovery of Toll-like receptors (TLRs) that were found to be crucial for induction of effective immune response. The number of studies, although sometimes with contradictory findings, associating TLRs and diabetes induction is steadily growing (Kim et al. 2007; Zipris 2010; Li et al. 2012a; Gülden et al. 2013; Lee 2013). For example, apoptotic β-cells cells undergoing secondary necrosis stimulated the priming of diabetogenic T cells through a TLR2-dependent, but TLR4-independent, activation of antigen presenting cells and the development of autoimmune diabetes was markedly inhibited in $Tlr2^{-/-}$ mice but not in $Tlr4^{-/-}$ mice (Kim et al. 2007). We hypothesize, that eosinophils could be involved in the development of autoimmune diabetes through their TLR-driven activation and subsequent degranulation related to tissue damage leading to auto-antigen processing and presentation to self-reactive T cells.

6. Conclusions

This thesis is based on three original articles, one submitted manuscript and unpublished data that contribute to our knowledge about the role of myeloid cells in embryonic development and disease. In addition, the presented thesis is supported by one methodologically related published article and one submitted manuscript. The results can be summed up as follows:

Toll like receptors and their adaptor proteins are expressed during embryogenesis. Apart from maternal myeloid cells and differentiated YS-derived phagocytes emerging around E9.5, TLRs are expressed on early hematopoietic progenitors. Hematopoietic precursors expressing TLR2 preferentially differentiate into myeloid lineage cells *in vivo* and *in vitro*, and TLR2 triggering enhances their proliferation rate as well as myeloid differentiation in a MyD88-dependent manner. In the presence of erythropoietin, TLR2$^+$ precursors display the capacity to mature into primitive erythroid cells. The appearance of TLR2$^+$ precursors in pre/early primitive streak embryo at E6.5 coincides with the onset of gastrulation, and these cells persist in both the yolk sac and the embryo proper before the establishment of circulation. However, only a subset of YS-derived TLR2$^+$ ckit$^+$ progenitors coexpresses CD41, CD150 and Runx1, markers of primitive as well as definitive hematopoiesis. Taken together, the expression of TLR2 marks the emergence of common embryonic hematopoietic progenitors of early erythro-myeloid lineages and endows them with the capacity to boost the production of myeloid cells.

Using BAC recombineering, we generated two transgenic *Tlr2* reporter mouse strains suitable for visualization and lineage tracing of cells with active *Tlr2* locus. We have shown that the *Tlr2* promoter is activated during early postgastrulation embryonic development in hematopoietic precursor cells that give rise to all lineages of adult type hematopoiesis.

E10.5 CD45$^+$ CD11b$^+$ F4/80$^+$ macrophages coexpress Toll-like receptors (TLRs) and CD14. These embryonic YS derived myeloid cell have the capability to engulf both apoptotic cells and bacteria, secrete upon TLR stimulation a broad spectrum of pro-inflammatory cytokines and chemokines, proving that these receptors are fully functional. E10.5 TLR2$^+$ embryonic phagocytes express a distinct set of genes as compared to adult peritoneal macrophages. In addition they possess a TLR2 regulatable protein machinery that is essential for the recycling of cellular iron.

The autophagic adaptor protein p62 accumulates in detergent-resistant membranes of macrophages at the early stages of microbe–host cell interaction upon *F. tularensis* infection *in vitro*.

Eosinophils isolated from peripheral capillary blood of type 1 diabetic patients express high levels of myeloid α-defensins and myeloperoxidase. Thus the transcriptionally active eosinophils in T1D patients could contribute to disease pathogenesis.

7. References

Adachi O, Kawai T, Takeda K, Matsumoto M, Tsutsui H, Sakagami M, Nakanishi K, Akira S. 1998. Targeted Disruption of the MyD88 Gene Results in Loss of IL-1- and IL-18-Mediated Function. *Immunity* **9**: 143-150.

Ajami B, Bennett JL, Krieger C, McNagny KM, Rossi FMV. 2011. Infiltrating monocytes trigger EAE progression, but do not contribute to the resident microglia pool. *Nat Neurosci* **14**: 1142-1149.

Akira S, Takeda K. 2004. Toll-like receptor signalling. *Nat Rev Immunol* **4**: 499-511.

Akira S, Takeda K, Kaisho T. 2001. Toll-like receptors: critical proteins linking innate and acquired immunity. *Nat Immunol* **2**: 675-680.

Akira S, Uematsu S, Takeuchi O. 2006. Pathogen Recognition and Innate Immunity. *Cell* **124**: 783-801.

Alexander WS. 1998. Cytokines in hematopoiesis. *Int Rev Immunol* **16**: 651-682.

Alliot F, Godin I, Pessac B. 1999. Microglia derive from progenitors, originating from the yolk sac, and which proliferate in the brain. *Brain Res Dev Brain Res* **117**: 145-152.

Anderson KV, Jürgens G, Nüsslein-Volhard C. 1985. Establishment of dorsal-ventral polarity in the Drosophila embryo: Genetic studies on the role of the Toll gene product. *Cell* **42**: 779-789.

Araki K, Imaizumi T, Okuyama K, Oike Y, Yamamura K-i. 1997. Efficiency of Recombination by Cre Transient Expression in Embryonic Stem Cells: Comparison of Various Promoters. *Journal of Biochemistry* **122**: 977-982.

Barbalat R, Lau L, Locksley RM, Barton GM. 2009. Toll-like receptor 2 on inflammatory monocytes induces type I interferon in response to viral but not bacterial ligands. *Nat Immunol* **10**: 1200-1207.

Barton GM, Kagan JC. 2009. A cell biological view of Toll-like receptor function: regulation through compartmentalization. *Nat Rev Immunol* **9**: 535-542.

Baumann CI, Bailey AS, Li W, Ferkowicz MJ, Yoder MC, Fleming WH. 2004. PECAM-1 is expressed on hematopoietic stem cells throughout ontogeny and identifies a population of erythroid progenitors. *Blood* **104**: 1010-1016.

Bertrand JY, Giroux S, Golub R, Klaine Ml, Jalil A, Boucontet L, Godin I, Cumano A. 2005a. Characterization of purified intraembryonic hematopoietic stem cells as a tool to define their site of origin. *Proceedings of the National Academy of Sciences of the United States of America* **102**: 134-139.

Bertrand JY, Jalil A, Klaine M, Jung S, Cumano A, Godin I. 2005b. Three pathways to mature macrophages in the early mouse yolk sac. *Blood* **106**: 3004-3011.

Bieneman AP, Chichester KL, Chen YH, Schroeder JT. 2005. Toll-like receptor 2 ligands activate human basophils for both IgE-dependent and IgE-independent secretion. *The Journal of allergy and clinical immunology* **115**: 295-301.

Blasius AL, Beutler B. 2010. Intracellular Toll-like Receptors. *Immunity* **32**: 305-315.

Boettcher S, Ziegler P, Schmid MA, Takizawa H, van Rooijen N, Kopf M, Heikenwalder M, Manz MG. 2012. Cutting Edge: LPS-Induced Emergency Myelopoiesis Depends on TLR4-Expressing Nonhematopoietic Cells. *The Journal of Immunology* **188**: 5824-5828.

Böiers C, Carrelha J, Lutteropp M, Luc S, Green Joanna CA, Azzoni E, Woll Petter S, Mead Adam J, Hultquist A, Swiers G et al. 2013. Lymphomyeloid Contribution of an Immune-Restricted Progenitor Emerging Prior to Definitive Hematopoietic Stem Cells. *Cell stem cell* **13**: 535-548.

Boiko JR, Borghesi L. 2011. Hematopoiesis sculpted by pathogens: Toll-like receptors and inflammatory mediators directly activate stem cells. *Cytokine* **57**: 1-8.

Boisset J-C, Robin C. 2012. On the origin of hematopoietic stem cells: Progress and controversy. *Stem Cell Res* **8**: 1-13.

Borregaard N, Sørensen OE, Theilgaard-Mönch K. 2007. Neutrophil granules: a library of innate immunity proteins. *Trends in Immunology* **28**: 340-345.

Bourke E, Bosisio D, Golay J, Polentarutti N, Mantovani A. 2003. The toll-like receptor repertoire of human B lymphocytes: inducible and selective expression of TLR9 and TLR10 in normal and transformed cells. *Blood* **102**: 956-963.

Brauner H, Elemans M, Lemos S, Broberger C, Holmberg D, Flodstrom-Tullberg M, Karre K, Hoglund P. 2010. Distinct phenotype and function of NK cells in the pancreas of nonobese diabetic mice. *Journal of immunology (Baltimore, Md : 1950)* **184**: 2272-2280.

Breier G, Breviario F, Caveda L, Berthier R, Schnurch H, Gotsch U, Vestweber D, Risau W, Dejana E. 1996. Molecular cloning and expression of murine vascular endothelial- cadherin in early stage development of cardiovascular system. *Blood* **87**: 630-641.

Brinkmann V, Reichard U, Goosmann C, Fauler B, Uhlemann Y, Weiss DS, Weinrauch Y, Zychlinsky A. 2004. Neutrophil Extracellular Traps Kill Bacteria. *Science* **303**: 1532-1535.

Bulek AM, Cole DK, Skowera A, Dolton G, Gras S, Madura F, Fuller A, Miles JJ, Gostick E, Price DA et al. 2012. Structural basis for the killing of human beta cells by CD8(+) T cells in type 1 diabetes. *Nat Immunol* **13**: 283-289.

Caramalho I, Lopes-Carvalho T, Ostler D, Zelenay S, Haury M, Demengeot J. 2003. Regulatory T Cells Selectively Express Toll-like Receptors and Are Activated by Lipopolysaccharide. *The Journal of Experimental Medicine* **197**: 403-411.

Costa G, Kouskoff V, Lacaud G. 2012. Origin of blood cells and HSC production in the embryo. *Trends Immunol* **33**: 215-223.

Cox SL, Silveira PA. 2009. Emerging roles for B lymphocytes in Type 1 diabetes. *Expert review of clinical immunology* **5**: 311-324.

Cumano A, Ferraz JC, Klaine M, Di Santo JP, Godin I. 2001. Intraembryonic, but Not Yolk Sac Hematopoietic Precursors, Isolated before Circulation, Provide Long-Term Multilineage Reconstitution. *Immunity* **15**: 477-485.

de Bruijn MFTR, Speck NA, Peeters MCE, Dzierzak E. 2000. Definitive hematopoietic stem cells first develop within the major arterial regions of the mouse embryo. *EMBO J* **19**: 2465-2474.

De Luca K, Frances-Duvert V, Asensio MJ, Ihsani R, Debien E, Taillardet M, Verhoeyen E, Bella C, Lantheaume S, Genestier L et al. 2009. The TLR1/2 agonist PAM3CSK4 instructs commitment of human hematopoietic stem cells to a myeloid cell fate. *Leukemia* **23**: 2063-2074.

Delgado MA, Deretic V. 2009. Toll-like receptors in control of immunological autophagy. *Cell Death Differ* **16**: 976-983.

Delgado MA, Elmaoued RA, Davis AS, Kyei G, Deretic V. 2008. Toll-like receptors control autophagy. *Embo j* **27**: 1110-1121.

Dengjel J, Schoor O, Fischer R, Reich M, Kraus M, Müller M, Kreymborg K, Altenberend F, Brandenburg J, Kalbacher H et al. 2005. Autophagy promotes MHC class II presentation of peptides from intracellular source proteins. *Proceedings of the National Academy of Sciences* **102**: 7922-7927.

Dennis DT, Inglesby TV, Henderson DA, Bartlett JG, Ascher MS, Eitzen E, Fine AD, Friedlander AM, Hauer J, Layton M et al. 2001. Tularemia as a biological weapon: medical and public health management. *JAMA : the journal of the American Medical Association* **285**: 2763-2773.

Donovan A, Lima CA, Pinkus JL, Pinkus GS, Zon LI, Robine S, Andrews NC. 2005. The iron exporter ferroportin/Slc40a1 is essential for iron homeostasis. *Cell metabolism* **1**: 191-200.

Dunne A, O'Neill LAJ. 2003. The Interleukin-1 Receptor/Toll-Like Receptor Superfamily: Signal Transduction During Inflammation and Host Defense. *Sci STKE* **2003**: 3-17.

Dzierzak E, Medvinsky A. 1995. Mouse embryonic hematopoiesis. *Trends Genet* **11**: 359-366.

Dzierzak E, Medvinsky A. 2008. The discovery of a source of adult hematopoietic cells in the embryo. *Development* **135**: 2343-2346.

Eichmann A, Corbel C, Nataf V, Vaigot P, Bréant C, Le Douarin NM. 1997. Ligand-dependent development of the endothelial and hemopoietic lineages from embryonic mesodermal cells expressing vascular endothelial growth factor receptor 2. *Proc Natl Acad Sci USA* **94**: 5141-5146.

Faloon P, Arentson E, Kazarov A, Deng CX, Porcher C, Orkin S, Choi K. 2000. Basic fibroblast growth factor positively regulates hematopoietic development. *Development* **127**: 1931-1941.

Ferkowicz MJ, Starr M, Xie X, Li W, Johnson SA, Shelley WC, Morrison PR, Yoder MC. 2003. CD41 expression defines the onset of primitive and definitive hematopoiesis in the murine embryo. *Development* **130**: 4393-4403.

Ferkowicz MJ, Yoder MC. 2005. Blood island formation: longstanding observations and modern interpretations. *Exp Hematol* **33**: 1041-1047.

Francois S, El Benna J, Dang PM, Pedruzzi E, Gougerot-Pocidalo MA, Elbim C. 2005. Inhibition of neutrophil apoptosis by TLR agonists in whole blood: involvement of the phosphoinositide 3-kinase/Akt and NF-kappaB signaling pathways, leading to increased levels of Mcl-1, A1, and phosphorylated Bad. *Journal of immunology (Baltimore, Md : 1950)* **174**: 3633-3642.

Fu Y, Maye P. 2011. Engineering BAC Reporter Gene Constructs for Mouse Transgenesis. in *Transgenic Mouse Methods and Protocols* (eds. MH Hofker, J Deursen), pp. 163-179. Humana Press.

Furuta C, Ema H, Takayanagi S-i, Ogaeri T, Okamura D, Matsui Y, Nakauchi H. 2006. Discordant developmental waves of angioblasts and hemangioblasts in the early gastrulating mouse embryo. *Development* **133**: 2771-2779.

Galli SJ, Borregaard N, Wynn TA. 2011. Phenotypic and functional plasticity of cells of innate immunity: macrophages, mast cells and neutrophils. *Nat Immunol* **12**: 1035-1044.

Gardner RL, Rossant J. 1979. Investigation of the fate of 4·5 day post-coitum mouse inner cell mass cells by blastocyst injection. *Journal of Embryology and Experimental Morphology* **52**: 141-152.

Gautier EL, Shay T, Miller J, Greter M, Jakubzick C, Ivanov S, Helft J, Chow A, Elpek KG, Gordonov S et al. 2012. Gene-expression profiles and transcriptional regulatory pathways that underlie the identity and diversity of mouse tissue macrophages. *Nat Immunol* **13**: 1118-1128.

Geering B, Stoeckle C, Conus S, Simon HU. 2013. Living and dying for inflammation: neutrophils, eosinophils, basophils. *Trends Immunol* **34**: 398-409.

Gewirtz AT, Navas TA, Lyons S, Godowski PJ, Madara JL. 2001. Cutting Edge: Bacterial Flagellin Activates Basolaterally Expressed TLR5 to Induce Epithelial Proinflammatory Gene Expression. *The Journal of Immunology* **167**: 1882-1885.

Gilliet M, Cao W, Liu Y-J. 2008. Plasmacytoid dendritic cells: sensing nucleic acids in viral infection and autoimmune diseases. *Nat Rev Immunol* **8**: 594-606.

Ginhoux F, Greter M, Leboeuf M, Nandi S, See P, Gokhan S, Mehler MF, Conway SJ, Ng LG, Stanley ER et al. 2010. Fate Mapping Analysis Reveals That Adult Microglia Derive from Primitive Macrophages. *Science* **330**: 841-845.

Gleich GJ. 2000. Mechanisms of eosinophil-associated inflammation. *The Journal of allergy and clinical immunology* **105**: 651-663.

Golub R, Cumano A. 2013. Embryonic hematopoiesis. *Blood Cells, Molecules, and Diseases* **Epub ahead of print**.

Gülden E, Ihira M, Ohashi A, Reinbeck AL, Freudenberg MA, Kolb H, Burkart V. 2013. Toll-Like Receptor 4 Deficiency Accelerates the Development of Insulin-Deficient Diabetes in Non-Obese Diabetic Mice. *PLoS ONE* **8**: e75385.

Gutierrez MG, Master SS, Singh SB, Taylor GA, Colombo MI, Deretic V. 2004. Autophagy Is a Defense Mechanism Inhibiting BCG and Mycobacterium tuberculosis Survival in Infected Macrophages. *Cell* **119**: 753-766.

Hall JD, Woolard MD, Gunn BM, Craven RR, Taft-Benz S, Frelinger JA, Kawula TH. 2008. Infected-host-cell repertoire and cellular response in the lung following inhalation of Francisella tularensis Schu S4, LVS, or U112. *Infection and immunity* **76**: 5843-5852.

Hamilton DL, Abremski K. 1984. Site-specific recombination by the bacteriophage P1 lox-Cre system: Cre-mediated synapsis of two lox sites. *Journal of Molecular Biology* **178**: 481-486.

Han D, Cai X, Wen J, Matheson D, Skyler JS, Kenyon NS, Chen Z. 2012. Innate and adaptive immune gene expression profiles as biomarkers in human type 1 diabetes. *Clinical and experimental immunology* **170**: 131-138.

Hansson GK, Hermansson A. 2011. The immune system in atherosclerosis. *Nat Immunol* **12**: 204-212.

Harju K, Glumoff V, Hallman M. 2001. Ontogeny of Toll-Like Receptors Tlr2 and Tlr4 in Mice. *Pediatr Res* **49**: 81-83.

Harris J, De Haro SA, Master SS, Keane J, Roberts EA, Delgado M, Deretic V. 2007. T Helper 2 Cytokines Inhibit Autophagic Control of Intracellular Mycobacterium tuberculosis. *Immunity* **27**: 505-517.

Hayashi F, Means TK, Luster AD. 2003. Toll-like receptors stimulate human neutrophil function. *Blood* **102**: 2660-2669.

Hessner MJ, Wang X, Meyer L, Geoffrey R, Jia S, Fuller J, Lernmark A, Ghosh S. 2004. Involvement of eotaxin, eosinophils, and pancreatic predisposition in development of type 1 diabetes mellitus in the BioBreeding rat. *Journal of immunology (Baltimore, Md : 1950)* **173**: 6993-7002.

Holl TM, Kelsoe G. 2006. Outside Influence: TLRs Direct Hematopoietic Cell Fates. *Immunity* **24**: 667-669.

Hornung V, Rothenfusser S, Britsch S, Krug A, Jahrsdörfer B, Giese T, Endres S, Hartmann G. 2002. Quantitative Expression of Toll-Like Receptor 1–10 mRNA in Cellular Subsets of Human Peripheral Blood Mononuclear Cells and Sensitivity to CpG Oligodeoxynucleotides. *The Journal of Immunology* **168**: 4531-4537.

Hou B, Reizis B, DeFranco AL. 2008. Toll-like Receptors Activate Innate and Adaptive Immunity by using Dendritic Cell-Intrinsic and -Extrinsic Mechanisms. *Immunity* **29**: 272-282.

Huber TL, Kouskoff V, Joerg Fehling H, Palis J, Keller G. 2004. Haemangioblast commitment is initiated in the primitive streak of the mouse embryo. *Nature* **432**: 625-630.

Hume DA, Perry VH, Gordon S. 1984. The mononuclear phagocyte system of the mouse defined by immunohistochemical localisation of antigen F4/80: macrophages associated with epithelia. *Anat Rec* **210**: 503-512.

Checroun C, Wehrly TD, Fischer ER, Hayes SF, Celli J. 2006. Autophagy-mediated reentry of Francisella tularensis into the endocytic compartment after cytoplasmic replication. *Proc Natl Acad Sci U S A* **103**: 14578-14583.

Chiu HC, Soni S, Kulp SK, Curry H, Wang D, Gunn JS, Schlesinger LS, Chen CS. 2009. Eradication of intracellular Francisella tularensis in THP-1 human macrophages with a novel autophagy inducing agent. *Journal of biomedical science* **16**: 110.

Choi K, Kennedy M, Kazarov A, Papadimitriou JC, Keller G. 1998. A common precursor for hematopoietic and endothelial cells. *Development* **125**: 725-732.

Choi YJ, Im E, Chung HK, Pothoulakis C, Rhee SH. 2010. TRIF Mediates Toll-like Receptor 5-induced Signaling in Intestinal Epithelial Cells. *Journal of Biological Chemistry* **285**: 37570-37578.

Chow A, Lucas D, Hidalgo A, Méndez-Ferrer S, Hashimoto D, Scheiermann C, Battista M, Leboeuf M, Prophete C, van Rooijen N et al. 2011. Bone marrow CD169+ macrophages promote the retention of hematopoietic stem and progenitor cells in the mesenchymal stem cell niche. *The Journal of Experimental Medicine* **208**: 261-271.

Ichii M, Shimazu T, Welner RS, Garrett KP, Zhang Q, Esplin BL, Kincade PW. 2010. Functional diversity of stem and progenitor cells with B-lymphopoietic potential. *Immunological Reviews* **237**: 10-21.

Iwasaki H, Akashi K. 2007. Myeloid Lineage Commitment from the Hematopoietic Stem Cell. *Immunity* **26**: 726-740.

Janeway CA, Jr. 1989. Approaching the asymptote? Evolution and revolution in immunology. *Cold Spring Harbor symposia on quantitative biology* **54 Pt 1**: 1-13.

Kamada N, Hisamatsu T, Okamoto S, Chinen H, Kobayashi T, Sato T, Sakuraba A, Kitazume MT, Sugita A, Koganei K et al. 2008. Unique CD14+ intestinal macrophages contribute to the pathogenesis of Crohn disease via IL-23/IFN-γ axis. *The Journal of Clinical Investigation* **118**: 2269-2280.

Katsura Y, Kawamoto H. 2001. Stepwise lineage restriction of progenitors in lympho-myelopoiesis. *Int Rev Immunol* **20**: 1-20.

Katz J, Benoist C, Mathis D. 1993. Major histocompatibility complex class I molecules are required for the development of insulitis in non-obese diabetic mice. *Eur J Immunol* **23**: 3358-3360.

Kaul D, Habbel P, Derkow K, Krüger C, Franzoni E, Wulczyn FG, Bereswill S, Nitsch R, Schott E, Veh R et al. 2012. Expression of Toll-Like Receptors in the Developing Brain. *PLoS ONE* **7**: e37767.

Kawai T, Akira S. 2006. TLR signaling. *Cell Death Differ* **13**: 816-825.

Kawai T, Akira S. 2010. The role of pattern-recognition receptors in innate immunity: update on Toll-like receptors. *Nat Immunol* **11**: 373-384.

Kawai T, Akira S. 2011. Toll-like Receptors and Their Crosstalk with Other Innate Receptors in Infection and Immunity. *Immunity* **34**: 637-650.

Kawamoto H, Katsura Y. 2009. A new paradigm for hematopoietic cell lineages: revision of the classical concept of the myeloid-lymphoid dichotomy. *Trends Immunol* **30**: 193-200.

Kawamoto H, Minato N. 2004. Myeloid cells. *The International Journal of Biochemistry & Cell Biology* **36**: 1374-1379.

Kawamoto H, Wada H, Katsura Y. 2010. A revised scheme for developmental pathways of hematopoietic cells: the myeloid-based model. *International Immunology* **22**: 65-70.

Kawane K, Fukuyama H, Kondoh G, Takeda J, Ohsawa Y, Uchiyama Y, Nagata S. 2001. Requirement of DNase II for definitive erythropoiesis in the mouse fetal liver. *Science* **292**: 1546-1549.

Keogh B, Parker AE. 2011. Toll-like receptors as targets for immune disorders. *Trends in Pharmacological Sciences* **32**: 435-442.

Khadra A, Pietropaolo M, Nepom GT, Sherman A. 2011. Investigating the role of T-cell avidity and killing efficacy in relation to type 1 diabetes prediction. *PLoS One* **6**: e14796.

Kiel MJ, Yilmaz OH, Iwashita T, Yilmaz OH, Terhorst C, Morrison SJ. 2005. SLAM Family Receptors Distinguish Hematopoietic Stem and Progenitor Cells and Reveal Endothelial Niches for Stem Cells. *Cell* **121**: 1109-1121.

Kim HS, Han MS, Chung KW, Kim S, Kim E, Kim MJ, Jang E, Lee HA, Youn J, Akira S et al. 2007. Toll-like receptor 2 senses beta-cell death and contributes to the initiation of autoimmune diabetes. *Immunity* **27**: 321-333.

Kim HS, Lee MS. 2009. Role of innate immunity in triggering and tuning of autoimmune diabetes. *Current molecular medicine* **9**: 30-44.

Kim S, Takahashi H, Lin W-W, Descargues P, Grivennikov S, Kim Y, Luo J-L, Karin M. 2009. Carcinoma-produced factors activate myeloid cells through TLR2 to stimulate metastasis. *Nature* **457**: 102-106.

Kinder SJ, Tsang TE, Quinlan GA, Hadjantonakis AK, Nagy A, Tam PP. 1999. The orderly allocation of mesodermal cells to the extraembryonic structures and the anteroposterior axis during gastrulation of the mouse embryo. *Development* **126**: 4691-4701.

King KY, Goodell MA. 2011. Inflammatory modulation of HSCs: viewing the HSC as a foundation for the immune response. *Nat Rev Immunol* **11**: 685-692.

Komiya A, Nagase H, Okugawa S, Ota Y, Suzukawa M, Kawakami A, Sekiya T, Matsushima K, Ohta K, Hirai K et al. 2006. Expression and function of toll-like receptors in human basophils. *International archives of allergy and immunology* **140 Suppl 1**: 23-27.

Kumar H, Kawai T, Akira S. 2011. Pathogen Recognition by the Innate Immune System. *International Reviews of Immunology* **30**: 16-34.

Kzhyshkowska J, Gratchev A, Goerdt S. 2006. Stabilin-1, a homeostatic scavenger receptor with multiple functions. *Journal of cellular and molecular medicine* **10**: 635-649.

Lacaud G, Gore L, Kennedy M, Kouskoff V, Kingsley P, Hogan C, Carlsson L, Speck N, Palis J, Keller G. 2002. Runx1 is essential for hematopoietic commitment at the hemangioblast stage of development in vitro. *Blood* **100**: 458-466.

Lancrin C, Sroczynska P, Stephenson C, Allen T, Kouskoff V, Lacaud G. 2009. The haemangioblast generates haematopoietic cells through a haemogenic endothelium stage. *Nature* **457**: 892-895.

Lawson KA, Meneses JJ, Pedersen RA. 1991. Clonal analysis of epiblast fate during germ layer formation in the mouse embryo. *Development* **113**: 891-911.

Lee EC, Yu D, Martinez de Velasco J, Tessarollo L, Swing DA, Court DL, Jenkins NA, Copeland NG. 2001. A Highly Efficient Escherichia coli-Based Chromosome Engineering System Adapted for Recombinogenic Targeting and Subcloning of BAC DNA. *Genomics* **73**: 56-65.

Lee M-S. 2013. Treatment of Autoimmune Diabetes by Inhibiting the Initial Event. *Immune Netw* **13**: 194-198.

Lehrer RI, Szklarek D, Barton A, Ganz T, Hamann KJ, Gleich GJ. 1989. Antibacterial properties of eosinophil major basic protein and eosinophil cationic protein. *Journal of immunology (Baltimore, Md : 1950)* **142**: 4428-4434.

Lemaitre B, Nicolas E, Michaut L, Reichhart J-M, Hoffmann JA. 1996. The Dorsoventral Regulatory Gene Cassette spätzle/Toll/cactus Controls the Potent Antifungal Response in Drosophila Adults. *Cell* **86**: 973-983.

Leuschner F, Rauch PJ, Ueno T, Gorbatov R, Marinelli B, Lee WW, Dutta P, Wei Y, Robbins C, Iwamoto Y et al. 2012. Rapid monocyte kinetics in acute myocardial infarction are sustained by extramedullary monocytopoiesis. *The Journal of Experimental Medicine* **209**: 123-137.

Levine B, Deretic V. 2007. Unveiling the roles of autophagy in innate and adaptive immunity. *Nat Rev Immunol* **7**: 767-777.

Li M, Song L, Gao X, Chang W, Qin X. 2012a. Toll-like receptor 4 on islet beta cells senses expression changes in high-mobility group box 1 and contributes to the initiation of type 1 diabetes. *Experimental & molecular medicine* **44**: 260-267.

Li Y, Du XF, Liu CS, Wen ZL, Du JL. 2012b. Reciprocal regulation between resting microglial dynamics and neuronal activity in vivo. *Developmental cell* **23**: 1189-1202.

Li Z, Chen MJ, Stacy T, Speck NA. 2006. Runx1 function in hematopoiesis is required in cells that express Tek. *Blood* **107**: 106-110.

Lindau D, Mussard J, Wagner BJ, Ribon M, Rönnefarth VM, Quettier M, Jelcic I, Boissier M-C, Rammensee H-G, Decker P. 2013. Primary blood neutrophils express a functional cell surface Toll-like receptor 9. *European Journal of Immunology* **43**: 2101-2113.

Lindgren H, Golovliov I, Baranov V, Ernst RK, Telepnev M, Sjostedt A. 2004. Factors affecting the escape of Francisella tularensis from the phagolysosome. *Journal of medical microbiology* **53**: 953-958.

Lunemann JD, Munz C. 2008. Autophagy in CD4+ T-cell immunity and tolerance. *Cell Death Differ* **16**: 79-86.

Lux CT, Yoshimoto M, McGrath K, Conway SJ, Palis J, Yoder MC. 2008. All primitive and definitive hematopoietic progenitor cells emerging before E10 in the mouse embryo are products of the yolk sac. *Blood* **111**: 3435-3438.

Mantovani A, Cassatella MA, Costantini C, Jaillon S. 2011. Neutrophils in the activation and regulation of innate and adaptive immunity. *Nat Rev Immunol* **11**: 519-531.

Marée AFM, Komba M, Dyck C, Łabęcki M, Finegood DT, Edelstein-Keshet L. 2005. Quantifying macrophage defects in type 1 diabetes. *Journal of Theoretical Biology* **233**: 533-551.

Massberg S, Schaerli P, Knezevic-Maramica I, Köllnberger M, Tubo N, Moseman EA, Huff IV, Junt T, Wagers AJ, Mazo IB et al. 2007. Immunosurveillance by Hematopoietic Progenitor Cells Trafficking through Blood, Lymph, and Peripheral Tissues. *Cell* **131**: 994-1008.

Matsuoka S, Tsuji K, Hisakawa H, Xu M-j, Ebihara Y, Ishii T, Sugiyama D, Manabe A, Tanaka R, Ikeda Y et al. 2001. Generation of definitive hematopoietic stem cells from murine early yolk sac and paraaortic splanchnopleures by aorta-gonad-mesonephros region-derived stromal cells. *Blood* **98**: 6-12.

McGrath KE, Koniski AD, Malik J, Palis J. 2003. Circulation is established in a stepwise pattern in the mammalian embryo. *Blood* **101**: 1669-1675.

McGrath KE, Palis J. 2005. Hematopoiesis in the yolk sac: more than meets the eye. *Experimental Hematology* **33**: 1021-1028.

Medvinsky A, Dzierzak E. 1996. Definitive Hematopoiesis Is Autonomously Initiated by the AGM Region. *Cell* **86**: 897-906.

Medvinsky A, Rybtsov S, Taoudi S. 2011. Embryonic origin of the adult hematopoietic system: advances and questions. *Development* **138**: 1017-1031.

Medzhitov R. 2001. Toll-like receptors and innate immunity. *Nat Rev Immunol* **1**: 135-145.

Medzhitov R. 2007. Recognition of microorganisms and activation of the immune response. *Nature* **449**: 819-826.

Medzhitov R, Preston-Hurlburt P, Janeway C. 1997. A human homologue of the Drosophila Toll protein signals activation of adaptive immunity. *Nature* **388**: 394-397.

Mikkola HKA, Fujiwara Y, Schlaeger TM, Traver D, Orkin SH. 2003. Expression of CD41 marks the initiation of definitive hematopoiesis in the mouse embryo. *Blood* **101**: 508-516.

Miller BC, Zhao Z, Stephenson LM, Cadwell K, Pua HH, Lee HK, Mizushima N, Iwasaki A, He Y-W, Swat W et al. 2008. The autophagy gene ATG5 plays an essential role in B lymphocyte development. *Autophagy* **4**: 309-314.

Min B, Brown MA, Legros G. 2012. Understanding the roles of basophils: breaking dawn. *Immunology* **135**: 192-197.

Mitjavila-Garcia MT, Cailleret M, Godin I, Nogueira MM, Cohen-Solal K, Schiavon V, Lecluse Y, Le Pesteur F, Lagrue AH, Vainchenker W. 2002. Expression of CD41 on hematopoietic progenitors derived from embryonic hematopoietic cells. *Development* **129**: 2003-2013.

Miyake K, Onji M. 2013. Endocytosis-free DNA sensing by cell surface TLR9 in neutrophils: Rapid defense with autoimmune risks. *European Journal of Immunology* **43**: 2006-2009.

Mizushima N, Ohsumi Y, Yoshimori T. 2002. Autophagosome formation in mammalian cells. *Cell structure and function* **27**: 421-429.

Moore M, Metcalf D. 1970. Ontogeny of the haemopoietic system: yolk sac origin of in vivo and in vitro colony forming cells in the developing mouse embryo. *Br J Haematol* **18**: 279-296.

Morita Y, Ema H, Nakauchi H. 2010. Heterogeneity and hierarchy within the most primitive hematopoietic stem cell compartment. *J Exp Med* **207**: 1173-1182.

Muller AM, Medvinsky A, Strouboulis J, Grosveld F, Dzierzakt E. 1994. Development of hematopoietic stem cell activity in the mouse embryo. *Immunity* **1**: 291-301.

Murray PJ, Wynn TA. 2011. Protective and pathogenic functions of macrophage subsets. *Nat Rev Immunol* **11**: 723-737.

Muzio M, Bosisio D, Polentarutti N, D'amico G, Stoppacciaro A, Mancinelli R, van't Veer C, Penton-Rol G, Ruco LP, Allavena P et al. 2000. Differential Expression and Regulation of Toll-Like Receptors (TLR) in Human Leukocytes: Selective Expression of TLR3 in Dendritic Cells. *The Journal of Immunology* **164**: 5998-6004.

Nagai Y, Garrett KP, Ohta S, Bahrun U, Kouro T, Akira S, Takatsu K, Kincade PW. 2006. Toll-like Receptors on Hematopoietic Progenitor Cells Stimulate Innate Immune System Replenishment. *Immunity* **24**: 801-812.

Nagase H, Okugawa S, Ota Y, Yamaguchi M, Tomizawa H, Matsushima K, Ohta K, Yamamoto K, Hirai K. 2003. Expression and Function of Toll-Like Receptors in Eosinophils: Activation by Toll-Like Receptor 7 Ligand. *The Journal of Immunology* **171**: 3977-3982.

Nagy A. 2000. Cre recombinase: The universal reagent for genome tailoring. *genesis* **26**: 99-109.

Nakagawa I, Amano A, Mizushima N, Yamamoto A, Yamaguchi H, Kamimoto T, Nara A, Funao J, Nakata M, Tsuda K et al. 2004. Autophagy defends cells against invading group A Streptococcus. *Science* **306**: 1037-1040.

Nathan C, Ding A. 2010. Nonresolving Inflammation. *Cell* **140**: 871-882.

Nedjic J, Aichinger M, Emmerich J, Mizushima N, Klein L. 2008. Autophagy in thymic epithelium shapes the T-cell repertoire and is essential for tolerance. *Nature* **455**: 396-400.

Nejepinska J, Malik R, Filkowski J, Flemr M, Filipowicz W, Svoboda P. 2012. dsRNA expression in the mouse elicits RNAi in oocytes and low adenosine deamination in somatic cells. *Nucleic Acids Res* **40**: 399-413.

Nguyen KD, Qiu Y, Cui X, Goh YPS, Mwangi J, David T, Mukundan L, Brombacher F, Locksley RM, Chawla A. 2011. Alternatively activated macrophages produce catecholamines to sustain adaptive thermogenesis. *Nature* **480**: 104-108.

Nishikawa M, Tahara T, Hinohara A, Miyajima A, Nakahata T, Shimosaka A. 2001. Role of the microenvironment of the embryonic aorta-gonad-mesonephros region in hematopoiesis. *Ann N Y Acad Sci* **938**: 109-116.

Nishikawa SI, Nishikawa S, Hirashima M, Matsuyoshi N, Kodama H. 1998. Progressive lineage analysis by cell sorting and culture identifies FLK1+VE-cadherin+ cells at a diverging point of endothelial and hemopoietic lineages. *Development* **125**: 1747-1757.

North T, Gu TL, Stacy T, Wang Q, Howard L, Binder M, Marin-Padilla M, Speck NA. 1999. Cbfa2 is required for the formation of intra-aortic hematopoietic clusters. *Development* **126**: 2563-2575.

Odegaard JI, Ricardo-Gonzalez RR, Goforth MH, Morel CR, Subramanian V, Mukundan L, Eagle AR, Vats D, Brombacher F, Ferrante AW et al. 2007. Macrophage-specific PPAR[ggr] controls alternative activation and improves insulin resistance. *Nature* **447**: 1116-1120.

Okuda T, van Deursen J, Hiebert SW, Grosveld G, Downing JR. 1996. AML1, the Target of Multiple Chromosomal Translocations in Human Leukemia, Is Essential for Normal Fetal Liver Hematopoiesis. *Cell* **84**: 321-330.

Orkin SH, Zon LI. 2008. Hematopoiesis: An Evolving Paradigm for Stem Cell Biology. *Cell* **132**: 631-644.

Palis J. 2006. Yolk Sac Development in Mice. in *Hematopoietic Stem Cell Development* (eds. I Godin, A Cumano), p. 62. Springer, Boston, MA.

Palis J, Robertson S, Kennedy M, Wall C, Keller G. 1999. Development of erythroid and myeloid progenitors in the yolk sac and embryo proper of the mouse. *Development* **126**: 5073-5084.

Palis J, Yoder MC. 2001. Yolk-sac hematopoiesis: The first blood cells of mouse and man. *Experimental Hematology* **29**: 927-936.

Paludan C, Schmid D, Landthaler M, Vockerodt M, Kube D, Tuschl T, Munz C. 2005. Endogenous MHC class II processing of a viral nuclear antigen after autophagy. *Science* **307**: 593-596.

Pandey S, Agrawal DK. 2006. Immunobiology of Toll-like receptors: Emerging trends. *Immunol Cell Biol* **84**: 333-341.

Paolicelli RC, Bolasco G, Pagani F, Maggi L, Scianni M, Panzanelli P, Giustetto M, Ferreira TA, Guiducci E, Dumas L et al. 2011. Synaptic pruning by microglia is necessary for normal brain development. *Science* **333**: 1456-1458.

Petrenko O, Beavis A, Klaine M, Kittappa R, Godin I, Lemischka IR. 1999. The Molecular Characterization of the Fetal Stem Cell Marker AA4. *Immunity* **10**: 691-700.

Pivarcsi A, Bodai L, Réthi B, Kenderessy-Szabó A, Koreck A, Széll M, Beer Z, Bata-Csörgoő Z, Magócsi M, Rajnavölgyi É et al. 2003. Expression and function of Toll-like receptors 2 and 4 in human keratinocytes. *International Immunology* **15**: 721-730.

Pohar J, Pirher N, Benčina M, Manček-Keber M, Jerala R. 2013. The Role of UNC93B1 Protein in Surface Localization of TLR3 Receptor and in Cell Priming to Nucleic Acid Agonists. *Journal of Biological Chemistry* **288**: 442-454.

Pollard JW. 2009. Trophic macrophages in development and disease. *Nat Rev Immunol* **9**: 259-270.

Poltorak A, He X, Smirnova I, Liu M-Y, Huffel CV, Du X, Birdwell D, Alejos E, Silva M, Galanos C et al. 1998. Defective LPS Signaling in C3H/HeJ and C57BL/10ScCr Mice: Mutations in Tlr4 Gene. *Science* **282**: 2085-2088.

Pua HH, He Y-W. 2007. Maintaining T Lymphocyte Homeostasis: Another Duty of Autophagy. *Autophagy* **3**: 266-267.

Purton LE, Scadden DT. 2007. Limiting Factors in Murine Hematopoietic Stem Cell Assays. *Cell Stem Cell* **1**: 263-270.

Qian B-Z, Pollard JW. 2010. Macrophage Diversity Enhances Tumor Progression and Metastasis. *Cell* **141**: 39-51.

Rae F, Woods K, Sasmono T, Campanale N, Taylor D, Ovchinnikov DA, Grimmond SM, Hume DA, Ricardo SD, Little MH. 2007. Characterisation and trophic functions of murine embryonic macrophages based upon the use of a Csf1r-EGFP transgene reporter. *Dev Biol* **308**: 232-246.

Rao S, Lobov IB, Vallance JE, Tsujikawa K, Shiojima I, Akunuru S, Walsh K, Benjamin LE, Lang RA. 2007. Obligatory participation of macrophages in an angiopoietin 2-mediated cell death switch. *Development* **134**: 4449-4458.

Recalcati S, Locati M, Gammella E, Invernizzi P, Cairo G. 2012. Iron levels in polarized macrophages: regulation of immunity and autoimmunity. *Autoimmunity reviews* **11**: 883-889.

Reizis B, Colonna M, Trinchieri G, Barrat F, Gilliet M. 2011. Plasmacytoid dendritic cells: one-trick ponies or workhorses of the immune system? *Nat Rev Immunol* **11**: 558-565.

Rhodes KE, Gekas C, Wang Y, Lux CT, Francis CS, Chan DN, Conway S, Orkin SH, Yoder MC, Mikkola HKA. 2008. The Emergence of Hematopoietic Stem Cells Is Initiated in the Placental Vasculature in the Absence of Circulation. *Cell Stem Cell* **2**: 252-263.

Rosenberg HF, Dyer KD, Foster PS. 2013. Eosinophils: changing perspectives in health and disease. *Nat Rev Immunol* **13**: 9-22.

Sabroe I, Jones EC, Usher LR, Whyte MKB, Dower SK. 2002. Toll-Like Receptor (TLR)2 and TLR4 in Human Peripheral Blood Granulocytes: A Critical Role for Monocytes in Leukocyte Lipopolysaccharide Responses. *The Journal of Immunology* **168**: 4701-4710.

Saint André Av, Blackwell NM, Hall LR, Hoerauf A, Brattig NW, Volkmann L, Taylor MJ, Ford L, Hise AG, Lass JH et al. 2002. The Role of Endosymbiotic Wolbachia Bacteria in the Pathogenesis of River Blindness. *Science* **295**: 1892-1895.

Salomon B, Lenschow DJ, Rhee L, Ashourian N, Singh B, Sharpe A, Bluestone JA. 2000. B7/CD28 costimulation is essential for the homeostasis of the CD4+CD25+ immunoregulatory T cells that control autoimmune diabetes. *Immunity* **12**: 431-440.

Samokhvalov IM, Samokhvalova NI, Nishikawa S-i. 2007. Cell tracing shows the contribution of the yolk sac to adult haematopoiesis. *Nature* **446**: 1056-1061.

Samuel Varman T, Shulman Gerald I. 2012. Mechanisms for Insulin Resistance: Common Threads and Missing Links. *Cell* **148**: 852-871.

Sanjuan MA, Dillon CP, Tait SWG, Moshiach S, Dorsey F, Connell S, Komatsu M, Tanaka K, Cleveland JL, Withoff S et al. 2007. Toll-like receptor signalling in macrophages links the autophagy pathway to phagocytosis. *Nature* **450**: 1253-1257.

Santic M, Asare R, Skrobonja I, Jones S, Abu Kwaik Y. 2008. Acquisition of the vacuolar ATPase proton pump and phagosome acidification are essential for escape of Francisella tularensis into the macrophage cytosol. *Infection and immunity* **76**: 2671-2677.

Seto S, Tsujimura K, Horii T, Koide Y. 2013. Autophagy adaptor protein p62/SQSTM1 and autophagy-related gene Atg5 mediate autophagosome formation in response to Mycobacterium tuberculosis infection in dendritic cells. *PLoS One* **8**: e86017.

Shalaby F, Ho J, Stanford WL, Fischer K-D, Schuh AC, Schwartz L, Bernstein A, Rossant J. 1997. A Requirement for Flk1 in Primitive and Definitive Hematopoiesis and Vasculogenesis. *Cell* **89**: 981-990.

Sharan SK, Thomason LC, Kuznetsov SG, Court DL. 2009. Recombineering: a homologous recombination-based method of genetic engineering. *Nat Protocols* **4**: 206-223.

Shi C-S, Kehrl JH. 2008. MyD88 and Trif Target Beclin 1 to Trigger Autophagy in Macrophages. *Journal of Biological Chemistry* **283**: 33175-33182.

Schroeder JT, MacGlashan DW, Jr., Lichtenstein LM. 2001. Human basophils: mediator release and cytokine production. *Advances in immunology* **77**: 93-122.

Schulz C, Perdiguero EG, Chorro L, Szabo-Rogers H, Cagnard N, Kierdorf K, Prinz M, Wu B, Jacobsen SEW, Pollard JW et al. 2012. A Lineage of Myeloid Cells Independent of Myb and Hematopoietic Stem Cells. *Science* **336**: 86-90.

Silver L, Palis J. 1997. Initiation of Murine Embryonic Erythropoiesis: A Spatial Analysis. *Blood* **89**: 1154-1164.

Sioud M, Floisand Y, Forfang L, Lund-Johansen F. 2006. Signaling through Toll-like Receptor 7/8 Induces the Differentiation of Human Bone Marrow CD34+ Progenitor Cells along the Myeloid Lineage. *J Mol Biol* **364**: 945-954.

Smith JL, Gesteland KM, Schoenwolf GC. 1994. Prospective fate map of the mouse primitive streak at 7.5 days of gestation. *Dev Dynam* **201**: 279-289.

Spencer LA, Szela CT, Perez SA, Kirchhoffer CL, Neves JS, Radke AL, Weller PF. 2009. Human eosinophils constitutively express multiple Th1, Th2, and immunoregulatory cytokines that are secreted rapidly and differentially. *J Leukoc Biol* **85**: 117-123.

Srinivas S, Watanabe T, Lin C-S, William C, Tanabe Y, Jessell T, Costantini F. 2001. Cre reporter strains produced by targeted insertion of EYFP and ECFP into the ROSA26 locus. *BMC Developmental Biology* **1**: 4.

Stefater Iii JA, Lewkowich I, Rao S, Mariggi G, Carpenter AC, Burr AR, Fan J, Ajima R, Molkentin JD, Williams BO et al. 2011. Regulation of angiogenesis by a non-canonical Wnt-Flt1 pathway in myeloid cells. *Nature* **474**: 511-515.

Sugiyama D, Ogawa M, Nakao K, Osumi N, Nishikawa S, Nishikawa S-i, Arai K-i, Nakahata T, Tsuji K. 2007. B cell potential can be obtained from pre-circulatory yolk sac, but with low frequency. *Dev Biol* **301**: 53-61.

Summers C, Rankin SM, Condliffe AM, Singh N, Peters AM, Chilvers ER. 2010. Neutrophil kinetics in health and disease. *Trends in Immunology* **31**: 318-324.

Suurmond J, Stoop JN, Rivellese F, Bakker AM, Huizinga TWJ, Toes REM. 2014. Activation of human basophils by combined toll-like receptor- and FcεRI-triggering can promote Th2 skewing of naive T helper cells. *European Journal of Immunology* **44**: 386-396.

Takeuchi O, Hoshino K, Kawai T, Sanjo H, Takada H, Ogawa T, Takeda K, Akira S. 1999. Differential Roles of TLR2 and TLR4 in Recognition of Gram-Negative and Gram-Positive Bacterial Cell Wall Components. *Immunity* **11**: 443-451.

Takizawa H, Boettcher S, Manz MG. 2012. Demand-adapted regulation of early hematopoiesis in infection and inflammation. *Blood* **119**: 2991-3002.

Tam PP, Beddington RS. 1987. The formation of mesodermal tissues in the mouse embryo during gastrulation and early organogenesis. *Development* **99**: 109-126.

Tamilselvam B, Daefler S. 2008. Francisella targets cholesterol-rich host cell membrane domains for entry into macrophages. *Journal of immunology (Baltimore, Md : 1950)* **180**: 8262-8271.

Tanaka Y, Hayashi M, Kubota Y, Nagai H, Sheng G, Nishikawa S-I, Samokhvalov IM. 2012. Early ontogenic origin of the hematopoietic stem cell lineage. *Proc Natl Acad Sci USA* **109**: 4515-4520.

Taoudi S, Morrison AM, Inoue H, Gribi R, Ure J, Medvinsky A. 2005. Progressive divergence of definitive haematopoietic stem cells from the endothelial compartment does not depend on contact with the foetal liver. *Development* **132**: 4179-4191.

Tarnvik A, Berglund L. 2003. Tularaemia. *The European respiratory journal* **21**: 361-373.

Till JE, McCulloch E. 1961. A direct measurement of the radiation sensitivity of normal mouse bone marrow cells. *Radiation research* **14**: 213-222.

Tonkin DR, Haskins K. 2009. Regulatory T cells enter the pancreas during suppression of type 1 diabetes and inhibit effector T cells and macrophages in a TGF-beta-dependent manner. *Eur J Immunol* **39**: 1313-1322.

Trumpp A, Essers M, Wilson A. 2010. Awakening dormant haematopoietic stem cells. *Nat Rev Immunol* **10**: 201-209.

Ueda Y, Kondo M, Kelsoe G. 2005. Inflammation and the reciprocal production of granulocytes and lymphocytes in bone marrow. *J Exp Med* **201**: 1771-1780.

Ueno H, Klechevsky E, Morita R, Aspord C, Cao T, Matsui T, Di Pucchio T, Connolly J, Fay JW, Pascual V et al. 2007. Dendritic cell subsets in health and disease. *Immunol Rev* **219**: 118-142.

Ueno H, Weissman IL. 2007. Stem cells: Blood lines from embryo to adult. *Nature* **446**: 996-997.

Ueno H, Weissman IL. 2010. The origin and fate of yolk sac hematopoiesis: application of chimera analyses to developmental studies. *Int J Dev Biol* **54**: 1019-1031.

Wallander ML, Leibold EA, Eisenstein RS. 2006. Molecular control of vertebrate iron homeostasis by iron regulatory proteins. *Biochimica et biophysica acta* **1763**: 668-689.

Wang HB, Ghiran I, Matthaei K, Weller PF. 2007. Airway eosinophils: allergic inflammation recruited professional antigen-presenting cells. *Journal of immunology (Baltimore, Md : 1950)* **179**: 7585-7592.

Weller PF. 1994. Eosinophils: structure and functions. *Curr Opin Immunol* **6**: 85-90.

Welner RS, Kincade PW. 2007. Stem Cells on Patrol. *Cell* **131**: 842-844.

Wentworth JM, Naselli G, Brown WA, Doyle L, Phipson B, Smyth GK, Wabitsch M, O'Brien PE, Harrison LC. 2010. Pro-inflammatory CD11c+CD206+ adipose tissue macrophages are associated with insulin resistance in human obesity. *Diabetes* **59**: 1648-1656.

Wolfs TGAM, Buurman WA, van Schadewijk A, de Vries B, Daemen MARC, Hiemstra PS, van 't Veer C. 2002. In Vivo Expression of Toll-Like Receptor 2 and 4 by Renal Epithelial Cells: IFN-γ and TNF-α Mediated Up-Regulation During Inflammation. *The Journal of Immunology* **168**: 1286-1293.

Wong CK, Cheung PF, Ip WK, Lam CW. 2007. Intracellular signaling mechanisms regulating toll-like receptor-mediated activation of eosinophils. *American journal of respiratory cell and molecular biology* **37**: 85-96.

Wright DE, Wagers AJ, Gulati AP, Johnson FL, Weissman IL. 2001. Physiological Migration of Hematopoietic Stem and Progenitor Cells. *Science* **294**: 1933-1936.

Wynn TA, Chawla A, Pollard JW. 2013. Macrophage biology in development, homeostasis and disease. *Nature* **496**: 445-455.

Xu M-j, Matsuoka S, Yang F-C, Ebihara Y, Manabe A, Tanaka R, Eguchi M, Asano S, Nakahata T, Tsuji K. 2001. Evidence for the presence of murine primitive megakarycytopoiesis in the early yolk sac. *Blood* **97**: 2016-2022.

Xu Y, Jagannath C, Liu X-D, Sharafkhaneh A, Kolodziejska KE, Eissa NT. 2007. Toll-like Receptor 4 Is a Sensor for Autophagy Associated with Innate Immunity. *Immunity* **27**: 135-144.

Yanez A, Goodridge HS, Gozalbo D, Gil ML. 2013. TLRs control hematopoiesis during infection. *Eur J Immunol* **43**: 2526-2533.

Yang F, Liu XB, Quinones M, Melby PC, Ghio A, Haile DJ. 2002. Regulation of reticuloendothelial iron transporter MTP1 (Slc11a3) by inflammation. *The Journal of biological chemistry* **277**: 39786-39791.

Yoder MC, Hiatt K, Mukherjee P. 1997. In vivo repopulating hematopoietic stem cells are present in the murine yolk sac at day 9.0 postcoitus. *Proceedings of the National Academy of Sciences* **94**: 6776-6780.

Yokomizo T, Hasegawa K, Ishitobi H, Osato M, Ema M, Ito Y, Yamamoto M, Takahashi S. 2008. Runx1 is involved in primitive erythropoiesis in the mouse. *Blood* **111**: 4075-4080.

Yona S, Kim K-W, Wolf Y, Mildner A, Varol D, Breker M, Strauss-Ayali D, Viukov S, Guilliams M, Misharin A et al. 2013. Fate Mapping Reveals Origins and Dynamics of Monocytes and Tissue Macrophages under Homeostasis. *Immunity* **38**: 79-91.

Yoshimoto M, Porayette P, Glosson NL, Conway SJ, Carlesso N, Cardoso AA, Kaplan MH, Yoder MC. 2012. Autonomous murine T-cell progenitor production in the extra-embryonic yolk sac before HSC emergence. *Blood* **119**: 5706-5714.

Yousefi S, Gold JA, Andina N, Lee JJ, Kelly AM, Kozlowski E, Schmid I, Straumann A, Reichenbach J, Gleich GJ et al. 2008. Catapult-like release of mitochondrial DNA by eosinophils contributes to antibacterial defense. *Nat Med* **14**: 949-953.

Yousefi S, Simon D, Simon H-U. 2012. Eosinophil extracellular DNA traps: molecular mechanisms and potential roles in disease. *Current Opinion in Immunology* **24**: 736-739.

Zeigler BM, Sugiyama D, Chen M, Guo Y, Downs KM, Speck NA. 2006. The allantois and chorion, when isolated before circulation or chorio-allantoic fusion, have hematopoietic potential. *Development* **133**: 4183-4192.

Zipris D. 2010. Toll-like receptors and type 1 diabetes. *Advances in experimental medicine and biology* **654**: 585-610.

Zuniga-Pflucker JC, Lenardo MJ. 1996. Regulation of thymocyte development from immature progenitors. *Curr Opin Immunol* **8**: 215-224.